

ÉCOLE DE TECHNOLOGIE SUPÉRIEURE
UNIVERSITÉ DU QUÉBEC

THESIS PRESENTED TO
ÉCOLE DE TECHNOLOGIE SUPÉRIEURE

IN PARTIAL FULFILLMENT OF THE REQUIREMENTS FOR
THE DEGREE OF DOCTOR OF PHILOSOPHY
Ph.D.

BY
Mohammad Hany YASSIN

NONLINEAR SEISMIC SOIL-PILE INTERACTION ANALYSIS FOR BRIDGES
FOUNDED IN QUEBEC SOIL

MONTREAL, DECEMBER 15, 2015

©Copyright Mohammad Hany Yassin, 2015 All rights reserved

© Copyright

Reproduction, saving or sharing of the content of this document, in whole or in part, is prohibited. A reader who wishes to print this document or save it on any medium must first obtain the author's permission.

BOARD OF EXAMINERS

THIS THESIS HAS BEEN EVALUATED

BY THE FOLLOWING BOARD OF EXAMINERS

Mr. Omar Chaallal, Thesis Supervisor
Department of Construction Engineering at École de technologie Supérieure

Mr. Hakim Bouzid, Chair, Board of Examiners
Department of Mechanical Engineering at École de technologie supérieure

Mr. Amar Khaled, Member of the jury
Department of Construction Engineering at École de technologie supérieure

Mr. Nouredine Ghlamallah, External Evaluator
Directeur de service LVM, une division de Englobe Corp.

THIS THESIS WAS PRESENTED AND DEFENDED

IN THE PRESENCE OF A BOARD OF EXAMINERS AND THE PUBLIC

ON JUNE 16, 2015

AT ÉCOLE DE TECHNOLOGIE SUPÉRIEURE

ACKNOWLEDGMENTS

I would like to express my special appreciation and thanks to my advisor Professor Dr. Omar Chaallal, you have been a tremendous mentor for me. I would like to thank you for encouraging my research and for allowing me to grow as a research engineer. Your advice on both research as well as on my career have been priceless. I would also like to thank my committee members, Professor Hakim Bouzid, Professor Amar Khaled, Doctor Nouredine Ghlamallah for serving as my committee members even at hardship. I would especially like to thank my research colleagues, work fellows and friend for their consistent encouragement, advices and help they offered in order to complete this work.

A special thanks to my family. Words cannot express how grateful I am to my father, my mother, my brothers and sisters for all of the sacrifices that you've made on my behalf. Your prayer for me was what sustained me thus far. I would also like to thank all of my friends who supported me in writing, and incited me to strive towards my goal. At the end I would like express appreciation to my beloved wife Huda. Without her sacrifices and patience this work would have not been completed.

NONLINEAR SEISMIC SOIL-PILE INTERACTION ANALYSIS FOR BRIDGES FOUNDED IN QUEBEC SOIL

Mohammad Hany YASSIN

ABSTRACT

This doctorate program focuses on the nonlinear behavior of seismic soil-structure interaction of deep foundations with particular emphasis in Quebec soil. Soil-structure interaction (SSI) plays a crucial role when analyzing and designing important or essential structures, such as skyscrapers, nuclear reactor facilities and highway bridges. For the latter, deep foundations are commonly used to support the bridge superstructure. Historically, the analysis of the interaction between the piles and the embedment soil under lateral loadings used the beam on Winkler theory which is implemented through the p-y curves general method. The commonly-used springs are driven originally from full-scale tests on piles with static or slow cyclic lateral load application. Evidences, from disturbed or damaged structures after earthquake, indicate that SSI follows different curve from the static p-y curve used in the design. The main objective of this research study is to contribute bridge the gap by carrying comprehensive nonlinear seismic analyses on soil-pile interaction for Quebec soils. Extensive numerical investigations have been conducted on 600 parametrical models in order to evaluate these variations and gaps. Results from this research study shows that the following parameters have a direct impact on the seismic soil-pile interaction: the length of the pile, the mass of the structure, as well as the intensity of the seismic record. The seismic soil-pile interaction (SPSI) is normally investigated by dynamic time history analysis on continuum soil-structure models. However, this process is long and time consuming particularly in engineering practice. A new simplified method is proposed in this study to scale the static p-y curves in order to simulate the dynamic behavior of SPSI. The results indicate a reasonable matching between the results from time-history and static analysis. Scaling the current p-y curves in order to simulate the SPSI, would results in a more accurate estimation for the seismic demands on the bridge. Furthermore it will reduce the computation cost by benefiting from currently-used and fast to implement p-y curve method. Field experiments on several types of soil are recommended in order to normalize these findings for engineering practice.

Keywords: Piles, Soil-structure interaction, Seismic, Nonlinear, p-y curve.

NONLINEAR SEISMIC SOIL-PILE INTERACTION ANALYSIS FOR BRIDGES FOUNDED IN QUEBEC SOIL

Mohammad Hany YASSIN

RÉSUMÉ

Cette thèse de doctorat traite du comportement non linéaire de l'interaction dynamique sol-structure des fondations profondes. L'étude considère en particulier les sols québécois. L'interaction sol-structure (ISS) joue un rôle crucial dans l'analyse et la conception de structures importantes ou essentielles. On peut citer les gratte-ciels, les réacteurs nucléaires ou les ponts routiers, autoroutiers et ferroviaires. En particulier, les fondations profondes sont souvent utilisées pour supporter la superstructure de ponts. Historiquement, l'analyse de l'interaction entre les pieux/caissons et le sol dans lequel ils sont fondés était basée sur la théorie de la poutre de Winkler à travers les courbes p-y généralisées. Les modèles de comportement des ressorts de Winkler utilisés étaient originalement déduits à partir d'essais statiques ou cycliques quasi-statiques. Cependant, les enseignements post-séismes sur les structures incluant les pieux/caissons ayant subi des dommages ont révélé que l'ISS introduit une courbe p-y différente de la courbe statique utilisée dans la pratique pour la conception des pieux/caissons.

L'objectif principal de la présente recherche est de contribuer à la compréhension de cette différence en menant une étude compréhensive et des analyses sismiques non linéaires poussées sur le comportement de l'interaction sol-pieu pour les sols québécois. Des investigations numériques extensives ont été menées dans le cadre de la présente étude. Un total de 600 modèles paramétriques ont été considérés afin d'évaluer cette différence. Les résultats de ces investigations ont permis de ressortir les paramètres majeurs qui impactent le plus le comportement sismique de l'interaction sol-pieu/caisson. On peut citer la longueur du pieu/caisson, la masse de la structure, et l'intensité de l'enregistrement sismique. L'interaction sismique sol-pieu/caisson est normalement analysée en réalisant une analyse dynamique pas-à-pas sur des modèles de continuum sol-structure. Ceci peut s'avérer long et fastidieux. Une nouvelle méthode est proposée dans le cadre de cette recherche permettant de calibrer les courbes p-y statiques pour les rendre capables de simuler le comportement dynamique de l'interaction sol-pieu/caisson. Les résultats obtenus indiquent une concordance raisonnable entre l'analyse dynamique rigoureuse pas-à-pas et l'analyse pseudo-statique approximative équivalente. L'utilisation des courbes p-y existantes calibrées pour simuler l'interaction dynamique sol-pieu/caisson permettra d'obtenir une estimation de la demande sismique sur les ponts plus précise et s'approchant plus de la réalité. Par ailleurs, elle permettra de réduire le temps de simulations numériques en bénéficiant des outils informatiques et des logiciels existants qui ont été développés durant les dernières années en se basant sur les courbes p-y statiques. Des essais in-situ sur des différents sols représentatifs

du Québec sont recommandés afin de valider et normaliser les résultats obtenus dans le cadre de cette étude pour les rendre utilisables en pratique.

Mots clés : Pieu/caisson, interaction sol-structure, sismique, non linéaire, courbe p-y.

TABLE OF CONTENTS

| | Page |
|--|------|
| INTRODUCTION | 1 |
| 0.1 Introduction..... | 1 |
| 0.2 Performance of deep foundation of bridges during seismic events | 2 |
| 0.3 Effects of SSI on the dynamic response of bridge structures | 2 |
| 0.4 Objectives | 4 |
| 0.5 Research significance..... | 5 |
| 0.6 Organization of the dissertation | 5 |
| CHAPTER 1 LITERATURE REVIEW | 7 |
| 1.1 Introduction..... | 7 |
| 1.2 Models of Soil-pile interaction under seismic loading | 8 |
| 1.3 Analytical models | 9 |
| 1.4 Beam-on-Elastic Foundation Models (subgrade reaction method) | 11 |
| 1.5 Beam-on-Winkler Foundation Models (“p-y” method)..... | 14 |
| 1.6 Continuum Models..... | 24 |
| 1.7 Finite Element Models..... | 26 |
| 1.8 Experimental models | 29 |
| 1.9 The pressuremeter method..... | 30 |
| 1.10 The flat dilatometer method..... | 32 |
| 1.11 The cone penetration test | 32 |
| 1.12 Codes recommendations and common practice..... | 33 |
| CHAPTER 2 MODELING ISSUES FOR PILES UNDER LATERAL LOADING..... | 37 |
| 2.1 Introduction..... | 37 |
| 2.2 Major elements in the soil-pile interaction problem | 37 |
| 2.3 Pile head fixity (kinematic seismic response of single piles – Gazetas)..... | 38 |
| 2.4 Soil stiffness..... | 39 |
| 2.5 In-situ horizontal stresses..... | 42 |
| 2.6 Pile/soil friction..... | 44 |
| 2.7 Sloping ground..... | 44 |
| 2.8 Pore pressure effects | 46 |
| 2.9 Pile diameter effect | 47 |
| 2.10 Group effect | 49 |
| CHAPTER 3 SITE CHARACTERIZATION | 57 |
| 3.1 Introduction..... | 57 |
| 3.2 Bécancour site..... | 57 |
| 3.2.1 Location | 58 |
| 3.2.2 Local geology..... | 58 |
| 3.2.3 Data analysis | 59 |

| | | |
|---|---|-----|
| 3.2.4 | Summary of work done..... | 59 |
| 3.2.5 | Summary of the stratigraphy..... | 64 |
| 3.2.6 | Presentation of the profile for analysis | 71 |
| 3.3 | Québec City site..... | 72 |
| 3.3.1 | Location | 72 |
| 3.3.2 | Local geology..... | 73 |
| 3.3.3 | Data analysis | 74 |
| 3.3.4 | Summary of work done..... | 74 |
| 3.3.5 | Summary of the stratigraphy..... | 80 |
| 3.3.6 | Presentation of the profile for analysis | 87 |
| 3.4 | Conclusions..... | 88 |
| CHAPTER 4 SELECTION OF EARTHQUAKE PARAMETERS | | 89 |
| 4.1 | Selection of seismic parameters for Bécancour site | 89 |
| 4.1.1 | Response spectrum by NBC 2010 | 89 |
| 4.1.2 | Deaggregation of the seismic hazard | 91 |
| 4.1.3 | Natural period of the soil deposit..... | 93 |
| 4.1.4 | Selection of earthquakes signals | 94 |
| 4.1.5 | Scaling of response spectra..... | 95 |
| 4.2 | Selection of seismic parameters for Quebec site | 100 |
| 4.3 | Conclusion | 100 |
| CHAPTER 5 PSEUDO-STATIC ANALYSIS OF TEST PILES | | 103 |
| 5.1 | Introduction..... | 103 |
| 5.2 | Methodology..... | 103 |
| 5.3 | Bécancour Site | 106 |
| 5.3.1 | The Models | 107 |
| 5.3.2 | Analysis Procedure and Results..... | 110 |
| 5.4 | Québec City Site | 121 |
| 5.4.1 | The Models | 121 |
| 5.4.2 | Analysis Procedure and Results..... | 123 |
| 5.5 | FLAC Models | 129 |
| 5.6 | Comparison of Results: FLAC vs LPILE | 131 |
| CHAPTER 6 SEISMIC ANALYSIS: PRESENTATION OF RESULTS AND DISCUSSION | | 137 |
| 6.1 | Introduction..... | 137 |
| 6.2 | Research Methodology | 139 |
| 6.2.1 | Site Seismic Response Analysis | 140 |
| 6.2.2 | Soil-Structure Seismic Analysis | 142 |
| 6.2.3 | Description of the model..... | 143 |
| 6.2.4 | Validating the FE model with LPILE for static load case | 146 |
| 6.2.5 | Analysis matrix | 146 |
| 6.2.6 | Post-processing of results | 147 |
| 6.2.7 | Presentation and discussion of results..... | 159 |

| | |
|--|-----|
| 6.2.8 Application of DS ratio in L-Pile and comparison of results..... | 185 |
| CONCLUSIONS AND RECOMMENDATIONS | 196 |
| APPENDIX I NON-LINEAR TIME HISTORY ANALYSIS RESULTS..... | 201 |
| BIBLIOGRAPHY | 249 |

LIST OF FIGURES

| | Page |
|-------------|---|
| Figure 1.1 | Beam-on-elastic-foundation problem 11 |
| Figure 1.2 | Failure modes proposed for short and long pile for free and fixed head conditions..... 13 |
| Figure 1.3 | Model of laterally loaded pile: (a) Elevation view; (b) As elastic line; (c) p - y curves 15 |
| Figure 1.4 | Discrete Load-Transfer (DLT) approach to obtain p - y curves 16 |
| Figure 1.5 | p - y curves extracted from cyclic load experiment 18 |
| Figure 1.6 | Hysteretic backbone curve..... 20 |
| Figure 1.7 | Degradation coefficient vs. Pore pressure ratio 22 |
| Figure 1.8 | Laterally loaded pile and pressuremeter analogy..... 31 |
| Figure 2.1 | Soil Stiffness Curve 40 |
| Figure 2.2 | Typical p - y Curves..... 42 |
| Figure 2.3 | Relation between Soil modulus and p - y Curves 42 |
| Figure 2.4 | Effect of Soil Weight and In-Situ Stress on the p - y Curve..... 43 |
| Figure 2.5 | Proposed Model for Soil–Pile Analysis in Pile-Stabilized Slopes..... 45 |
| Figure 2.6 | Coefficient C_u (p -multiplier) versus Pore Pressure Ratio r_u 47 |
| Figure 2.7 | Schematic of Pile Group Resistance 50 |
| Figure 2.8 | Top View of Typical Laterally Loaded Group Configuration..... 51 |
| Figure 2.9 | Estimating Factor α 54 |
| Figure 2.10 | Group Effect on p - y Curve : (a) p -multiplier concept; (b) y -multiplier concept 55 |
| Figure 3.1 | Location of the Bécancour Site..... 58 |
| Figure 3.2 | Location plan of boreholes and borings in the central zone 60 |

| | | |
|-------------|---|-----|
| Figure 3.3 | Stratigraphic profile of Bécancour Site..... | 65 |
| Figure 3.4 | Profiles of S_u and $(N_1)_{60}$ for Bécancour Site | 69 |
| Figure 3.5 | Profile of ϕ' and γ_{sat} for Bécancour Site | 70 |
| Figure 3.6 | Profiles of G_{max} and E'_{max} for Bécancour Site..... | 71 |
| Figure 3.7 | Profile of Stratigraphy and Geotechnical Properties Used for Analysis for Bécancour..... | 72 |
| Figure 3.8 | Location of the Québec Site..... | 73 |
| Figure 3.9 | Location of the Boreholes: Site of Québec City | 75 |
| Figure 3.10 | Stratigraphy of Quebec City Site (F-09 to F16)..... | 81 |
| Figure 3.11 | Profile of $(N_1)_{60}$ Index as a Function of Elevation..... | 85 |
| Figure 3.12 | Profile of ϕ' and γ_{sat} for the Site of Québec City | 86 |
| Figure 3.13 | Profiles of G_{max} and E'_{max} for the site of Quebec City | 87 |
| Figure 3.14 | Stratigraphy and Geotechnical Properties for the Site of Québec City | 88 |
| Figure 4.1 | Response spectra NBC 2010 - Site of Bécancour..... | 90 |
| Figure 4.2 | Distribution to a bimodal fashion and the contribution to the seismic hazard..... | 92 |
| Figure 5.1 | Summary of the Model for the Bécancour Pile | 108 |
| Figure 5.2 | Bending stiffness of the circular pile section..... | 109 |
| Figure 5.3 | Moment curvature of the circular pile section | 110 |
| Figure 5.4 | p - y Curves at Different Location along the Pile (depths are from the pile top) | 112 |
| Figure 5.5 | Bending Moment along the Pile | 113 |
| Figure 5.6 | Lateral Displacement of the Pile..... | 114 |
| Figure 5.7 | Shear along the Pile | 115 |
| Figure 5.8 | Effect the Superstructure Mass Variation versus Normalized Shear Measured from the Ground Surface Level..... | 116 |

| | | |
|-------------|--|-----|
| Figure 5.9 | Effect of the Superstructure Mass Variation versus Normalized Bending Moment Measured from the Ground Surface Level | 118 |
| Figure 5.10 | Effect of the Superstructure Mass Variation versus Normalized Deflection Measured from the Ground Surface Level..... | 119 |
| Figure 5.11 | Effect of the Superstructure Mass Variation versus Normalized Shear Measured from the Ground Surface Level..... | 120 |
| Figure 5.12 | Summary of Model for Québec City Pile | 123 |
| Figure 5.13 | p - y Curves at Different Location along the Pile | 125 |
| Figure 5.14 | Bending moment along the pile | 126 |
| Figure 5.15 | Shear along the pile..... | 127 |
| Figure 5.16 | Lateral displacement of the pile..... | 128 |
| Figure 5.17 | FLAC Model for the Bécancour Pile | 131 |
| Figure 5.18 | FLAC vs LPILE : Displacement, Shear and Moment for Series 1 for Bécancour Pile | 132 |
| Figure 5.19 | FLAC vs LPILE : Displacement, Shear and Moment for Series 2 for Bécancour Pile | 133 |
| Figure 5.20 | FLAC vs LPILE : Displacement, Shear and Moment for Series 3 for Bécancour Pile | 134 |
| Figure 5.21 | FLAC vs LPILE : Displacement, Shear and Moment for Series 1 for Bécancour Pile | 135 |
| Figure 6.1 | Full model of subsoil and structure, and source of the loading $P_e(t)$ (Truty, 2010)..... | 141 |
| Figure 6.2 | Typical soil-structure interaction problem components with DRM method (Truty, 2010): (a) Background Model (b) Reduced Model (c) viscous dampers at the side walls in the DRM model and (d) Boundaries in the DRM model | 143 |
| Figure 6.3 | Several soil models and Real soil behavior | 145 |
| Figure 6.4 | Idealization of soil behavior with Mohr-Coulomb Model..... | 145 |
| Figure 6.5 | DLT integration flowchart for p - y back calculations | 148 |

| | | |
|-------------|---|-----|
| Figure 6.6 | Back-calculated p-y curves for BECR1M2 | 149 |
| Figure 6.7 | Back-calculated p-y curves for BECR1M3 | 149 |
| Figure 6.8 | Back-calculated p-y curves for BECR1M4 | 150 |
| Figure 6.9 | Back-calculated p-y curves for QCR1M2..... | 150 |
| Figure 6.10 | Back-calculated p-y curves for QCR1M3..... | 151 |
| Figure 6.11 | Back-calculated p-y curves for QCR1M4..... | 151 |
| Figure 6.12 | Back-calculated p-y curves for QCR2M2..... | 152 |
| Figure 6.13 | Back-calculated p-y curves for QCR2M3..... | 152 |
| Figure 6.14 | Back-calculated p-y curves for QCR2M4..... | 153 |
| Figure 6.15 | P-M interaction curve for the pile section for applied axial loads..... | 154 |
| Figure 6.16 | Nonlinear EI vs bending moment for the pile section | 154 |
| Figure 6.17 | P-M interaction envelope..... | 155 |
| Figure 6.18 | Pile head deformation for varying values of I_b/I_c (Silva, 2008) | 161 |
| Figure 6.19 | BECR1 seismic scaled bending moment | 163 |
| Figure 6.20 | BECR1 static scaled bending moment..... | 164 |
| Figure 6.21 | BECR1 seismic scaled displacements | 165 |
| Figure 6.22 | BECR1 static scaled displacements..... | 166 |
| Figure 6.23 | BECR1 seismic and static scaled bending moment envelopes..... | 167 |
| Figure 6.24 | Seismic scaled bending moment envelopes of BECR1 and BECR2 | 168 |
| Figure 6.25 | BECR2 seismic scaled bending moment | 169 |
| Figure 6.26 | BECR2 static scaled bending moment..... | 170 |
| Figure 6.27 | BECR2 seismic displacements | 171 |
| Figure 6.28 | BECR2 static displacements | 172 |
| Figure 6.29 | BECR2 seismic and static scaled bending moment envelopes..... | 173 |

| | | |
|-------------|--|-----|
| Figure 6.30 | QCR1 seismic scaled bending moment | 174 |
| Figure 6.31 | QCR1 static scaled bending moment..... | 175 |
| Figure 6.32 | QCR1 seismic scaled displacements..... | 176 |
| Figure 6.33 | QCR1 static scaled displacements | 177 |
| Figure 6.34 | QCR1 seismic and static scaled bending moment envelopes | 178 |
| Figure 6.35 | Seismic scaled bending moment envelopes of QCR1 and QCR2 | 179 |
| Figure 6.36 | QCR2 seismic scaled bending moment | 180 |
| Figure 6.37 | QCR2 static scaled bending moment..... | 181 |
| Figure 6.38 | QCR2 seismic scaled displacements..... | 182 |
| Figure 6.39 | QCR2 static scaled displacements | 183 |
| Figure 6.40 | QCR2 seismic and static scaled bending moment envelopes | 184 |
| Figure 6.41 | Seismic vs static scaled displacements from the modified soil model of BECR1 | 187 |
| Figure 6.42 | Seismic vs static scaled bending moment from the modified soil model of BECR1 | 188 |
| Figure 6.43 | Seismic vs static scaled displacements from the modified soil model of BECR1 | 189 |
| Figure 6.44 | Seismic vs static scaled bending moment from the modified soil model of BECR2 | 190 |
| Figure 6.45 | Seismic vs static scaled displacements from the modified soil model of QCR1 | 191 |
| Figure 6.46 | Seismic vs static scaled bending moment from the modified soil model of QCR1 | 192 |
| Figure 6.47 | Seismic vs static scaled displacements from the modified soil model of QCR2 | 193 |
| Figure 6.48 | Seismic vs static scaled bending moment from the modified soil model of QCR2 | 194 |

LIST OF TABLES

| | Page |
|------------|--|
| Table 0.1 | Tabulated results from inelastic analysis of the Hanshin bridge response4 |
| Table 1.1 | Analytical soil-pile interaction models10 |
| Table 1.2 | The Discrete Load-Transfer (DLT) approach.....17 |
| Table 2.1 | Deflection Parameters of Clay <i>p-y</i> Curves as Affected by Pile Diameter48 |
| Table 3.1 | Summary of Tests and Borings Carried Out.....60 |
| Table 3.2 | SPT and Laboratory Test Results for Boreholes FG-19 and FG-2162 |
| Table 3.3 | Summary of Bedrock Characteristics for Bécancour Site65 |
| Table 3.4 | Friction Angle of Bécancour Clay68 |
| Table 3.5 | Summary of Boreholes Considered in this Study74 |
| Table 3.6 | Overall SPT and Laboratory Results (F-09 to F-11)77 |
| Table 3.7 | Overall SPT and Laboratory Results (F-12 to F-14)78 |
| Table 3.8 | Overall SPT and Laboratory Results (F-15 to F-16)79 |
| Table 3.9 | Water Table Depths for Boreholes F-09 to F-1679 |
| Table 3.10 | Summary of the RQD Values for Boreholes of Québec site84 |
| Table 3.11 | Range of Values for E_m of Bedrock.....85 |
| Table 4.1 | Seismic hazard and processing site class C to class A.....90 |
| Table 4.2 | Deaggregation of the seismic hazard – Site of Bécancour92 |
| Table 4.3 | Calculating the average shear wave velocity93 |
| Table 4.4 | Selected Earthquakes94 |
| Table 4.5 | Original signal - Saguenay (1998)96 |
| Table 4.6 | Original signal – Nahanni (1985)97 |

| | | |
|-----------|---|-----|
| Table 4.7 | Transformed signals - City of Bécancour | 98 |
| Table 4.8 | Transformed signals - City of Bécancour | 98 |
| Table 4.9 | Transformed signals - Quebec City | 101 |
| Table 5.1 | Steps of the uniform load method procedure according to CAN/CSA-S6-14..... | 105 |
| Table 5.2 | Analysis matrix and labeling of the pseudo-static analyses..... | 106 |
| Table 5.3 | Soil properties for the Pseudo-static analysis of pile for Bécancour | 107 |
| Table 5.4 | Calculation summary for Bécancour site..... | 111 |
| Table 5.5 | Summary of the Lateral Displacements along the Pile Compared to the Yielding Criteria of the Soil Obtained from the p - y Curves..... | 117 |
| Table 5.6 | Soil Properties for the Pseudo-Static Analysis of Pile for Québec City | 121 |
| Table 5.7 | Calculation Summary for Québec City Case | 124 |
| Table 5.8 | Summary of the Lateral Displacements along the First 10m of the Pile | 129 |
| Table 5.9 | Analysis Cases using FLAC | 130 |
| Table 6.1 | Analysis matrix table | 146 |

NOMENCLATURE

| | |
|--------------|--|
| $(N_1)_{60}$ | SPT N value corrected for field procedure |
| $[C]$ | Represents the damping matrix |
| $[m]$ | Represents the mass matrix |
| A | Zonal acceleration ratio |
| c | Constant depends on the I_b/I_c |
| C_B | Correction for the hole diameter |
| C_E | Correction factor related to the ratio of energy of the hammer |
| C_N | Factor to normalize the index at 1 atm |
| CPT_u | Cone penetration testing |
| C_R | Correction for length of tubing |
| C_S | Correction for the type of sampler used |
| C_{sm} | Elastic seismic response coefficient |
| C_u | Undrained shear strength |
| D | The embedment depth of the pile |
| d | The pile diameter |
| DS | Dynamic to static response ratio |
| DS | Dynamic to Static scaling factor |
| DS_M | Dynamic to static bending moment ratio |
| DS_y | Dynamic to static displacement ratio |
| dz | Tributary length for nodes of numerical pile |
| E_{beam} | Modulus of elasticity of pile material |
| EI_p | Flexure rigidity of pile section |
| E'_{max} | Effective soil modulus of elasticity |

| | |
|---------------------|---|
| E_p | Modulus of elasticity of pile material |
| E_{py-max} | Elastic modulus of p - y curve |
| E_{soil} | Modulus of elasticity of soil material |
| g | Acceleration due to gravity, m/sec ² |
| G_{max} | Shear modulus of soil |
| I | Importance factor based on the importance category |
| I_{beam} | Lateral deflection of the j^{th} pile in the group |
| I_{ij} | Elastic interaction factor of load at node j on node i |
| I_p | Second moment of area of pile section |
| k | Lateral stiffness of the system |
| K | Lateral stiffness of the bridge |
| L | Total length of the bridge |
| L | The distance between the superstructure and the point of fixity of the pile |
| m | Total number of piles in the group |
| $M_{Dyn-max}^{zi}$ | Maximum dynamic bending moment at depth z_i |
| $M_{Stat-max}^{zi}$ | Maximum static bending moment at depth z_i |
| n | Total number of pile nodes |
| N_{60} | SPT N value corrected for field procedure |
| N_m | In-situ index |
| OCR | Over consolidation ratio |
| p | The reaction of soil on the pile |
| P_l | The limit pressure from the pressuremeter test |
| P_a | Atmospheric pressure |
| P_{atm} | Atmospheric pressure |
| P_{dyn} | Dynamic soil reaction |
| P_e | Equivalent static load |
| P_i | Lateral load on the i^{th} pile in the group |

| | |
|-----------------|--|
| p_j | Lateral load acting on node j |
| P_{stat} | Static soil reaction |
| P_u | Ultimate soil reaction |
| P_{u_seism} | Ultimate seismic soil reaction |
| P_{u_static} | Ultimate static soil reaction |
| q_c | Uncorrected tip resistance |
| q_j | Lateral pressure acting over tributary length for node j |
| R_h | The ultimate horizontal resistance of the pile |
| S | Site coefficient specified |
| $SCPT_u$ | Seismic Cone penetration testing |
| S_u | Shear strength of soil |
| T | Fundamental period of the structure |
| T | Fundamental period of vibration |
| T | Fundamental period of the bridge |
| t_i | Time instance |
| u | Nodal displacement |
| u_i | Additional lateral displacement at node i from adjacent pile |
| u_i | Represents the structure displacements vector in the direction and its first and second derivatives respectively |
| V_s | Shear wave velocity |
| $V_{s,max}$ | Maximum static displacement of the bridge due to an arbitrary uniform lateral load |
| W | Effective weight of the bridge |
| W | The weight of the superstructure |
| x | The depth below the soil surface |
| y | The pile deflection |
| y_c | Cyclic displacement |
| y_{Dyn} | Dynamic displacement |

| | |
|----------------------|---|
| y_{stat} | Static displacement |
| $y_{dyn-max}^{zi}$ | Maximum dynamic displacement at depth z_i |
| $y_{Stat-max}^{zi}$ | Maximum static displacement at depth z_i |
| $\alpha\delta_{pjk}$ | Influence factor on the j^{th} pile from the k^{th} pile in the group |
| γ_{sat} | Saturated density of soil material |
| $\delta_{p=l}$ | Lateral deflection of a single pile due to lateral unit load application |
| ν_{soil} | Poisson reatio of soil material |
| σ'_m | Mean effective stress |
| ϕ' | Effective friction angle of soil |

ABBREVIATIONS

| | |
|--------|--|
| AASHTO | The American Association of State Highway and Transportation Officials |
| API | American Petroleum Institute |
| BNQ | Sols – Analyse granulométrique des sols inorganiques |
| CH | Fine grained soil -very strong |
| CID | Canadian Standards Association |
| CL | Fine grained soil -weak |
| CPT | Cone Penetration Test |
| CSA | Canadian Standards Association |
| DLT | Discrete Load-Transfer |
| DOF | Degree of Freedom |
| DRM | Domain Reduction Method |
| EW | East-West |
| FE | Finite Element |
| FEM | Finite Element Method |
| kPa | Killo Pascal |
| MC | Mohr-Coulomb |
| MDOF | Multi degrees of freedom |
| MPa | Mega Pascal |
| MRNF | Ministère des Ressources Naturelles et de la Faune du Québec |
| MTQ | Ministry of Transport of Quebec |
| N-D | Non-Drained |
| NS | North-South |
| OCR | The over consolidation ratio |
| PI | Plasticity Index |
| PRA | Peak rock acceleration |
| PSPI | Pile-Soil-Pile Interaction |
| RQD | Rock Quality Designation |
| SBT | Standard Penetration Test |
| SDOF | Single-degree-of-freedom |
| SPI | Soil-Pile Interaction |
| SPT | Standard Penetration Test |
| SSI | Soil-Structure Interaction |
| SSPSI | Seismic Soil-Structure-Pile Interaction |
| VBA | Visual Basic for Applications |

INTRODUCTION

0.1 Introduction

Soil-structure interaction (SSI) has a direct effect on the performance and integrity of structures subjected to earthquakes. Accounting for this effect is crucial for the design of important structures such as skyscrapers, nuclear reactor facilities and long bridges. During an earthquake, changes occur in the mechanical properties of the soil supporting the foundation. Degradation in the strength of the soil is typically observed during an intense seismic event which makes loss of soil lateral support a possible scenario. In this case different soil models have to be considered in the foundation design. The current common practice for designing deep foundations under lateral load is to implement the p-y curve method. These curves were initially driven from full scale test with either static or slow cyclic load application. Many analytical, experimental and continuum finite element (FE) models were also developed and practically applied in the design of complex structures. These models vary in their complexity and applicability to analysis and design procedures. However, with the advances in computations and programming, many unconventional models are gaining in popularity and are more readily applicable in design.

Commonly, bridge designers follow typical procedure in the design where the assumption of fixed substructure at the pile cap level applies. The reactions at the pile cap level from different loads are then transmitted to the geotechnical engineer in order to size and design the foundation for the extreme case. This procedure includes discontinuity and inaccuracy in estimating the correct reactions at the pile head. The discontinuity resource comes from the fact that there are two separate structural models, one for the bridge and another for the pile. This procedure is not accurate because it assumes that the foundation is fixed at the pile head elevation where in reality the fixity occurs at deeper levels as we will see in Chapter 5 and 6. However, it might be suitable for the preliminary design stages.

Therefore, a more global modeling approach that considers the pile-bridge system is required for the final design. In order to accomplish this modeling procedure, the supporting soil surrounding the piles has also to be considered. The selection of the appropriate soil modeling procedure is related to the degree of importance of the structure and the available resources. A review of the evolution of the different methods and models developed in order to simulate the SSI effects with focus on the SSI for deep foundations of bridges under seismic loading.

0.2 Performance of deep foundation of bridges during seismic events

Piles are commonly used to support bridge structures. The global performance of the bridge during an earthquake is related directly to the type of foundation and its interaction with the supporting soil. It is also related to other parameters such as the impediment of the foundation, the weight of the superstructure and the nature of the seismic record. For deep foundations, the length of the pile plays an important role in the overall response of the structure to lateral load. In general, long piles in weak soil are more flexible and results in higher fundamental period and lower seismic demands on the foundations, whereas for structures with stubby shafts it is the opposite. The impact of these factors will be investigated and evaluated in this study with particular emphasis on piles founded in Quebec soil.

0.3 Effects of SSI on the dynamic response of bridge structures

In a recent technical seminar conducted at the University of British Colombia (Finn 2010) about modeling soil-structure interaction in the analysis of buildings and bridges, the effect of incorporating SSI in the design of structures was presented. The following general beneficial effects of including the SSI in design emerged:

1. Increase in the fundamental period of the system,
2. Decrease in the value of design base shear,

3. Increase in the damping of the soil-structure system by adding hysteretic soil and radiation damping,
4. Large foundation slabs can reduce the high frequency free field motions significantly and hence reduce the input motions to the structure, i.e., reduction of seismic demand on the structures depending on period,

However, these effects are problem-dependent and can vary based on the following factors:

- (i) Type of the structure, i.e., material, geometry, etc.,
- (ii) Type and geometry of the foundation system,
- (iii) Site properties, i.e., soil stratigraphy, geotechnical properties, water table, etc.,
- (iv) Seismic record characteristics.

Ventura (2010) reported that considering the SSI in design would lead to an increase in the seismic demand and the ductility demand of the system (beneficial effect), whereas in another study which examined the role of soil on the collapse of 18 piers of the Hanshin expressway in the Kobe earthquake using three different seismic records, two effects were found to exist as can be seen in Table 0.1.

As can be seen in this table, considering the SSI effects in the analysis can either be beneficial or detrimental to design. Therefore, the accuracy in evaluating the dynamic characteristics of the system might be effected by eliminating the SSI from the analysis which might lead to unconservative design (Gazetas and Mylonakis 1998, Meymand 1998, Wolf and Song 2002). This effect will be investigated throughout the chapters of this study.

Table 0.1 Tabulated results from inelastic analysis of the Hanshin bridge response after Mylonakis (2006)

| Excitation | Analysis type | Effective natural period (s) | Peak deck acceleration (g) | Peak deck displacement (cm) | Peak drift displacement (cm) | R | System ductility μ_s | Column ductility μ_c | Role of SSI |
|-----------------|---------------|------------------------------|----------------------------|-----------------------------|------------------------------|------|--------------------------|--------------------------|--------------------|
| JMA | Fixed base | 0.65 | 0.87 | 21.0 | 21.0 | 2.67 | 2.86 | 2.86 | <i>beneficial</i> |
| | Flexible base | 0.93 | 0.89 | 21.0 | 19.0 | 2.13 | 1.93 | 2.58 | |
| Fukiai | Fixed base | 0.65 | 0.80 | 14.6 | 14.6 | 1.95 | 1.99 | 1.99 | <i>detrimental</i> |
| | Flexible base | 0.93 | 1.02 | 41.9 | 31.2 | 2.56 | 2.79 | 4.24 | |
| Takatori | Fixed base | 0.65 | 0.74 | 10.0 | 10.0 | 1.36 | 1.34 | 1.34 | <i>detrimental</i> |
| | Flexible base | 0.93 | 0.79 | 24.4 | 13.4 | 1.67 | 1.62 | 1.83 | |

0.4 Objectives

The main objective of this study is to investigate the effect of earthquake on the soil-structure interaction for deep foundations founded in Quebec soil.

Specific objectives are set as follows:

1. Carry out comprehensive nonlinear seismic analyses on soil-pile interaction for Quebec soils.
2. Define the effects of the dynamic seismic load on current models of p - y curves which were derived from static or slow cyclic lateral load application.
3. Develop a simplified methodology to evaluate the effect of an earthquake on the commonly used static p - y curves in order to accurately account for the strength loss in soil from earthquake in the design of deep foundation for bridge structures.

0.5 Research significance

This research introduces a new methodology for performing nonlinear seismic analysis for deep foundation. It involves the development of many data analyses VBA scripts that can process millions of lines of data results from seismic analysis and transform it to useful engineering information. These procedures can also be used for future work on other soil or pile cases. Another set of procedures were developed in Matlab to extract p - y curves from hysteretic p - y loop that is obtained from numerical or experimental analysis. It also proposed a simplified procedure for applying the currently used p - y curves for the seismic design of piles by factoring the static curves to match the dynamic response of the pile under seismic load.

0.6 Organization of the dissertation

This document consists of five chapters in addition to the introduction chapter. The first chapter reviews the state of the art of the soil-structure interaction and the progress of research in this field. Chapter two discusses the effect of several elements on the soil-structure interaction problem. Chapter three describes the soil characteristics of the selected sites. Chapter four presents the results of a preliminary study based on an equivalent static load procedure. Chapter five presents the results from dynamic analysis and proposes a simplified procedure to reduce the p - y curves to obtain equivalent seismic p - y curves for daily practice engineering. Finally, a set of representative data that includes hysteretic p - y loops and results envelopes with time and depth for the bending moment and pile displacement from nonlinear time history analysis is presented in Appendix I for selected cases.

CHAPTER 1

LITERATURE REVIEW

This chapter presents a review of the developments of major methods for solving the SSI problem for deep foundation with focus on the application of seismically loaded bridges. These models are mainly based on the four following theories: (i) Beam-on-Elastic Foundation (subgrade reaction method); (ii) Beam-on-Winkler Foundation (so-called “p-y” method); (iii) Continuum Models; and (iv) Finite Element Method.

1.1 Introduction

The study of the interaction between the soil and the structure phenomenon has been an active area of research for decades. The nature of the SSI problem has a mutual soil-structure effect. In other words the existence of soil affects the structure response to external loads and vice versa. This has been driving the attention of many researchers for very long time. It started in the 19th century when Winkler developed his first model for foundation on linearly elastic homogeneous strata of soil. However, it was not until the late 1960s when the construction of nuclear plant started on large scale and concerns were raised about the safety of these structures during earthquakes. More importantly the numerous research studies accompanied these projects made it possible to develop new numerical and computational methods for solving challenging analytical models of SSI problems. Add to that the advances in computers which helped in solving complex problems within relatively small time. Since then, many models and techniques were developed to tackle very complex SSI problems over the last forty years. SSI models range in their complexity from simplified practical models to sophisticated impractical ones. Nevertheless, the selection of the appropriate model is problem-dependent. In other words, one cannot claim that a uniform global model is valid for all SSI problems that cover a wide range of soils and structures types.

The problem conditions and parameters play an important role in selecting the appropriate, accurate and inexpensive SSI model and solution approach. Having said that, one can say that some models and methods are much more desirable in the daily practice than other methods due to their simplicity and practicality. Therefore, many of these methods are recommended by codes and design standards.

In this study, the focus will be on the deep foundation for bridges under seismic load. The related methods and models are reviewed and presented hereafter.

1.2 Models of Soil-pile interaction under seismic loading

Different models and solution procedures were developed during the past four decades in order to simulate and capture the performance of piled structures during earthquake taking into consideration the SSI effects. Models were developed initially for single pile in soil problem, later on the group effect on the pile performance was considered. SSI models can be classified into simple and complex models. The simple models are easy to apply, fast to solve and suitable for daily practice but they might result in conservative design which is desirable in many cases. The sophisticated models requires very skilled engineer to apply, consume time to model and to solve. Therefore they can be expensive and not required in many projects. Nevertheless, these models result in very accurate and realistic outcomes which are required for the design of sensitive and important structures. One can also categorize the SSI models basically based on their deriving approach into analytical models and experimental models.

Nevertheless, as will be seen later, a combined approach is often required for achieving the final solution. This combination allows for enhancement of one model, derived from an analytical approach for example, by calibrating its solution to match the solution from another method such as the experimental model. Many commonly-used models, such as the well-known p - y curves method, are initially analytical-based solutions that were calibrated with experimental results.

In the following sections an objective review of these models is presented. The reader is referred to the original source of each method for a complete explanation on the solution methodology and procedure.

1.3 Analytical models

The need of developing analytical models of soil-pile interaction (SPI) problem was objectively motivated and accelerated by the numerous projects of offshore oil platforms and nuclear power plants in the late sixties. In the last fifteen years, the SPI become an interesting subject for the design of tall buildings and long bridges too. Having said so, several analytical models were developed to tackle this problem. These models are mainly based on four theories that were developed and evaluated chronologically as follows:

- (i) Beam-on-Elastic Foundation (subgrade reaction method),
- (ii) Beam-on-Winkler Foundation (so-called “ p - y ” method),
- (iii) Continuum,
- (iv) Finite Element Method.

A brief description of each one of these theories and methods as well as summary of features and applications is presented in Table 1.1.

Table 1.1 Analytical soil-pile interaction models

| Analytical model | Theory | Features | | Applications |
|---|---|--|---|---|
| | | Pros | cons | |
| Beam-on-Elastic Foundation Models (Hetényi, 1946) (subgrade reaction method) | The governing equation; $(EI)_{pile} \frac{d^4 y}{dx^4} = p$ Where: $p = -E_{soil} y$ | <ul style="list-style-type: none"> – Simplified approximate solution. | <ul style="list-style-type: none"> – Analytical solutions are not available for arbitrary distributions of soil or pile stiffness; – Solution depends on the appropriate selection of subgrade reaction; – It is recognized that this method is physically and theoretically limited. | <ul style="list-style-type: none"> – Static lateral loading; – Pile head stiffness estimation for the superstructure analysis. |
| Beam-on-Winkler Foundation Models (p-y method) – see Figure 1.3 | Based on the Winkler's foundation assumption (Winkler, 1876) that each layer of soil responds independently to adjacent layers. | <ul style="list-style-type: none"> – Developed analytically for static loading then extended to cyclic loading conditions; – Calibrated with large scale tests; – Pile is modeled by a beam lays on discrete spring system (linear or nonlinear); and – Widely accepted. | <ul style="list-style-type: none"> – Ignores the shear transfer between layers of soil – Two-dimensional simplification of the soil-pile contact, which ignores the radial and three dimensional components of interaction. | <ul style="list-style-type: none"> – Static, cyclic or dynamic lateral load problems; – Routinely applied to dynamic or earthquake loading cases. |
| Continuum Models | Soil is dealt with as continuum viscous medium (elastic or plastic) and pile is embedded in it. | <ul style="list-style-type: none"> – Purely theoretically-based approach comparing to the p-y method; – 2D or 3D modeling capabilities; – Finite element or finite difference discretization can be employed to obtain the solution. | <ul style="list-style-type: none"> – Localized yielding at the soil-pile interface is not adequately characterized in the elastic solution. | <ul style="list-style-type: none"> – Dynamic soil-pile analysis; – Better suited to relatively low levels of seismic loading |
| Finite Elements Models | Finite elements | <ul style="list-style-type: none"> – Suitable for big and complex structures; – Discretization can be in spatial, time or properties domains; and – Computer packages are available. | <ul style="list-style-type: none"> – Not suitable for routine design and require specialized users; – Results reliability is based on the selection and calibration of an appropriate soil constitutive model.; and – Expensive solution– in terms of the time, effort and experience required to build the model. | Static or dynamic soil-pile problems. |

1.4 Beam-on-Elastic Foundation Models (subgrade reaction method)

Laterally loaded single pile is a typical SSI problem in which both pile and soil strengths properties contribute to the pile response. Therefore, it is very important to appreciate this correlation when evaluating performance. This fundamental rule of considering the combined properties of both the soil and pile is epitomized in the classical beam-on-elastic-foundation problem (Dodds, 2007a) – see Figure 1.1.

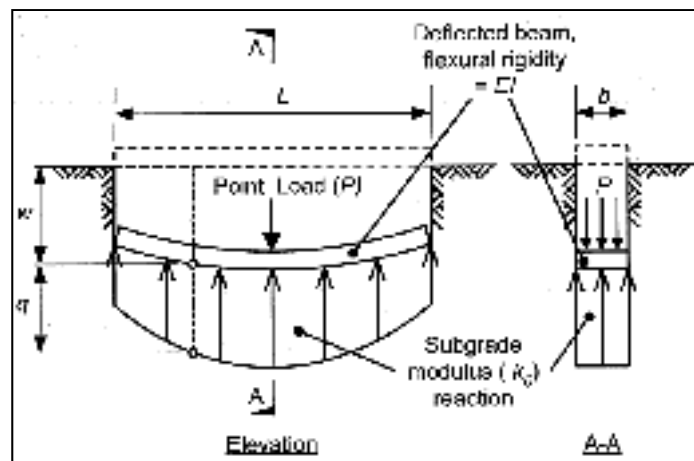


Figure 1.1 Beam-on-elastic-foundation problem after Dodds (2007a)

The evolution of this approach will be presented in a chronological form as follows:

Hetényi (1946) introduced the subgrade reaction method in the form of Equations (1.1) and (1.2):

$$EI \frac{d^4 y}{dx^4} = p \quad (1.1)$$

$$p = -E_s y \quad (1.2)$$

Where:

- EI is the elastic flexure modulus of the pile;
- y is the pile deflection;
- x is the depth below the soil surface;

E_s is the subgrade reaction modulus; and
 p is the reaction of soil on the pile.

Terzaghi (1955) indicated that readily obtainable solutions were possible, but the selection of an appropriate subgrade modulus presented a real problem, emphasizing the basic limitations involved with subgrade reaction theory, and the difficulty of obtaining an appropriate value for the subgrade modulus.

Rowe (1956) examined the effect of the two options, flexible or rigid piles in sand under lateral load. He founded that back-calculated subgrade reactions differ significantly based on the selected assumption.

McClelland and Focht (1958) observed that the subgrade modulus is not an exclusive property of the soil, but simply a convenient mathematical parameter that expresses the ratio of soil reaction to pile deflection. They introduced an analysis procedure for correlating triaxial stress strain data to a pile load-deflection curve at discrete depths, estimating the modulus of subgrade reaction at each layer.

Matlock and Reese (1960) generalized iterative solution method that considered two forms of varying modulus with depth applied to rigid and flexible laterally loaded piles embedded in soil.

Davisson and Gill (1963) introduced constant modulus of subgrade reaction in each soil layer. They concluded that the near surface modulus was the controlling factor for the pile response laterally loaded pile embedded in a layered soil system.

Broms (1964a; 1964b) introduced a new design method applying the limit equilibrium approach. He established a method for analysis and design of lateral pile response depending on Terzaghi's (1955) values for modulus of subgrade reaction. For undrained conditions in cohesive soil, he proposed the use of constant subgrade modulus accompanied with the value of $9S_u$ for the ultimate lateral soil resistance. For drained conditions, he used a linearly variable subgrade modulus that increases with depth. To estimate the ultimate lateral resistance a Rankine earth pressure-based method was used with a value equal to $3K_p D_p \sigma'_v$ for cohesive and cohesionless soils. He defined two failure modes for the pile under lateral load as presented in Figure 1.2. The controlling failure mode depends on the pile length. For

long piles it takes the shape of plastic hinging where for stubby piles it takes the form of mobilization of ultimate lateral resistance. These failure modes recognized the relative importance of either pile or soil strength in governing the ultimate capacity of long or short piles, respectively.

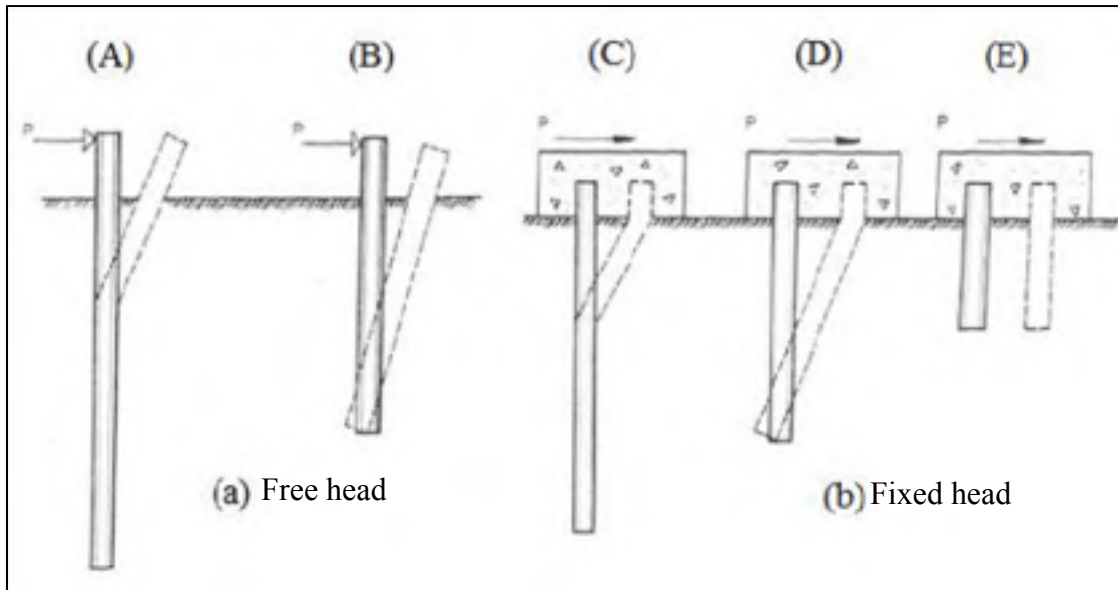


Figure 1.2 Failure modes proposed for short and long pile for free and fixed head conditions
Taken from Broms (1964a), (1964b)

Jamilokowski and Garassino (1977) discussed soil modulus and ultimate soil resistance laterally loaded piles. They acknowledged the limitation of this method in their review of soil moduli for laterally loaded piles, highlighting the important observation made earlier by McClelland and Focht (1958).

Randolph and Houlsby (1984) studied the lower and upper bound values of the limiting pressure classical plasticity theory applied to undrained laterally loaded pile that ranged from approximately 9 to 12 S_u as a function of pile roughness.

Reese (1986) discussed the dependence of lateral behavior on pile length, noting that short piles can deflect a large amount at the groundline given movement of the pile tip, but with

increasing depth of penetration the soil resistance at the pile tip increases until a point is reached at which groundline deflection reaches a limiting value.

Hansbro (1995) revisited Broms' computation of drained ultimate lateral resistance based on results of centrifuge tests conducted by Barton (1982). He suggested that a drained ultimate lateral resistance of $K_p^2 D_p \sigma'_v$ is more appropriate for cohesionless soils.

Kulhawy and Chen (1995) applied Broms' concepts to drilled shafts, recognizing the components of resistance to lateral loading unique to drilled shafts, and noted the importance of conducting appropriate laboratory tests laterally loaded pile and drilled shaft analysis.

1.5 Beam-on-Winkler Foundation Models (“p-y” method)

Idealizing the soil foundation based on the Winkler (1876) foundation assumption, that consists of a bed of infinitely closely spaced, independent springs each possessing a linear vertical pressure per unit area versus vertical deflection (Dodds, 2007a), a beam on discrete spring system may be adopted to model pile lateral loading– see Figure 1.3. Although this assumption ignores the shear transfer between layers of soil, it has proven to be a popular and effective method for static and dynamic lateral pile response analyses (Meymand, 1998). This assumption was validated with Föppl's classical experiment (Föppl, 1922) for a large variety of soils (Hetényi, 1946).

This model was developed based on instrumented full-scale field tests, soil testing, and numerical and analytical studies. Introducing prominently are what may be termed “conventional” p - y curve formulations that have essentially developed the McClelland and Focht (1958) idea to a stage fit for practice. In their original work, McClelland and Focht (1958) formalized the procedure to obtain p and y based on the Discrete Load-Transfer (DLT) approach. This fundamental method is illustrated in the flowchart depicted in Figure 0.5.

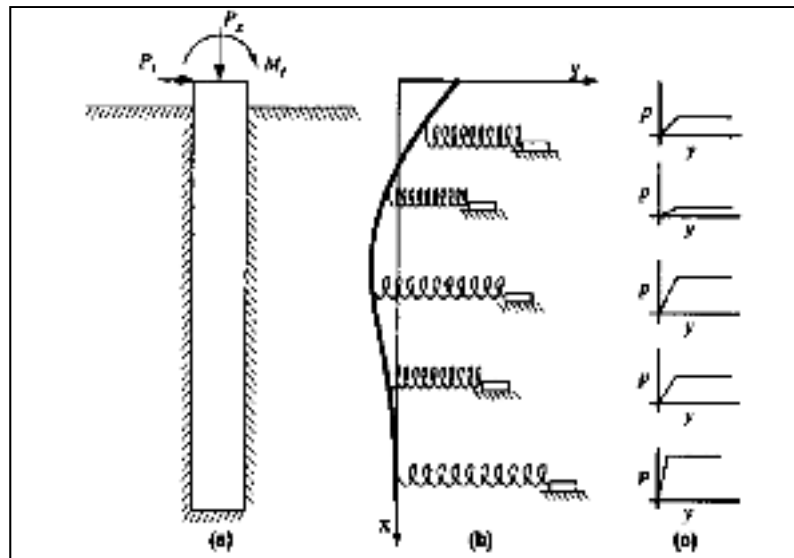


Figure 1.3 Model of laterally loaded pile: (a) Elevation view;
(b) As elastic line; (c) p - y curves (Reese, 1997)

The DLT approach depends on the beam theory to obtain the soil-pile response to a lateral load. The moment diagrams along the pile derived from the strain gauges data at successive stages during a full-scale pile test are twice differentiated and twice integrated, respectively, to obtain several response quantities such as the displacements (y), the slope (θ), the shear (V), and the loading (p) as illustrated in Table 1.2.

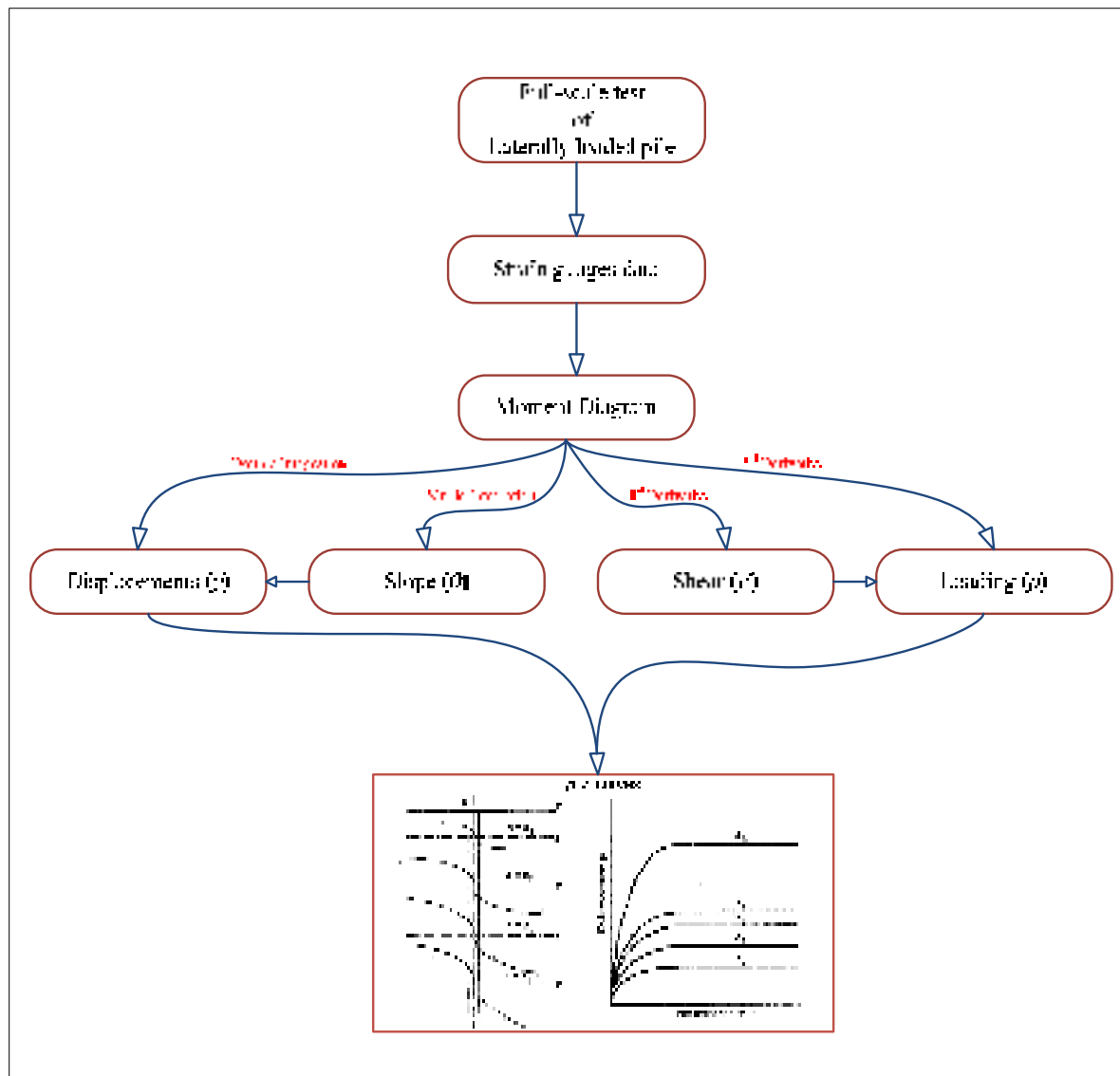


Figure 1.4 Discrete Load-Transfer (DLT) approach to obtain p - y curves

Table 1.2 The Discrete Load-Transfer (DLT) approach
after Dodds (2007a)

| Displacement | Slope | Moment | Shear | Loading |
|--------------|----------------------|------------------------------|------------------------------|------------------------------|
| y | $\int \frac{dy}{dz}$ | $E_p I_p \frac{d^2 y}{dz^2}$ | $E_p I_p \frac{d^3 y}{dz^3}$ | $E_p I_p \frac{d^4 y}{dz^4}$ |

The popular p - y routine is an effective method for static and dynamic lateral pile response analyses. General frameworks that have helped to rationalize and improve the understanding of lateral pile-soil interaction were built (Dodds, 2007a). One of the main disadvantages in this method is ignoring the radial and three dimensional components of interaction. Reliability studies of springs used in analysis of seismic soil-pile interaction conducted using nonlinear springs such as those recommended by API (1993) drew attention to the so called “limitations in the ability to predict single pile-soil-pile interaction” (Finn, 2010). These limitations rise from the fact that p - y springs were developed for static and slow cyclic loading – not seismic loading which strains credibility further. However, many improvements and amendments on the original principles of p - y curves have been established, featuring phenomena such as soil-pile gapping, cyclic degradation of soil strength, and strain rate dependency. The chronological evolution of p - y method is presented as follows;

Winkler’s foundation assumption (1876): Each layer of soil foundation responds independently to adjacent layers. The pile is modeled as a beam and discrete spring system. This principle ignores the shear transfer between adjacent soil layers

McClelland and Focht (1958) are the originators of the p - y method of laterally loaded pile. They introduced an analysis procedure for correlating triaxial stress strain data to a pile load-deflection curve at discrete depths. They formalized the procedure to obtain p and y based on the DLT approach.

Matlock (1962) conducted static and cyclic field and laboratory tests of laterally loaded piles in soft clay describing the p - y concept as the relationship that relates the soil resistance “ p ” arising from the nonuniform stress field surrounding the pile mobilized in response to a lateral soil displacement “ y ”.

Penzien et al. (1964) presented a method for seismic pile response analysis. A MDOF discrete parameter system for modeling the soil medium response initiated by seismic base excitation of bridge structures supported on long piles driven through soft clays.

Matlock (1970) proposed p - y curves for static and cyclic loading of piles in soft clay in the form of the following equation:

$$p = 0.5p_u \left(y/y_c \right)^{0.33} \quad (1.3)$$

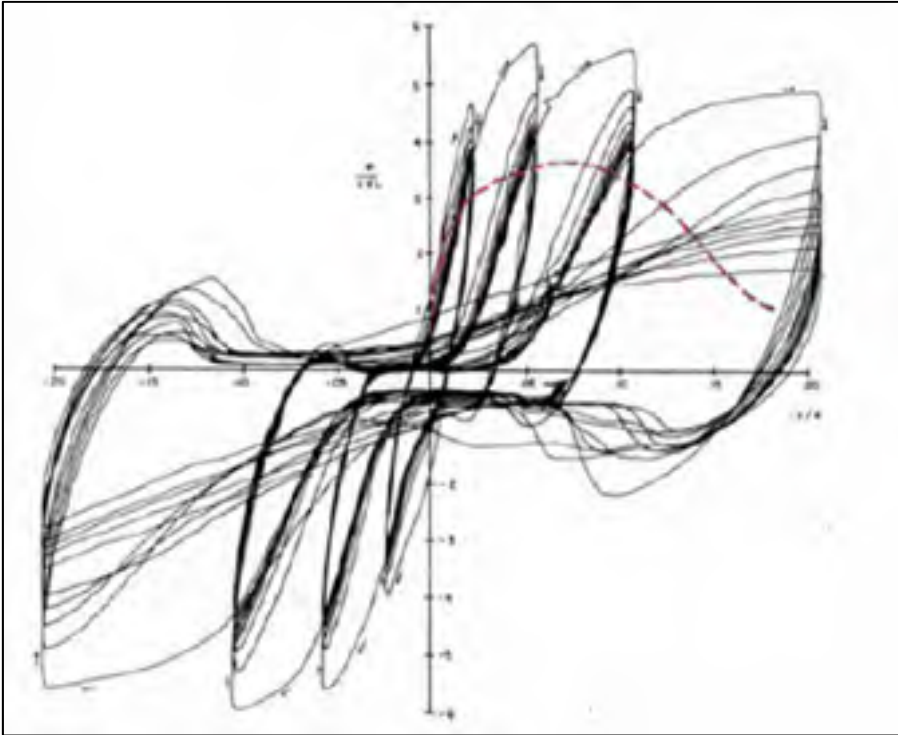


Figure 1.5 p - y curves extracted from cyclic load experiment
Taken from Matlock (1970)

Parker and Reese (1970) introduced continuous hyperbolic tangent curve that proved to be the most accurate for both static and cyclic loading, and relatively easy to implement. The curve has the form of the following equation;

$$p = \eta A p_u \tanh \left[\left(k_z / A p_u \right)^y \right] \quad (1.4)$$

Reese et al. (1974) performed static and cyclic lateral load test from which API method for constructing p - y curves in sand was extracted. Later, he introduced a segmented p - y curve.

Reese et al. (1975) conducted lateral pile load tests in an over consolidated strain-softening stiff clay deposit. This work presented the characteristic static and cyclic-loading p - y curves currently recommended by API as design curves.

Reese (1977) introduced COM624, a free analytical tools provides highly efficient platforms for p - y analysis of static or cyclic laterally loaded piles in layered soils.

Matlock and Foo (1978) innovated SPASM8, a beam-on-dynamic-Winkler-foundation analysis program with discrete elements. The linear elastic pile was linked to a fully nonlinear hysteretic degrading soil support model with gapping capability.

Lee et al. (1978) introduced the effective stress site response code DESRA II for soil liquefaction analysis.

Stevens and Audibert (1979) amended existing p - y curve formulations and correlated to the pile diameter. The derived expression prorates the pile deflection to the square root of pile diameter.

Bea and Audibert (1979) studied loading rate and load cycling effects on axial and lateral dynamic pile response.

Bogard and Matlock (1980) suggested a modification to the current p - y curves.

Matlock and Foo (1980) described the computer code DRIVE 7, a model for axial loading of piles with similar features as SPASM8. The software is capable of conducting static, cyclic, or dynamic loading analysis, including pile driving simulation.

Kagawa and Kraft (1980) presented a nonlinear dynamic Winkler model using the equivalent linear method. Soil spring stiffness values were determined from the hysteretic backbone curve as shown in Figure 1.6.

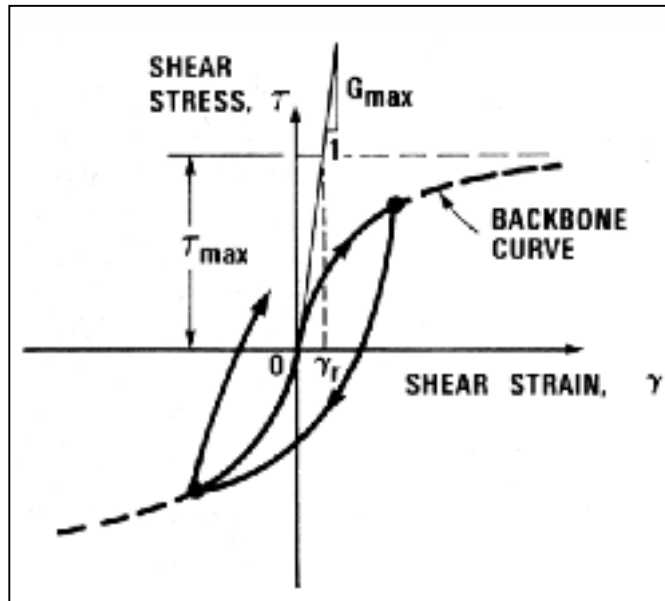


Figure 1.6 Hysteretic backbone curve
after Kagawa (1980)

Kagawa and Kraft (1981) reformulated the nonlinear soil model as an effective stress model, where cyclic degradation of soil resistance was governed by pore pressure generation.

McClelland Engineers (1983) introduced the computer code NONSPS that implemented the Kagawa and Kraft (1981) model.

Matlock et al. (1981) presented a method for simulating soil-pile response in liquefiable cohesionless soils during earthquake shaking using the results of the computer code DESRA II (Lee, 1978) as input to the SPASM 8 model. The degradation of the p - y backbone curve carried out in proportion to the excess pore pressure generation calculated by DESRA II.

O'Neill and Murchison (1983) carried out a systematic evaluation of p - y relationships in sands and compared the predictive accuracy of four methods including the segmented curve of Reese et al. (1974) against a set of pile load test data.

Scott (1979) proposed a bilinear representation by and a continuous hyperbolic tangent curve described by Parker and Reese (1970).

Bogard and Matlock (1980) a modification suggested.

O'Neill and Gaziglu (1984) investigated p - y relationships in cohesive soils and attempted to develop a unified method for both soft and stiff clay. The method has not been widely adopted.

Reese(1984) established criterion for laterally loaded pile analysis in soft clays in the commonly used computer program COM624P.

Carter (1984) proposed a nonlinear soil-pile interaction model.

Nogami (1985) and Nogami and Konagi (1988b) described the transfer matrix approach that was used to solve the equations of motion for a pile subject to soil-pile interaction forces, and functions of the near field and far field soil element properties.

Bea (1988) introduced the analytical model PAR, a three-dimensional, time domain, nonlinear, discrete element method for computing single pile dynamic response. PAR is a hybrid model that performs site response analysis in the far field soil finite elements, and models soil-pile interaction with near field springs and dashpots. Pile group effects are not impeded in the model.

Nogami et al. (1988a) developed hybrid near field/far field soil-pile interaction models for dynamic loading.

Reese and Wang (1989) introduced LPILE, a commercial analytical tool that provides highly efficient platforms for p - y analysis static cyclic laterally loaded piles in layered soils.

Nogami et al. (1991) and (1992) formulated solutions for single pile and pile group axial and lateral response in both the time and frequency domains, incorporating nonlinear soil-pile response, degradation, gapping, slip, radiation damping, and loading rate effects. They also provided a detailed comparison of the features and performance of Matlock's, Novak's, and Nogami's Winkler foundation models for lateral pile response. Nogami's far field element consisted of three Kelvin-Voigt parallel spring-dashpot pairs designed to simulate an infinite elastic plane strain medium, and a shear element in series to simulate interaction of adjacent soil layers. Gapping was provided by an elasto-plastic interface element. His model can be

used to compute pile head impedance functions, or input excitations can be directly applied to the discrete end nodes of the model.

API (1993) codified Matlock's (1970) method in the API Recommended Practice.

Chacko (1993) examined the computer code NONSPS in recent model simulation studies conducted at U.C. Davis and found it to have only fair performance.

Makris (1994) has presented an analytical solution for pile kinematic response due to the passage of Rayleigh waves, applicable to near field earthquake response earthquake

Makris and Badoni (1995a) introduced a so-called macroscopic model based on the Bouc-Wen model of visco-plasticity. They used distributed nonlinear springs to approximate the soil-pile reaction. Radiation damping was provided by a frequency dependent viscous dashpot that attenuated at large pile deflections. The model required that two parameters be fit by experimental data.

Liu and Dobry (1995) introduced a promising approach for modeling p - y curves for liquefied soils was. In a centrifuge, they first subjected loose sand to seismic shaking to generate pore pressures. Then they immediately performed a cyclic lateral load pile test before the pore pressures could dissipate. The p - y curves developed from such load tests were compared with static p - y curves for un-liquefiable sands to develop scaling factors for various pore pressure ratios as shown in Figure 1.7.

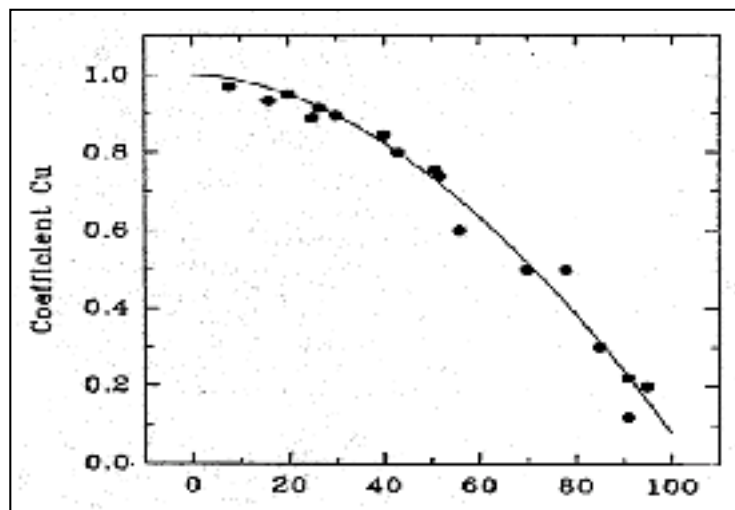


Figure 1.7 Degradation coefficient vs. Pore pressure ratio (Liu, 1995)

Pender and Pranjoto (1996) updated Carter (1984) model to include the effects of gapping. Compression-only springs were attached to both sides of the pile, preloaded to reflect the effects of pile installation, and provided with the ability to detach and form a gap when the spring force reached zero. A hyperbolic form of the nonlinear spring stiffness was adopted, defined by initial stiffness and ultimate resistance parameters. The model demonstrated very well progressive gapping with depth and with the number of load cycles, and the consequent reduction in pile head lateral stiffness. The authors acknowledged the need to extend the model to dynamic loading.

Lok (1999) develop fully-coupled analyses wherein both soil and soil-pile superstructure response can be simultaneously evaluated.

Boulanger et al.(2004) through a series of centrifuge test on pile in soil, described the observed p - y response as “deformation hardening” especially when past displacement values were exceeded. The study accredited this phenomenon to dilative response of the soil under nearly undrained loading conditions.

Brandenberg et al.(2005) studied the behavior of single piles and pile groups in liquefiable and laterally spreading ground. He performed eight dynamic model tests on 9 m radius centrifuge. The results of this study showed that the peak lateral loads were predicted well by Matlock’s (1970) “static” p - y curves, whereas his “cyclic loading” p - y curves were very unconservative. The peak loading produced by down slope spreading of the clay crust is more closely approximated by a static monotonic loading mechanism than by the displacement-controlled cyclic loading used in Matlock’s studies.

Liang, R. Y. (2007) recognized the need to a new p - y criterion developed specifically for cohesive intermediate geomaterials. He proposed new hyperbolic p - y criterion for cohesive soil and intermediate geomaterials based on 3-D FEM simulation results and verified by using the results of six full-scale lateral load tests on fully instrumented drilled shafts with diameters ranging from 0.76 m to 1.83 m in the geo-medium ranging from soft clays to intermediate geomaterials.

1.6 Continuum Models

As mentioned earlier, the Winkler Foundation method suffer two major drawbacks: (i) the independence behavior among Winkler foundation adjacent springs – and hence ignoring the shear transfer between soil layers; and (ii) the limitations in simulating the radial and three dimensional components of soil-pile interaction. This bounds the application of Winkler Foundation method to the problem whereby disregarding these two components does not influence the analysis significantly. However, real soil is inherently a particulate material and thus derives its resistance through innumerable load paths that can generally be considered in a continuous, interactive sense (Dodds, 2007a).

Consequently, continuum elastic and plastic models were widely applied to the geotechnical problems including the seismic soil-pile interaction problem. This field is still being investigated and needs further research, yet the undertaken work to this point has pushed the general understanding of seismic soil-pile interaction to new limits. Prominently, it provides an appropriate basis for consideration of more sophisticated problem such as the pile-soil-pile interaction effects which dominates the general seismic pile group performance.

Continuum approaches, as defined here, comprise an assortment of solution techniques utilizing either the theory of elasticity alone or both the theory of elasticity and plasticity (Dodds, 2007a). Models including fully coupled or uncoupled three dimensional analyses and simplifications using two-dimensional analyses (plane strain or plane stress) were developed in the last century. The recent computing and simulating advances opened the opportunity for very complicated models to be realistically examined. The development of this approach is presented in chronological order in the following section.

Mindlin's (1936) presented his closed form solution for the application of point loads to a semi-infinite mass. The accuracy of the solution depends on the Young's modulus evaluation. This model can be applied for small strain and steady state vibration problems. Layered soil profiles cannot be accommodated and only solutions for constant, linearly increasing, and parabolically increasing soil modulus with depth have been derived.

Tajimi (1966) described a dynamic soil-pile interaction solution based on elastic continuum theory. He used a linear Kelvin-Voigt visco-elastic stratum to model the soil and ignored the vertical components of dynamic response.

Poulos (1971a; 1971b) presented elastic continuum solutions for laterally loaded single piles and groups under static loading.

Novak (1974) adopted a plane strain, complex transmitting boundary adjacent to the pile for solution of pile stiffness and damping coefficients. The plane strain condition is equivalent to incorporating the Winkler assumption into the continuum model, and formed the basis for his future work. The solution was applied to pile dynamics problem.

Nogami and Novak (1976) formulated more rigorous solutions for axial and lateral pile response, respectively, in a linear visco-elastic medium in a similar way as in Tajimi (1966).

Novak (1977) studied the axial response of floating piles; specifically, the particular sensitivity of response to the pile tip condition, i.e. end-bearing or floating.

Novak and Aboul-Ella (1978) improved the previous model of Novak (1977) by considering layered soil media, imperfect fixity of the pile tip, and material damping of the soil.

Novak and Sheta (1980) proposed a cylindrical boundary zone around the pile. The zone was characterized by decreased modulus and increased damping relative to the free field, and with no mass to prevent wave reflections from the fictitious interface between the cylindrical zone and the outer region.

Poulos and Davis (1980) presented a set of analysis and design methods for pile foundations based on elastic continuum theory.

Poulos (1982) described a procedure for degradation of soil-pile resistance under cyclic lateral loading and compared it to several case studies.

Swane and Poulos (1984) proposed a subgrade reaction method that can capture a progressive soil-pile gapping with bilinear elasto-plastic springs and friction slider blocks.

Gazetas and Dobry (1984) derived a method for substructuring the seismic soil-pile-structure interaction problem based on kinematics and includes inertial components. They performed a parametric finite element study based on the work of Blaney et al. (1976).

Davies and Budhu (1986) and Budhu and Davies ((1987), (1988)) used the boundary element method to develop convenient design equations for the analysis of static laterally loaded fixed and free headed piles. The model accounted for nonlinear soil response with yield influence factors in profiles of both constant and linearly varying soil modulus with depth. Applications of the method are static laterally loaded fixed and free headed piles problems.

Tazoh et al. (1988) modified and extended Tajimi (1966) model to include superstructure inertial effects.

Poulos (1989) presented a compendium of his work on axial pile loading axial pile loading.

Gazetas (1991) made a complete survey of foundation vibration problems in which he included detailed design charts and equations for direct computation of pile head lateral and axial stiffness and damping coefficients in the three soil profiles.

Novak and his co-workers (1993) have issued the computer code DYNA4 which implemented their studies of single and pile group lateral and axial dynamic response.

1.7 Finite Element Models

The finite element method (FEM) potentially provides the most rigorous and powerful analytical methods for conducting seismic soil-pile interaction analyses. When implemented by competent users, FEM can account for factors difficult if not impossible to simulate with other techniques. However, the technique has not yet been fully realized as a practical tool. The advantages of a finite element approach include the capability of performing the SSPSI analysis of pile groups in a fully-coupled manner, without resorting to independent calculations of site or superstructure response, or application of pile group interaction factors. Obviously it is possible to model any arbitrary soil profile, and to study 3-D effects. Challenges to successful implementation of this technique lie in providing appropriate soil constitutive models that can capture small to very large strain behavior, rate dependency, degradation of resistance, and still prove practical for use. Special features to account for pile installation effects and soil-pile gapping should also be implemented (Meymand, 1998).

The most sophisticated and accurate method based on a continuum approach is FEM. FEM analysis can account for the shaft, soil, and rock mass behaviors more rigorously than the approximate methods described herein. But FEM analyses are not suitable for routine design of foundations in most cases. First, the results are only as reliable as the input parameters. In most cases the material properties of the rock mass are not known with sufficient reliability to warrant the most sophisticated analysis. Second, the design engineer should have the appropriate level of knowledge of the mathematical techniques incorporated into the FEM analyses. Finally, the time, effort, and expense required for conducting FEM analyses are often not warranted. For very large or critical bridge structures, sophisticated FEMs may be warranted and the agency might benefit from the investment required in computer codes, personnel training, and field and laboratory testing needed to take advantage of such techniques.

The development of this approach as applied to SSPSI problem is presented in chronological order in the following section.

Yegian and Wright (1973) implemented a finite element analysis with a radial soil-pile interface element. The model described the nonlinear lateral pile response of single piles and pairs of piles to static loading.

Blaney et al. (1976) based on work by Kausel et al. (1975) used a finite element formulation with a consistent boundary matrix to represent the free-field, subjected to both pile head and seismic base excitations, and derived dynamic pile stiffness coefficients as a function of dimensionless frequency.

Desai and Appel (1976) presented a three dimensional finite element solution with interface elements for the laterally loaded pile problem.

Emery and Nair (1977) studied an axisymmetric finite element model that incorporated non-symmetric free-field acceleration boundary excitations from wave propagation analyses.

Randolph and Wroth (1978) modeled the linear elastic deformation of axially-loaded piles.

Kuhlemeyer (1979a) offered efficient static and dynamic solutions for lateral soil-pile elastic response.

Kuhlemeyer (1979b) used a finite element model of dynamic axially loaded piles to verify Novak's (1977) solution and a simplified method presented by the author.

Angelides and Roesset (1981) extended Blaney's work with an equivalent linearization scheme to model nonlinear soil-pile response.

Stevens and Audibert (1979) developed force-deflection relations and compared favorably with the p-y curves suggested.

Randolph (1981) derived simplified expressions for the response of single piles and groups from a finite element parametric study.

Dobry et al. (1982) performed a parametric study of the dynamic response of head loaded single piles in uniform soil using Blaney's method and proposed revised pile stiffness and damping coefficients as a function of E_s and E_p .

Kay et al. (1983) promoted a site-specific design methodology for laterally loaded piles consisting of pressuremeter test data as input to an axisymmetric finite element program.

Lewis and Gonzalez (1985) compared field test results of drilled piers to a 3-D finite element study that included nonlinear soil response and soil-pile gapping.

Trochianis et al. (1988) investigated nonlinear monotonic and cyclic soil-pile response in both lateral and axial modes with a 3-D finite element model of single and pairs of piles, incorporating slippage and gapping at the soil-pile interface. They deduced a simplified model accommodating pile head loading only.

Koojiman (1989) described a quasi-3-D finite element model that substructured the soil-pile mesh into independent layers with a Winkler type assumption.

Brown et al. (1989) obtained p-y curves from 3-D finite element simulations that showed only fair comparison with field observations.

Wong et al. (1989) modeled soil-drilled shaft interaction with a specially developed 3-D thin layer interface element.

Bhomik and Long (1991) devised 2-D and 3-D finite element models that used a bounding surface plasticity soil model and provided for soil-pile gapping.

Brown and Shie (1991) used a 3-D finite element model to study group effects on modification of p-y curves.

Urao et al. (1992) contrasted results from a dynamic 3-D finite element analysis of a composite pile/ diaphragm wall foundation with an axisymmetric model.

Cai et al. (1995) analyzed a 3-D nonlinear finite element subsystem model consisting of substructured solutions of the superstructure and soil-pile systems.

Wu and Finn ((1997a), (1997b)) presented a quasi-3-D finite element formulation with relaxed boundary conditions that permitted: a) dynamic nonlinear analysis of pile groups in the time domain, and b) dynamic elastic analysis of pile groups in the frequency domain. These methods showed good comparison to more rigorous techniques, but at reduced computational cost.

Fujii et al. (1998) compared the results of a fully-coupled 2-D effective stress SSI model to measured performance of a pile supported structure in the Kobe earthquake.

1.8 Experimental models

Full-scale instrumented pile test in the field or well-built lab-scale pile testing is considered a good reliable accurate solution in the SPI problem. Full-scale test, which can also be conducted on pile in laboratory soil, is to some extent considered to be a practical solution in the states (Dodds, 2007a) as well as in the Canadian practice. The Canadian Foundation Engineering Manual (Society, 2006) indicates in section 18.4 that *"...often the best method is still the one based on well-planned and well-executed lateral test loading"*. The manual also recommends alternative experimental-based solutions to the analytical models of laterally loaded pile problem such as the pressuremeter method.

Other field-based methods utilizing the pressuremeter, flat dilatometer or cone penetrometer testing devices accompanied with a theory-based method utilizing the so-called "Strain Wedge" model can be used in this problem (Dodds, 2007a). Recalling the expenses, experience and time required in the approach, this solution might be particularly worthy for

important and large projects. The following section describe on each of these alternative methods.

1.9 The pressuremeter method

The pressuremeter considers the strong analogy between the behavior of soils around a laterally loaded pile and around the pressuremeter probe as can be perceived clearly in Figure 1.8. The Canadian Foundation Engineering Manual (Society, 2006) recommends Menard (1962) empirical method for calculating the horizontal resistance R_u from pressuremeter test data for a short head-restrained pile as presented in the following equation;

$$R_h = P_1 d(D - d) \quad (1.5)$$

Where

- R_h is the ultimate horizontal resistance of the pile;
- P_1 is the limit pressure from the pressuremeter test;
- D is the embedment depth of the pile; and
- d is the pile diameter.

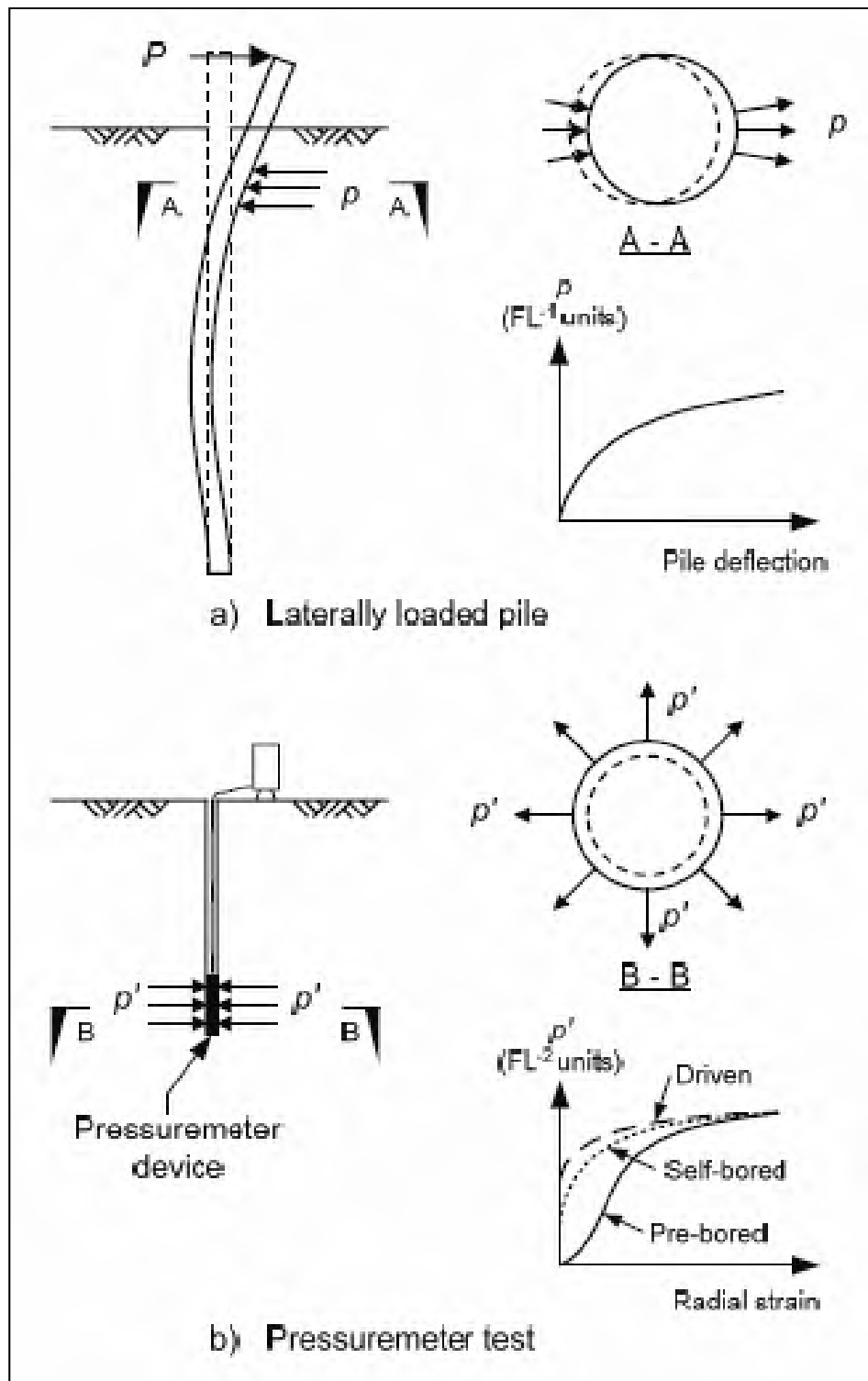


Figure 1.8 Laterally loaded pile and pressuremeter analogy
after Briaud (1984); Robertson (1984)

As shown, the all-round pressure (p') developed against the radially expanded pressuremeter resembles the soil resistance (p) developed against the front of a laterally loaded pile. Furthermore, the ability of the pressuremeter to measure both the resistance and deformation of the soil (the latter recorded in terms of radial strain), enables a direct comparison to be made between the pressuremeter response curve and the p - y curve for a pile.

Pressuremeter methods to derive p - y curves have been presented for the case of prebored pressuremeter tests ((Briaud, 1984); Briaud, Smith and Tucker, 1985) and pushed-in (driven) pressuremeter tests (Robertson, 1984). Briaud et al.(1984) also noted four other methods for prebored tests and two methods for self-bored tests.

1.10 The flat dilatometer method

The flat dilatometer has also found use in establishing p - y curves, although its capabilities are not to the same extent as the pressuremeter. In the flat dilatometer test, the technique of inflating a 60 mm diameter steel membrane into the soil in the horizontal direction to achieve 1 mm of deflection at the center, can only reasonably be expected to correlate well with the initial stiffness of p - y curves. Robertson, Davies and Campanella (1989) and Gabr, Lunne and Powell (1994) provided evidence in this respect, successfully predicting field test data using p - y curves that utilized dilatometer data to characterize the stiffness, and the conventional mechanistic approaches to establish ultimate resistance values. Anderson et al. (2003) also compared case histories against computer predictions using dilatometer-derived p - y curves, but recommended a restrictive application to low load levels (25% of ultimate), as predictions at higher load levels were too stiff.

1.11 The cone penetration test

The cone penetration test (CPT) is an attractive alternative given its ability to provide practically continuous profiling of soil behavior in terms of cone resistance and shaft friction correlations. Given that the behavior of the soil near the ground surface plays the most important role in defining laterally loaded pile behavior, obtaining detailed knowledge in this

zone to characterize p-y curves is an improvement. Evidence of this improvement was suggested by the findings of Anderson et al. (2003), who concluded that p-y curves using friction angle and undrained shear strength input parameters derived from standard CPT correlations produced the best prediction of field behavior, compared to p-y curves using input parameters from standard penetration test (SPT) correlations, or p-y curves derived from pressuremeter and flat dilatometer methods. Another CPT approach is the centrifuge work by Dyson and Randolph (2001), where the cone resistance was used to quantify the resistance component of a p-y curve described by a power law relationship.

1.12 Codes recommendations and common practice

| Code | Recommended procedure |
|--|--|
| AASHTO LRFD (The American Association of State Highway and Transportation Officials, 2014) | The <i>p-y</i> curves method for piles with small diameter and the strain wedge method for piles/shafts with large diameter |
| 2. ASCE E41-06 (American Society of Civil Engineers, 2007) | Clauses 3.2.6 and 3.2.6.2 indicate that ‘the soil-pile interaction shall be evaluated for buildings in which the increase due to the soil-pile effects will result in an increase in spectral accelerations in the fundamental period. The soil-pile effect is calculated using the explicit modeling procedure, or other approved rational procedure. |
| 3. CALIFORNIA DEPARTMENT OF TRANSPORTATION (CALTRANS, 2009) | Recommends the use of point-of-fixity method in seismic design of piles. Two procedures, preliminary and rigorous, are suggested to obtain the equivalent column length of pile foundation (Bridge Design Aids Chapter 12). |

| | |
|---|---|
| <p>4. CANADIAN FOUNDATION ENGINEERING MANUAL, 4TH EDITION (Canadian Geotechnical Society, 2006)</p> | <p>In section 6.9, it is indicated that ‘the soil-pile interaction occur during the seismic excitation governs the response of foundations’.</p> <p>‘Calculating the soil-pile effect using the explicit modeling procedure is based on a mathematical model that includes the flexibility and damping of individual foundation elements’.</p> <p>In section 6.9.2, it is indicated that ‘the main features that should be considered in theses analysis are the nonlinear behavior of the soil adjacent to the piles’.</p> <p>The methods recommended in this manual are:</p> <ul style="list-style-type: none"> • Broms’ method; • Pressuremeter method; • The p-y curves approach; and • The elastic continuum theory. |
| <p>5. CANADIAN HIGHWAY BRIDGE DESIGN CODE CAN/CSA-S6-14 (Canadian Standards Association, 2014)</p> | <p>Clause 6.8.7.3 states that ‘the pile is modeled as a beam-column supported by springs equivalent to the passive reaction distributed along the shaft’.</p> |
| <p>6. CONCRETE DESIGN HANDBOOK/ CSA A23.3-04 (Canadian Standards Association. Cement Association of Canada, 2006)</p> | <p>In clause 9.5.1.2.1, it is indicated that ‘the most common approach is to use finite element analysis software to model the pile as a beam on elastic foundation. This approach can easily consider the changes in soil constants along the height of the pile.</p> <p>The subgrade response characteristics (spring constants) are normally established by geotechnical engineers.</p> |

| | |
|---|---|
| 7. NEVADA STATE DOT (NDOT, 2008) | Section 17.5 mentions that in the initial stages of design, when using driven piles or drilled shafts, estimate the preliminary point-of-fixity at the top of the pile (bottom of the column) for the final design, a structural model with site-specific p - y curves is used to represent the soil and determine the lateral resistance of piles or shafts. The soil surrounding the piles is modeled as a set of equivalent non-linear springs’. |
| 8. WASHINGTON STATE BRIDGE DESIGN MANUAL (Washington-State-DOT, 2010) | For laterally loaded deep foundation, the following methods are recommended (clause 7.2.5): <ul style="list-style-type: none">• the equivalent cantilever column (the-fixity-point) method;• the equivalent base springs method;• the non-linear soil springs method (p-y curves) implemented in FEM programs. |

CHAPTER 2

MODELING ISSUES FOR PILES UNDER LATERAL LOADING

This chapter presents the major problems and issues related to piles under lateral loadings. The effects of these issues which can be related either to the soil or to the pile properties are described and discussed.

2.1 Introduction

Modeling soil-pile interaction (SPI) problems is a very challenging task, especially under earthquake loading conditions. This is because the solution is sensitive to the boundary conditions and to the input parameters of the problem. Therefore, it may be unrealistic to envision a unique modeling solution that covers all these parameters and cases. Nevertheless, the main elements that should be considered in the modeling of the seismic SPI problem are determined in most of the cases. This chapter attempts to examine these parameters and provide an explanation of the effect of each of these issues on the response and performance of piles.

2.2 Major elements in the soil-pile interaction problem

The soil-structure interaction of deep foundations under earthquake loading is a complex and cumbersome problem. This is due to the numerous elements and factors that contribute to the overall response of the system. Some factors are related to the structural properties of the foundation, others are related to the site and soil properties. In the following section a total of ten major aspects that affect soil-pile-interaction (SPI) modeling have been identified and will be discussed in the next sections. These aspects are as follows: (1) Pile head fixity; (2) Soil stiffness; (3) In-situ stresses; (4) Pile/soil friction; (5) Sloping ground;

(6) Pore pressure effects; (7) Pile diameter; (8) Nonlinear Pile section properties; (9) Water table effect; (10) Cap mass or superstructure inertial forces; and (11) Group effects.

The contribution of these factors to the overall performance of the system can be significant as will be seen later. Therefore, their effect should be assessed when analyzing seismic soil-pile interaction. Obviously the occurrence or existence of factors acting simultaneously for all cases is very seldom. Therefore, care should be exercised when defining the problem and its boundary conditions in order to build the appropriate model for the problem at hand.

The following sections will attempt to shed some light on the effect of these factors on the results of any model that describes the soil-pile interaction during an earthquake.

2.3 Pile head fixity (kinematic seismic response of single piles – Gazetas)

The displacements at the pile head during an earthquake correspond to the displacements of the pile cap in the model coordinate system. However, the slope or rotation of the pile head is not always equal to the rotation of the pile cap. The relation between the two rotations depends on the type of pile-cap connection and the degree of fixity. The pile-cap connection varies between two boundaries, i.e., hinged (pinned) connection and rigid (fixed connection). In between, the fixity may be a portion of the free rotational degree of freedom (DOF).

It may be instructive at this point to differentiate between the type of pile-cap connection and the type of the connection to the superstructure which affects the reactions applied at the pile top level. The pile-cap connection type will induce boundary displacements to the system whereas the pile-superstructure connection will apply forces at the pile-head level.

Fan and Ahmad (1991) reported that increasing the degree of fixity at the pile-cap level (from hinged- or free-head to fixed-head piles) has a direct effect on the input motion to pile model. They stated that by doing so the "effective" pile-cap input motion in an earthquake excitation will tend to be less severe. On the other hand, they noticed that in homogeneous deposits, single piles with free-head or hinged-at-the-cap experience shaking with low to

intermediate frequency. This implies an "effective" pile top motion greater than the free-field. In contrast, with fixed-head piles, this tendency for larger pile-top motion is completely suppressed. The study recognized also the importance of assessing the rotational component of the pile cap during the earthquake which occurs in both conditions, i.e., pinned or fixed cap connection and for a single pile or pile group.

2.4 Soil stiffness

The term soil stiffness generally stands for the Young's moduli of the soil. The soil performance at low levels of strains can be practically estimated from the linear elastic continuum model in which the elastic soil properties such as Young's modulus (E_{soil}) and Poisson's ratio (ν_{soil}) control the soil performance. These properties can be obtained from the results of triaxial tests for drained (E') or undrained (E_u) conditions. It can also be obtained from compression test on hard or weak rock.

The triaxial test provides a complete history of the degradation of the soil stiffness as the strain level increases. Figure 2.1 illustrates this variation of the soil stiffness with the strain level. As can be seen from this figure the curve has an initial straight horizontal line portion that reflects the elastic behavior region which is associated with maximum soil modulus. At certain strain level the soil starts to yield and the soil stiffness degrades until it reaches a very small residual value when large deflections occur. The horizontal segment, which represents the small-strain behavior of the soil, is an essential part of constitutive modeling – especially when the analysis focuses on the soil deformations. Ignoring this phenomenon can result in the prediction of patterns of movement considerably different to those observed in the field (David, 2001).

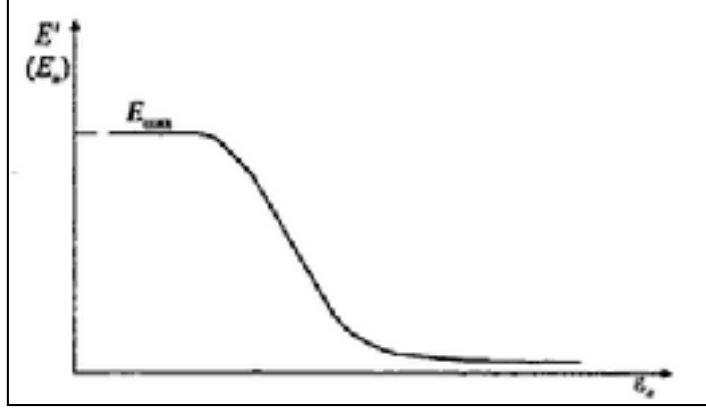


Figure 2.1 Soil Stiffness Curve after David (2001)

In the soil-pile interaction problem the initial stiffness of the p - y curves (E_{py-max}), or what can be considered as the horizontal subgrade reaction of the soil k_h , is strongly correlated to the elastic stiffness of the soil. As recommended by Dodds (2007b), the subgrade reaction of the soil can be estimated from Vesić (1961)'equation related to the infinite elastic beam on elastic soil as follows:

$$k_{\infty} = \frac{0.65E_{soil}}{1 - \nu_{soil}^2} \sqrt[12]{\frac{E_{soil}b^4}{E_{beam}I_{beam}}} \quad (2.1)$$

By considering the values of ν_{soil} for most soils (0.1 to 0.3 for sands and 0.5 for saturated clay in undrained conditions) and noting that the fraction inside the radical sign is close to unity, it can be concluded that $k_{\infty} \approx E_{soil}$.

Vesić (1961) showed that infinity length effect can be minimal when the beam (pile in our case) is *sufficiently long* and the beam (pile) performs flexibly (as in most pile cases). The beam is considered *sufficiently long* when its dimensionless length (λL) is greater than 2.25, where λ is defined by the following equation:

$$\lambda = \sqrt[4]{\frac{k}{4 E_{beam} I_{beam}}} \quad (2.2)$$

Where k is the subgrade modulus of the beam and L is the beam length.

The soil stiffness affects the soil-pile interaction during the earthquake. The initial value of the moduli (i.e., for low strain levels) controls the yielding limit of the soil at the soil-pile interface. In contrast, the degradation in these moduli, due to larger strains, dominates the soil-pile interaction relationship.

The effect of the soil modulus distribution with depth has a significant but complex effect on the unrestrained pile head stiffness (Pender, 2004). Vasquez (2006) reported the relation between the soil moduli and the p - y curve as depicted in Figure 2.2. As can be seen, two dashed lines are shown. The slope of these lines indicates the soil modulus. The upper bound of the soil modulus represents the maximum E_s and corresponds to the horizontal portion of E_{max} in Figure 2.2. In a p - y relationship, as the deflection of the pile increases, the slope of a secant (known as the secant modulus) to the curve gets smaller. Thus the value of the soil modulus decreases with increasing deflection. Along the pile depth, the soil becomes stiffer, the pile deflection decreases and the maximum soil modulus increases, as illustrated in Figure 2.3. Thus E_s is a nonlinear function of pile deflection and depth.

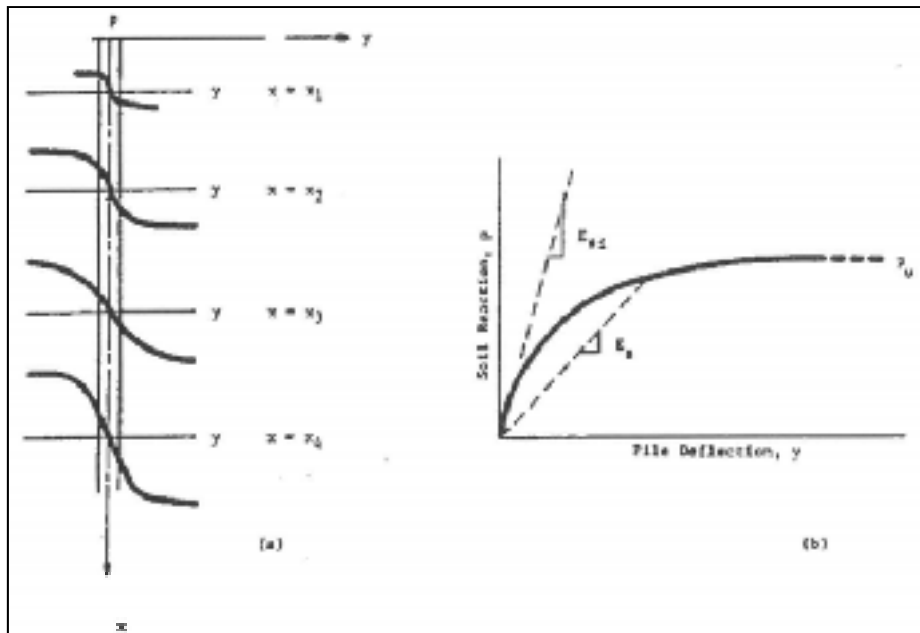


Figure 2.2 Typical $p-y$ Curves after Vasquez (2006)

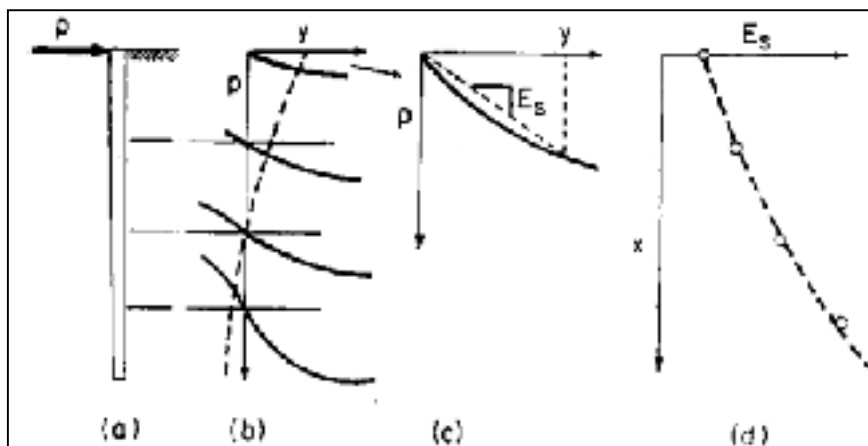


Figure 2.3 Relation between Soil modulus and $p-y$ Curves after Wang (2006)

2.5 In-situ horizontal stresses

The horizontal stress in the soil at certain level, or point, is proportional to the vertical stress resulting from the self-weight of the soil at that level, or point $\sigma_{h0} = k_0 \times \sigma_{v0}$. Brown (1991)

reported that the in-situ horizontal stress in the ground has no significant effects on the performance of the laterally loaded pile. In other word, p - y curves of piles in soil should not be modified when in-situ horizontal stresses in the soil exist. However, they found on the basis of pile head load-deformation plots, that the soil unit weight represents a small but significant portion of load resistance in the pile response. Therefore, and as illustrated in Figure 2.4, lateral pile response appears to be relatively insensitive to the in-situ horizontal stress in the ground. In contrast, the soil unit weight contributes significantly to soil resistance. This contribution of soil unit weight is reasonably captured by the existing Matlock criteria for soft clays.

The study of Brown (1991) did not consider the effect of the in-situ state of stress on the mobilized shear strength which might be an influential factor when constructing the p - y curves.

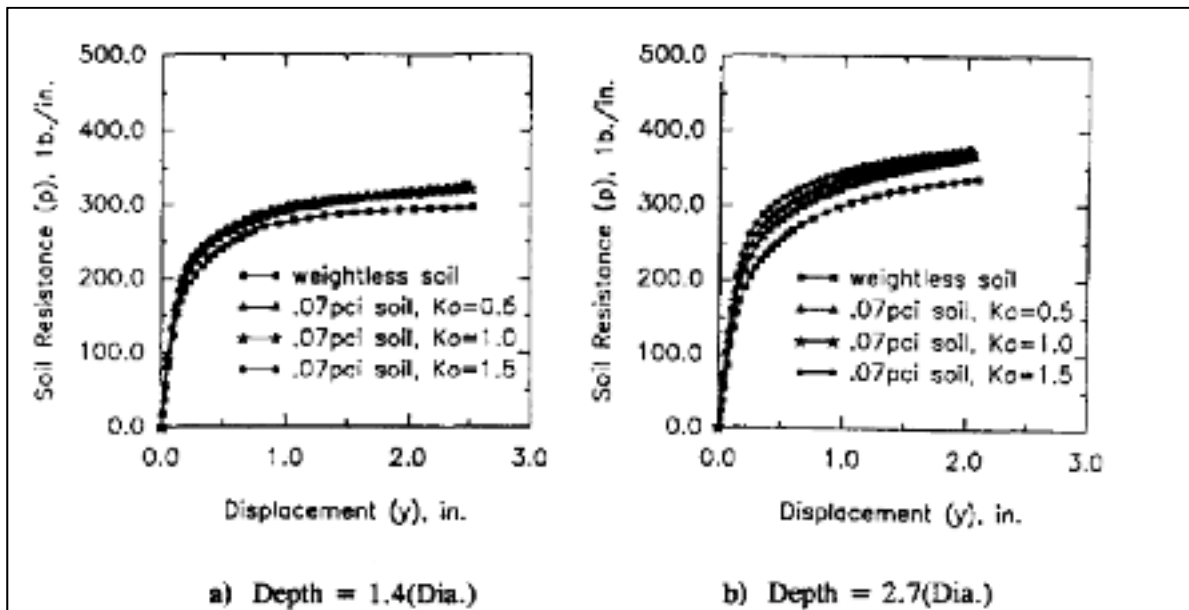


Figure 2.4 Effect of Soil Weight and In-Situ Stress on the p - y Curve
after Brown (1991)
(1 in.=25.4mm, 1lb=4.45 kN)

2.6 Pile/soil friction

One of the common techniques in designing piles for deep foundations relies on the relative friction between the pile and the soil that can be present at the soil/pile interface. The friction pile type is particularly suitable for soft clay with gradually increasing firmness with depth (McCarthy, 1998). The concept is based on resisting the axial thrust in the pile by the skin friction at the soil/pile interface. However, in laterally loaded piles, the soil resistance transferred to the pile is mobilized as a combination of normal stress and frictional resistance around the perimeter to the point at which separation or gapping occurs. Brown (1991) reported that the pile response is significantly affected by the interface friction, but relatively insensitive to the friction coefficient. The study concluded that an appropriate finite element model of the laterally loaded pile problem must include provisions for slippage, gapping and frictional resistance at the pile/soil interface. However, the lateral load response of the pile is not particularly sensitive to the friction coefficient used at the interface but to the frictional angle of the interface soil, as long as frictional behavior is provided.

2.7 Sloping ground

Piles in sloping ground interact with the soil differently from the piles in horizontal ground. This situation may be encountered by practicing engineers particularly when the piles are used to support the structure on inclined ground or when piles are used in slope stabilization. In this case, the piles are usually subjected to lateral forces due to horizontal movements of the surrounding soil and therefore are considered as passive piles. As noted by Ashour (2012), solutions to this problem can be obtained using Broms' method (1964a) as characterized in NAVFAC (1982) or the traditional p - y curve method. However, neither of these methods was in the beginning developed for sloped ground.

Brown (1991) investigated the effect of sloping ground on the p - y curves. Based on a numerical model, they derived new p - y curves for sloped soil conditions and compared them with those derived originally for soil with horizontal ground surface. They founded that slope

effect is most significant at shallow depths, and then only with respect to the maximum soil resistance P_u . In other words, the effect of slope diminishes with depth below the surface and this effect reduces the ultimate soil resistance by less than 30% in most cases. In addition, they found that the effect of sloping ground increases significantly with increasing slope. These findings were in agreement with the proposed model for soil–pile analysis in pile-stabilized slopes by Ashour (2012) work as illustrated in Figure 2.5.

As it can be noticed from this model, soil conditions below the sliding mass region is very similar to the conditions of the soil for which the original p - y curves were developed i.e. horizontal soil layers. However the ultimate soil resistance P_u should be adjusted to account for the slopping effect. This rises the importance of adjusting the currently used p - y curves for sloped surface conditions.

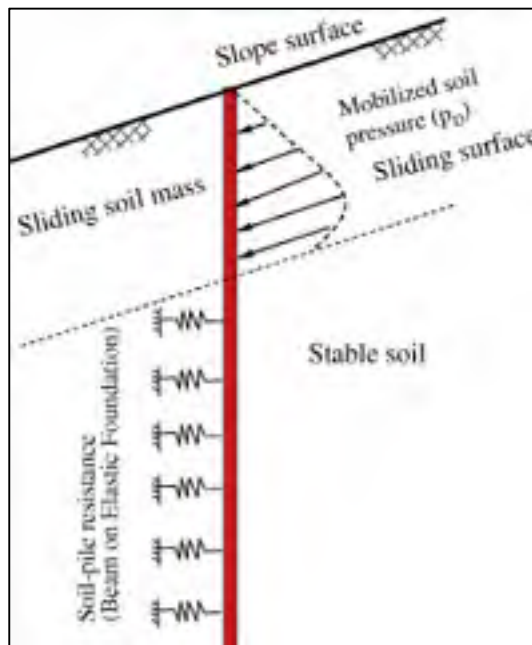


Figure 2.5 Proposed Model for Soil–Pile Analysis in Pile-Stabilized Slopes after Ashour (2012)

2.8 Pore pressure effects

It is well known that saturated sandy and silty soils under the course of seismic loading will suffer excessive and quick pore water pressure rise. This is due to the rapid loading and unloading of the soil within a short period of time that prevents the dissipation of the pressure and enforces the undrained loading conditions. This phenomenon leads to degradation of the soil shear strength during the earthquake which directly affects the p - y curves. If the degradation continues the soil may liquefy and fail.

Region of potential liquefaction when analyzing a seismic soil-pile interaction problem can be identified using the normalized excess pore-pressure ratio (or cyclic pore-pressure ratio) (FLAC3D-Manual, 2012), u_e / σ'_c in which u_e represents the excess pore pressure and σ'_c the initial effective confining stress. This pore pressure occurring during the earthquake shaking is usually normalized with the static pore pressure.

Dobry (1999) examined the effect of pore pressure rise on the p - y curves of pile in loose sand subjected to seismic shaking. The curves developed from this study were compared to the original static p - y curves. A reduction scale expressed through a coefficient C_u (not to be confused with C_u for shear resistance) was introduced for different pore water pressure ratios as illustrated in Figure 2.6.

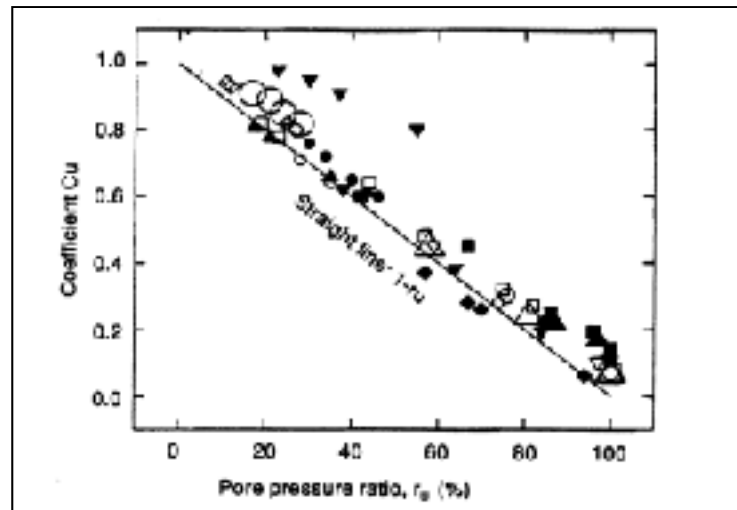


Figure 2.6 Coefficient C_u (p -multiplier) versus Pore Pressure Ratio r_u after Dobry (1999)

This coefficient C_u can be used as a p -multiplier to the static regular p - y curves to take into account the excess pore pressure effect. A prior site-response analysis is warranted to determine the pore-pressure ratios during the earthquake. Then using the curves (see Figure 2.6) suggested by Dobry (1999), a corresponding p -multiplier can be obtained and used accordingly to reduce the p - y ultimate capacity. For example, if the pore-pressure ratio is 0.4, the p - y curve is reduced by 20% accordingly.

2.9 Pile diameter effect

The effect of pile diameter on the pile performance and its interaction with the surrounding soil under lateral load has been studied by several researchers. This effect is attributed to the direct relation between the ultimate soil resistance per unit length of pile P_u and the pile width (or diameter) d .

In the early work of Terzaghi (1955), the subgrade modulus of the soil was found to be independent of the pile diameter. This conclusion was inconsistent with the field observation as stated by Dodds (2007b).

In other words, the pile diameter contributes to the p - y curves and to the performance of the soil surrounding the pile. Reese et al. (1975) compared the bending moment values calculated from the analytical expressions of p - y curves with the tests results of piles 152mm- and 641mm- diameter piles at Manor site. He found good agreement with the experimental values; however the commuted deflections did not match. This mismatch could not be explained at the time of the experiment but was later attributed to the use of first power diameter term in the p - y equations (Reese, 2009).

Common sense as well as field observation support the fact that piles under lateral loading become stiffer when the diameter gets larger, as reported by several studies such as the work of (Stevens and Audibert 1979, Pender 1993, Idriss 2001, Reese 2009, O'Neil and Dunnavant 1984 and 1985).

In terms of the p - y formulation, Dunnavant (1984 and 1985) found that for clay soil, the site-specific response of the soil surrounding the pile could be characterized by a nonlinear function of the diameter (Reese, 2009). Other research studies reached similar finding so that the characteristic soil deflection is related to the square root of the diameter as presented in Table 2.1.

Table 2.1 Deflection Parameters of Clay p - y Curves as Affected by Pile Diameter
adapted from Dodds (2007b)

| Characteristic Deflection Parameter | |
|---|----------------------------|
| $y_c = 8.9\varepsilon_{50}\sqrt{d}$ | Steven and Audibert (1979) |
| $y_c = 0.8\varepsilon_{50}\sqrt{d}\left(\frac{E_p I_p}{E_s}\right)^{0.125}$ | Gazioglu and O'Neil (1984) |

Reese (2006 and 2009) stated that the diameter of the pile should not appear as a linear function in p - y curves for cyclic loading in clays below the water table. In contrast, for cemented sand, (Ashford, 2003) found that the pile diameter has no effect on the p - y curves when modeling of cast-in-drilled-hole (CIDH) piles.

Pender (2004) has explained the diameter effects by considering the real possibility of soil modulus distributions increasing either linearly with depth or with the square root of the depth, as opposed to constant with depth. This distribution is also consistent with the one introduced by Vasquez (2006). Pender (2004) pointed out that the ratio of unrestrained lateral pile head stiffness to pile diameter remains constant with changes in diameter for the case of a constant soil modulus profile, whereas the ratio increases with increasing diameter for the non-constant soil modulus cases. By doubling the pile diameter in the linear modulus case, for example, the lateral stiffness increased by a factor greater than two. Thus a seemingly stiffer response with increasing pile diameter was attributed to a varying soil modulus distribution with depth.

2.10 Group effect

Soil-pile interaction (SPI) of a laterally loaded single pile is affected by the existence of other piles nearby. This is known as pile-soil-pile interaction (PSPI). The PSPI effect results mainly from the extra strain-induced load applied to the pile from other piles. In other terms, a typical isolated pile has higher lateral load capacity and undergoes less deflection compared with the behavior of the same pile as part of a group of piles. This effect depends mainly on the pile spacing and may be influenced by the pile configuration, distribution of soil modulus with depth, size of the group, pile head restraint type, soil types and between-piles soil conditions. These factors are depicted in Figure 2.7.

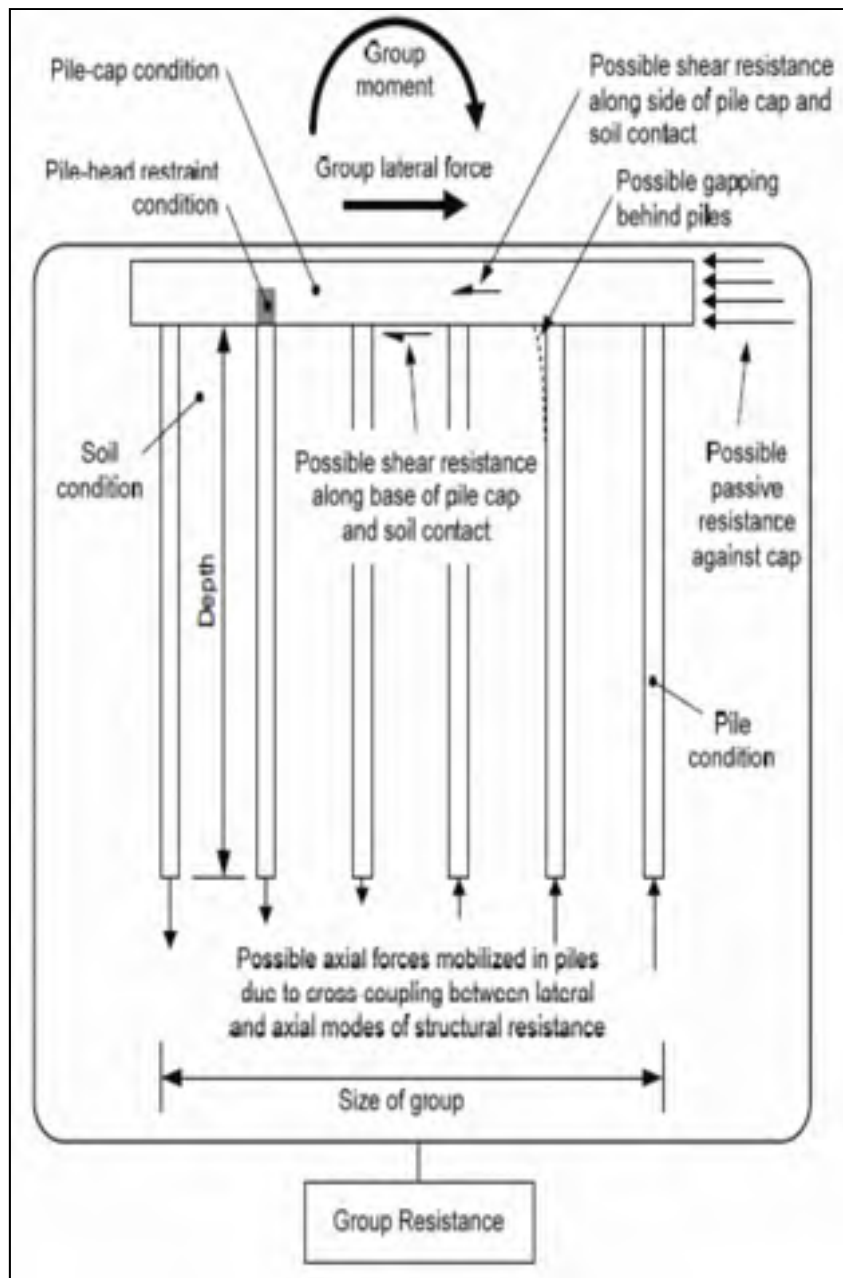


Figure 2.7 Schematic of Pile Group Resistance
after Dodds (2007b)

In this regard, pile groups can be categorized into: spaced group, widely spaced group, large or small groups. The group effect is more pronounced when piles are closely spaced especially in a large group.

Observation from full-scale lateral loading test of group piles (such as the work of Focht and Koch, 1973) demonstrated the unsymmetrical distribution of load among piles of laterally loaded pile group. These studies identified the so-called shadowing effect phenomenon in which the trailing rows of piles, which are in the shadow of the leading front row experience more lateral displacement and therefore have a reduced lateral resistance compared to the leading row (see Figure 2.8). Ochoa and O'Neill (1989) explained this phenomenon by the fact that piles in the leading row have more soil support than the ones in the shadow and that a local reduction in the lateral support of the soil in front of the pile as the pile located ahead displaces leaving the soil behind with less or no support (gaping effect).

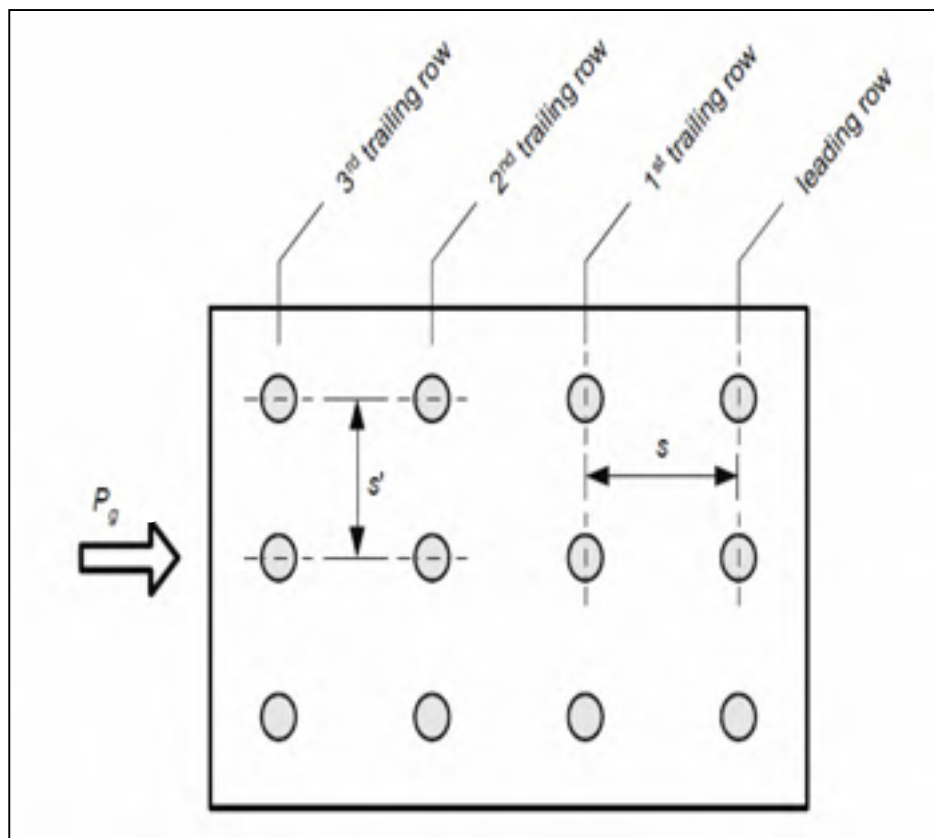


Figure 2.8 Top View of Typical Laterally Loaded Group Configuration after Dodds (2007b)

It was also found that the PSPI in the direction of the lateral loading is as much as twice the one in the direction perpendicular to the load and that interaction is reduced with depth especially in the case when soil modulus increases downward along the pile length. Another interesting finding is that PSPI factors are inversely proportional to the pile-to-pile spacing (Poulos 1971b, Poulos 1979, Randolph 1981) as cited by (Dodds, 2007b).

Quantifying the group effect on the behavior of laterally loaded single pile has been obtained theoretically and experimentally. Nevertheless, both approaches result in reducing the lateral resistance capacity of the singular pile in the group. Several methods have been introduced to estimate this reduction by either increasing the displacement of a single pile induced by other piles or by reducing the soil resistance at the pile-soil interface, i.e. by modifying the p - y curve elements.

An example of an increased displacement introduced to a single pile to account for the group effect is the one based on the elastic-based approach introduced by Poulos (1971b) in which the group interaction is defined by an influence factor α as follows:

$$\alpha = \frac{\text{additional movement caused by adjacent pile}}{\text{movement of pile caused by its own loading}} \quad (2.3)$$

Using the method, the lateral displacement of a pile δ_j in group can be estimated using the following equation (rotation can be defined similarly):

$$\delta_j = \bar{\delta}_{P=1} \left(\sum_{\substack{k=1 \\ k \neq j}}^m P_k \alpha_{\delta P j k} + P_j \right) \quad (2.3)$$

Where

δ_j = Lateral deflection of the j^{th} pile in the group;

$\bar{\delta}_{P=1}$ = Lateral deflection of a single pile due to lateral unit load application;

P_i = Lateral load on the i^{th} pile in the group;

$\alpha_{\delta Pjk}$ = Influence factor on the j^{th} pile from the k^{th} pile in the group;

m = Total number of piles in the group.

The factor α is estimated from prior discretization analysis as presented in Figure 2.9 and equations (2.4) and (2.5).

$$p_j = q_j dz \quad (2.4)$$

$$u_i = \sum_{j=1}^n I_{ij} p_j \quad (2.5)$$

Where

p_j = Lateral load acting on node j ;

q_j = Lateral pressure acting over tributary length for node j ;

dz = Tributary length for nodes of numerical pile;

u_i = Additional lateral displacement at node i from adjacent pile;

I_{ij} = Elastic interaction factor of load at node j on node i ; and

n = Total number of pile nodes.

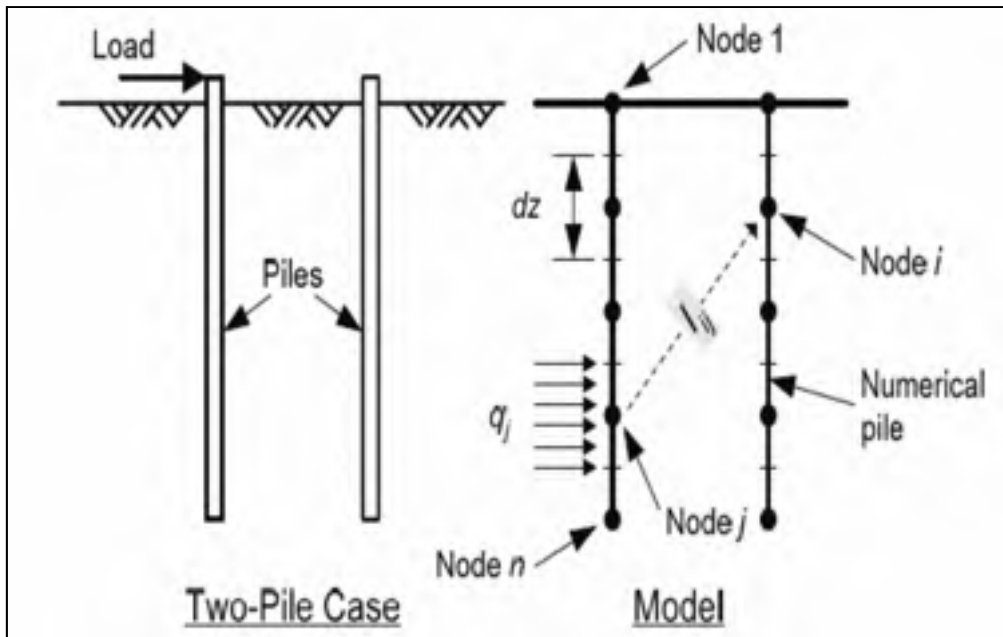


Figure 2.9 Estimating Factor α

The mathematical expression of Equation (2.5) and the evidence of shadow effect together demonstrate the need to modify p - y curves of pile in group to account for the reduced lateral capacity and/or the additional displacement induced by neighboring piles, especially on the trailing piles. This has led to the concept of p -multiplier and y -multiplier in which the original p - y curve is stretched vertically or horizontally to account for the group effect (see Figure 2.10).

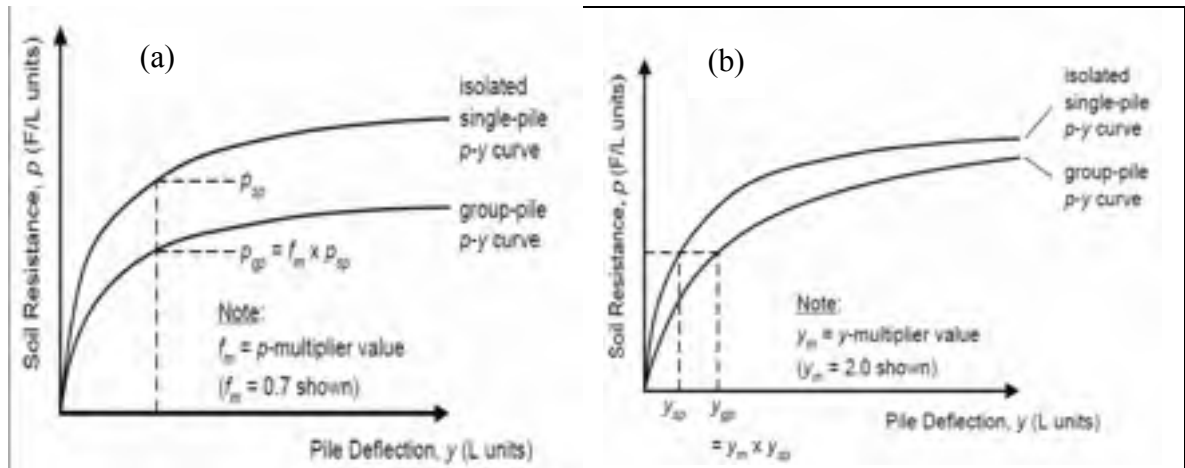


Figure 2.10 Group Effect on p - y Curve : (a) p -multiplier concept; (b) y -multiplier concept after Dodds (2007b)

CHAPTER 3

SITE CHARACTERIZATION

This chapter presents the site characterization and geotechnical properties of soil for the Quebec sites considered for the present study, namely: Bécancour and Québec City. For each of the two sites a brief description of the local stratigraphy and results of field and laboratory tests are presented.

3.1 Introduction

This chapter presents the stratigraphic and geotechnical soil properties for the Quebec sites that will be studied and modeled in this study. The sites chosen are: Bécancour and Quebec City. The selected sites represents typical soil stratigraphy for the province of Quebec. Bécancour site consists mainly of clay, silt and sandy silt soil, Quebec site however represents a deep layer of sand. Using results of field work and laboratory provided by the Ministry of Transport of Quebec (MTQ), two profiles were created. For each of the two sites, the location of the site, a synthesis of the work, a brief description of the local stratigraphy and a discussion of the results of field and laboratory work are presented. The stratigraphy retained, along with profiles of S_u , $(N_1)_{60}$, γ_{sat} , G_{max} , E'_{max} and ϕ' are also presented.

3.2 Bécancour site

This section describes the Bécancour site location, as well as the various analyzes that have led to the creation of the profile used in subsequent modeling.

3.2.1 Location

The first site is located in the Saint-Grégoire sector in the city Bécancour, Montérégie. Figure 3.1 shows the location of the project, along Highway 55, at the intersection with the Acadians Boulevard.



Figure 3.1 Location of the Bécancour Site (MTQ 2010, Qualitas 2011)

3.2.2 Local geology

Located in the lowlands of the St.-Lawrence, the region of Bécancour city suffered invasion by the waters of the Champlain Sea 8,500 to 12,500 years ago. This created the deposit of fine sediments and the formation of a significant deposit of cohesive soils (Leroueil, 1983). This deposit is based on granular soil composed of dense to very dense sand and silt (Qualitas, 2011).

3.2.3 Data analysis

This section summarizes the work performed on site and presents a description of the general stratigraphy of the site and test results that have led to the creation of the geotechnical profiles for the Bécancour site.

3.2.4 Summary of work done

A total of seven boreholes, two Nilcon vane tests, thirty piezocone penetration tests (CPTu) and three seismic cone penetration tests (SCPTu) were conducted on a distance of 2.9 km along Highway 55 (Qualitas, 2011). This work was conducted by the Qualitas Group and the results were reported in January 2011. The project was divided into three zones: northern, central and southern zone. Owing to large scope of work and the soil heterogeneity along the highway, only the central area of the project was selected for this study. This choice was motivated by the fact that the central zone featured a thick layer of clay and was close to two wells, three piezocone penetration tests (CPTu), a seismic cone penetration test (SCPTu) test and a Nilcon vane test along a line transverse to the highway at km p.k. 5+050. This was in line with the objective of the study and warranted reliable geotechnical data for further analysis. The proximity of the test locations reduces the uncertainty associated with the heterogeneity of soils and allows a representative soil profile in place to be achieved for subsequent modeling. Figure 3.2 shows a location plan of boreholes and drill holes, where the selected area, defined in a rectangular, is located at the intersection of Highway 55 and the Acadians Boulevard. Table 3.1 shows a summary of surveys and borings carried out.

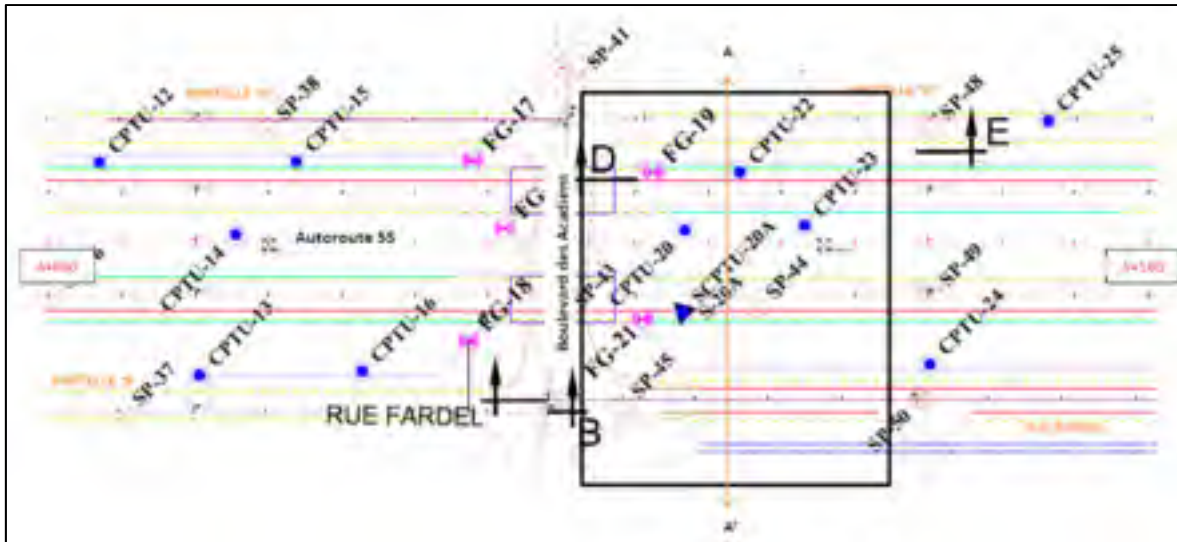


Figure 3.2 Location plan of boreholes and borings in the central zone (Qualitas 2011)

Table 3.1 Summary of Tests and Borings Carried Out (Qualitas 2011)

| | Surface Elevation | Depth | Base Elevation |
|-----------------|-------------------|-------|----------------|
| Drilling / Poll | (m) | (m) | (m) |
| FG-19 | 25.11 | 20.20 | 4.91 |
| FG-21 | 24.02 | 19.00 | 5.02 |
| CPTU-20 | 24.78 | 15.09 | 9.69 |
| SCPTU-20A | 23.88 | 12.05 | 11.83 |
| CPTU-22 | 25.02 | 11.57 | 13.45 |
| CPTU-23 | 24.58 | 11.88 | 12.70 |
| S-20A | 23.88 | 7.50 | 16.38 |

In addition to field and in-situ testing, the following laboratory tests were performed on samples collected during drilling (Qualitas, 2011):

- Sedimentometry (BNQ 2501-025)
- Particle size analysis by mechanical sieving (BNQ-2501-025)
- Water content (BNQ-2501-170)

- Specific gravity by weighing
- Plasticity and liquidity limits (BNQ-2501-092)
- Relative density of grains (BNQ 2501-070)
- Sensitivity of cone falling (BNQ 2501-110)
- Oedometer consolidation test (ASTM D2435-96)

Table 3.2 shows the laboratory results for boreholes FG-19 and FG-21. The N index, suitable for granular soil layers, is not corrected and is taken directly from SPT test results recorded on the boring reports. Rock Quality Designation (RQD) index, used to describe the rock quality, is also indicated in the table.

Finally, Casagrande type piezometers were installed at the location of boreholes FG-19 and FG-21. The reading of borehole FG-21 indicated the presence of a water table at 0.68 m depth in November (Qualitas, 2011). Therefore, a water table at surface was considered in the analysis for this site. This is justified by the fact that snowmelt is likely to cause an enhancement of the water table level.

Table 3.2 SPT and Laboratory Test Results for Boreholes FG-19 and FG-21

| Depth (m) from | to | Soil | % FC | w (%) | w _L (%) | w _p (%) | I _p (%) | I _L (%) | γ_{sat} (kN/m ³) | e | N/S _u (c/300mm/kPa) | St | OCR | σ'_p (kPa) | C _r | C _c | Compact/ Consistency |
|-------------------|-------|-----------------------------|---------|----------|-----------------------|-----------------------|-----------------------|-----------------------|--|-------|-----------------------------------|-----|------|----------------------|----------------|----------------|-------------------------|
| Drilling FG-19 | | | | | | | | | | | | | | | | | |
| 0.00 | 2.22 | sandy embankment | 9.9 | 9.0 | - | - | - | - | - | - | 45 | - | | | | | dense to very dense |
| 2.22 | 5.50 | clay and silt | 99.2 | 55.2 | 76.8 | 24 | 52.8 | 0.59 | 16.7 | 1.482 | 46.9 | 3.8 | | | | | firm |
| 5.50 | 8.45 | silt and clay | 99.1 | 43.0 | 37.0 | 16.4 | 20.6 | 1.29 | 17.7 | 1.397 | 18.3 | 6.8 | 1.07 | 75 | 0.047 | 0.68 | soft |
| 8.45 | 9.50 | clayey silt | - | - | - | - | - | - | 17.5 | - | - | - | | | | | stiff |
| 9.50 | 13.20 | silt and sand | - | - | - | - | - | - | - | - | 29 | - | | | | | medium to dense |
| 13.20 | 17.95 | sandy silt | - | - | - | - | - | - | - | - | 86 | - | | | | | very dense |
| 17.95 | 18.70 | dark gray shale | - | - | - | - | - | - | - | - | - | - | | | | | RQD = 0 % |
| 18.70 | 19.30 | dark brown to gray shale | - | - | - | - | - | - | - | - | - | - | | | | | RQD = 70 % |
| 19.30 | 20.20 | brown shale | - | - | - | - | - | - | - | - | - | - | | | | | RQD = 90 % |

| Depth (m) | | Soil | % FC | w (%) | w _L (%) | w _p (%) | I _p (%) | I _L (%) | γ _{sat} (kN/m ³) | e | N/S _u (c/300mm/kPa) | St | OCR | σ' _p (kPa) | C _r | C _c | Compact/ Consistency |
|-----------|-------|--------------------------------|------|-------|--------------------|--------------------|--------------------|--------------------|---------------------------------------|-------|--------------------------------|------|------|-----------------------|----------------|----------------|----------------------|
| from | to | | | | | | | | | | | | | | | | |
| | | Drilling FG-21 | | | | | | | | | | | | | | | |
| 0.00 | 0.68 | sandy-clayey silt | - | - | - | - | - | - | 17.0 | - | - | - | | | | | hard |
| 0.68 | 2.15 | silty clay | - | - | - | - | - | - | 17.0 | - | - | - | | | | | stiff to hard |
| 2.15 | 3.55 | silty clay | 99.6 | 64.5 | 64.4 | 23.8 | 40.6 | 1.00 | 15.8 | 2.053 | 30.9 | 17.2 | 3.04 | 95 | 0.047 | 1.735 | firm to soft |
| 3.55 | 5.15 | silty clay | 99.4 | 76.5 | 63.1 | 21 | 42.1 | 1.32 | 15.4 | 2.283 | 21.8 | 31.1 | 2.33 | 90 | 0.047 | 2.671 | soft |
| 5.15 | 6.25 | clay and silt to silt and clay | - | 43.3 | 38.6 | 17 | 21.6 | 1.22 | 17.5 | 1.048 | 25.5 | 31.9 | 1.69 | 91 | 0.025 | 0.557 | soft |
| 6.25 | 7.95 | silt and clay | 88.6 | 39.6 | - | - | - | - | 19.3 | 0.843 | - | - | | | | | soft |
| 7.95 | 8.55 | silty sand | - | - | - | - | - | - | - | - | 27 | - | | | | | medium |
| 8.55 | 14.70 | silt and sand | 56.2 | 11.0 | - | - | - | - | - | - | 33 | - | | | | | medium to dense |
| 14.70 | 16.05 | sand and silt | 43.3 | 9.0 | - | - | - | - | - | - | 62 | - | | | | | very dense |
| 16.05 | 16.70 | weathered shale | - | - | - | - | - | - | - | - | - | - | | | | | |
| 16.70 | 17.60 | brown shale | - | - | - | - | - | - | - | - | - | - | | | | | RQD = 17 % |
| 17.60 | 19.00 | brown shale | - | - | - | - | - | - | - | - | - | - | | | | | RQD = 69 % |

3.2.5 **Summary of the stratigraphy**

This section presents the general stratigraphy encountered for studied site. Figure 3.3, prepared by Qualitas (2011), illustrates the different soil deposits for different elevations.

Granular fill (roadway surface structure)

A 2-m deep granular fill covers the cohesive soil at the location of borehole FG-19. This fill contains less than 10% of fine particles and is densely compacted with an N index equal to 45.

Deposit of cohesive soil

A deposit of cohesive soil is encountered beneath the granular fill at the location of borehole FG-19, and at surface at the location of borehole FG-21. Its thickness is about 7.5 meters. This means that the silty clay is becoming silt and clay at greater depth. Thus the percentage of silt increases with depth.

Its consistency changes from hard/firm surface (clay crust) to soft with undrained shear strength of approximately 20 kPa. The measured OCR varies from 1.07 to 3.04 and the measured pre-consolidation stress (σ'_p) is 90 kPa on average (Qualitas, 2011). This is a CL and CH soil since the plasticity index (I_p) ranges from 20.6% to 52.8%.

Deposit of granular soil

The deposit of cohesive soil lays on a granular soil, the density of which is medium to very dense and increases with depth. The N index varies from 27 to 89. The soil consists of silt and sand to sand and silt. The percentage of fine particles ranges from 56.2% to 43.3%. The thickness of the deposit is equal to 8.25 meters on average.

Bedrock

The bedrock is reached at a depth of 17.95 meters for borehole FG-19 and at 16.05 meters for borehole FG-21. It is brown shale, which is disintegrated on its surface to a depth of about 70 cm. Thereafter, RQD varies from 17% to 89% indicating that the rock quality varies from very poor to excellent. A summary of results are provided in Table 3.3.

Table 3.3 Summary of Bedrock Characteristics for Bécancour Site

| Drilling | Type of Rock | Sample | Depth (m) | | Average elevation | RQD (%) | Remarks |
|----------|--------------|--------|-----------|-------|-------------------|---------|---------------|
| | | | From | To | | | |
| FG-19 | Shale | CF-21 | 17.95 | 18.70 | 6.79 | 0 | Friable rock |
| FG-19 | Shale | CR-22 | 18.70 | 19.00 | 6.26 | 70 | |
| FG-19 | Shale | CR-23 | 19.00 | 20.20 | 5.51 | 75 | |
| FG-21 | Shale | CR-19 | 16.05 | 16.70 | 7.65 | - | Disaggregated |
| FG-21 | Shale | CR-19 | 16.70 | 17.60 | 6.87 | 17 | |
| FG-21 | Shale | CR-20 | 17.60 | 19.00 | 5.72 | 69 | |

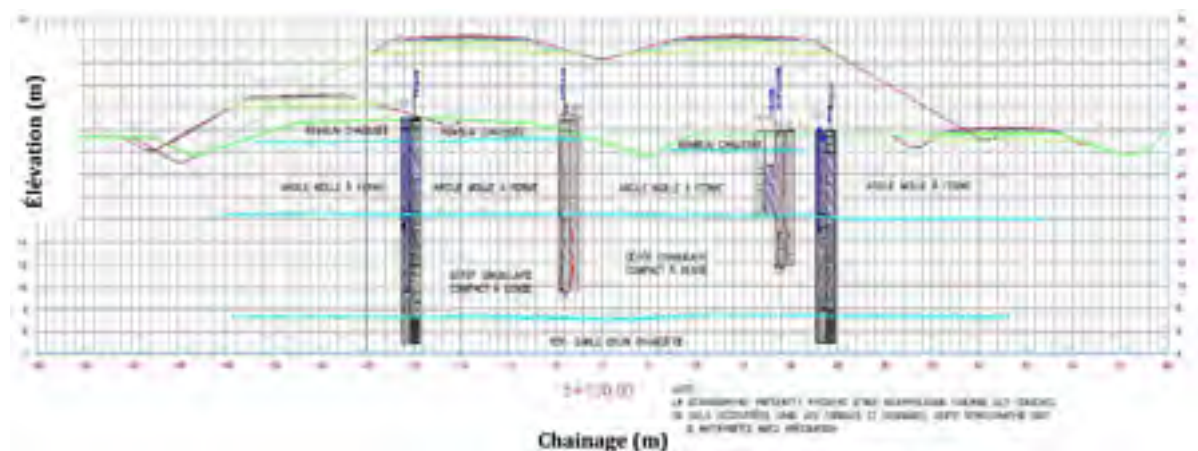


Figure 3.3 Stratigraphic profile of Bécancour Site (Qualitas 2011)

Presentation of results and choice of geotechnical parameters

This section presents the geotechnical parameters of the site soil, as obtained by tests conducted by Qualitas (2011). The profiles of the shear strength for cohesive soils and of the $(N_1)_{60}$ index for granular soils, are first presented. Subsequently, the choice of friction angle (ϕ') and saturated unit weight (γ_{sat}) is indicated. Finally, the moduli G_{max} and E'_{max} , as a function of depth, are presented and discussed.

Profiles of S_u and $(N_1)_{60}$

In the layer of cohesive soil, the shear strengths were obtained from three sources, all illustrated in Figure 3.4. The shear strength S_u derived from the falling cone tests on samples from boreholes FG-19 and FG-20 are indicated. The resistance profile obtained using Nilcon vane (borehole S-20A) is shown in the figure. Finally, the corrected toe resistance (q_T), obtained from seismic cone penetration and cone penetration tests (see SCPTU-20A, CPTU-22 and CPTU-23 in Figure 3.4) were transformed into S_u using the following equation (Leroueil, 1983):

$$S_u = \frac{\sigma_{VO} - q_t}{N_{KT}} \quad (3.1)$$

Where N_{KT} is the cone factor and is equal to 18 for this site (Qualitas, 2011). Note that the strengths obtained through Nilcon vane were used to derive the factor N_{KT} (Qualitas, 2011).

The N indices obtained from SPT testing for boreholes FG-19 and FG-21 were normalized to obtain $(N_1)_{60}$ index using the method described by Youd and Idriss (2001) using the following equation:

$$(N_1)_{60} = N_m C_N C_E C_B C_R C_S \quad (3.2)$$

Where N_m = in-situ index, C_N = factor to normalize the index at 1 atm, C_E = correction factor related to the ratio of energy of the hammer, C_B = correction for the hole diameter, C_R = correction for length of tubing and C_S = correction for the type of sampler used. The tip

resistances (q_c) were transformed into N_{60} indices using the method of Robertson et al. (1986). This method allow for the Cone Penetration Method (CPT) to be obtained through a diagram which relates SPT to the soil type encountered. The N_{60} index is then obtained using the following equation:

$$N_{60} \frac{q_c/P_a}{SBT} \quad (3.3)$$

where P_a = atmospheric pressure and q_c = uncorrected tip resistance. The conversion of q_c was performed by Qualitas (2011). Standardization of N_{60} to $(N_1)_{60}$ was performed using the method described above, assuming a factor of C_E of 1. The $(N_1)_{60}$ indices are shown in Figure 3.4 for boreholes FG-19 and FG-21 and tests CPTU-20, CPTU-22, CPTU-23 and SCPTU-20A.

After analyzing the various values S_u and $(N_1)_{60}$, a profile was developed and is shown in Figure 3.4. The corresponding stratigraphy is also shown. This stratigraphy corresponds to soil strata encountered in borehole FG-21, which was not drilled through a roadway surface structure. This choice was made with the aim to model the natural soil deposit encountered at Bécancour site.

Profile of ϕ' and γ_{sat}

Clays in Quebec generally feature a friction angle, over consolidated in the field, between 25° and 34° , with a tendency to decrease with an increase of the plasticity index (PI) (Leroueil et al., 1983). Leroueil et al. (1983) have developed a chart to relate PI to the friction angle. Table 3.4 shows the $\phi'_{n.c.}$ obtained using this chart for boreholes FG-19 and FG-21. These angles were used to determine the profile shown in Figure 3.5. The values range from 26° to 32° . In addition, CID tests, carried out by Lefebvre et al. (1981), showed an angle ϕ' of 27.1° in the critical state for the Batiscan clay, a value which fits well with the friction angle range selected. Note that the city of Batiscan is located only at about 25 km northeast of the Bécancour site. For the underlying layer of granular soil, Table 3.1 of the

manual entitled: "Bearing capacity of soil" of the U.S. Army Corps of Engineers (1992), was used to derive the friction angles. This table relates the $(N_1)_{60}$ index to a range of values of ϕ' . The profile of $(N_1)_{60}$, which was developed previously, was used. The values thus obtained vary from 34° to 42° .

Table 3.4 Friction Angle of Bécancour Clay (Qualitas 2011)

| FG-19 | | | | FG-21 | | | |
|-----------|-----------|-----------|---------|-----------|-----------|-----------|---------|
| Depth (m) | Elev. (m) | I_p (%) | ϕ' | Depth (m) | Elev. (m) | I_p (%) | ϕ' |
| 3.6 | 21.51 | 52.8 | 24.8 | 2.9 | 21.12 | 40.6 | 27 |
| 7.45 | 17.66 | 20.6 | 30.2 | 4.3 | 19.72 | 42.1 | 26.4 |
| | | | | 6.1 | 17.92 | 21.6 | 30.3 |

For the crust clay, an average γ_{sat} of 17.6 kN/m^3 was used, based on values obtained by Trak et al. (1980) in St-Alban, just north of the site under consideration. An average γ_{sat} of 16.82 kN/m^3 was selected to characterize the clay layer, based on all laboratory tests performed (Qualitas, 2011). Finally, the profile of γ_{sat} for the granular soil layer was derived on the basis of the tables developed by Holtz and Kovacs (1991). These tables relate various usual soil properties as a function of their density. Thus, the obtained values range from 19.5 kN/m^3 to 23 kN/m^3 in depth. The profile obtained is shown on Figure 3.5.

Profile of G_{max} and E'_{max}

To determine the profile of G_{max} as a function of depth, the shear wave velocity (V_s) obtained by the seismic cone penetration test (SCPTU-20A) was used. The following relation relates V_s to G_{max} (Kramer, 1996):

$$G_{\text{max}} = \rho V_s^2 \quad (3.4)$$

Where ρ =density of the layer. An average density of 1715 kg/m^3 was used for the clay layer and an average density of 1988 kg/m^3 for the granular layer. The following classical elasticity relation was then used to determine the profile of E'_{\max} :

$$E'_{\max} = 2G_{\max}(1 + \nu') \quad (3.5)$$

Where a Poisson's ratio (ν') of 0.3 was assumed for all soil deposits (Holtz and Kovacs, 1991). The values of G_{\max} range from 8 to 32 MPa for the clay and from 86 to 132 MPa for the granular layers. The values of E'_{\max} range from 22.47 to 81.25 MPa for the clay layer and from 225.68 to 341.36 MPa for the granular soil layer. The obtained profiles of G_{\max} and E'_{\max} are illustrated in Figure 3.6.

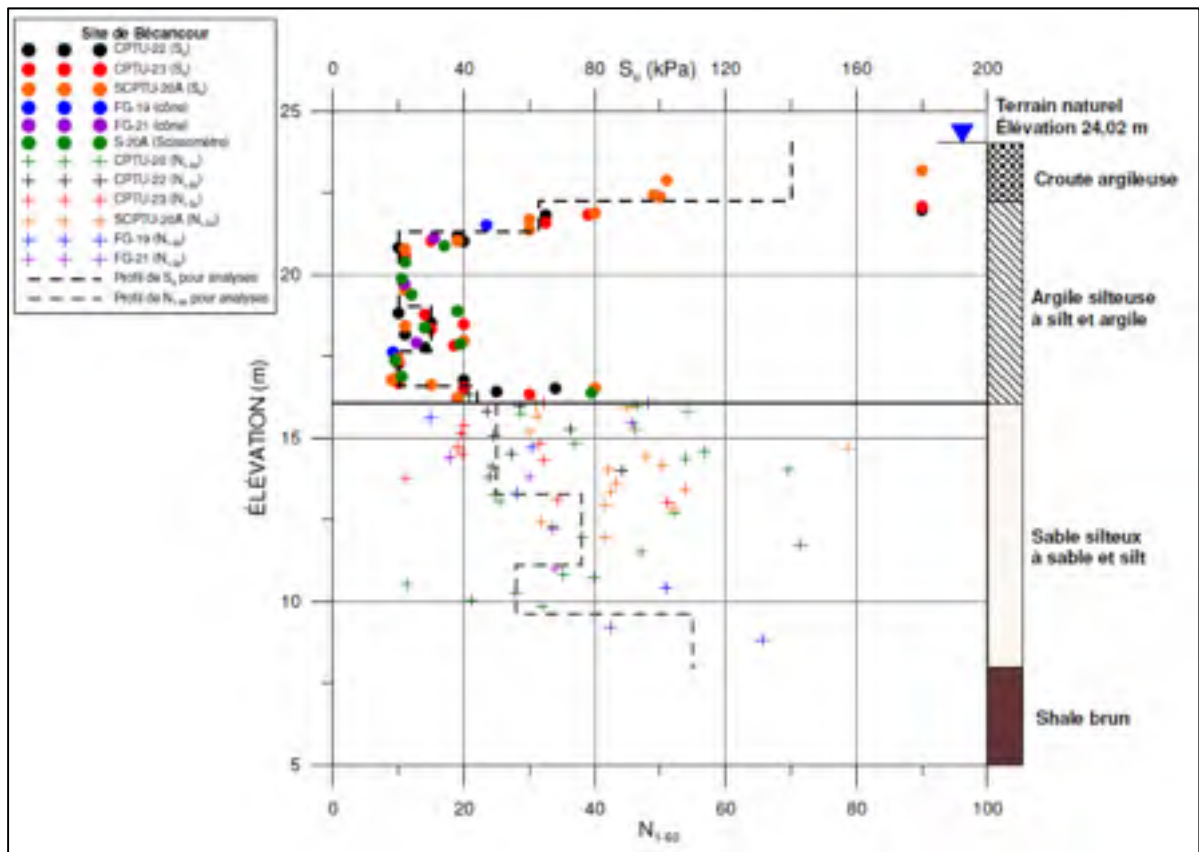


Figure 3.4 Profiles of S_u and $(N_1)_{60}$ for Bécancour Site

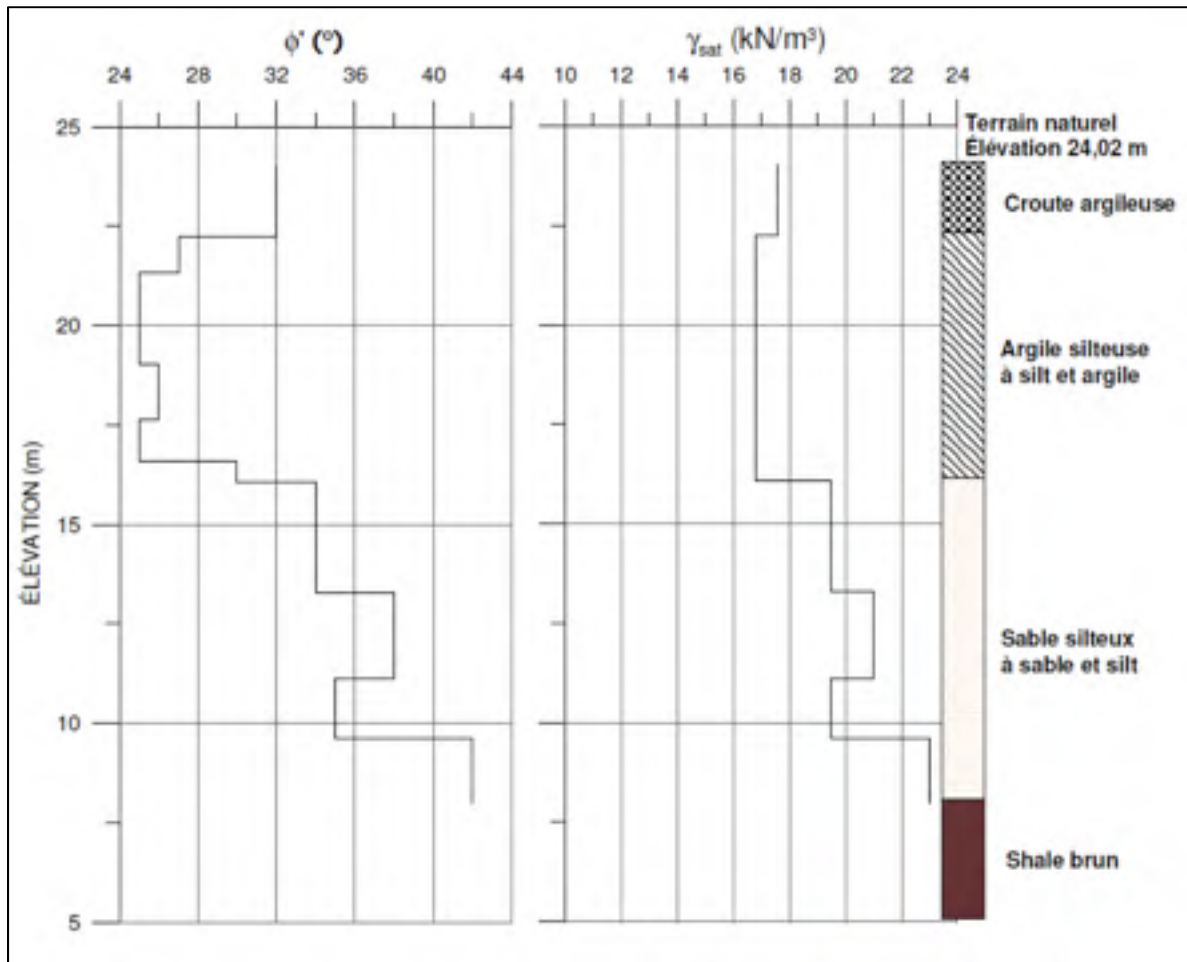


Figure 3.5 Profile of ϕ' and γ_{sat} for Bécancour Site

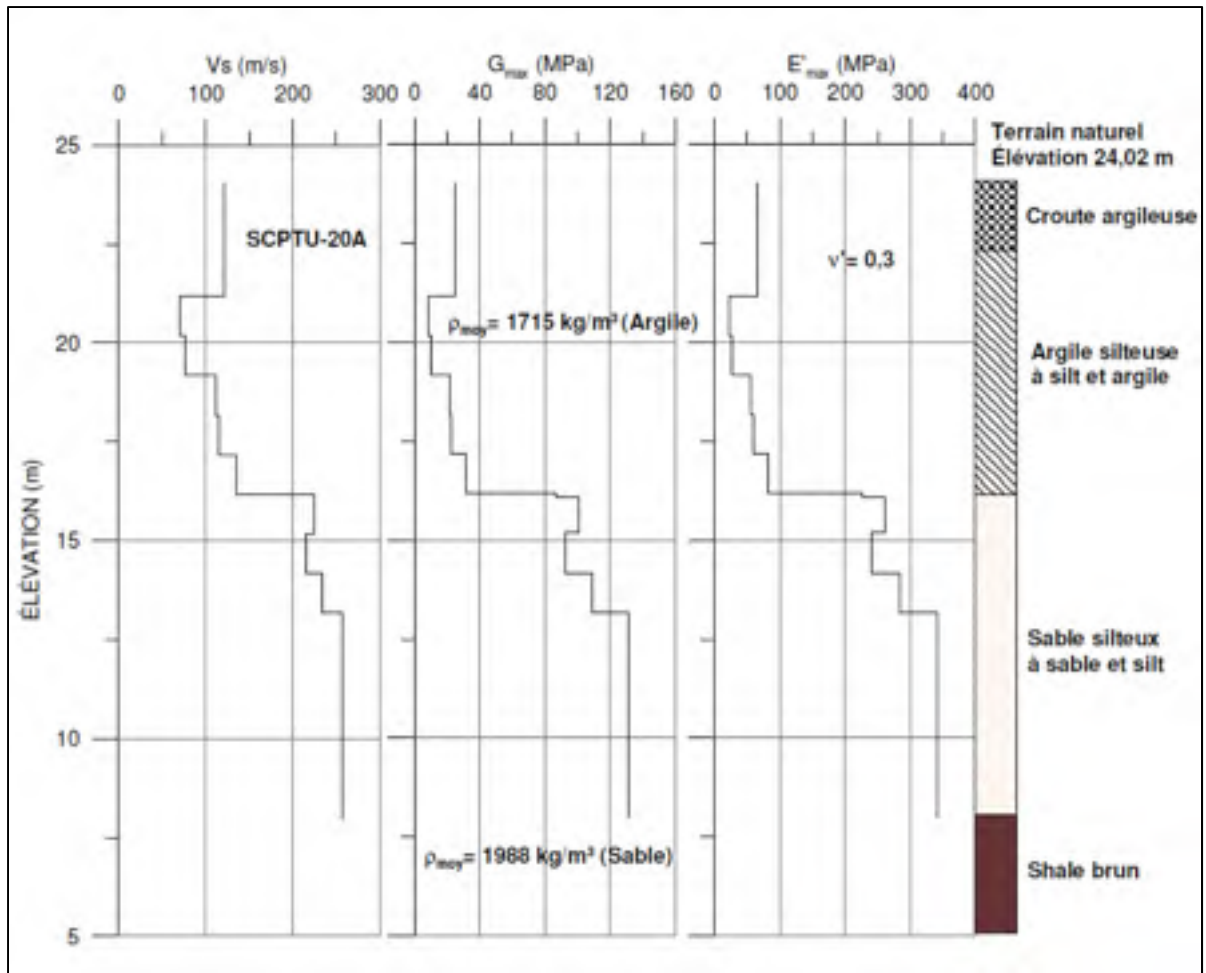


Figure 3.6 Profiles of G_{max} and E'_{max} for Bécancour Site

3.2.6 Presentation of the profile for analysis

Figure 3.7 presents a summary of the stratigraphy and geotechnical properties of the different layers for Bécancour site. This profile will be used for modeling. Note that the value of drained cohesion (c') of the clay layer is derived from tests performed by Lefebvre et al. (1981) on the soft clay of the city of Bastican, which is located close to Bécancour site.

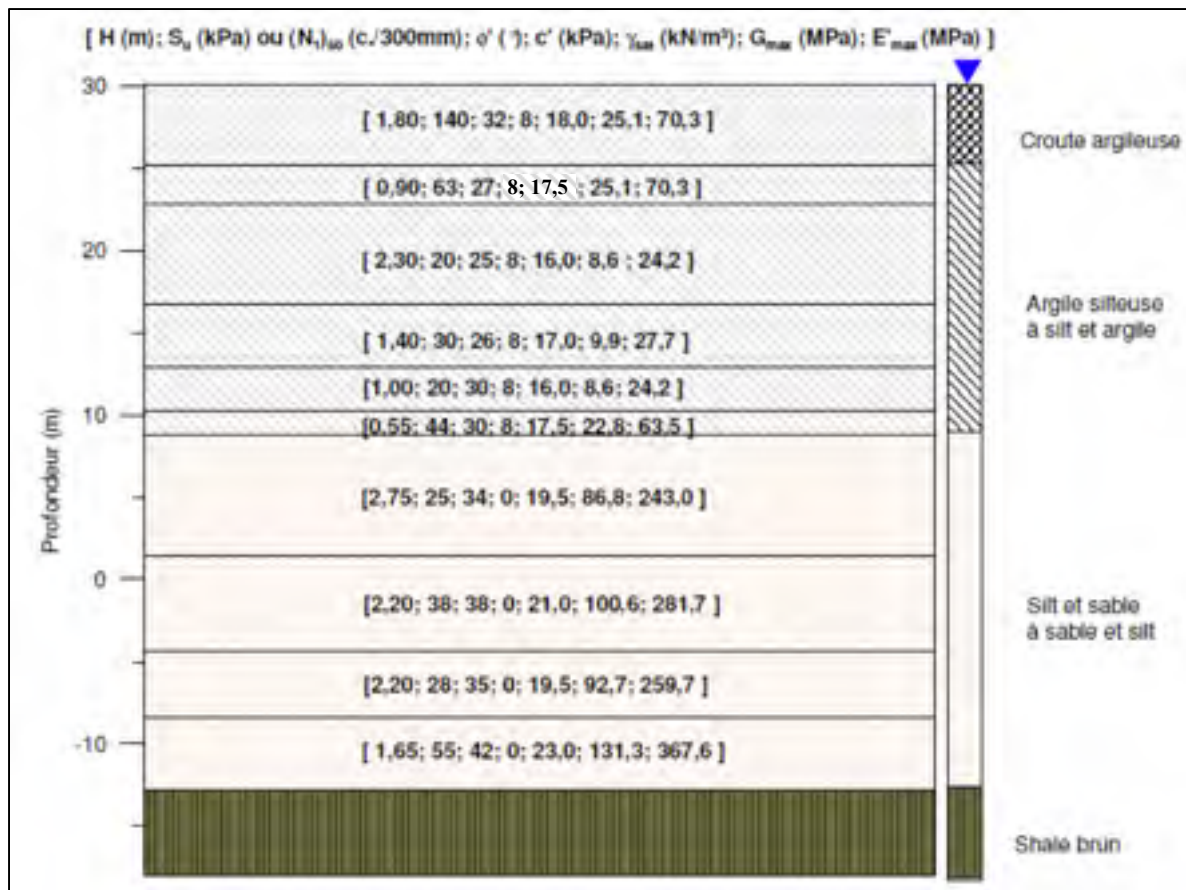


Figure 3.7 Profile of Stratigraphy and Geotechnical Properties Used for Analysis for Bécancour

3.3 Québec City site

This section describes the second site (Quebec City) location. It also presents the process that led to the selection of geotechnical and stratigraphic profiles to be used in modeling and analysis.

3.3.1 Location

The second site is located in the borough of Ste-Foy in Québec City. Figure 3.8 illustrates the geographical location of the project, at the intersection of Robert-Bourassa (A740) and Charest (A440) Highways.



Figure 3.8 Location of the Québec Site (MTQ 2009, Google 2012)

3.3.2 Local geology

The soil of Québec City is made up of three geological provinces as follows: North, the Canadian Shield (Province of Greenville) in the north, the lowlands of the St. Lawrence in the center, and finally, the Appalachian Mountains in the south (*Ministère des Ressources Naturelles et de la Faune du Québec*, MRNF, 2012). The Logan Fault defines the boundary between the Lower Town of Québec (Lowlands of St-Lawrence), and the Upper Town (Appalachian Mountains) (MRNF, 2012). This fault runs through the city of Cap-Rouge to downtown. The study site is located directly on the border between the Lowlands and the Appalachian Mountains. The erosion of the mountains due to the icecap moving during the glacial periods caused the deposit of thick layers of sand and gravel. These sand and gravel deposits are present at the study site (Natural Resources Canada, 2012).

3.3.3 Data analysis

This section summarizes the work performed on site and presents a description of the stratigraphy encountered. Subsequently, details of the main results will be processed, allowing the development of a representative soil profile at the intersection of Robert-Bourassa and Charest Highways.

3.3.4 Summary of work done

Given the broad extent of the project, this study targets a particular section of borehole data, developed by the Department of Transportation of Québec in 2008 and 2009. This particular section is related to the soil under the ramp linking the southbound of Robert-Bourassa Highway to the westbound of Charest Highway. This choice was made because of easier access to the site in case further investigations were to be required during the course of the present study. In addition, the fact that the zone of Einstein Street is safe with no major traffic motivated the choice of nearby soil boreholes F-09 to F-16 on a total of sixteen boreholes realized in that section. Figure 3.9 shows the location plan of the boreholes related to the targeted work zone of this study. Table 3.5 presents a summary of the boreholes considered in the present study. The terrain is relatively flat and the depth of drilling varied from 9.41 m to 12.00 m.

Table 3.5 Summary of Boreholes Considered in this Study

| | Surface Elevation | Depth | Base Elevation |
|----------|-------------------|-------|----------------|
| Drilling | (m) | (m) | (m) |
| F-09 | 19.82 | 9.41 | 10.41 |
| F-10 | 19.50 | 12.00 | 7.50 |
| F-11 | 19.04 | 11.51 | 7.53 |
| F-12 | 19.70 | 11.75 | 7.95 |
| F-13 | 18.90 | 9.89 | 9.01 |
| F-14 | 19.64 | 18.58 | 1.06 |
| F-15 | 18.73 | 10.35 | 8.38 |
| F-16 | 19.13 | 10.30 | 8.83 |

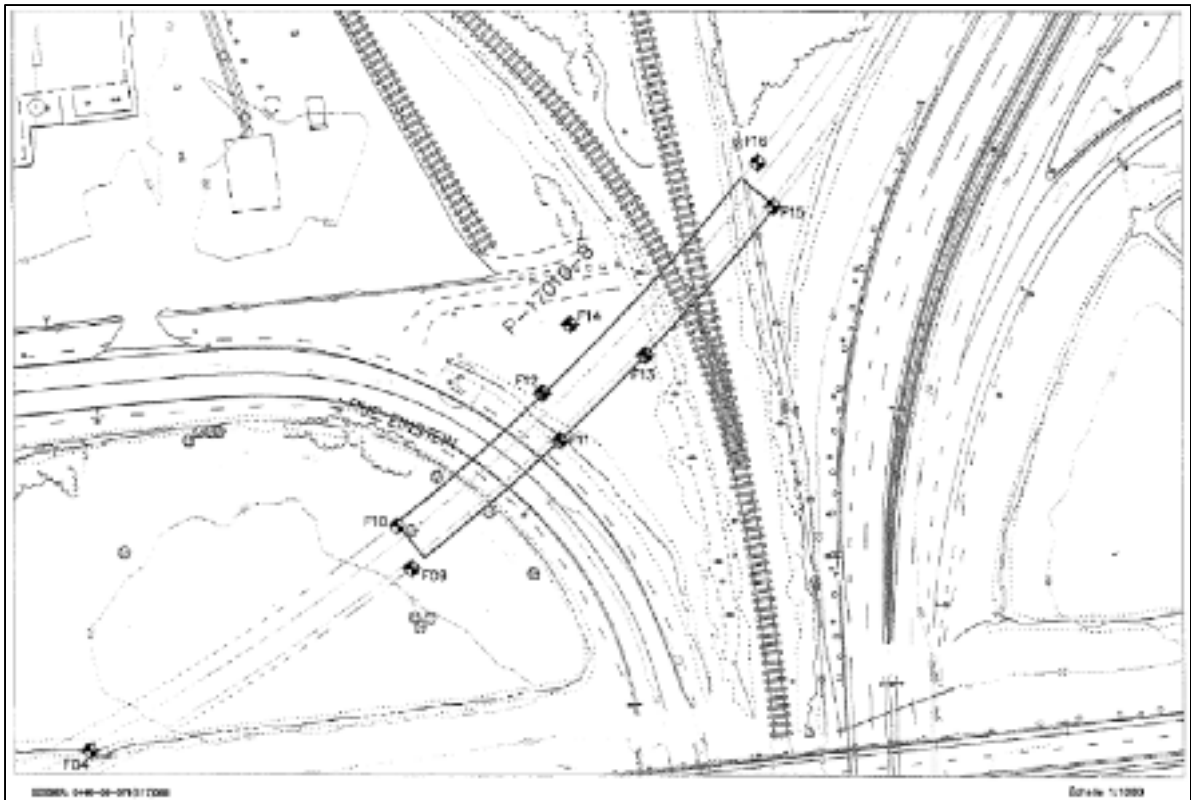


Figure 3.9 Location of the Boreholes: Site of Québec City (MTQ 2009)

In addition to the boreholes and the visual observations that were realized, the following laboratory tests were performed on selected samples taken during the in-situ work:

- Particle size analysis by mechanical sieving (BNQ-2501-025)
- Sedimentometry (BNQ-2501-025)
- Water content (BNQ-2501-170)
- Plasticity and liquidity limits (BNQ-2501-092)

Tables 3.6 through 3.8 present the overall results obtained in the field and in laboratory. Note that the SPT N index has not been corrected. The results are raw data extracted from boring reports of drillings. The RQD for the bedrock reached during the drilling is also indicated, when available. An examination of these tables show that the soil is mainly granular, and the

layer of silt and sand on surface has a low to medium plasticity if we refer to w_L and I_p obtained from tests (Holtz and Kovacs, 1991).

Casagrande type piezometers were installed at the locations of F-09, F-10 and F-12 to F-16. Table 3.9 shows all the elevations and depths of water tables observed. It is seen that the shallowest water table, observed in borehole F-13, was only at 0.2m depth in January. Therefore, the water table will be considered on surface during subsequent analyses. Indeed, the spring season will likely lead to fluctuating surface water as the snow will melt.

Finally, dilatometer tests were performed in the bedrock at the locations of boreholes F-11 and F-14, in order to determine the parameters of elastic moduli (E_m). The tests were conducted at depths of 19.1 m, 18.1 m, 17.1 m, 15.1 m, 14.1 m and 13.1 m. The results at various depths yield a profile of the rigidity of the rock in the elastic range.

Table 3.6 Overall SPT and Laboratory Results (F-09 to F-11)

| Depth (m) from to | | Soil | % FC | w (%) | w _L (%) | I _p (%) | N (c/300 mm) | Compactness |
|----------------------|-------|---------------------------------|---------|----------|-----------------------|-----------------------|-----------------|---|
| Drilling F-09 | | | | | | | | |
| 0.00 | 1.00 | topsoil | - | - | - | - | - | - |
| 1.00 | 2.30 | silt and sand | - | - | - | - | 9 | loose |
| 2.30 | 3.80 | silt and sand | - | - | - | - | 12 | medium |
| 3.80 | 4.60 | silt, sand, and rock climbed | - | - | - | - | refusal | very dense refusal on rock fragments |
| 4.60 | 5.00 | sand and silt | - | - | - | - | 56 | very dense |
| 5.00 | 7.60 | sand and silt | - | - | - | - | 18 | medium |
| 7.60 | 8.00 | sand and silt (gritty) | - | - | - | - | 41 | dense |
| 8.00 | 9.30 | sand and silt (gritty) | - | - | - | - | 21 | compact |
| 9.30 | 9.41 | shale | - | - | - | - | - | very poor quality |
| Drilling F-10 | | | | | | | | |
| 0.00 | 1.10 | topsoil | - | - | - | - | - | - |
| 1.10 | 1.50 | silt and sand | - | - | - | - | 4 | very loose |
| 1.50 | 3.05 | clayey silt | 89.1 | - | 34.2 | 14.2 | 9 | loose |
| 3.05 | 4.50 | silty sand | 38.9 | - | 18.0 | 2.0 | 7 | loose |
| 4.50 | 5.30 | gravel | - | - | - | - | 12 | medium |
| 5.30 | 8.50 | sand and silt | 37.5 | - | 16.0 | 1.0 | 18 | medium |
| 8.50 | 9.27 | shale | - | - | - | - | - | very poor quality |
| 9.27 | 12.00 | shale | - | - | - | - | - | RQD = 34% |
| Drilling F-11 | | | | | | | | |
| 0.00 | 1.60 | silt and sand (embankment) | 62.0 | - | 30.0 | 10.0 | 4 | very loose |
| 1.60 | 2.20 | silty sand | - | - | - | - | 21.0 | compact |
| 2.20 | 4.40 | silty sand | 39.5 | - | 17.0 | 1.0 | 10 | loose |
| 4.40 | 5.20 | silty sand | - | - | - | - | 60 | very dense |
| 5.20 | 6.00 | silty sand | 37.5 | - | 15.0 | 0.0 | 17 | medium |
| 6.00 | 7.68 | silty sand | 44.0 | - | 18.0 | 2.0 | 31 | dense |
| 7.68 | 9.03 | gravelly silty sand | - | - | - | - | refusal | very dense |
| 9.03 | 11.51 | shale | - | - | - | - | - | RQD = 0% |
| 11.51 | 19.67 | shale | - | - | - | - | - | RQD = 0 to 61% to 14% |

Table 3.7 Overall SPT and Laboratory Results (F-12 to F-14)

| Depth (m) from | to | Soil | % FC | w (%) | w _L (%) | I _p (%) | N (c/300 mm) | Compactness |
|----------------------|-------|-----------------------------|---------|----------|-----------------------|-----------------------|-----------------|-------------|
| Drilling F-12 | | | | | | | | |
| 0.00 | 0.15 | topsoil | - | - | - | - | - | - |
| 0.15 | 1.58 | sandy silt (embankment) | - | - | - | - | 9 | loose |
| 1.58 | 2.40 | silt and sand | 61.5 | 20.0 | 30.0 | 12.0 | 11 | medium |
| 2.40 | 3.00 | sand and silt | - | - | - | - | 17.0 | medium |
| 3.00 | 4.50 | sand and silt | - | - | - | - | 12 | medium |
| 4.50 | 5.30 | sand and silt | 43.9 | 10.0 | 19.0 | 2.0 | 4 | very loose |
| 5.30 | 6.10 | sand and silt | - | - | - | - | 28.0 | compact |
| 6.10 | 6.80 | sandy silt | - | - | - | - | 14.0 | medium |
| 6.80 | 7.92 | sandy silt | - | - | - | - | 52.0 | very dense |
| 7.92 | 10.35 | shale | - | - | - | - | - | RQD = 0% |
| 10.35 | 11.75 | shale | - | - | - | - | - | RQD = 78% |
| Drilling F-13 | | | | | | | | |
| 0.00 | 0.10 | topsoil | - | - | - | - | - | - |
| 0.10 | 2.30 | silty sand (embankment) | 34.4 | 17.0 | 23.0 | 6.0 | 2.0 | very loose |
| 2.30 | 3.00 | sand with traces of silt | - | - | - | - | 2 | very loose |
| 3.00 | 3.80 | silty sand | - | - | - | - | 7 | loose |
| 3.80 | 4.50 | sand and silt | 43.2 | 12.0 | 18.0 | 2.0 | 5 | loose |
| 4.50 | 5.20 | sand and silt | - | - | - | - | 17.0 | medium |
| 5.20 | 6.00 | silty sand | 28.2 | 9.0 | 15.0 | 1.0 | 59 | very dense |
| 6.00 | 6.80 | silty sand | - | - | - | - | 17 | medium |
| 6.80 | 7.77 | shale | - | - | - | - | - | RQD = 0% |
| 7.77 | 9.29 | shale | - | - | - | - | - | RQD = 43% |
| 9.29 | 9.89 | shale | - | - | - | - | - | RQD = 0% |
| Drilling F-14 | | | | | | | | |
| 0.00 | 0.10 | topsoil | - | - | - | - | - | - |
| 0.10 | 1.30 | sandy silt (embankment) | - | - | - | - | 9.0 | loose |
| 1.30 | 2.00 | sandy silt (embankment) | - | - | - | - | 27 | compact |
| 2.00 | 3.80 | sand and silt | - | - | - | - | 18 | medium |
| 3.80 | 6.00 | sand and silt | 43.9 | 12.0 | 18.0 | 2.0 | 6 | loose |
| 6.00 | 6.70 | sand and silt | - | - | - | - | 46.0 | dense |
| 6.70 | 7.50 | sand, and little silt | - | - | - | - | 0 | very loose |
| 7.50 | 8.30 | sand and silt | 37.9 | 10.0 | 17.0 | 1.0 | 18 | medium |
| 8.30 | 10.02 | shale | - | - | - | - | - | RQD = 0% |
| 10.02 | 10.98 | shale | - | - | - | - | - | RQD = 28% |
| 10.98 | 14.02 | shale | - | - | - | - | - | RQD = 69% |
| 14.02 | 18.58 | shale (friable) | - | - | - | - | - | RQD = 26% |

Table 3.8 Overall SPT and Laboratory Results (F-15 to F-16)

| Depth from | to | Soil | % FC | w (%) | w _L (%) | I _p (%) | N (c/300 mm) | Compactness |
|----------------------|-------|---------------|---------|----------|-----------------------|-----------------------|-----------------|-------------|
| Drilling F-15 | | | | | | | | |
| 0.00 | 0.15 | topsoil | - | - | - | - | - | - |
| 0.15 | 1.40 | silty sand | - | - | - | - | 22.0 | compact |
| 1.40 | 3.81 | sand and silt | 42.1 | 12.0 | 19.0 | 2.0 | 4 | very loose |
| 3.81 | 4.50 | silty sand | 36.5 | 10.0 | 18.0 | 1.0 | 12 | medium |
| 4.50 | 5.70 | silt and sand | - | - | - | - | 7 | loose |
| 5.70 | 6.40 | silty sand | 26.0 | 10.0 | 17.0 | 0.5 | 11.0 | medium |
| 6.40 | 10.35 | shale | - | - | - | - | - | RQD = 0% |
| Drilling F-16 | | | | | | | | |
| 0.00 | 0.30 | topsoil | - | - | - | - | - | - |
| 0.30 | 1.50 | silty sand | - | - | - | - | 10.0 | loose |
| 1.50 | 2.00 | sand and silt | - | - | - | - | 17 | medium |
| 2.00 | 3.81 | silty sand | - | - | - | - | 11 | medium |
| 3.81 | 6.00 | sand and silt | 41.6 | 11.0 | 18.0 | 1.0 | 5 | loose |
| 6.00 | 6.80 | silty sand | 34.9 | 8.0 | 17.0 | 1.0 | 45.0 | dense |
| 6.80 | 8.78 | shale | - | - | - | - | - | RQD = 0% |
| 8.78 | 10.30 | shale | - | - | - | - | - | RQD = 9% |

Table 3.9 Water Table Depths for Boreholes F-09 to F-16

| | Depth | Elevation | Date of survey |
|----------|-------|-----------|----------------|
| Drilling | (m) | (m) | |
| F-09 | 0.30 | 19.52 | 2008-11-05 |
| F-10 | 0.30 | 19.20 | 2008-11-05 |
| F-12 | 0.30 | 19.40 | 2009-01-15 |
| F-13 | 0.20 | 18.70 | 2009-01-22 |
| F-14 | 1.20 | 18.44 | 2009-01-27 |
| F-15 | 0.90 | 17.83 | 2009-02-05 |
| F-16 | 1.70 | 17.43 | 2009-02-05 |

3.3.5 Summary of the stratigraphy

This section presents the general stratigraphy encountered at the site of Quebec City. Each soil layer will be described and discussed. Figure 3.10 provides a comprehensive overview of the soil based on soil type encountered in the different layers of the eight wells tested.

Topsoil

A layer between 0.1 m and 1.0 m thick topsoil was encountered at the location of borehole F-09, F-10 and F-12 to F-16.

Fill (silt and sand)

An embankment composed of silt and sand was observed beneath the topsoil at the locations of boreholes F-09 to F-12 and F-14. Gravel and stones were present at the base of this layer in borehole F-09. The layer was loose to dense and its N index varied from 4 to 27. Given its liquidity index (w_L) ranging between 30% to 34.2% and its plasticity index (I_p) ranging from 10% to 14.2%, the soil can be qualified as having low to medium plasticity (Holtz and Kovacs, 1991). The percentage of fine particles ranges from 61.5% to 89.1%. The fill thickness varies from 1.6 m (F-11) to 3.6 m (F-09).

Deposit of granular soil

A granular soil deposit consisting of sand and silt is present beneath the fill for boreholes F-09 to F-12 and F-14 and beneath the topsoil for boreholes F-13, F-15 and F-16. The silt content decreased and the deposit became gradually silty sand as depth increased. The proportion of fine particles of soil varied from 26% to 44% and the N index ranged from 2 (surface) to 59 (deep). Therefore, the soil varies from very loose to very dense. The thickness of the deposit varies from 4.7 m (F-09) to 7.43 m (F-11).

Bedrock

The bedrock was reached for all boreholes at a depth varying from 6.40 m (F-15) to 9.3 m (F-09). The bedrock is a shale of very poor quality ($RQD = 0\%$) within a thickness of 2.15 m on

average. The quality of the cradle then improved as the depth increased, becoming even very good (RQD = 79%) at borehole F-12. At greater depth (15.52 m), the quality of the shale starts to deteriorate at borehole F-11. Indeed, the RQD index fell from 61% to 14% and then to 0%. Its quality, however, tends to increase again thereafter.

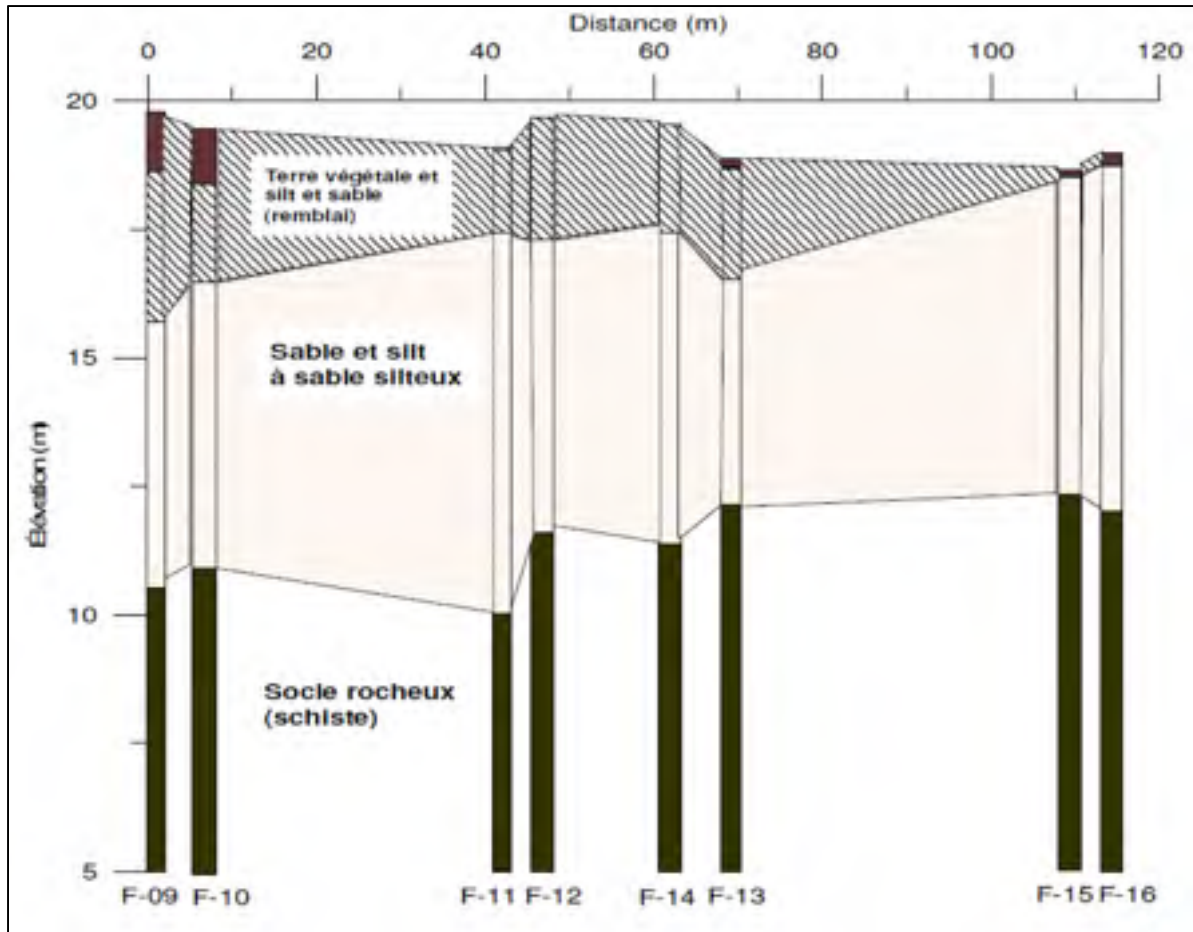


Figure 3.10 Stratigraphy of Quebec City Site (F-09 to F16)

Presentation of results and choice of geotechnical parameters

This section presents the steps that led to the selection of geotechnical parameters representative of the existing soil at the site of Quebec City. The index profiles $(N_1)_{60}$, ϕ' , of γ_{sat} , of G_{max} and E'_{max} are illustrated.

Profile of $(N_1)_{60}$

Similarly to the site of Bécancour, the N indices obtained using SPT tests were normalized to obtain corresponding $(N_1)_{60}$ Indices. The same methodology described earlier for Bécancour site was used for normalization. A correction factor of 0.75 was used for the energy ratio (C_E) due to the use of a "Donut" hammer. Figure 3.11 shows the $(N_1)_{60}$ indices obtained for the boreholes F-09 to F-16 as a function of elevation. The corresponding stratigraphy is also depicted in the figure. The layer thicknesses correspond to those encountered in borehole F-11. These thicknesses were selected because no topsoil was encountered in this borehole, and it is also at this location that the dilatometer test in the bedrock was carried out. The properties of the bedrock are therefore better defined compared to other boreholes.

Profile of ϕ' and γ_{sat}

The friction angles were derived using Table 3.1 of the manual entitled: "Bearing capacity of soil", by the USACE (1992) on one hand and values of the profile index $(N_1)_{60}$, built at the previous section, on the other hand. Thus, the obtained values vary from 29° at the surface to 32° in depth. The γ_{sat} profile was elaborated based on the density of the soils encountered, using the tables elaborated by Holtz and Kovacs (1991). The γ_{sat} values range from 18.5 to 19.5 kN/m³. Figure 3.12 illustrates the profiles selected for subsequent analyzes.

Profile of G_{max} and E'_{max}

The profile of the shear modulus G_{max} was calculated using the following equation:

$$G_{max} = 21.7(P_{atm}) K_{2,max} \sqrt{\frac{\sigma'_m}{P_{atm}}} \quad (3.6)$$

where P_{atm} = atmospheric pressure (101.3 kPa), σ'_m = mean effective stress = $(\sigma'_1 + \sigma'_2 + \sigma'_3)/3$ and

$$K_{2,max} = 20 ((N_1)_{60})^{(1/3)} \quad (3.7)$$

The mean effective stress was assessed by setting $\sigma'_2 = \sigma'_3$, and using the following equations:

$$K_0 = 1 - \sin \phi' \quad (3.8)$$

$$\sigma'_3 = K_0 \sigma'_1 \quad (3.9)$$

Thereafter, the profile of E'_{\max} has been evaluated using the theory of elasticity and the same equation as for Bécancour site (see section 3.2.3) and a Poisson's ratio of 0.3 (Holtz and Kovacs, 1991). The values of G_{\max} varied from 16.20 MPa to 42.13 MPa, whereas the values of E'_{\max} varied from 76.52 MPa to 198.95 MPa. Figure 3.13 shows the profiles of G_{\max} and E'_{\max} for the site of Quebec City.

Profiles of elastic modulus of the bedrock

Table 3.10 presents a summary of the RQD values for the boreholes performed in the Québec site. It is seen that the RQD index varied between 0% and 78%. These indices can be used to derive certain parameters of the bedrock through empirical equations.

Using the data obtained from dilatometer tests, the values of E_m were derived for different depths at the locations of boreholes FG-11 and FG-14 by the MTQ (2009). It was observed that the values of the moduli were very sensitive to the choice of the data points of the experimental curves. Therefore, the MTQ developed ranges of values taking into consideration this uncertainty. Table 3.11 presents the range of values thus obtained for E_m . It is seen that the minimum values range from 255 to 950 MPa, whereas the maximum values vary from 330 to 1210 MPa.

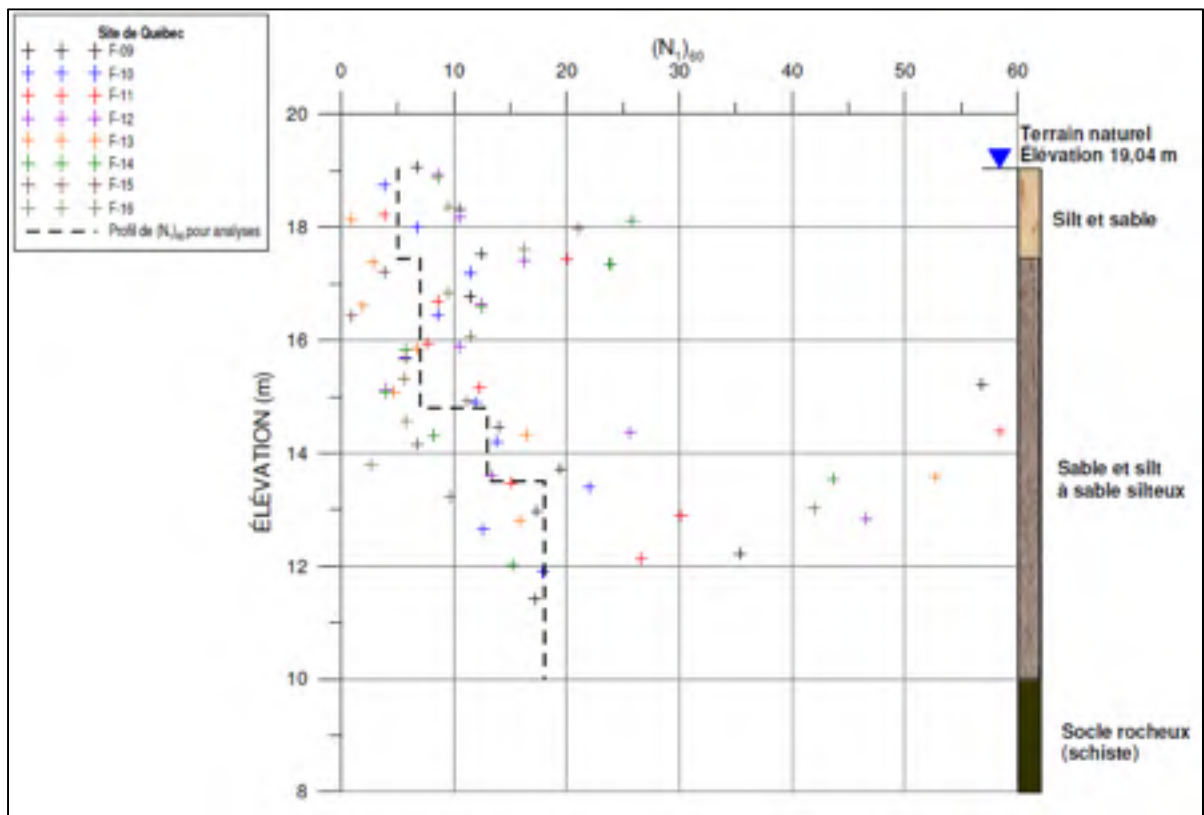
Table 3.10 Summary of the RQD Values for Boreholes of Québec site

| Drilling | Type of Rock | Sample | Depth (m) | | Average elevation | RQD (%) | Remarks |
|----------|--------------|--------|-----------|-------|-------------------|---------|------------------|
| | | | From | To | | | |
| F-10 | Schist | CR-6 | 9.15 | 10.40 | 9.73 | 39 | |
| F-10 | Schist | CR-7 | 10.40 | 12.00 | 8.30 | 29 | |
| F-11 | Schist | CR-1 | 8.96 | 9.60 | 9.76 | 0 | |
| F-11 | Schist | CR-2 | 10.46 | 10.65 | 8.49 | 0 | |
| F-11 | Schist | CR-3 | 11.51 | 12.58 | 7.00 | 25 | |
| F-11 | Schist | CR-4 | 12.85 | 14.15 | 5.54 | 36 | Dilatometer test |
| F-11 | Schist | CR-5 | 14.15 | 15.52 | 4.21 | 61 | Dilatometer test |
| F-11 | Schist | CR-6 | 15.52 | 17.05 | 2.76 | 14 | |
| F-11 | Schist | CR-7 | 17.05 | 17.40 | 1.82 | 0 | Dilatometer test |
| F-11 | Schist | CR-8 | 17.40 | 18.57 | 1.06 | 44 | Dilatometer test |
| F-11 | Schist | CR-9 | 18.57 | 19.67 | -0.08 | 20 | Dilatometer test |
| F-12 | Schist | CR-11 | 7.92 | 9.15 | 11.17 | 0 | |
| F-12 | Schist | CR-12 | 9.15 | 10.35 | 9.95 | 0 | |
| F-12 | Schist | CR-13 | 10.35 | 11.75 | 8.65 | 78 | |
| F-13 | Schist | CR-41 | 6.86 | 7.77 | 11.59 | 0 | |
| F-13 | Schist | CR-42 | 7.77 | 9.29 | 10.37 | 43 | |
| F-13 | Schist | CR-43 | 9.29 | 9.89 | 9.31 | 0 | |
| F-14 | Schist | CR-25 | 8.38 | 10.02 | 10.44 | 0 | |
| F-14 | Schist | CR-26 | 10.02 | 10.98 | 9.14 | 28 | |
| F-14 | Schist | CR-27 | 10.98 | 12.50 | 7.90 | 61 | Dilatometer test |
| F-14 | Schist | CR-28 | 12.50 | 14.02 | 6.38 | 78 | Dilatometer test |
| F-14 | Schist | CR-29 | 14.02 | 15.54 | 4.86 | 28 | |
| F-14 | Schist | CR-30 | 15.54 | 17.06 | 3.34 | 26 | Dilatometer test |
| F-14 | Schist | CR-31 | 17.06 | 18.58 | 1.82 | 24 | Dilatometer test |
| F-15 | Schist | CR-85 | 6.75 | 7.53 | 11.59 | 0 | |
| F-15 | Schist | CR-86 | 7.53 | 8.95 | 10.49 | 0 | |
| F-15 | Schist | CR-87 | 8.95 | 10.35 | 9.08 | 0 | |
| F-16 | Schist | CR-75 | 6.86 | 8.78 | 11.31 | 0 | |
| F-16 | Schist | CR-76 | 8.78 | 10.30 | 9.59 | 9 | |

Table 3.11 Range of Values for E_m of Bedrock

| Depth (m) | Elevation (m) | Minumin E_m (MPa) | Maximum E_m (MPa) |
|--------------|---------------|---------------------|---------------------|
| FG-11 | | | |
| 13.10 | 5.94 | 785 | 920 |
| 14.10 | 4.94 | 810 | 915 |
| 15.10 | 3.94 | 255 | 330 |
| 17.10 | 1.94 | - | 80* |
| 18.10 | 0.94 | 950 | 1210 |
| 19.10 | -0.06 | 450 | 600 |
| FG-14 | | | |
| 11.00 | 8.64 | 380 | 500 |
| 12.00 | 7.64 | 400 | 450 |
| 13.00 | 6.64 | 805 | 940 |
| 14.00 | 5.64 | 485 | 535 |
| 15.66 | 3.98 | 860 | 1045 |
| 17.66 | 1.98 | 335 | 335 |

*Doubtful test

Figure 3.11 Profile of $(N_1)_{60}$ Index as a Function of Elevation

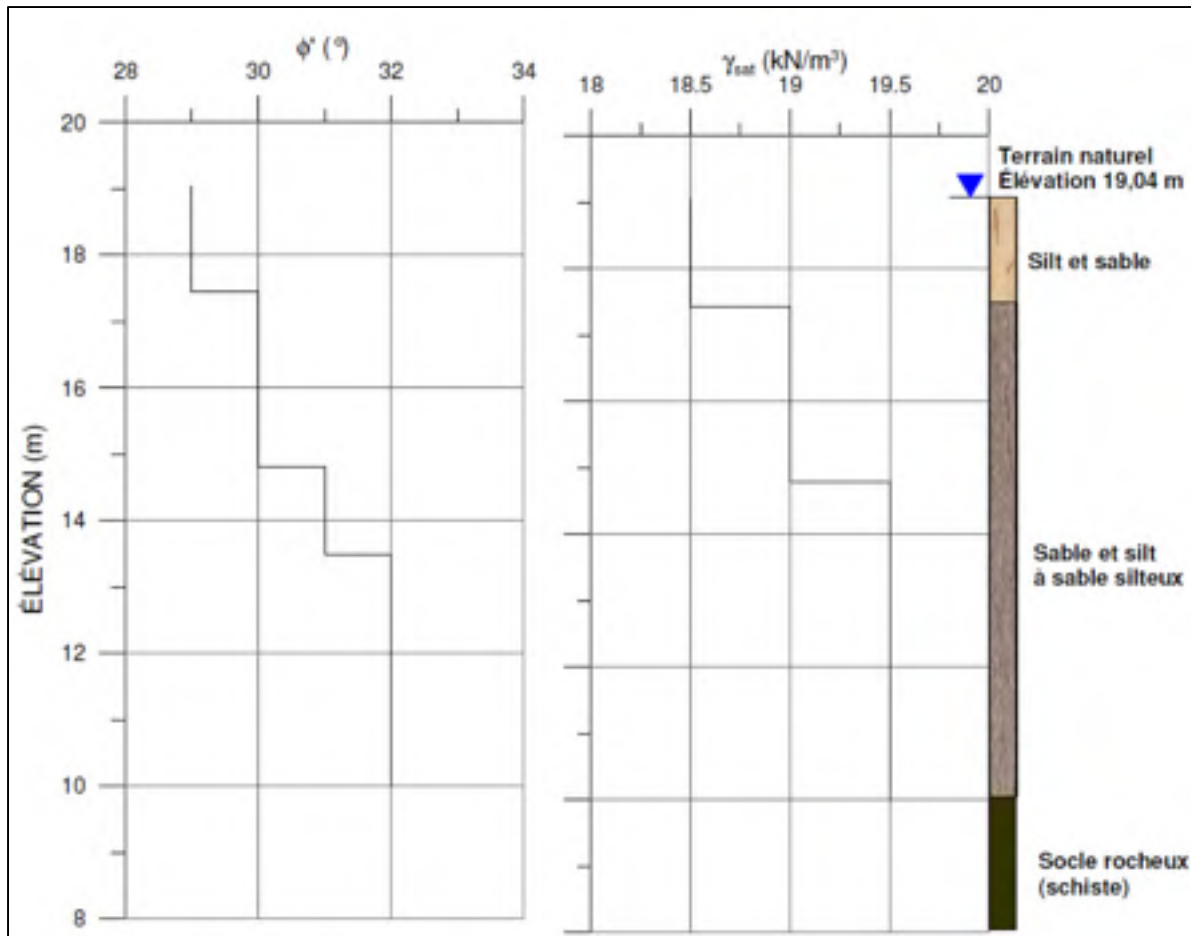


Figure 3.12 Profile of ϕ' and γ_{sat} for the Site of Québec City

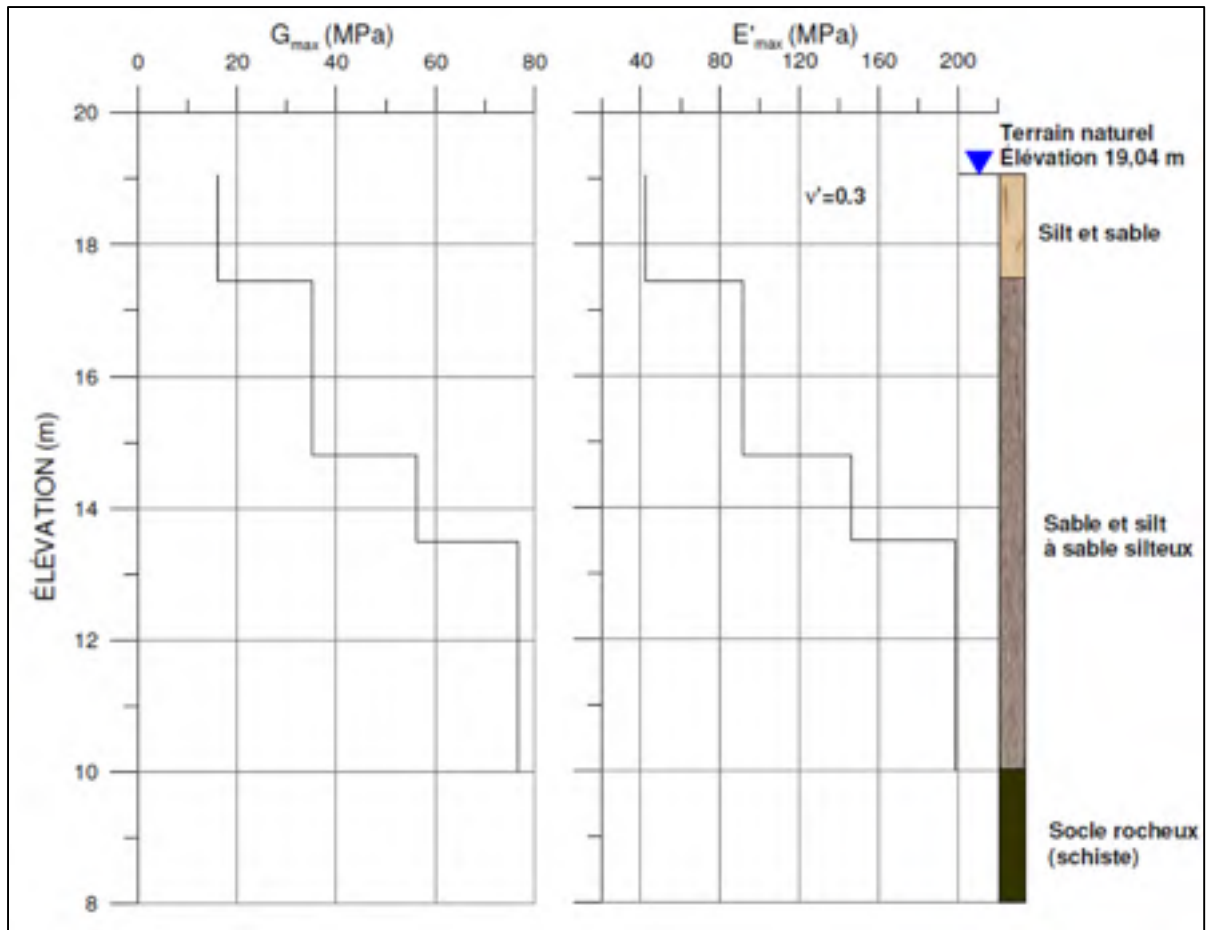


Figure 3.13 Profiles of G_{max} and E'_{max} for the site of Quebec City

3.3.6 Presentation of the profile for analysis

Figure 3.14 presents a summary of the stratigraphy and geotechnical properties selected for the different layers of soil at the site of Quebec City. This profile will be used for modeling.

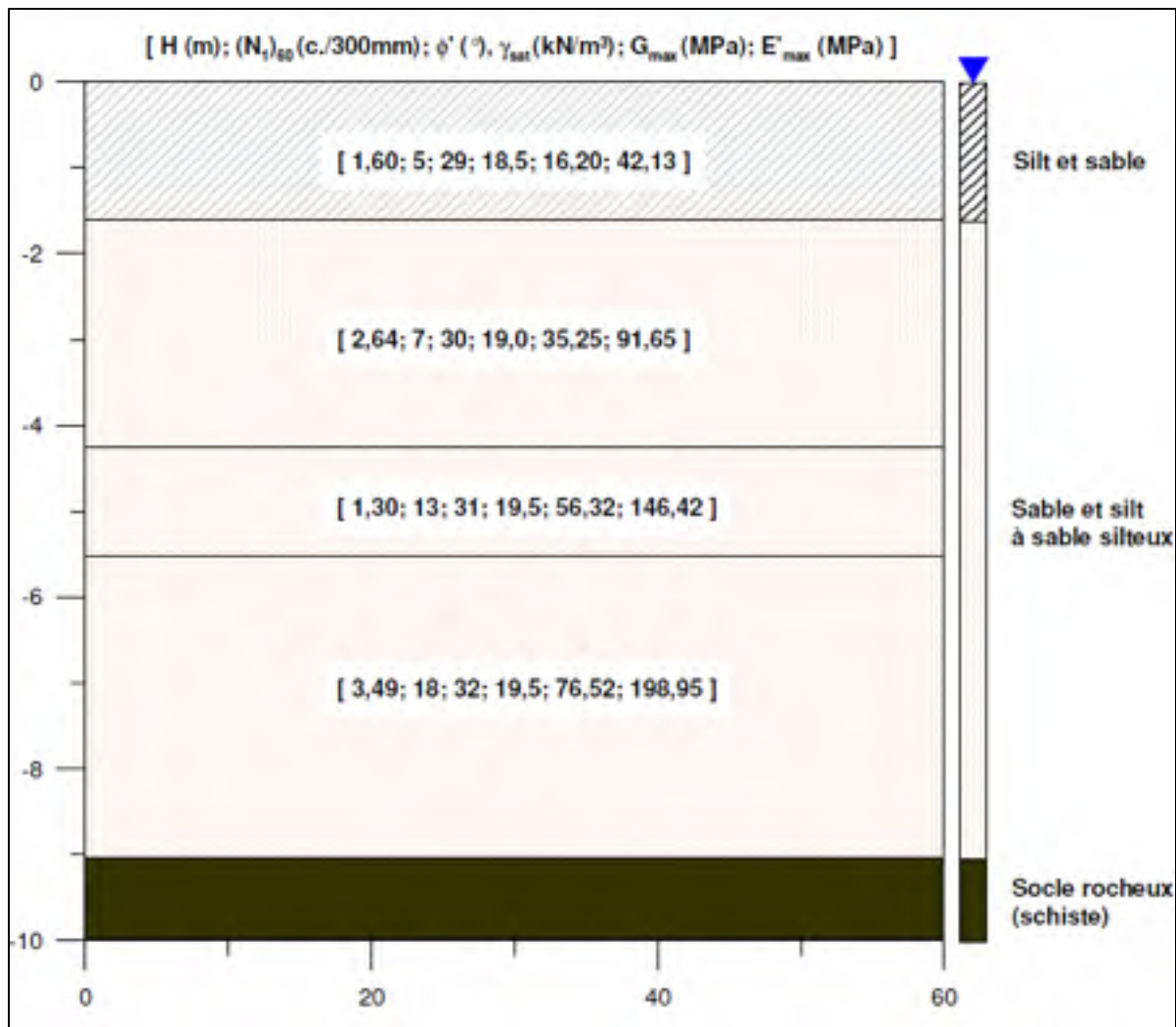


Figure 3.14 Stratigraphy and Geotechnical Properties for the Site of Québec City

3.4 Conclusions

Analysis of data from various field and laboratory, provided by the MTQ, allowed the development of two stratigraphic and corresponding geotechnical profiles representative of the soil and bedrock encountered at the site of Becancour and Quebec City. The first consists of a large clay deposit, supported by a deposit of granular soil. The second consists of an embankment of sand and silt, supported by a deposit of granular soil.

CHAPTER 4

SELECTION OF EARTHQUAKE PARAMETERS

This chapter presents the methodology for selecting the seismic record inputs for the nonlinear time history analysis. The objective of this part of work is to produce seismic signals compatible with the response spectrum at bedrock of the selected sites in the study. The generation of response spectra for the selected sites, according to the NBC 2010, is performed first. Subsequently, deaggregation of the seismic hazard analysis is performed in order to obtain seismic signals. Finally, RspMatch software is used to match the selected signals with the response spectra for the selected sites.

4.1 Selection of seismic parameters for Bécancour site

This section develops the methodology that led to the creation of seismic signals that will be applied at bedrock when modeling the site of the city of Bécancour.

4.1.1 Response spectrum by NBC 2010

Using the coordinates of the selected sites, the seismic hazard was obtained using the tool available on the website of the Geological Survey of Canada (GSC) (www.SeismesCanada.ca). The seismic hazard is given for various probabilities. In this study, a probability of occurrence of 2% in 50 years (0.000404 / year) was selected. The hazard obtained corresponds to a site of class C (i.e. shear wave velocity V_s is between 360 and 750 m /s). Since the seismic signals are to be applied at the bedrock, the transformation of this hazard for class A site (i.e. $V_s > 1500$ m/s) is required. The method of amplification factors proposed by Finn and Wightman (2003), is used for the processing, in accordance with the NBC 2010. This approach requires a number of input factors like F_a and F_v for short periods ($T=0.2$ sec) and long periods ($T=1$ sec), respectively.

These factors, according to the spectral response of 0.2 sec and 1 sec, are presented in tabular form in Appendix C of the NBC 2010. For the studied site, the values of F_a and F_v are 0.737 and 0.500 respectively. Figure 4.1 and Table 4.1 present the response spectra obtained for class C and Class A sites.

Table 4.1 Seismic hazard and processing site class C to class A

| Calculation of seismic hazard NBC 2010 (CGC) | | | | | | Transformation for Class A (Bedrock) (NBC 2010) | | | | | | |
|--|------------|------------|----------|----------|-------|---|-------|---------------------|------------|----------|----------|-------|
| Bécancour (Class C) | | | | | | Factor Class A | | Bécancour (Class A) | | | | |
| Probability | $S_a(0.2)$ | $S_a(0.5)$ | $S_a(1)$ | $S_a(2)$ | PRA | F_A | F_v | $S_a(0.2)$ | $S_a(0.5)$ | $S_a(1)$ | $S_a(2)$ | PRA |
| 2% in 50 years | 0.592 | 0.294 | 0.128 | 0.045 | 0.314 | 0.737 | 0.500 | 0.436 | 0.147 | 0.064 | 0.023 | 0.231 |
| 10% in 50 years | 0.229 | 0.116 | 0.055 | 0.018 | 0.113 | 0.700 | 0.500 | 0.160 | 0.058 | 0.028 | 0.009 | 0.079 |

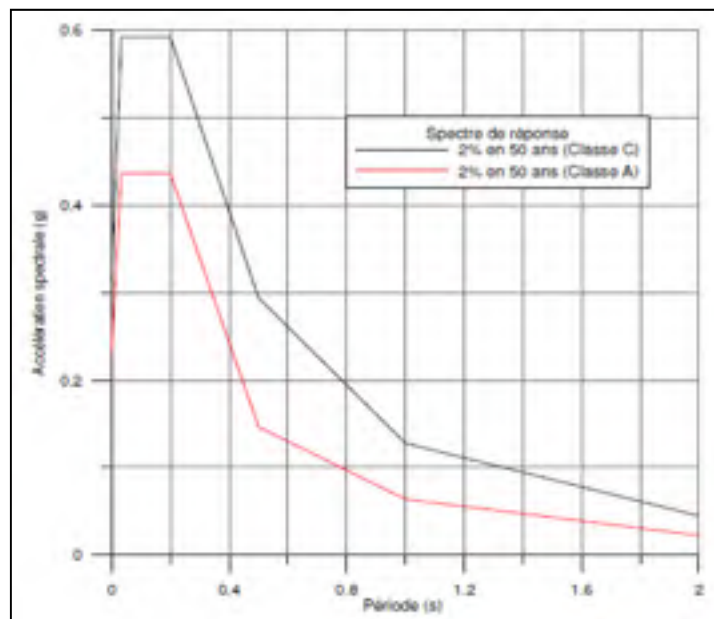


Figure 4.1 Response spectra NBC 2010 - Site of Bécancour

4.1.2 Deaggregation of the seismic hazard

The deaggregation of the seismic hazard identifies an event of a certain magnitude and distance from the site, which contributes most to the seismic hazard for a given probability (Chapman, 1995). Using attenuation law, the spectral response for various periods is calculated from different events of variable magnitudes and distances.

Two potential earthquake source zones have been used for the new Canadian seismic hazard model (Adams and Halchuk, 2003; Adams et al., 1995). The historical (H) model benefits from historical epicentres data that are based on the Canadian earthquake catalog. The regional model or (R) model is also based on historical seismicity, but combined with seismological analyzes. Geological Survey of Canada (GSC) uses two models of seismic zoning in the seismic hazard analysis.

GSC provides for a specific site, a probabilistic seismic hazard graph that relates the contribution of several seismic events to the seismic hazard (percent). The modal values corresponding to the event that contributes the most to the seismic hazard is selected. This event has the most probable occurrences during the selected return period. The choice of another event depends on the type of distribution of contributions to the seismic hazard. Figure 4.2 illustrates a distribution with single mode and double mode distributions.

Determination of averaged and most probable values can easily be achieved from single mode distribution whereas for double mode distribution the selection of mean values has to be between the two maxima.

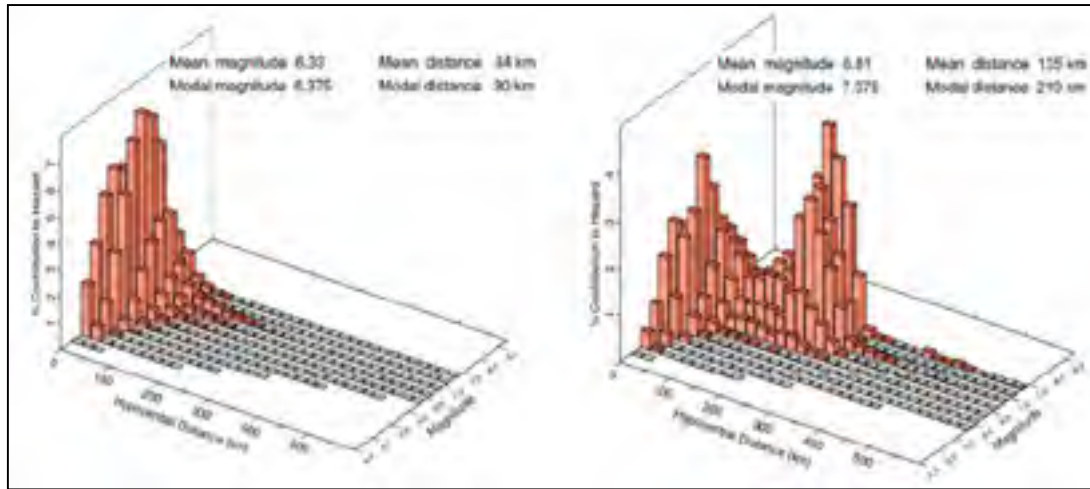


Figure 4.2 Distribution to a bimodal fashion and the contribution to the seismic hazard (GSC, 2012)

Table 4.2 indicates the values of magnitude and hypocentre distance obtained from the disaggregation of the seismic hazard at Bécancour site. The magnitudes are expressed in terms of magnitude Nuttli (m_{bLg}). The average values and modal are listed.

Table 4.2 Deaggregation of the seismic hazard – Site of Bécancour

| | | Model H | | | | Model R | | | |
|-----|-----------|---------|-----------|-------|-----------|---------|-----------|-------|--|
| | | Average | | Modal | | Average | | Modal | |
| T | M | R_H | M | R_H | M | R_H | M | R_H | |
| s | m_{bLg} | km | m_{bLg} | km | m_{bLg} | km | m_{bLg} | km | |
| 0.0 | 5.6 | 29.0 | 4.9 | 10.0 | 5.9 | 24.0 | 5.6 | 10.0 | |
| 0.2 | 6.2 | 69.0 | 5.9 | 30.0 | 6.3 | 34.0 | 6.4 | 30.0 | |
| 0.5 | 6.8 | 135.0 | 7.4 | 210.0 | 6.7 | 57.0 | 6.6 | 30.0 | |
| 1.0 | 7.0 | 149.0 | 7.4 | 210.0 | 6.8 | 70.0 | 6.9 | 30.0 | |
| 2.0 | 7.0 | 166.0 | 7.4 | 210.0 | 6.8 | 83.0 | 6.6 | 30.0 | |

4.1.3 Natural period of the soil deposit

In order to complete the seismic records selection, the natural period of the soil deposit at Becancour site is calculated. The average shear wave velocity used in this calculation is obtained from (NBC, 2010) and is given in the Equation (4.1). The results of this calculation step are presented in Table 4.3.

$$\bar{V}_S = \sum H_i / \sum \frac{H_i}{V_S} \quad (4.1)$$

Table 4.3 Calculating the average shear wave velocity

| H_i | V_s | H_i/V_s |
|----------------------|----------------------|------------------------------------|
| m | m/s | s |
| 1.80 | 118.30 | 0.0152 |
| 0.90 | 121.00 | 0.0074 |
| 2.30 | 70.80 | 0.0325 |
| 1.40 | 76.00 | 0.0184 |
| 1.00 | 70.80 | 0.0141 |
| 0.55 | 115.30 | 0.0048 |
| 2.75 | 208.90 | 0.0132 |
| 2.20 | 216.70 | 0.0102 |
| 2.20 | 215.90 | 0.0102 |
| 1.65 | 236.60 | 0.0070 |
| 16.75 | | 0.1329 |

The average shear wave velocity at Bécancour is 126 m / s. The natural period of the soil deposit is calculated as follows (Kramer, 1996):

$$T_n = \frac{4H_s}{V_s} = \frac{4(16.75)}{126} = 0.5 \text{ s} \quad (4.2)$$

4.1.4 Selection of earthquakes signals

The selection of earthquakes signals for nonlinear time history analysis is typically based on three aspects:

- 1) Geology similar to the studied site.
- 2) Similar magnitude, according to the deaggregation of seismic hazard at the site and for the natural period of the soil deposit.
- 3) Recorded data for seismic station located at a distance equivalent to the natural period of the soil deposit from the disintegration of the seismic hazard analysis.

Therefore, the selected seismic records must have been occurred in soil similar to the soil of Bécancour. Since the natural period of the soil deposit is 0.5 s, the selected earthquakes will have a magnitude of 6.8 and nearly m_{bLg} . Selected stations will be between 30 and 210 km from the hypocenter. Based on these data, two earthquakes which their data is available will be the subject of the study. Table 4.4 presents the main features for the selected earthquakes.

Table 4.4 Selected Earthquakes

| City | Location | Date | Time | m_{bLg} | m_b | M_s | Depth (km) |
|----------|----------------|------------|-------|-----------|-------|-------|------------|
| Saguenay | Eastern Canada | 1988-11-25 | 18h46 | 6.5 | 5.7 | 6.0 | 29 |
| Nahanni | Western Canada | 1985-23-12 | 5h16 | 6.1 | 6.4 | 6.9 | 18 |

Table 4.5 presents the original signals selected for the Saguenay earthquake. The selection was performed according to the hypocentral distance at each recording station. This distance has to be within the previously defined range. The hypocentral distance is calculated using trigonometry, knowing the epicentral distances (Munro and Weichert, 1989) and the depth of the hypocenter. Table 4.6 presents the original signals selected for the Nahanni earthquake. The epicentral distances and locations of the stations are from the open file number 13-30 Geological Survey of Canada written by Weichert et al (1986).

4.1.5 Scaling of response spectra

To make the response spectra of the original signals similar to the response spectra obtained from the NBC 2010 for Bécancour, the RspMatch software is utilized. RspMatch converts the frequency content of the seismic signals input to response spectrum and match the spectrum with a response target defined by the user. The spectrum used is that corresponding to a site of class A, since the signals will be applied at the bedrock. Output signals have response spectra similar to the ones obtained from the seismic hazard analysis of Bécancour. Table 4.7 presents the signals that will be used later in the nonlinear time history analysis, and some of its characteristics. The following figures illustrate the accelerograms of each signal, together with a comparison of their respective response spectrum and seismic hazard for Bécancour site (Class A site). An additional correction was made to the signals in order to obtain zero displacements at the end of the seismic events. Several errors, especially in the high frequency range, take place in the process of the integration of the acceleration which affects the accuracy of displacement profile. A cubic baseline correction was applied to the signals in SeismoSpect software to correct this error.

Table 4.5 Original signal - Saguenay (1998)

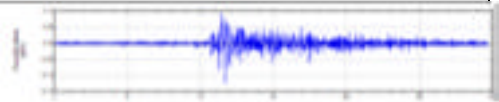
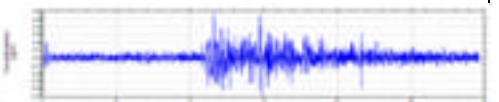

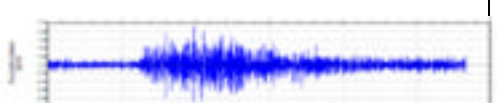
| Station | Location | Foundation | Orientation | Distance | | Tp | Time Trifunac | AMS | Accelerogram |
|---------|-------------------------|------------|--------------|------------|-------------|-------|------------------|-------|---|
| | | | | Epicentral | Hypocentral | | | | |
| | | | | km | km | s | s | g | |
| 8 | La Malbaie | Bedrock | Longitudinal | 93.0 | 97.4 | 0.120 | 11.0 | 0.124 |  |
| 8 | La Malbaie | Bedrock | Cross | 93.0 | 97.4 | 0.250 | 15.4 | 0.059 |  |
| 17 | St-André-du-Lac-St-Jean | Bedrock | Longitudinal | 63.6 | 69.9 | 0.045 | 12.5 | 0.155 |  |
| 17 | St-André-du-Lac-St-Jean | Bedrock | Cross | 63.6 | 69.9 | 0.035 | 15.1 | 0.091 |  |

Table 4.6 Original signal – Nahanni (1985)

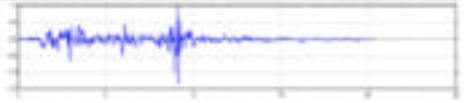
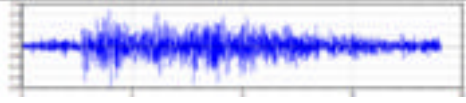
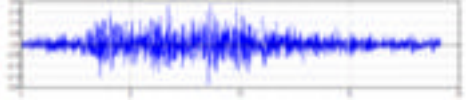
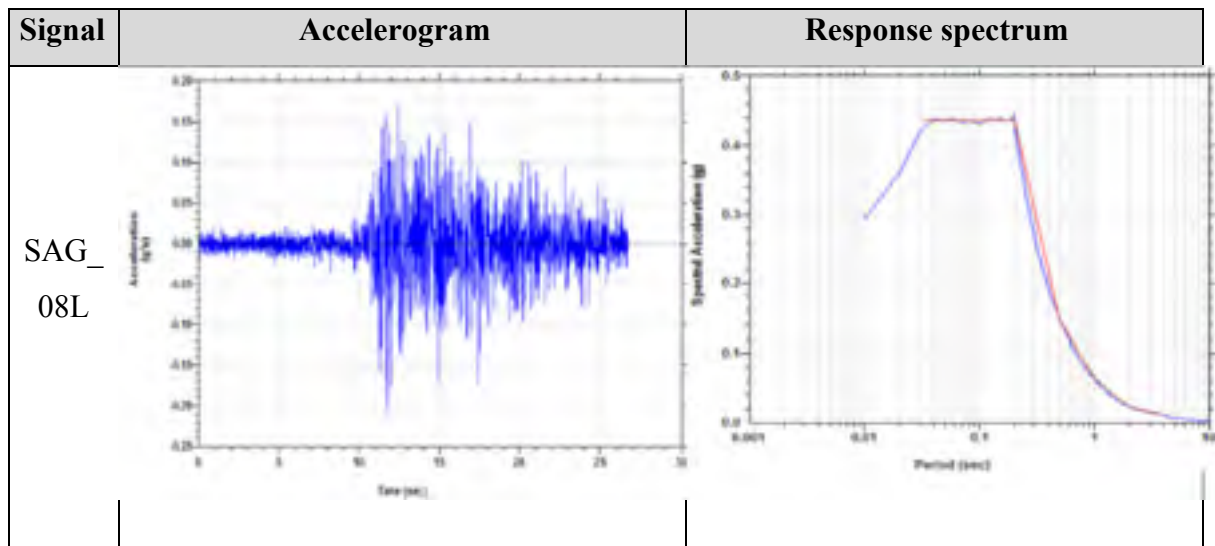
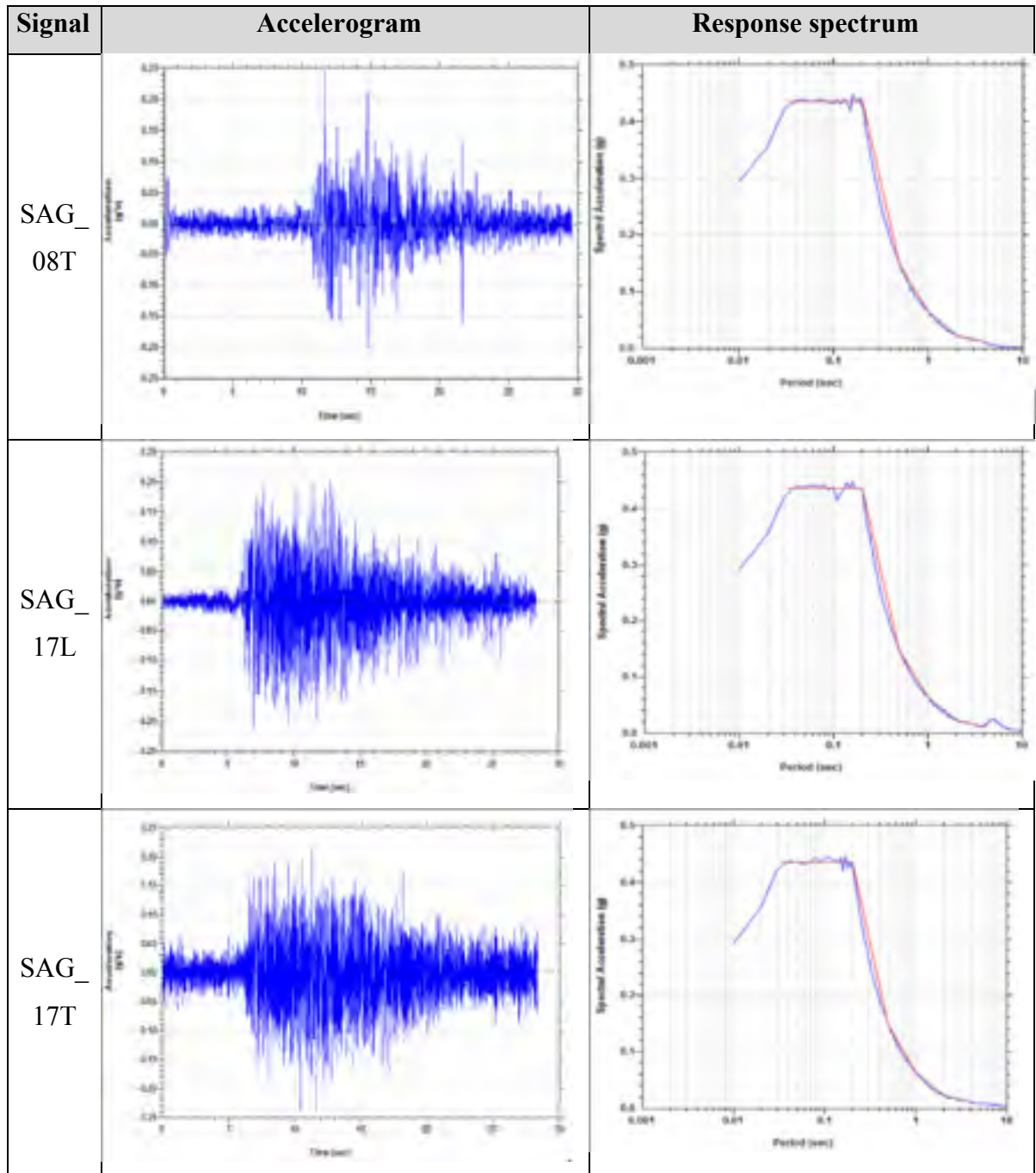
| Station | Location | Foundation | Orientation | Distance | | Tp | Time Trifunac | MS | Accelerogram |
|---------|---------------------|------------|--------------|------------------|-------------------|-------|------------------|-----|---|
| | | | | Epicentral km | Hypocentral km | | | | |
| 1 | Iverson | Bedrock | Cross | 7.6 | 19.5 | 0.065 | 7.9 | 345 |  |
| 3 | Battlement Creek | Bedrock | Longitudinal | 22.2 | 28.6 | 0.065 | 12.0 | 193 |  |
| 3 | Battlement Creek | Bedrock | Cross | 22.2 | 28.6 | 0.065 | 11.2 | 186 |  |

Table 4.7 Transformed signals - City of Bécancour

| Signal | Tp | Time Trifunac | AMS |
|----------|-------|---------------|-------|
| | s | s | g |
| SAG_08L | 0.150 | 12.8 | 0.204 |
| SAG_08T | 0.171 | 12.3 | 0.252 |
| SAG_17L | 0.195 | 15.3 | 0.210 |
| SAG_17T | 0.245 | 18.2 | 0.245 |
| SAG_20L | 0.210 | 10.4 | 0.216 |
| SAG_20T | 0.090 | 15.9 | 0.192 |
| NAH1_S1T | 0.195 | 11.9 | 0.262 |
| NAH1_S3L | 0.200 | 11.3 | 0.177 |
| NAH1_S3T | 0.248 | 11.2 | 0.179 |

Table 4.8 Transformed signals - City of Bécancour





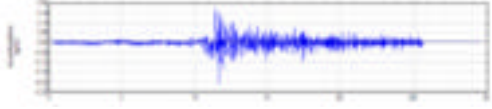
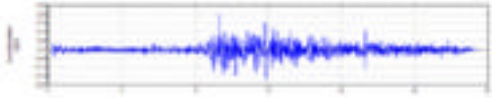
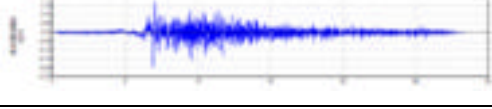
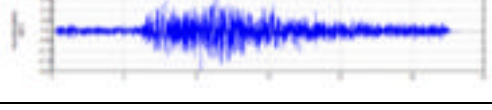
4.2 Selection of seismic parameters for Quebec site

Similar procedure was followed in the selection of earthquake signals for Quebec city site. The signals were also processed in similar fashion in order to adjust their frequency content. This part of analysis was performed by Mr. Denis LeBoeuf, at University of Laval for a project site located in the same region. The outcome of his work is therefore applied in this study. Table 4.9 presents the characteristics of these signals. The signals were recorded during the 1988 Saguenay earthquake. The S1280, S320 and S3360 signals are simulated with the goal of obtaining a synthetic response spectrum similar to the seismic hazard of Quebec City.

4.3 Conclusion

The process performed in this chapter has enabled the establishment of signals that have frequency content similar to the seismic hazard of Bécancour and Quebec City sites. These signals will be implemented in software modeling in subsequent sections.

Table 4.9 Transformed signals - Quebec City

| Signal | Tp | Time Trifunac | AMS | Sa(0,2) | Sa(0,5) | Sa(1,0) | Sa(2,0) | Accelerogram |
|---------|-------|------------------|-------|---------|---------|---------|---------|---|
| | s | s | g | g | g | g | g | |
| SAG_08L | 0.248 | 9.9 | 0.207 | 0.380 | 0.158 | 0.074 | 0.025 |  |
| SAG_08T | 0.218 | 13.1 | 0.202 | 0.388 | 0.158 | 0.075 | 0.026 |  |
| SAG_17L | 0.126 | 11.4 | 0.200 | 0.382 | 0.158 | 0.075 | 0.025 |  |
| SAG_17T | 0.055 | 14.5 | 0.197 | 0.385 | 0.156 | 0.076 | 0.025 |  |

CHAPTER 5

PSEUDO-STATIC ANALYSIS OF TEST PILES

This chapter presents results of a seismic pseudo-static analysis of bridge foundation piles for the two sites considered, Bécancour and Québec City. A typical bridge pile with a lumped mass representative of the deck was modeled as a single degree of freedom and subjected to seismic equivalent static loads calculated according to CSA-S6-14 Standard for Montreal region. Four masses were considered for analysis encompassing a wide range of bridge decks from light to heavy. The analyses were performed using Lpile software and results compared to those from Flac. The pseudo-static analysis procedure provides a good approximation to estimate the pile performance under earthquake loadings.

5.1 Introduction

The pseudo-static analysis procedure provides a good approximation to estimate the pile performance under earthquake loadings. The procedure prescribed in the CAN/CSA-S6-14 Standard will be followed to calculate the equivalent static load for single DOF model of a typical bridge with pile foundation for the two targeted sites, namely Bécancour and Québec City. The objectives of this analysis are:

- (1) To study the effect of increasing the lumped mass on top of the pile on the pile performance.
- (2) To validate the static analysis of laterally loaded pile in Lpile with Flac.

5.2 Methodology

Single-degree-of-freedom (SDOF) models of the pile with lumped masses at the top were built and studied. The pile used in this study is 670 mm diameter steel pile with 19 mm wall thickness and a total length that expands along the stratigraphy of the selected sites down to

the rock layer. An arbitrary lumped mass of 10.2 tonne, that represents the mass of two-span superstructure, is applied at the pile head at 3.81 m above the ground surface. This distance was warranted to provide sufficient inertial lateral loading and a sufficiently large moment in the pile during the earthquake.

In the pseudo-static procedure, a static load equivalent to the earthquake load is applied laterally to the structure. This is followed by static analysis to estimate the base shear in buildings or internal forces in the piers of bridge at the base level in order to select the appropriate footing design. In our case the objective is to evaluate the internal forces in the pile and the soil and determine the strain level at which they may fail.

The uniform load method defined in the CAN/CSA-S6-14 was followed to calculate the equivalent static lateral load P_e . Steps of this procedure are summarized in Table 5.1. A typical lifeline bridge with an importance factor of 3 was assumed in the analysis.

The equivalent static load P_e was calculated based on the sites properties and for four (04) different masses to encompass a wide spectrum of loading possibilities. The first mass, m_1 , represents the typical load coming from the superstructure. The second mass, m_2 , is larger than the first one but in a way that does not cause any damage to the soil or the structure. The third mass, m_3 , is greater than m_2 and generates a lateral load sufficient to damage the soil in the shallow depths around the pile. Finally, the forth one, m_4 , is selected to be large enough to initiate yielding in the pile as well as in surrounding soil due to the lateral push. Two representative sites for the province of Québec were studied namely: Bécancour and Québec city. Full description and characterization of these two sites have already been reported in Chapter 3. The labels of the analyses matrix performed are presented in Table 5.2. The computer program LPILE (Incorporated, 2007) was used for the analysis of the piles.

Table 5.1 Steps of the uniform load method procedure according to CAN/CSA-S6-14

| | |
|---|---|
| 1) Apply an arbitrary lateral load to superstructure P_0 | |
| 2) Calculate the lateral stiffness of the system k | $k = \frac{P_0}{V_{s,max}}$ <p>where K = lateral stiffness of the bridge $V_{s,max}$ = maximum static displacement of the bridge due to an arbitrary uniform lateral load, P_0</p> |
| 3) Calculate the fundamental period of the structure T | $T = 2\pi \sqrt{\frac{W}{gK}}$ <p>where W = effective weight of the bridge g = acceleration due to gravity, m/sec² K = lateral stiffness of the bridge</p> |
| 4) Determine the zonal acceleration ratio, A - Clause 4.4.3 and the site coefficient S - Clause 4.4.6 | |
| 5) Calculate the elastic seismic response coefficient, C_{sm} | $C_{sm} = \frac{1.2 AIS}{T^{2/3}} \leq 2.5AI$ <p>where A = zonal acceleration ratio specified in Clause 4.4.3 S = site coefficient specified in Clause 4.4.6 T = fundamental period of vibration, s I = importance factor based on the importance category specified in Clause 4.4.2 (= 3.0 for lifeline bridges)</p> |

| | |
|---|---|
| 6) Calculate the equivalent static load P_e | $P_e = \frac{C_{sm}W}{L}$ <p>where</p> <p>W = effective weight of the bridge*</p> <p>L = total length of the bridge</p> <p>* the actual weight shall be taken as the effective</p> <p>Weight (Clause 4.5.1)</p> |
|---|---|

Table 5.2 Analysis matrix and labeling of the pseudo-static analyses

| Site | Model with m_1 | Model with m_2 | Model with m_3 | Model with m_4 |
|-------------------------|------------------|------------------|------------------|------------------|
| Bécancour site | BM1 | BM2 | BM3 | BM4 |
| Québec City site | QM1 | QM2 | QM3 | QM4 |

5.3 Bécancour Site

The properties of the soil in this site were determined based on the soil properties described in Chapter 3 for the city of Bécancour. The p - y modulus K and the strain ε_{50} were determined based on the soil type, the effective unit weight γ , the average undrained shear strength c' and the friction angle ϕ from the tables recommended in LPILE (Incorporated, 2007). A summary of the soil and rock properties used in the analysis for this location is presented in Table 5.3.

Table 5.3 Soil properties for the Pseudo-static analysis of pile for Bécancour

| Layer thickness (m) | Soil type | γ (kN/m ³) | c' (kPa) | ϕ | K (MN/ m ³) | ε_{50} |
|---------------------|-------------------------------|-------------------------------|----------------------|--------|---------------------------|--------------------|
| 1.80 | Silt with clay | 18.0 | 8 | 32° | 24.4 | 0.02 |
| 0.90 | Silt with clay | 17.5 | 8 | 27° | 6.80 | 0.02 |
| 2.30 | Silt with clay | 16.0 | 8 | 25° | 6.80 | 0.02 |
| 1.40 | Silt with clay | 17.0 | 8 | 26° | 6.80 | 0.02 |
| 1.00 | Silt with clay | 16.0 | 8 | 30° | 24.4 | 0.02 |
| 0.55 | Silt with clay | 17.5 | 8 | 30° | 24.4 | 0.02 |
| 2.75 | Medium sand | 19.5 | 0 | 34° | 24.4 | - |
| 2.20 | Dense sand | 21.0 | 0 | 38° | 61.0 | - |
| 2.20 | Medium sand | 19.5 | 0 | 35° | 24.4 | - |
| 1.65 | Dense sand | 23.0 | 0 | 42° | 61.0 | - |
| Rock layer | | | | | | |
| Layer thickness (m) | γ (kN/m ³) | E_r (kPa) | Comp. strength (kPa) | RQD | K_{rm} | |
| 2.00 | 14 | 8000000 | 15000 | 50 | 0.0005 | |

5.3.1 The Models

The pile model was built in LPILE for the site properties described in the previous section. Four analysis cases were defined with four levels of lateral loading at the top of the pile. Each lateral load corresponds to a different mass (or axial load in the model). The first analysis case mass (BM1) is selected to represent a typical bridge load transferred to a single pile in a group. The second analysis case mass (BM2), which is greater than the first one, is selected to keep the performance of the system within the elastic region in order to capture the mass variation effect on the performance of the soil-pile system. The third analysis case mass (BM3) is selected to generate a sufficient lateral load to damage the soil surrounding the pile. Finally, the forth analysis case mass (BM4) is selected to be large enough to cause

calculated nonlinear EI of the pipe section and the corresponding moment-curvature graphs are illustrated in Figures 0.07 and 0.8 for the different mass cases.

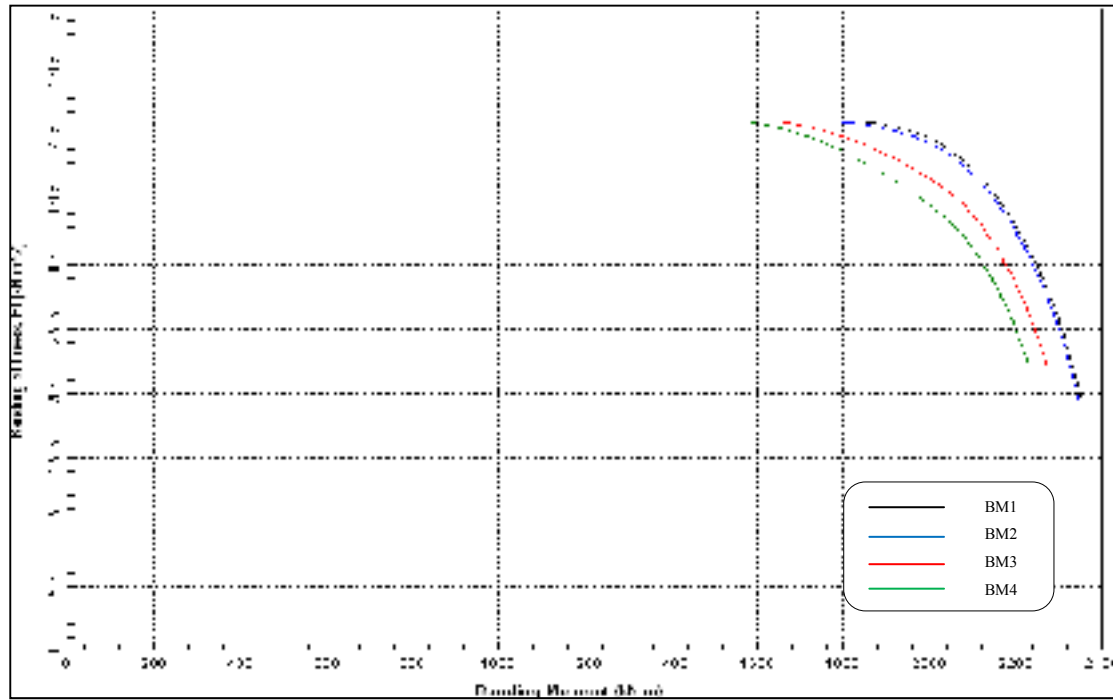


Figure 5.2 Bending stiffness of the circular pile section

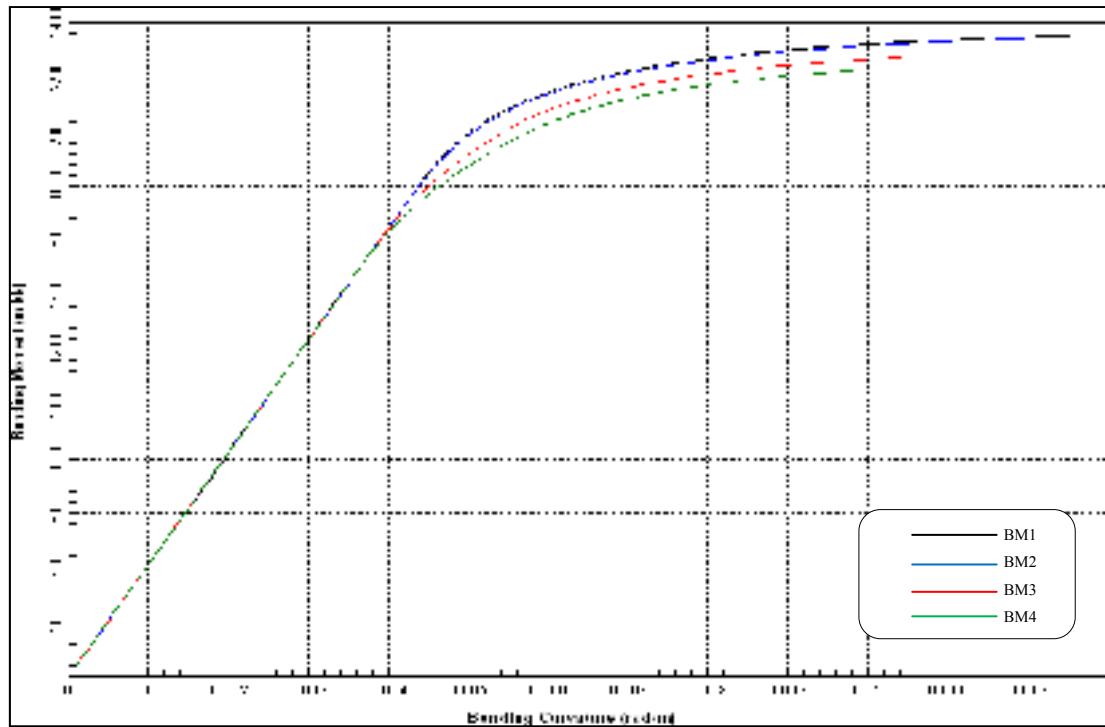


Figure 5.3 Moment curvature of the circular pile section

5.3.2 Analysis Procedure and Results

The procedure presented Table 5.1 was followed in calculating the equivalent static loads. An arbitrary lateral load of 100 kN was applied to the model in order to obtain the lateral stiffness K of the pile using LPILE. The calculation steps are summarized Table 5.4.

Table 5.4 Calculation summary for Bécancour site

| | |
|---|--|
| 1) Apply an arbitrary lateral load at the top of the pile $P_0 = 100kN$ and determine Δ $\Delta = 0.029972m$ | |
| 2) Calculate the lateral stiffness of the system k | $k = \frac{100 \times 10^3 N}{0.029972 m} = 3336447 N/m$ |
| 3) Calculate the fundamental period of the structure T | $T = 2\pi \sqrt{\frac{49100kg * 9.81m/sec^2}{9.81m/sec^2 * 3336447N/m}}$ $= 0.76sec$ |
| 4) Determine the zonal acceleration ratio, A - and the site coefficient S For Bécancour and from table A3.1.1; A=0.15 → Seismic Zone 3 From table 4.4.6.1; the soil type is III → S=1.5 | |
| 5) Calculate the elastic seismic response coefficient, C_{sm} | $C_{sm} = \frac{1.2 \times 0.15 \times 3 \times 1.5}{0.76^{2/3}} \leq 2.5 \times 0.15 \times 3$ $C_{sm} = 1.01 \approx 1 \leq 1.125 \text{ ok}$ |
| 6) Calculate the equivalent static load P_e | $P_e = 1 \times W$ $m_1 = 10.2ton \rightarrow W_1 = 100kN \rightarrow P_{e1} = 100$ $m_2 = 20.4ton \rightarrow W_2 = 200kN \rightarrow P_{e2} = 200$ $m_3 = 36.7ton \rightarrow W_3 = 360kN \rightarrow P_{e3} = 360kN$ $m_4 = 37.72on \rightarrow W_4 = 370kN \rightarrow P_{e4} = 370kN$ |

The p - y curves of the pile were printed at different depths to examine the yielding strains for the different load cases and are presented in Figure 5.4. The p - y curves presented here do not depend on the analysis case since they represent the soil-pile system characteristic. Therefore, they may be used for the four analysis cases.

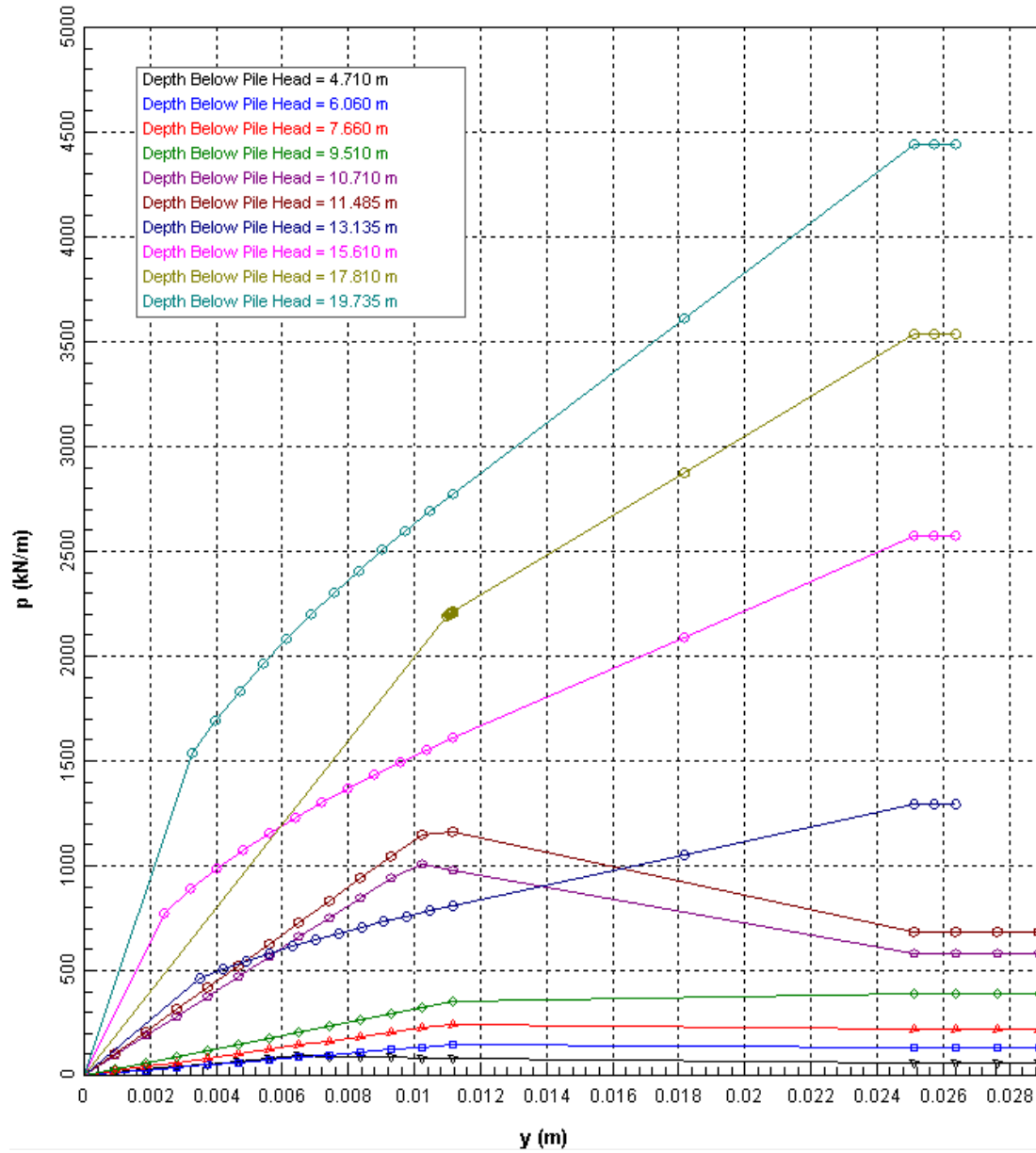


Figure 5.4 p - y Curves at Different Location along the Pile
(depths are from the pile top)

The p - y curves can be used to determine the displacement at which the soil is considered to be yielded. Comparing these limits to the actual displacements along the pile will be helpful in locating the failure region in the soil. The diagrams of bending moment, lateral displacements and shear force along the pile are provided in Figure 5.5 to 0.12 for the four analysis cases.

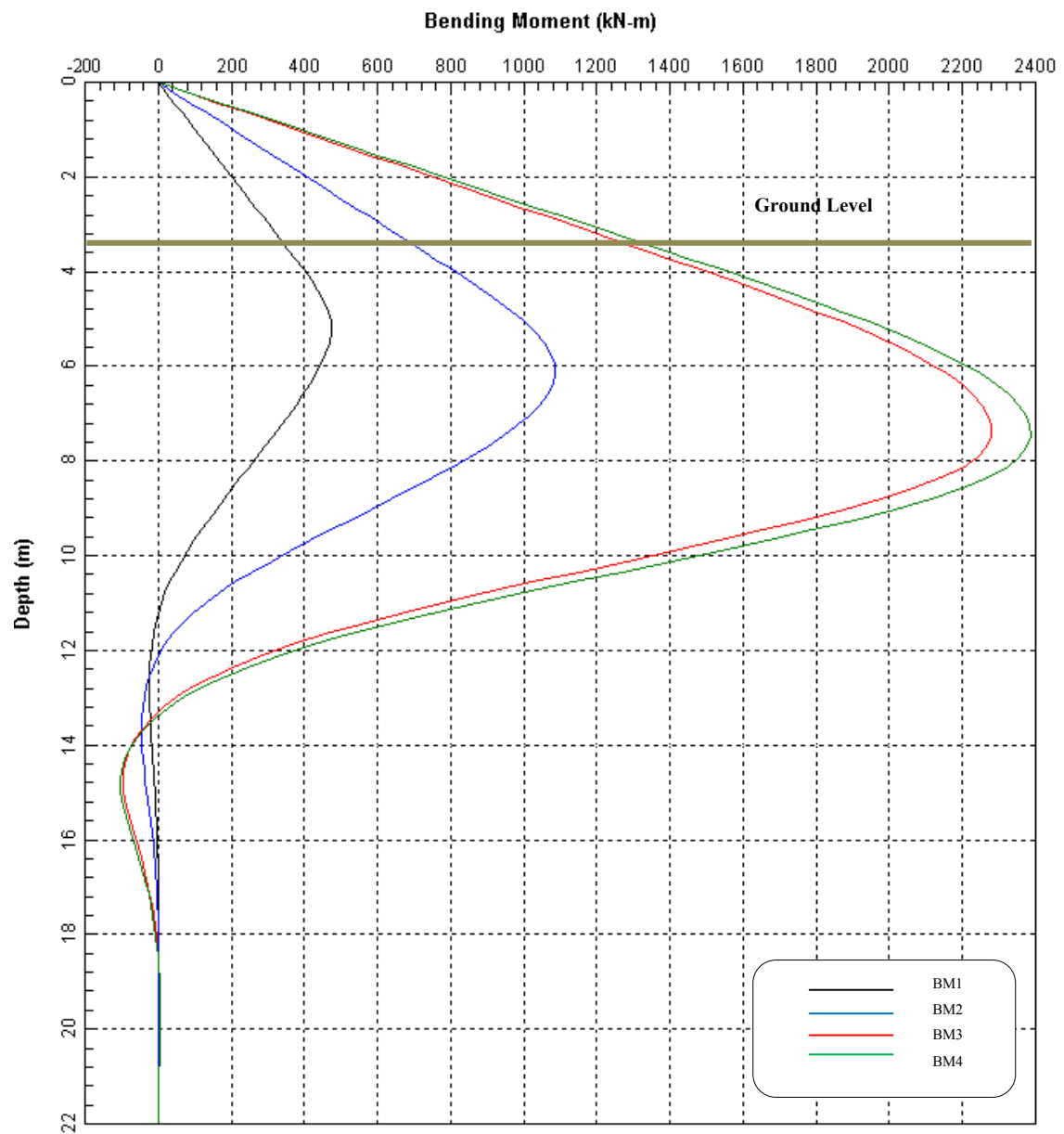


Figure 5.5 Bending Moment along the Pile

By comparing the bending moment values of the pile, from the bending moment diagram to the bending stiffness and the moment-curvature charts, It can be noted that the pile has yielded in bending in the forth case (BM4). The yielding encompasses the region between 4.6 m and 6.9 m under the pilehead. However, in the first three cases, i.e., BM1, BM2 and BM3, there is no indication of pile yielding.

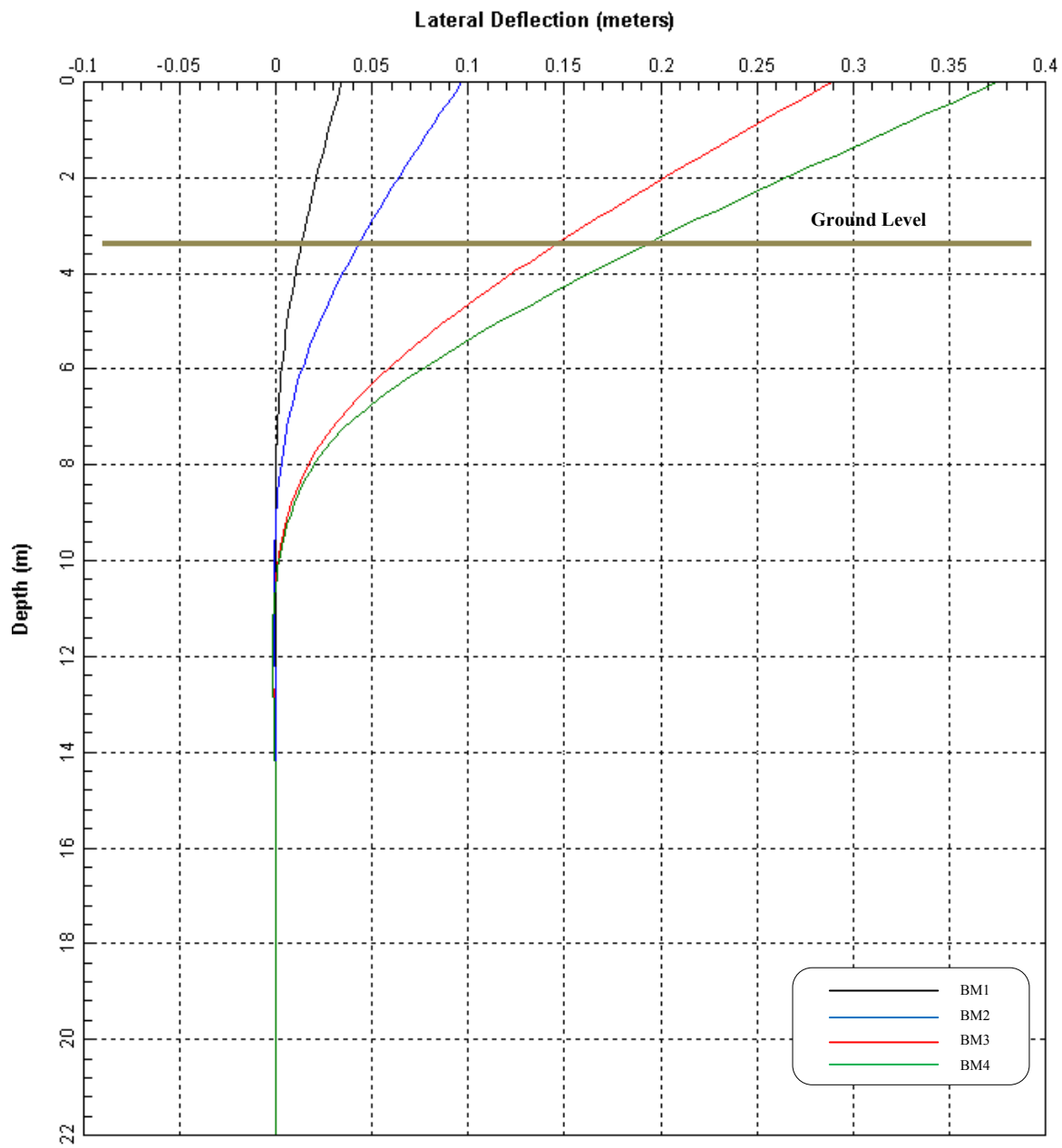


Figure 5.6 Lateral Displacement of the Pile

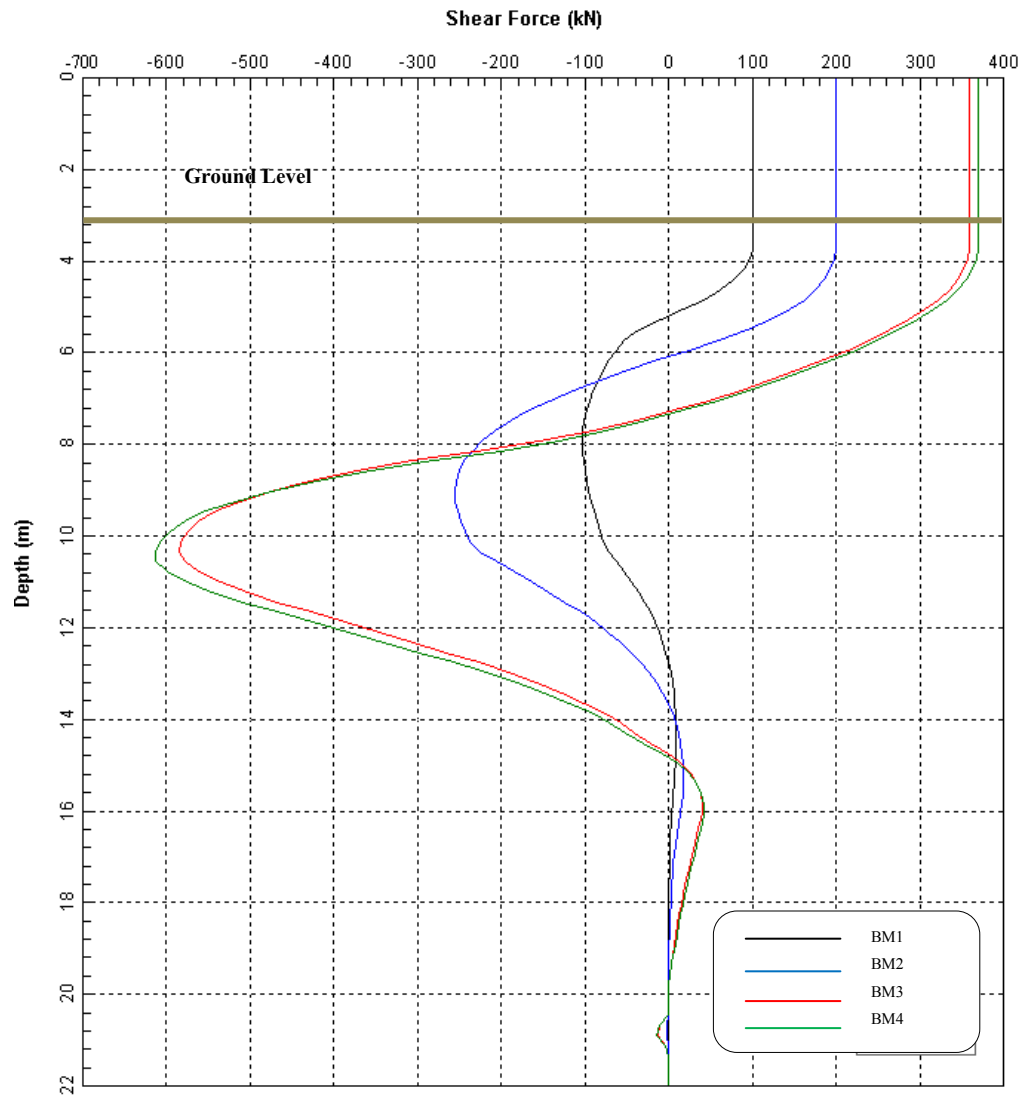


Figure 5.7 Shear along the Pile

The yielding displacements of the soil can be obtained from the p-y curves presented in Figure 5.4. Comparison between the actual pile displacement and the yielding displacements of the soil was examined within the first 6m below the ground surface and illustrated in Table 5.5.

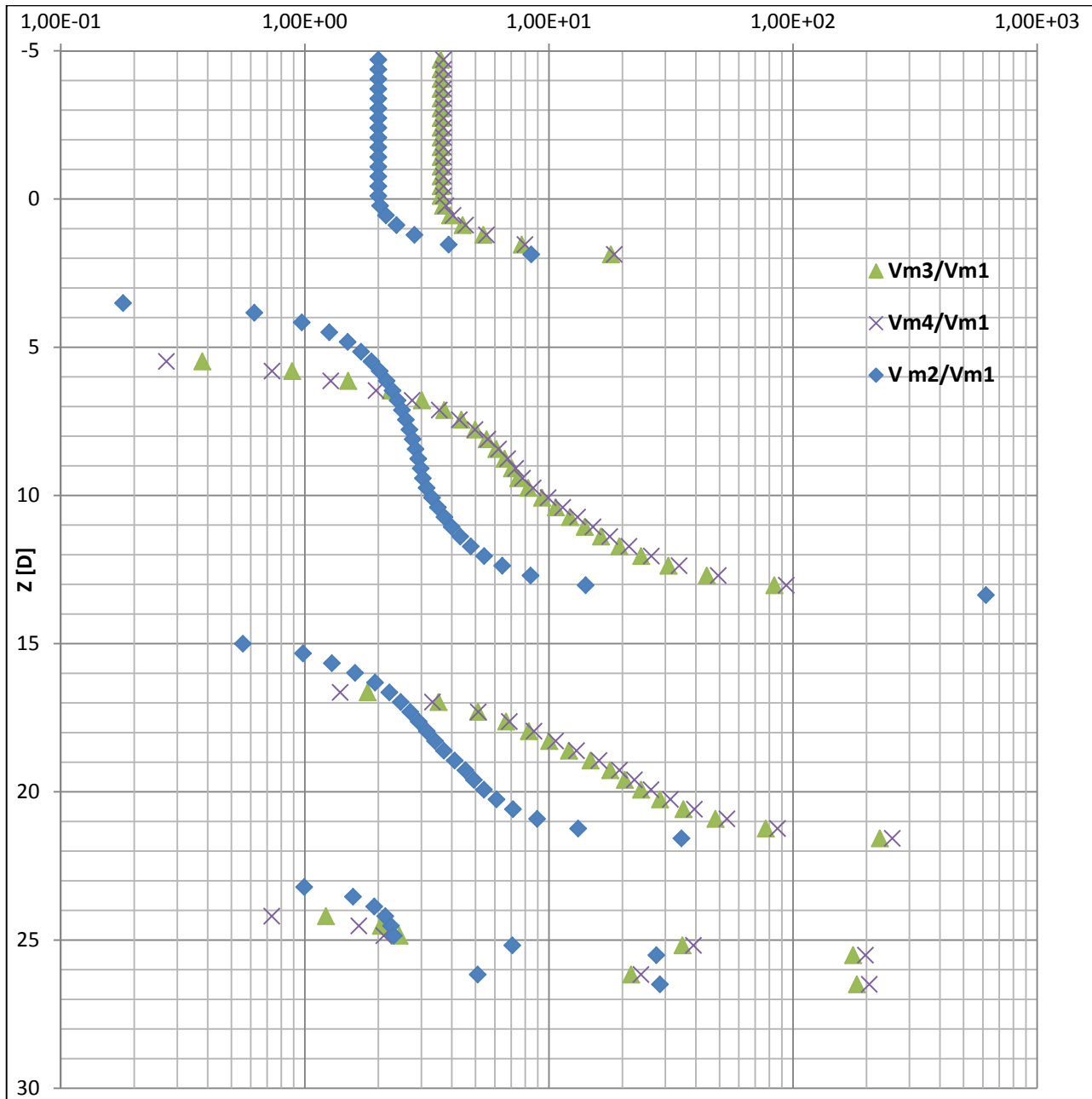


Figure 5.8 Effect the Superstructure Mass Variation versus Normalized Shear Measured from the Ground Surface Level

The table shows that failure in the soil occurs for the analysis cases BM3 and BM4. The soil in case BM3 fails under the lateral load within the first 1.70 m under the surface, this failure is not associated with structural failure. Therefore, analysis case BM3 is appropriate for the

case when soil failure is expected due to a strong earthquake motion and moderate structural weight. In contrast, analysis case BM4 represents the case of heavy bridges under seismic loading.

Table 5.5 Summary of the Lateral Displacements along the Pile Compared to the Yielding Criteria of the Soil Obtained from the p - y Curves

| Z | Z | P_u | P_{BM1} | Status | P_{BM2} | Status | P_{BM3} | Status | P_{BM4} | Status |
|------------|------------|----------------------|------------------------|---------------|------------------------|---------------|------------------------|---------------|------------------------|---------------|
| (m) | (D) | (kN/m) | (kN/m) | | (kN/m) | | (kN/m)) | | (kN/m)) | |
| 0.37 | 0.6 | 19.6 | -44.4 | Y | -28.0 | Y | -27.8 | Y | -27.7 | Y |
| 2.13 | 3.2 | 37.7 | -41.6 | Y | -152.7 | Y | -108.6 | Y | -108.5 | Y |
| 3.23 | 4.8 | 47.9 | -18.6 | NY | -121.8 | Y | -180.2 | Y | -180.0 | Y |
| 5.21 | 7.8 | 48.2 | 13.2 | NY | -1.4 | NY | -187.1 | Y | -219.5 | Y |
| 7.19 | 10.7 | 48.2 | 38.1 | NY | 93.8 | Y | 132.7 | Y | 125.2 | Y |
| 9.39 | 14.0 | 1316.0 | 8.2 | NY | 36.9 | NY | 143.9 | NY | 157.0 | NY |
| 11.37 | 17.0 | 2313.4 | -3.4 | NY | -0.4 | NY | 42.7 | NY | 50.4 | NY |
| 13.35 | 19.9 | 3159.0 | -1.3 | NY | -4.5 | NY | -12.8 | NY | -13.6 | NY |
| 15.33 | 22.9 | 4191.5 | -0.3 | NY | -2.0 | NY | -9.6 | NY | -10.6 | NY |
| 17.31 | 25.8 | 6591.5 | 0.7 | NY | 10.2 | NY | 61.0 | NY | 68.3 | NY |
| 18.19 | 27.1 | 12176.5 | 0.0 | NY | 0.0 | NY | 0.1 | NY | 0.1 | NY |

Notes: Y= Yielded; NY= Not yielded

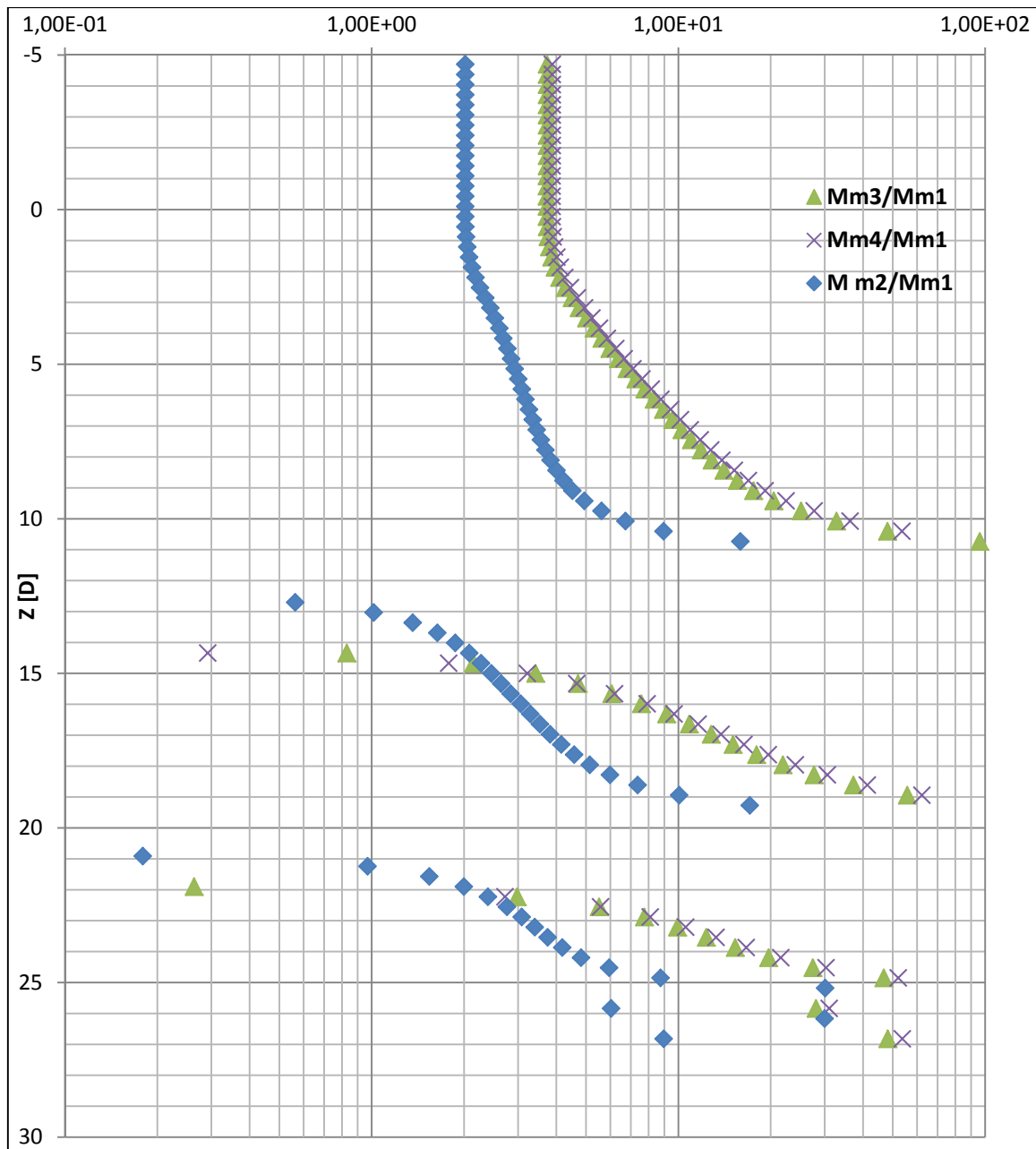


Figure 5.9 Effect of the Superstructure Mass Variation versus Normalized Bending Moment Measured from the Ground Surface Level

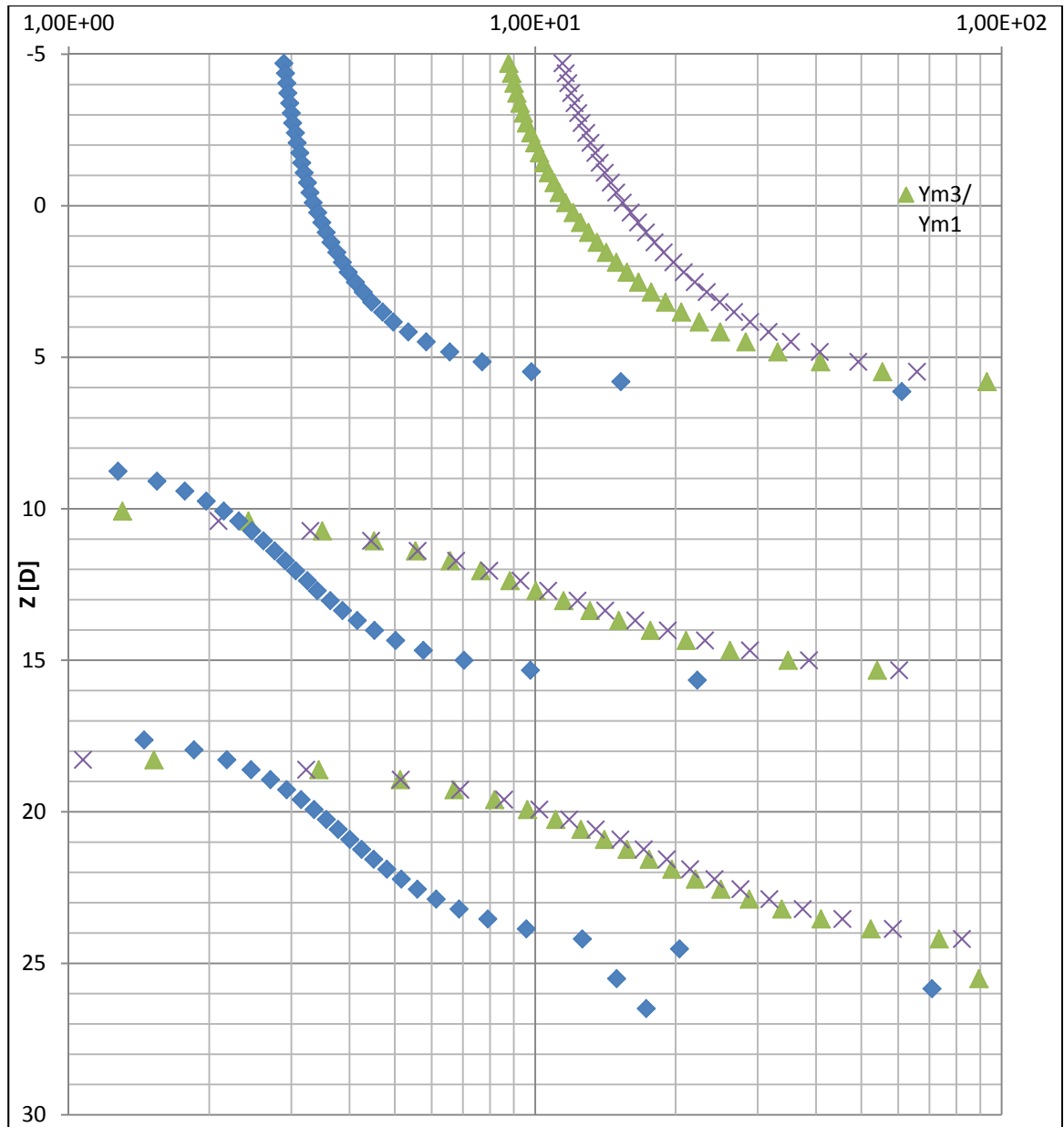


Figure 5.10 Effect of the Superstructure Mass Variation versus Normalized Deflection Measured from the Ground Surface Level

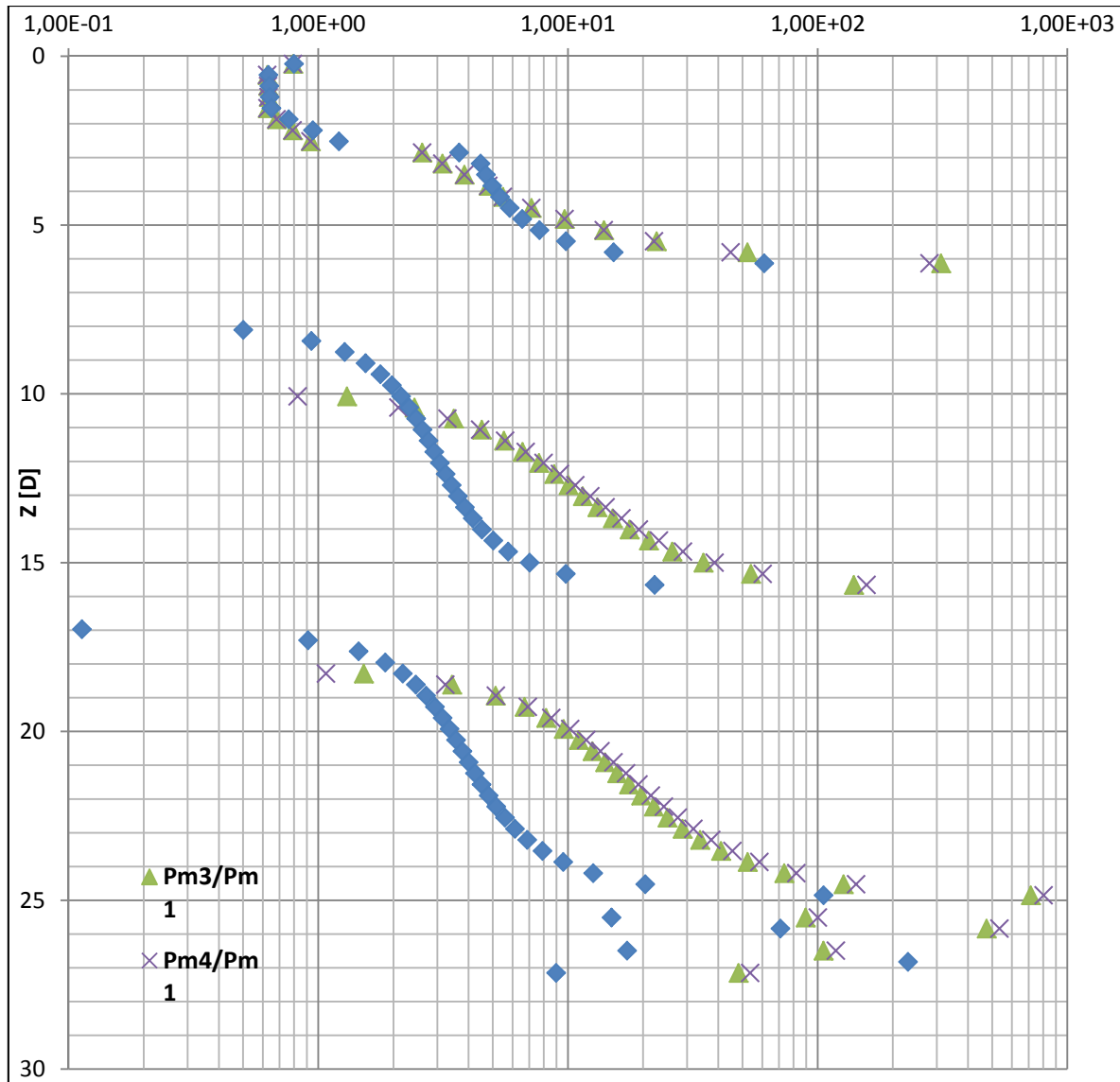


Figure 5.11 Effect of the Superstructure Mass Variation versus Normalized Shear Measured from the Ground Surface Level

The effect of mass variation on the pile response with depth has been examined by dividing the corresponding effect from all masses by the response of the pile from the first mass. This effect is presented through Figures 1.3 to Figure 5.11.

5.4 Québec City Site

The properties of the soil in this site were determined based on the soil properties described in Chapter 3 for Québec City. The p - y modulus K and the strain ε_{50} were determined based on the soil type, the effective unit weight γ , the average undrained shear strength c' and the friction angle ϕ from the tables recommended in LPILE (Incorporated, 2007). A summary of the soil and rock properties used in the analysis for this location is presented in Table 5.6.

Table 5.6 Soil Properties for the Pseudo-Static Analysis of Pile for Québec City

| Depth (m) | Soil type | γ (kN/m ³) | c' (kPa) | ϕ | K (MN/ m ³) | ε_{50} |
|------------|-------------------------------|-------------------------------|----------------------|--------|---------------------------|--------------------|
| 1.60 | Silt and Sand | 18.5 | - | 29° | 24.4 | 0.02 |
| 2.64 | Silty Sand | 19 | - | 30° | 6.8 | 0.02 |
| 1.30 | Silty Sand | 19.5 | - | 31° | 6.8 | 0.02 |
| 3.49 | Silty Sand | 19 | - | 32° | 6.8 | 0.02 |
| Rock layer | | | | | | |
| Depth (m) | γ (kN/m ³) | E_r (kPa) | Comp. strength (kPa) | RQD | K_{rm} | |
| 1 | 14 | 8000000 | 15000 | 50 | 0.0005 | |

5.4.1 The Models

The pile was modeled in the same way as the pile at Bécancour. LPILE was also used in the analysis in which the site properties described in the previous section were input. Likewise Bécancour site, four analysis cases were defined with four levels of lateral loading at the top of the pile. Each lateral load corresponds to a different mass (or axial load in the model).

The first analysis case mass (QM1) is selected to represent a typical bridge load transferred to a single pile in a group. The second analysis case mass (QM2), which is greater than the first one, is selected to keep the performance of the system within the elastic region in order

to capture the mass variation effect on the performance of the soil-pile system. The third analysis case mass (QM3) is selected to generate a sufficient lateral load to damage the soil surrounding the pile. Finally, the forth analysis case mass (QM4) is selected to be large enough to cause permanent damage in the pile and the surrounding soil. The model with the mass values for the four analysis cases is illustrated in Figure 5.12.

Although the soil type is a mix of silt and sand, no cohesion properties were introduced and therefore the Reese sand criteria were assumed in the analysis. The ground surface was assumed to be horizontal and the pile top extended 3.81 m above the surface. The circular steel pipe section was defined and the nonlinear sectional properties option was used in the analysis. The calculated nonlinear EI of the pipe section and the moment curvature graphs were illustrated in Figure 5.2 and Figure 5.3.

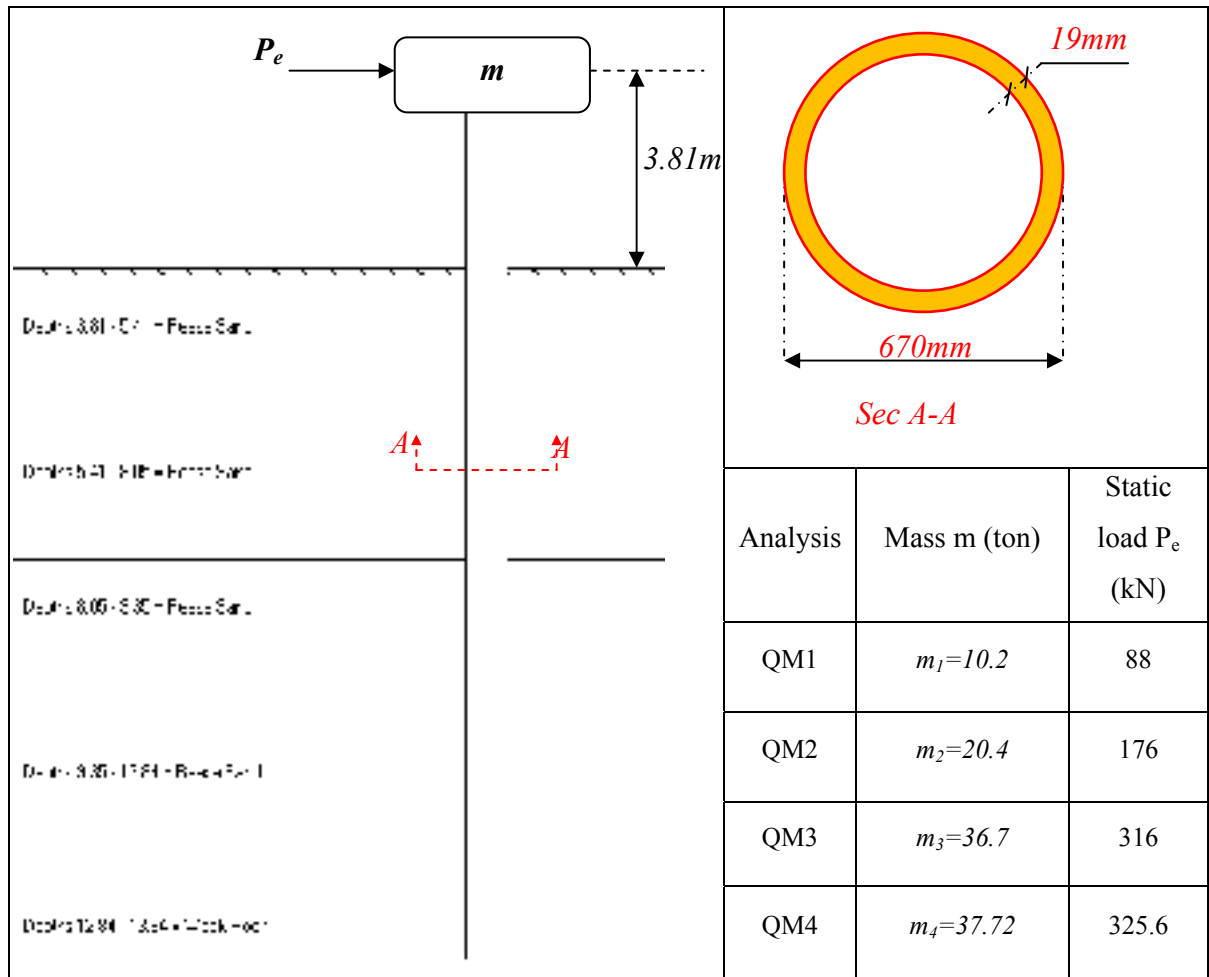


Figure 5.12 Summary of Model for Québec City Pile

5.4.2 Analysis Procedure and Results

The procedure presented in Table 5.1 was followed in calculating the equivalent static loads. An arbitrary lateral load of 100 kN was applied to the model in order to obtain the lateral stiffness K of the pile. The calculation steps are summarized in Table 5.7.

Table 5.7 Calculation Summary for Québec City Case

| | |
|---|--|
| 1) Apply an arbitrary lateral load to superstructure $P_0 = 100kN$ and determine Δ $\Delta = 0.040254m$ | |
| 2) Calculate the lateral stiffness of the system k | $k = \frac{100 \times 10^3 N}{0.040254 m} = 2484225 N/m$ |
| 3) Calculate the fundamental period of the structure T | $T = 2\pi \sqrt{\frac{49100kg * 9.81m/s^2}{9.81m/s^2 * 2484225N/m}}$ $= 0.88 \text{ sec}$ |
| 4) Determine the zonal acceleration ratio, A - and the site coefficient S For Québec city and from table A3.1.1; $A=0.20 \rightarrow$ Seismic Zone 3 From table 4.4.6.1; the soil type is III $\rightarrow S=1.5$ | |
| 5) Calculate the elastic seismic response coefficient, C_{sm} | $C_{sm} = \frac{1.2 \times 0.15 \times 3 \times 1.5}{0.883334^{2/3}} \leq 2.5 \times 0.15 \times 3$ $C_{sm} = 0.88 \leq 1.125 \text{ ok}$ |
| 6) Calculate the equivalent static load P_e | $P_e = 0.88 \times W$ $m_1=10.2\text{ton} \rightarrow W_1= 100kN \rightarrow P_{e1}= 88kN$ $m_2=20.4\text{ton} \rightarrow W_2= 200kN \rightarrow P_{e2}= 176kN$ $m_3=36.7\text{ton} \rightarrow W_3= 360kN \rightarrow P_{e3}= 316kN$ $m_4=37.72\text{ton} \rightarrow W_4=370kN \rightarrow P_{e4}=325.63kN$ |

The p - y curves of the pile were printed at different depths to examine the yielding strains for the different load cases. These curves are presented in Figure 5.13.

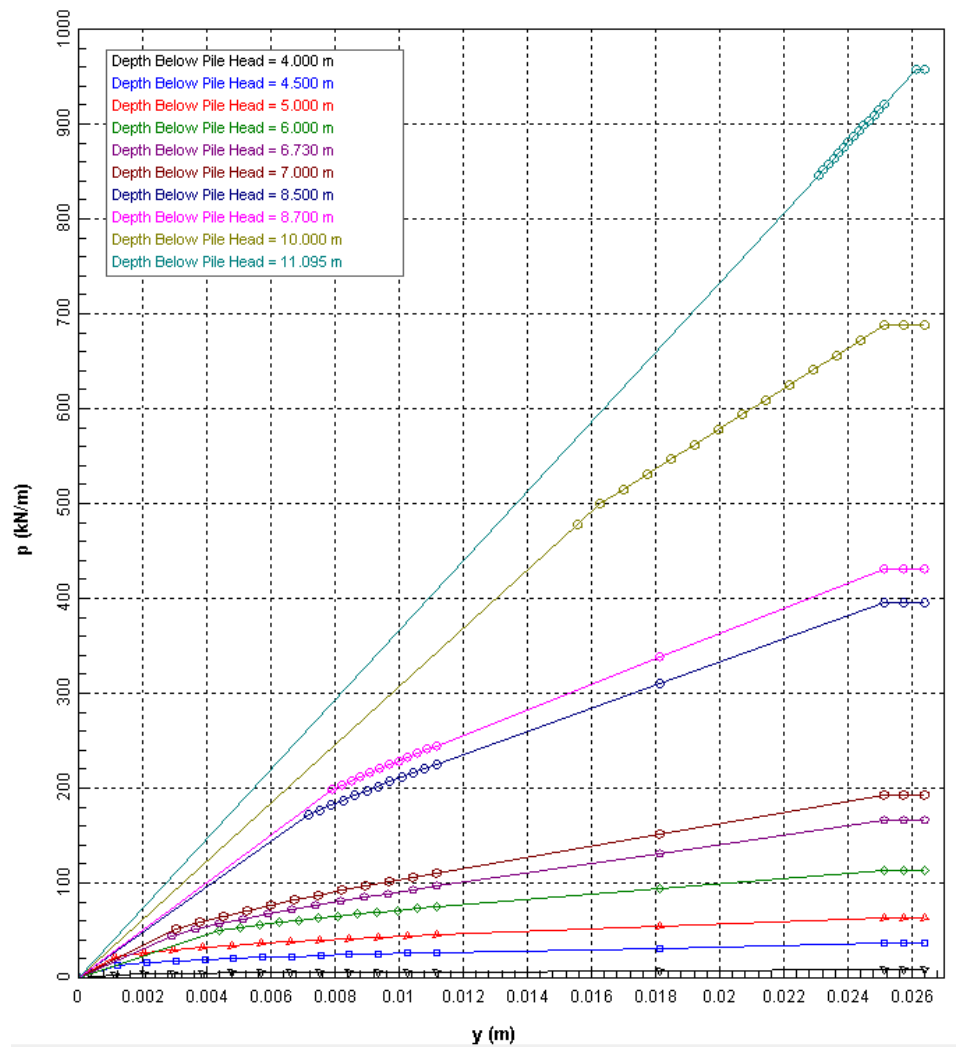


Figure 5.13 p - y Curves at Different Location along the Pile
(Depths are from the pile head)

The diagrams of the bending moment, the lateral displacements and shear force along the pile are presented for the four mass cases in Figure 5.14 to Figure 5.16.

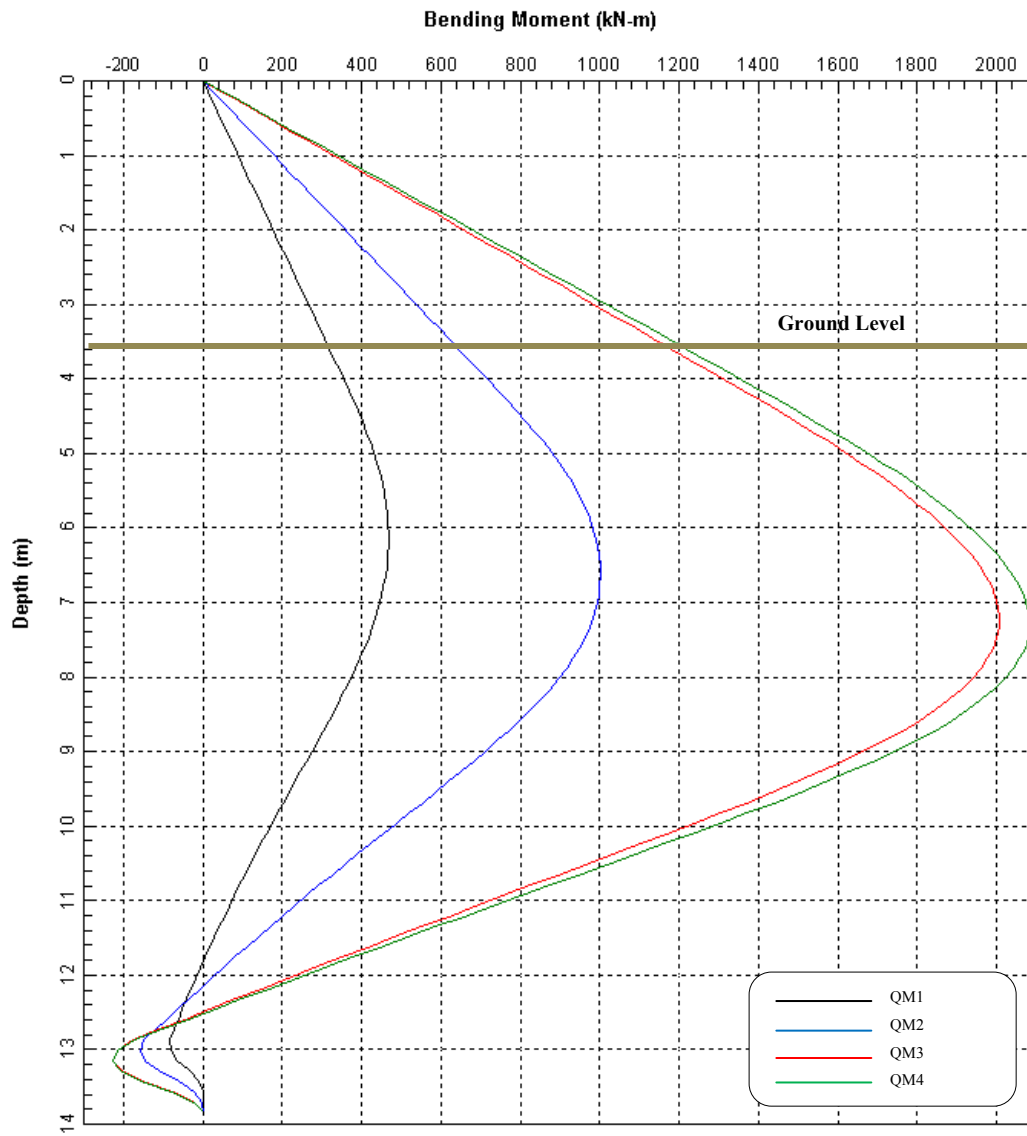


Figure 5.14 Bending moment along the pile

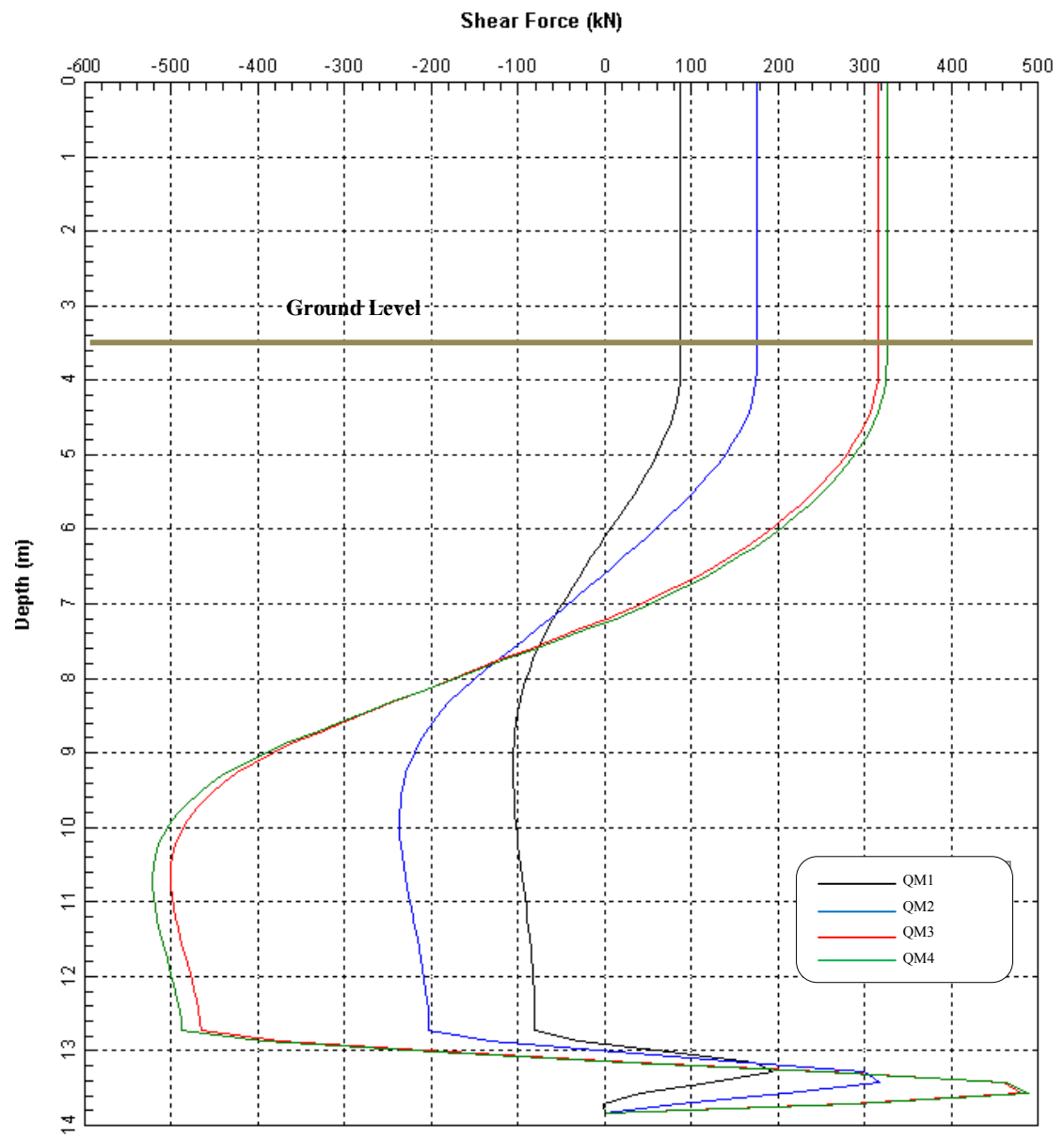


Figure 5.15 Shear along the pile

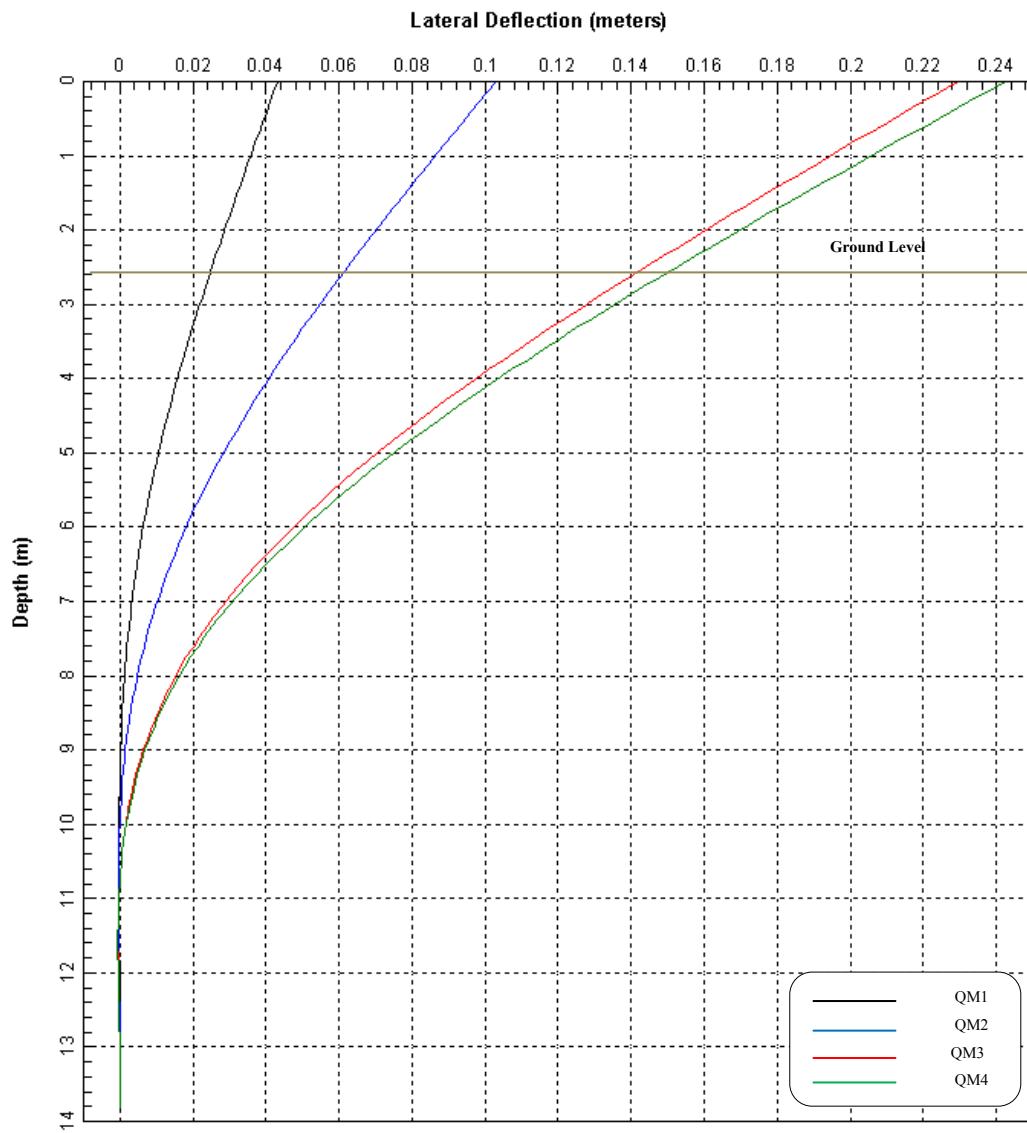


Figure 5.16 Lateral displacement of the pile

Table 5.8 Summary of the Lateral Displacements along the First 10m of the Pile Compared to the Yielding Criteria of the Soil Obtained from the p - y Curves

| Z | Z | P_u | P_{BM1} | Status | P_{BM2} | Status | P_{BM3} | Status | P_{BM4} | Status |
|------------|------------|----------------------|------------------------|---------------|------------------------|---------------|------------------------|---------------|------------------------|---------------|
| (m) | (D) | (kN/m) | (kN/m) | | (kN/m) | | (kN/m) | | (kN/m) | |
| 0.19 | 0.283582 | 8.834 | 0.0 | NY | -2.8 | NY | -2.8 | NY | -2.8 | NY |
| 0.69 | 1.029851 | 36.436 | 0.0 | NY | -32.4 | NY | -32.4 | NY | -32.4 | NY |
| 1.19 | 1.776119 | 62.823 | 0.0 | NY | -62.0 | NY | -62.0 | NY | -62.0 | NY |
| 2.19 | 3.268657 | 113.637 | 0.0 | NY | -92.8 | NY | -110.4 | NY | -110.4 | NY |
| 2.92 | 4.358209 | 165.576 | 0.0 | NY | -99.5 | NY | -157.2 | NY | -157.2 | NY |
| 3.19 | 4.761194 | 192.862 | 0.0 | NY | -104.4 | NY | -184.6 | NY | -184.6 | NY |
| 4.69 | 7 | 396.093 | 0.0 | NY | -73.1 | NY | -215.0 | NY | -224.2 | NY |
| 4.89 | 7.298507 | 430.62 | 0.0 | NY | -64.5 | NY | -212.1 | NY | -221.4 | NY |
| 6.19 | 9.238806 | 687.83 | 0.0 | NY | 1.3 | NY | -50.6 | NY | -56.8 | NY |
| 7.285 | 10.87313 | 957.429 | 0.0 | NY | 17.8 | NY | 15.4 | NY | 14.2 | NY |

Notes: Y= Yielded; NY= Not yielded

5.5 FLAC Models

Another study was conducted in parallel on the same prototype using FLAC software. The study was conducted at Université Laval (Maltais 2012) for the Bécancour case only. The analysis was conducted for the BM1 and BM3 load cases and considered two scenarios in terms of the existence of the water table. The analysis matrix for this study is presented in Maltais (2012) and the model is illustrated in Table 5.9 and Figure 5.17. The analysis also considered the drained and undrained conditions for the first two scenarios. The study was used to validate the LPILE model as a step towards the dynamic analysis model.

Table 5.9 Analysis Cases using FLAC

| | | | | | | Stratigraphy | | | | | | |
|--------------------|-----------|--------------|-----------|------------------------|-------------------------|--|------------------|-------------------------------|----------------------------|------------------|---------------------|-----------------------------|
| | | | | | | Crust clay and silty clay (layer 1 & 2) | | | Sand and silt (layer 3) | | | Brown Shale (layer 4) |
| Analysis series | Site | Mass load | Q (kN) | F _L (kN) | Water table level | Conditions | Soil behavior | Rupture criteria (soil) | Conditions | Soil behavior | Rupture criteria | Soil behavior |
| I | Bécancour | BM1 | 481.7 | 69.27 | Surface | ND | M-C | S _u | D | M-C | Φ' | E |
| II | Bécancour | BM1 | 481.7 | 69.27 | Surface | D | M-C | c'- Φ' | D | M-C | Φ' | E |
| III | Bécancour | BM1 | 481.7 | 69.27 | NA | D | M-C | c'- Φ' | D | M-C | Φ' | E |
| IV | Bécancour | BM3 | 1634 | 235 | NA | D | M-C | c'- Φ' | D | M-C | Φ' | E |

M-C: Mohr-Coulomb

N-D: Non-Drained

D: Drained

E: Elastic

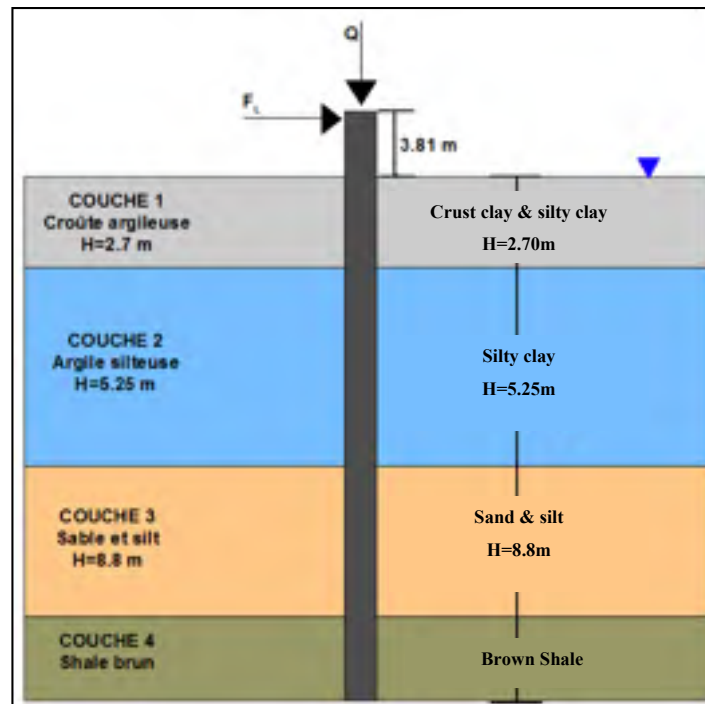


Figure 5.17 FLAC Model for the Bécancour Pile

5.6 Comparison of Results: FLAC vs LPILE

Analysis results using FLAC were compared to those obtained using LPILE for the Bécancour pile. Figures 2.3 to 0.26 illustrate this comparison in terms of the bending moment, the shear forces and the displacement for series 1 to 4, respectively. The comparison showed that the results are relatively in good agreement with slight differences. The differences were somehow expected since the soil model varies between the two software codes. The FLAC model implemented the Mohr-Coulomb criteria whereas the LPILE program is based on the p - y -curves. Nevertheless, the Mohr-Coulomb model, which rendered very reasonable results comparing to those of LPILE, is more suitable for the dynamic analysis which will be carried on later in this study as presented in Chapter 6.

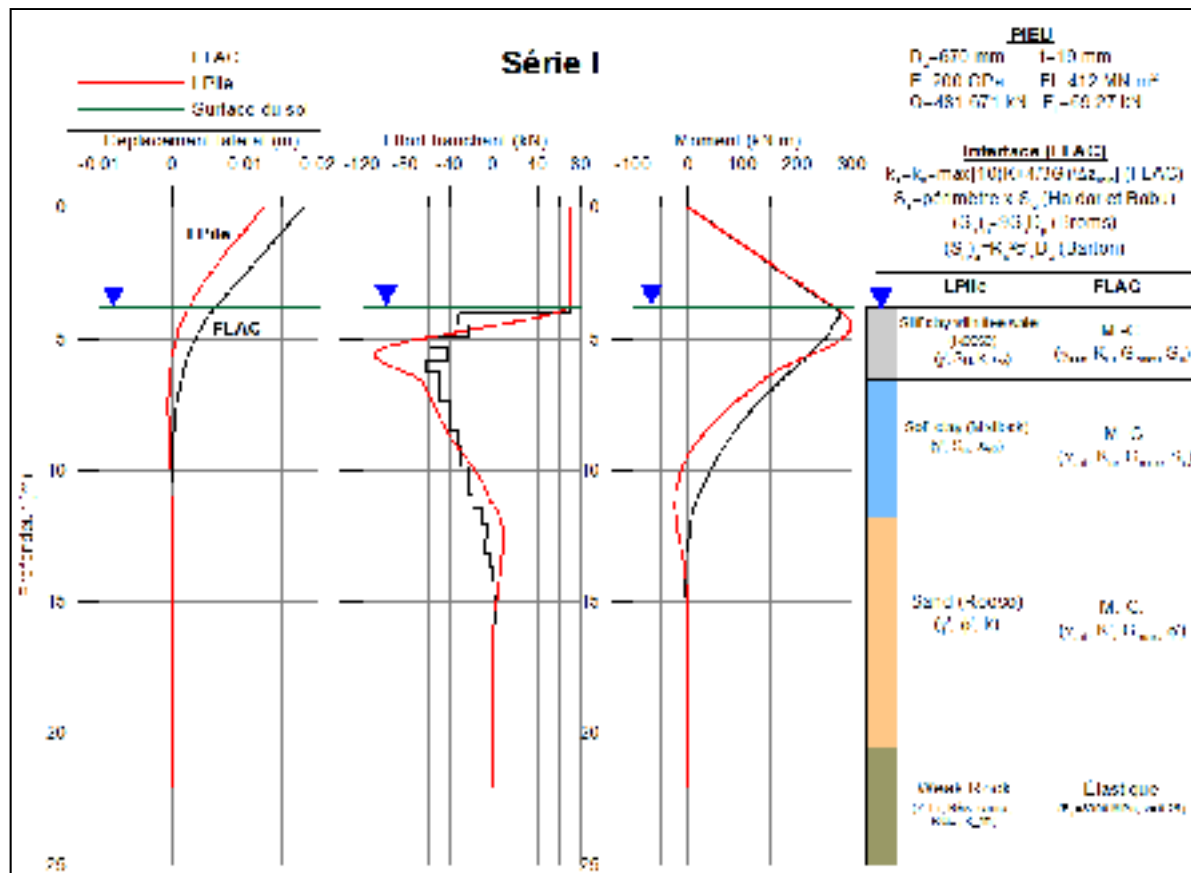


Figure 5.18 FLAC vs LPILE : Displacement, Shear and Moment for Series 1
for Bécancour Pile

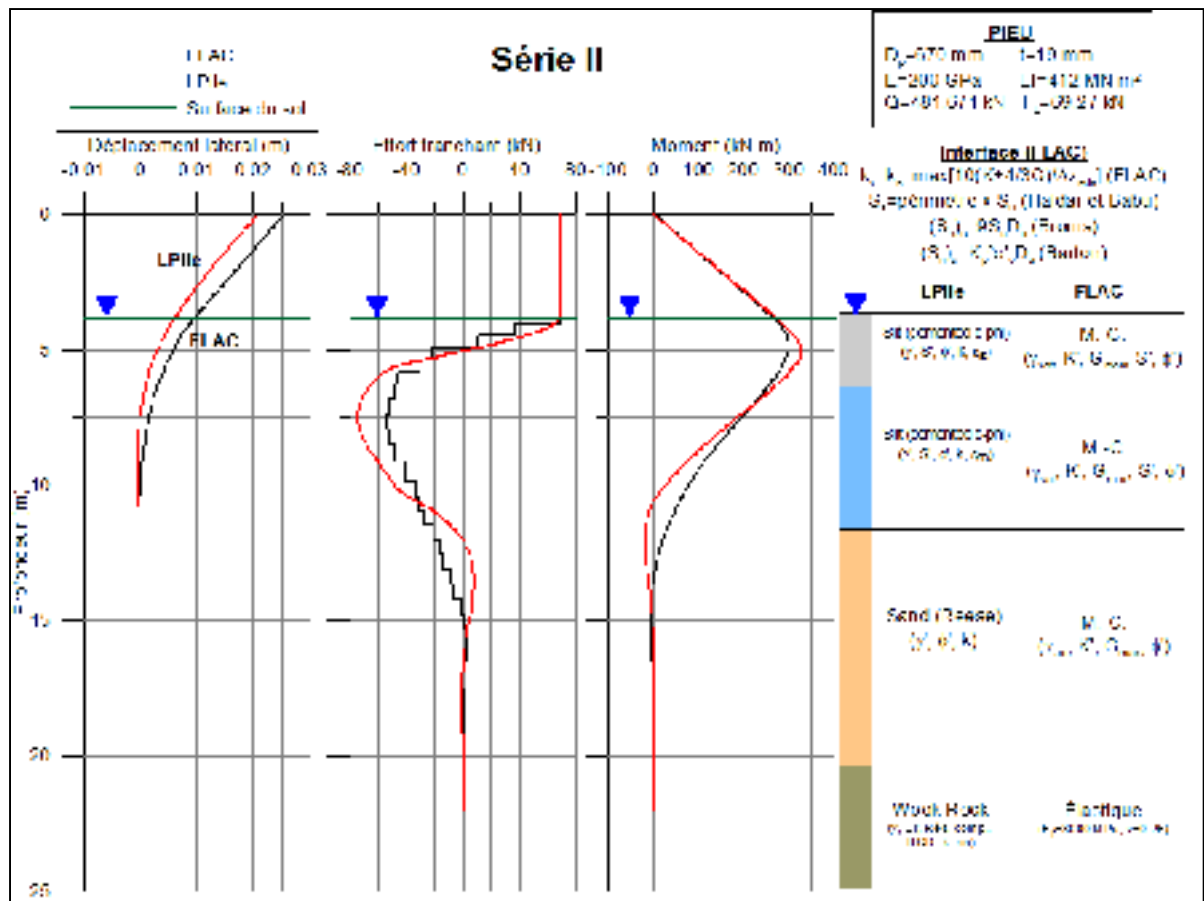


Figure 5.19 FLAC vs LPILE : Displacement, Shear and Moment for Series 2
for Bécancour Pile

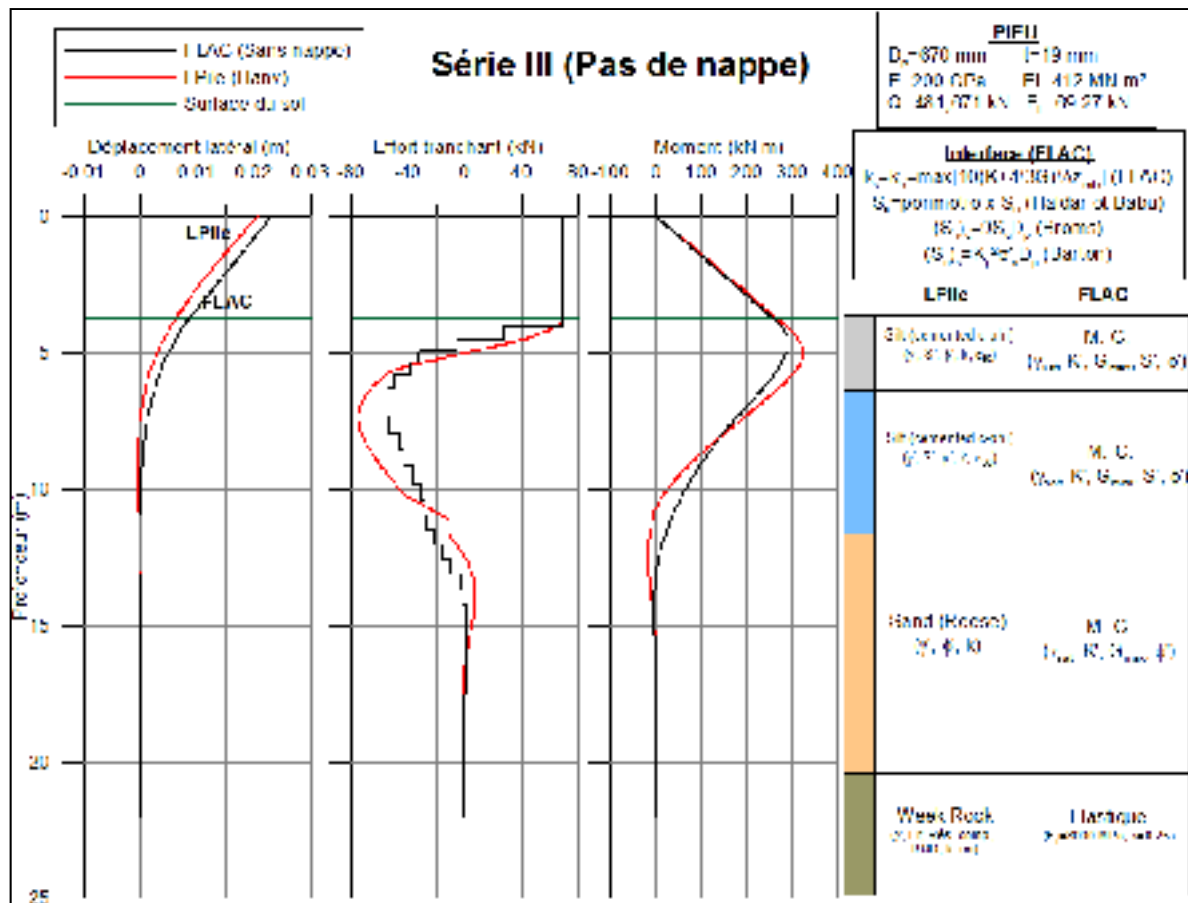


Figure 5.20 FLAC vs LPILE : Displacement, Shear and Moment for Series 3
for Bécancour Pile

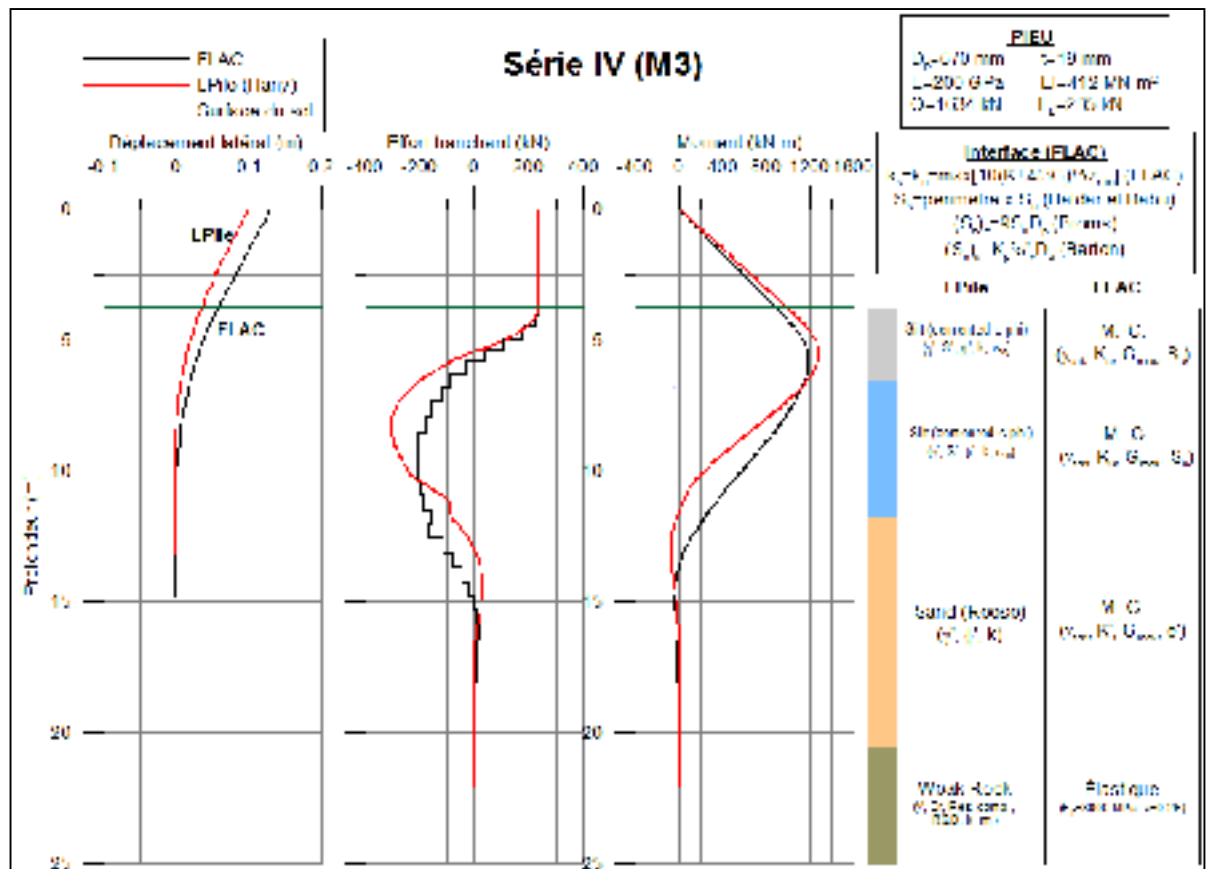


Figure 5.21 FLAC vs LPILE : Displacement, Shear and Moment for Series 1 for Bécancour Pile

CHAPTER 6

SEISMIC ANALYSIS: PRESENTATION OF RESULTS AND DISCUSSION

This chapter presents a description of the research methodology and presents results related to seismic analysis. Development of finite element models, results extracting procedure and post processing are also explained. A new method for obtaining p-y curves for dynamic analysis is introduced in this chapter. The finite element package Zsoil and Lpile were used in the analysis. Processing of results was implemented with special VBA and Matlab codes specifically developed for this study. A Dynamic to Static scaling factor DS is calculated and applied to static p-y curves in Lpile and static analyses for several load cases were performed. Results from dynamic and static analysis with dynamic p-y curves were compared and DS ratio was calibrated accordingly.

6.1 Introduction

The soil reaction P can be idealized based on Winkler theory by uniformly distributing the load applied to the beam, i.e. the pile in our case. The force P represents the reaction from the soil towards the pile in response to the soil disturbance from pile deformation. This reaction varies with depth of the pile due to the change in soil stiffness with Z . In this study the changes of bending moment occurs in the time domain as well as in the depth Z domain. Therefore, the load effects on the pile during the earthquake are a function of time and geometry.

Furthermore, the p-y curves are functions of several other parameters. This includes, beside the soil type and its nonlinear properties, the existence of water table and stratigraphy of soil layers. On the structure side, p-y curves are functions of pile diameter, pile length, free pile length above the ground and the structure mass.

The pile diameter plays an important role in the performance of long piles (Ashford, 2003; Juimnarongrit, 2001; Pender, 2004). This is also included in all original p-y equations as presented in Chapter 2. The soil reaction is applied to the leading pile-soil interface. In the case of the commonly used circular-section piles, this reaction is integrated along half of the pile perimeter. In this study the pile diameter was selected to minimize this effect. The studied pile section has a 670 mm outside diameter which results in 1.052 m half perimeter. This value made the 2D analysis results very close to the 3D analysis. Adopting a 2D analysis will minimize the analysis time and maximize the number of studied cases.

The lateral demands on the pile have an important impact on the ultimate p-y. The magnitude of this demand is proportional to the seismic intensity and the mass of the bridge. The seismic intensity is represented by the maximum ground acceleration or displacement during the earthquake and the predominant frequency of the seismic record. The predominant frequency of the seismic record influences the failure time at which the soil-pile interface reaches the yielding strain. However, the soil strains continue to increase after this point without increase in the lateral resistance.

The seismic records selected in this study represent the seismic activity of the studied locations, namely Bécancour and Quebec City as already described in Chapter 3.

The seismic force applied to a structure at each time instant follows the equation of motion. For a MDOF system, the equation of motion including the seismic force can be expressed as follows:

$$[m]\{\ddot{u}_i\} + [c]\{\dot{u}_i\} + [m]\{u_i\} = -[m]\{\ddot{u}_g\} \quad (6.1)$$

Where

- | | |
|-------|-------------------------------|
| $[m]$ | Represents the mass matrix |
| $[c]$ | Represents the damping matrix |

| | |
|--|---|
| $\{u_i\}, \{\dot{u}_i\}, \{\ddot{u}_i\}$ | Represents the structure displacements vector in the direction i and its first and second derivatives respectively, and |
| $\{\ddot{u}_g\}$ | Represents the ground acceleration vector. |

The left side of the equation represents the internal forces in the structure where the right side represents the external applied load, i.e., the seismic force. The seismic force is the product of the mass and the ground acceleration. For this study the acceleration term has not been scaled since it represents the site seismic characteristics. The mass factor has been scaled up gradually to increase the seismic demand. A total of 150 mass cases were studied. The initial mass applied represents mass1 case from the pseudo static analysis. This mass was monotonically scaled by factors between 1 and 150. For each mass case a time history analysis was performed. This process was repeated for the two records and for each of the sites. The total analysis matrix included 600 cases. In the following sections a description of the research methodology and modeling approach is presented.

6.2 Research Methodology

The research methodology involves the following aspects which will be developed stepwise in the following sections:

- (1) Site seismic response analysis
- (2) Soil-structure seismic analysis
- (3) Validation of results from the FE model
- (4) Parametric analysis
- (5) Extracting the results and post processing
- (6) Back calculations of p-y curves
- (7) Calculating p-y multiplier for seismic effect (DS ratio)
- (8) Applying p-y multiplier in static analysis model, i.e. LPILE
- (9) Comparing the results from the FE model and the LPILE model with the revised p-y and calibrating the multiplier DS.

The research is carried out based on the results from continuum finite element models that have been built in Zsoil student version. The models have been validated by comparing results from pushover analysis using Zsoil with those using LPILE.

The first two stages have been carried out using a time history analysis on finite element models that utilizes the Domain Reduction Method (DRM). The DRM was proposed by Bielac et al. (Bielak, 2003; Youshimura, 2003) in which the structure with the surrounding soil are modeled with Finite Element (FE) approach but with some enhancements. The DRM concept is explained in the following two sections.

6.2.1 Site Seismic Response Analysis

The main differences between the classical FE model and the DRM are the model size and the boundary conditions. In the classical FE model a large soil domain surrounding the structure, the pile in our case, has to be considered in the modeling. The soil domain diameter to be considered varies from site to site but it should be large enough to avoid wave reflection from rigid boundaries. In the DRM method the rigid boundaries are only needed in the beginning of the solution to calculate the reactions. In the next step, the rigid boundaries are removed from the model and replaced with the reactions from the previous step. Those forces will remain at all the subsequent solution steps. In this way the model size can be reduced significantly without affecting the results from accumulation of reflected waves. For example, in a small problem of spread footing-soil dynamic interaction, a 3600 m diameter of surrounding soil might be considered in the full model approach. Yet this distance can be reduced to 100 m with the DRM model (Truty, 2010).

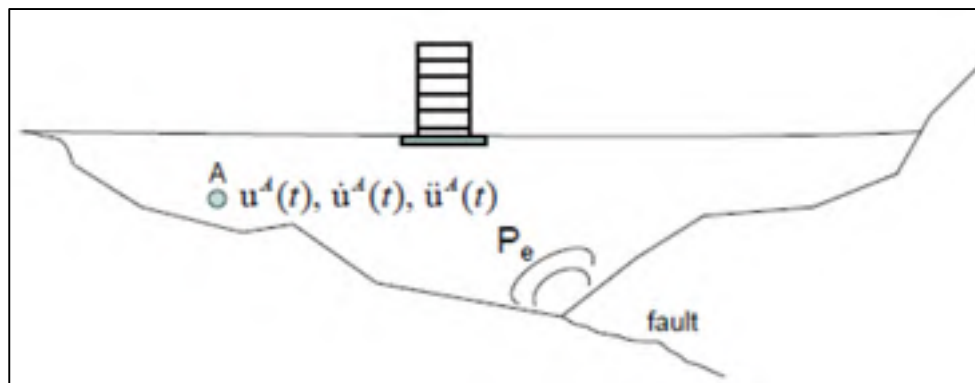


Figure 6.1 Full model of subsoil and structure, and source of the loading $P_e(t)$ (Truty, 2010)

The DRM modeling procedure consists of two consecutive stages: Background Model and Reduced Model. The Background Model will capture the response of the site to an input time function, whereas the Reduced Model will capture the structural aspects of the problem. In the Background Model stage the soil domain surrounding the structure is modeled without the structure. A time history analysis is carried out on the Background Model in order to determine the site response to base seismic excitation. The size of the model is relatively small in comparison with the classical FE models. The boundaries of the Background Model shall be defined in a way to avoid the effect of accumulation reflected waves from the rigid boundaries and yet satisfy equilibrium and stability at all analysis stages. Three different soil zones are defined in the model for this purpose, as follows:

a) The Exterior Domain: This represents the soil outside the limits of the model and at which the seismic excitation occurs. This represents typically the rock layer in the geotechnical problems. This region can be divided into two parts: the base and the side walls. The base, which is typically horizontal, is excited by an input time function. The function can be an acceleration or displacement time history record. The nodes of the horizontal base shall be restrained against gravity at all time steps during the analysis but free to displace in the horizontal direction. The vertical side walls represent the side support from the soil outside the limits of the model. The nodes on the side wall are restrained in the horizontal direction at the first time step in the analysis and free to displace in the following steps.

Nevertheless, the horizontal reactions on the side walls calculated from the first step will be maintained at all analysis steps in order to satisfy equilibrium. Another constraint shall be added here to lock the displacement of the left and right side walls during the analysis.

b) The Boundary Domain: This layer forms a transition between the exterior domain and the interior domain. The main purpose of this layer is to introduce absorption boundaries to eliminate the effect of wave reflections from rigid boundaries or structures. This can typically be achieved by defining a layer of viscous dampers at the side walls in the background model. The horizontal portion of this layer will transfer the excitation from the exterior domain to the interior domain. Both exterior and boundary domain will perform elastically.

c) The Interior Domain: This represents the actual soil layers and properties. An appropriate constitutive model shall be selected for each soil layer if the nonlinear performance of the soil element is to be captured. In this study the classical Mohr-Coulomb criterion has been considered in modeling the nonlinear behavior of the soil.

6.2.2 Soil-Structure Seismic Analysis

This analysis is conducted by performing time history analysis on the Reduced Model. The Reduced Model represents the soil as well as the structure. This model is similar to the Background Model but has an extra element: the structure. Boundary and exterior domains and rigid supports are similar to those used in the Background Model. The soil layers and soil properties are also identical. However, the structure nodes, elements, section and material properties shall be defined. The output from the Background Model is used as input to the Reduced Model. Therefore, a consistency between the two models shall be maintained when numbering and defining the nodes and elements. A time history analysis is carried out on the Reduced Model to capture the nonlinear structural performance of the pile during the earthquake.

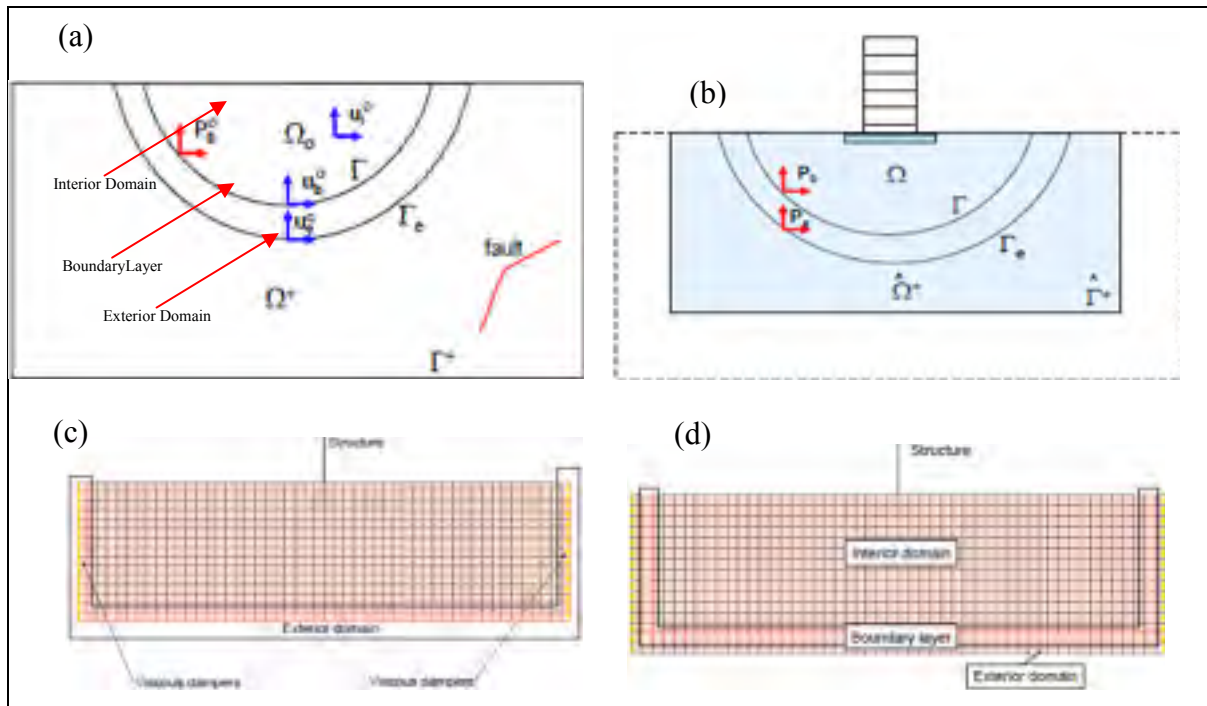


Figure 6.2 Typical soil-structure interaction problem components with DRM method (Truty, 2010): (a) Background Model (b) Reduced Model (c) viscous dampers at the side walls in the DRM model and (d) Boundaries in the DRM model

6.2.3 Description of the model

The modeling methodology explained earlier has been applied to this study. Two site response analyses were performed on each background model for the two seismic records. The background models do not include the pile. Separately, another model that includes the pile and 100 m of surrounding soil was modeled. The structural model is identical to the soil model in terms of node geometry, node numbering, continuum elements, materials and boundary conditions. The node deformations, i.e. displacements and rotations, from the background model represent the seismic input to the structural model. The soil was modeled with 2D continuum elements. The pile was modeled with classic beam element with three Gaussian points. The Gaussian point in the middle of the beam was considered for recording the results. The beams and soil elements shares the same nodes at the soil-pile interface. The possibility of separation between the soil and beam was also considered in the model. This

was possible by assigning cut-off properties to the nonlinear soil model. In this way if separation between the soil and pile element will take place when tension stresses in the soil exceed the stress limit defined in the material model.

The soil was assumed to follow Mohr-coulomb law (MC) with the effect of dilatancy. Tension resistance was assumed to be zero. The selection of MC model for this study was based on the fact that the studied soil is mostly c-phi soil and MC simplicity which results in faster analysis. Figures 9.3 and 10.4 depict several soil behavior models compared to the real nonlinear behavior and MC idealization. Pile material model was modeled with elastic steel properties. The nonlinear EI property of the steel section was not possible to consider directly in the model due to software limitations. However, the results for the time history analysis were limited to the yielding moments of the steel section, about 3 MN.m, which was obtained from a separate section analysis.

Lumped mass was applied at the pile head to represent the superstructure mass. The initial mass value was taken from the pseudo static analysis, see Chapter 5 for details. The results from the dynamic analysis were integrated to calculate p-y curves. Nevertheless, the calculated p-y curves were found to be under the ultimate capacity of the soil. In other words, the obtained curves represent the elastic soil and P_{ul} could not be achieved from the applied masses. This mass was later scaled up by an increasing factor from 1 to 150 until failure in soil is reached.

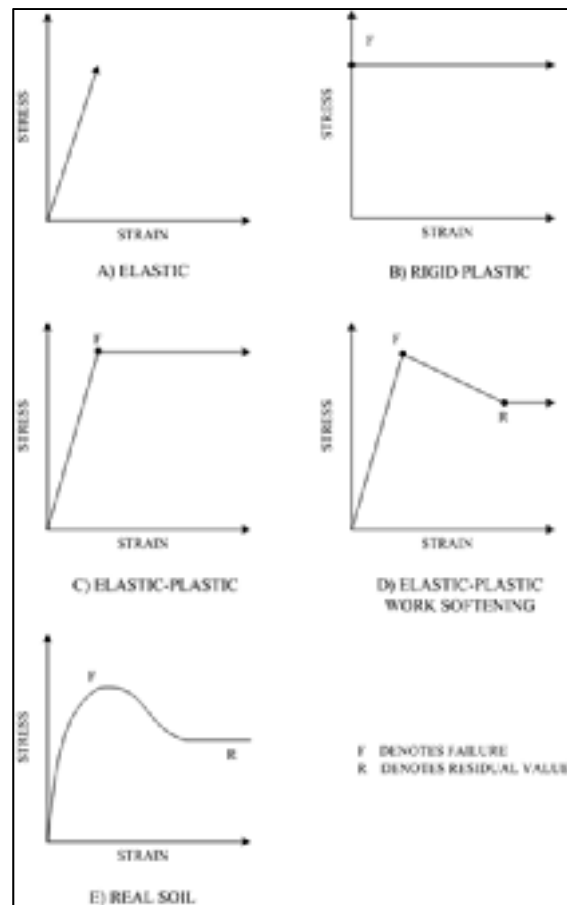


Figure 6.3 Several soil models and Real soil behavior

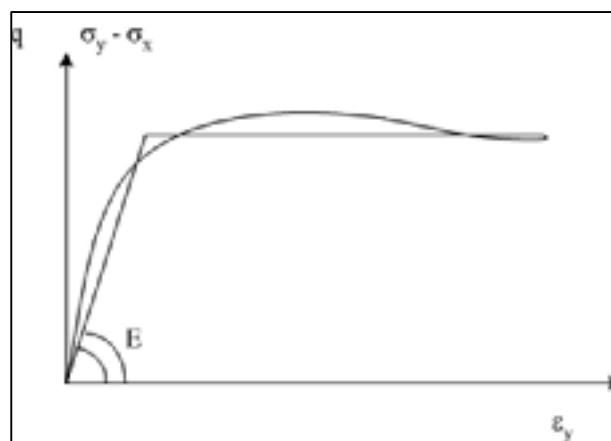


Figure 6.4 Idealization of soil behavior with Mohr-Coulomb Model

6.2.4 Validating the FE model with LPILE for static load case

The Zsoil model was validated with Lpile. A static push-over analysis was performed in Zsoil on the same model that is used later for dynamic analysis. The deformed shapes and bending moment diagrams were compared from both analysis and found to be reasonably matching.

6.2.5 Analysis matrix

The analyses were initially performed with masses that are equivalent to the base shear at the studied seismic region. The evaluation of the required masses at the top of the pile to generate an equivalent earthquake static load was presented in Chapter 5. The analysis was carried on with two seismic records for each site. The records were developed at the University of Laval as presented in Chapter 4. The analysis matrix includes a total of 12 cases as presented in Table 6.1.

Table 6.1 Analysis matrix table

| Site\ record | R1 | | | R2 | | |
|------------------|---------|---------|---------|---------|---------|---------|
| | Mass 2 | Mass3 | Mass4 | Mass 2 | Mass3 | Mass4 |
| Bécancour | BECR1M2 | BECR1M3 | BECR1M4 | BECR2M2 | BECR2M3 | BECR2M4 |
| Quebec | QCR1M2 | QCR1M3 | QCR1M4 | QCR2M2 | QCR2M3 | QCR2M4 |

6.2.6 Post-processing of results

The pile results were recorded at each 0.1 sec during the analyses for every node along the pile (approximately 0.5 m apart). The flexure moment, shear, and lateral deformation were extracted for each mass case and post processed for further analysis. The post processing phase includes four steps as follows:

Step 1- Back calculations of p-y curves from dynamic analysis

The results of this analysis include lateral displacements and bending moment captured at 0.1 sec intervals. The results were imported to MATLAB for post processing and back calculations of p-y curves. The discrete load transfer (DLT) approach is employed to obtain the p-y curve in which the following integrations are calculated at the pile nodes. The results of this analysis are presented in Figures 0.12to 0.20.

$$M(Z, t_i) = E_p I_p \frac{d^2 y_p}{dZ^2} = E_p I_p \frac{\varepsilon}{h} \quad (6.2)$$

$$P(Z, t_i) = \frac{d^2 M(z, t_i)}{dZ^2} = E_p I_p \frac{\varepsilon}{h} \quad (6.3)$$

$$y_p(Z, t_i) = \frac{1}{E_p I_p} \iint M(z, t_i) dz \quad (6.4)$$

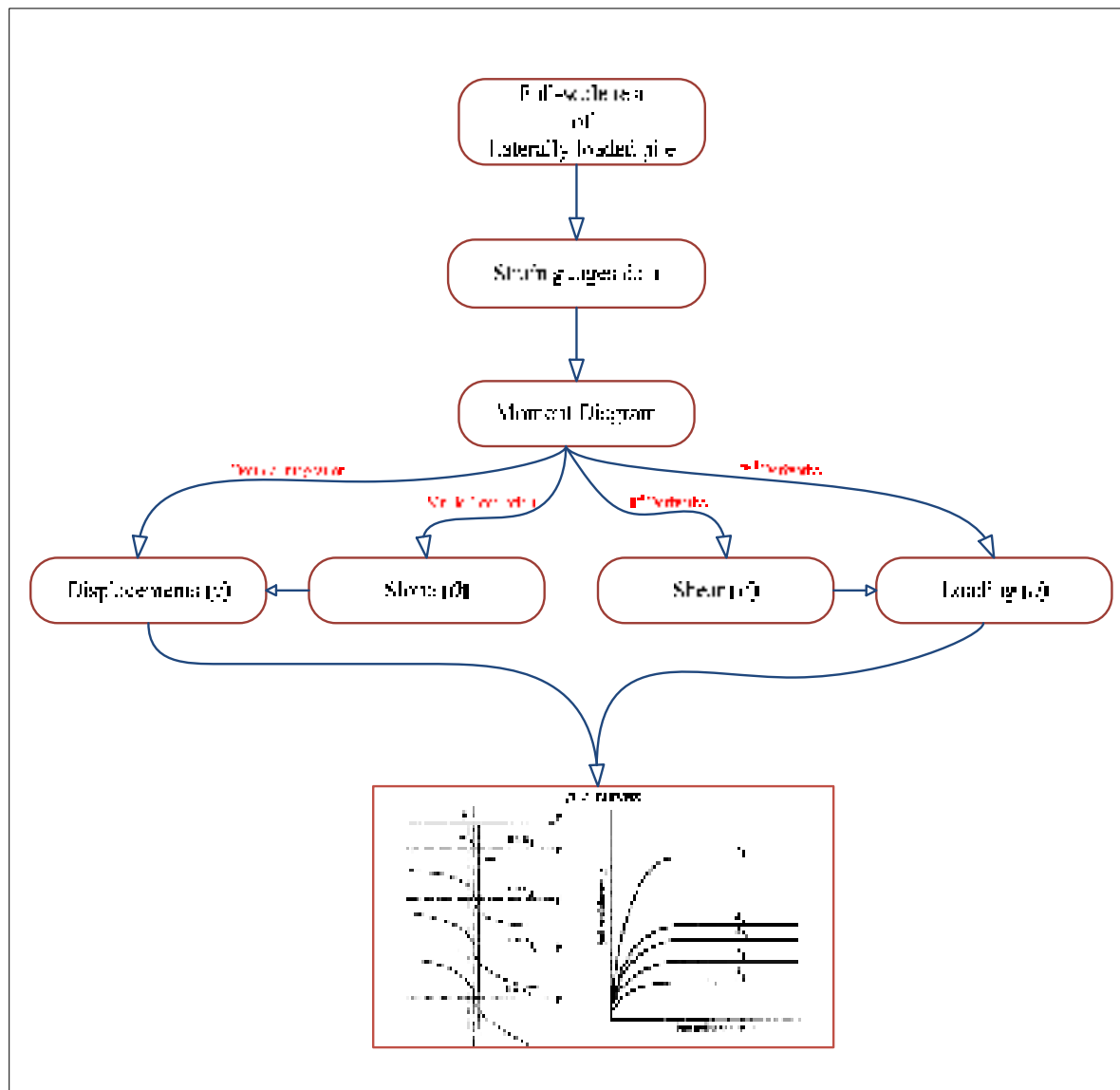


Figure 6.5 DLT integration flowchart for p-y back calculations

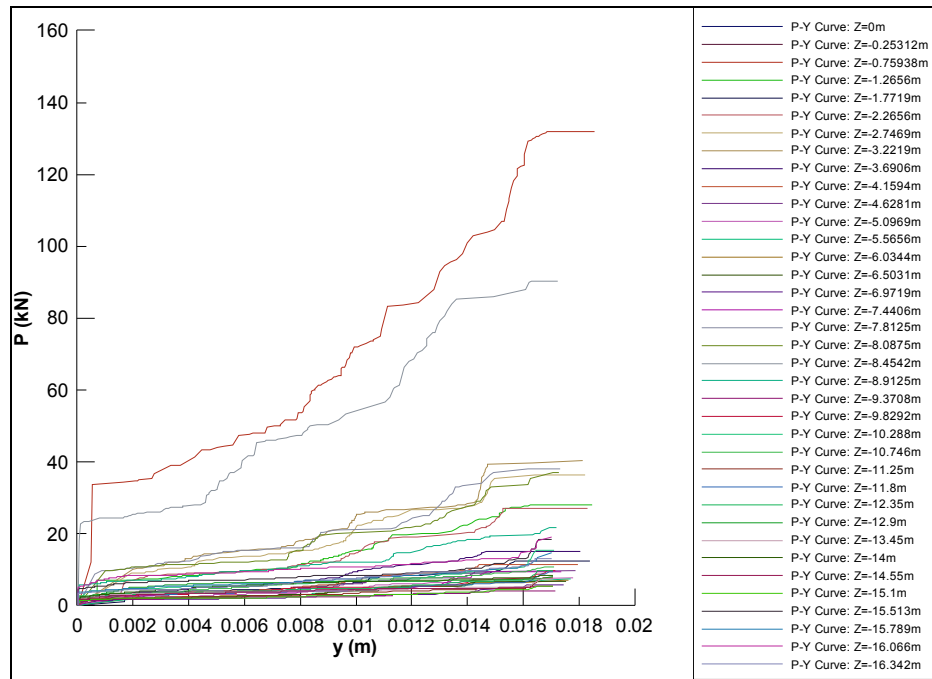


Figure 6.6 Back-calculated p-y curves for BECR1M2

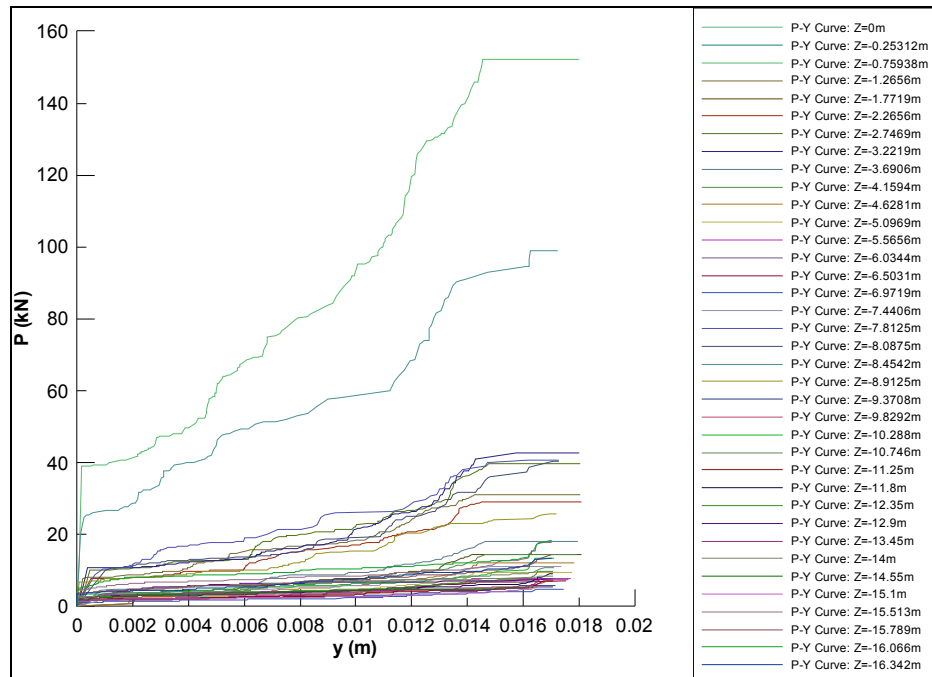


Figure 6.7 Back-calculated p-y curves for BECR1M3

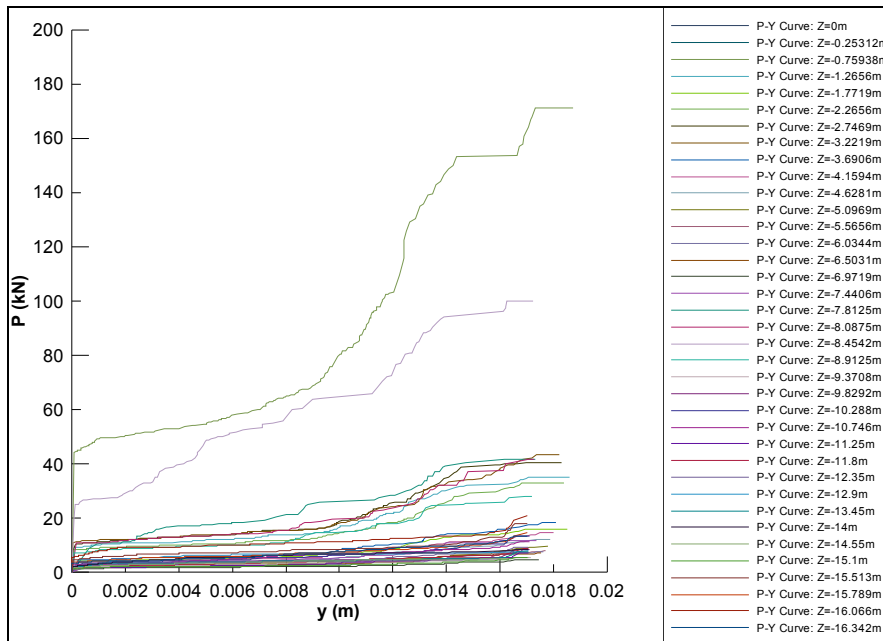


Figure 6.8 Back-calculated p-y curves for BECR1M4

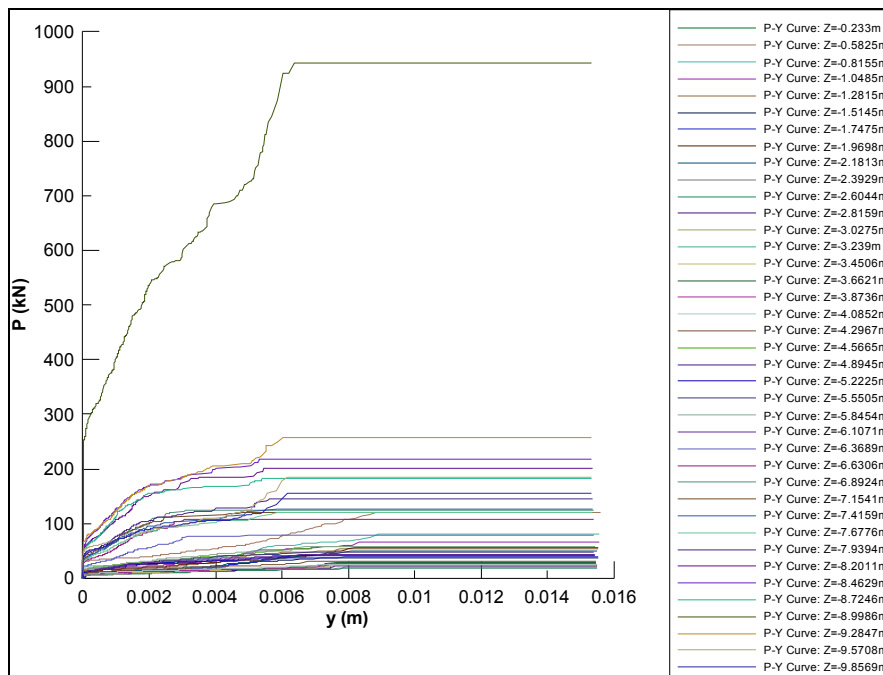


Figure 6.9 Back-calculated p-y curves for QCR1M2

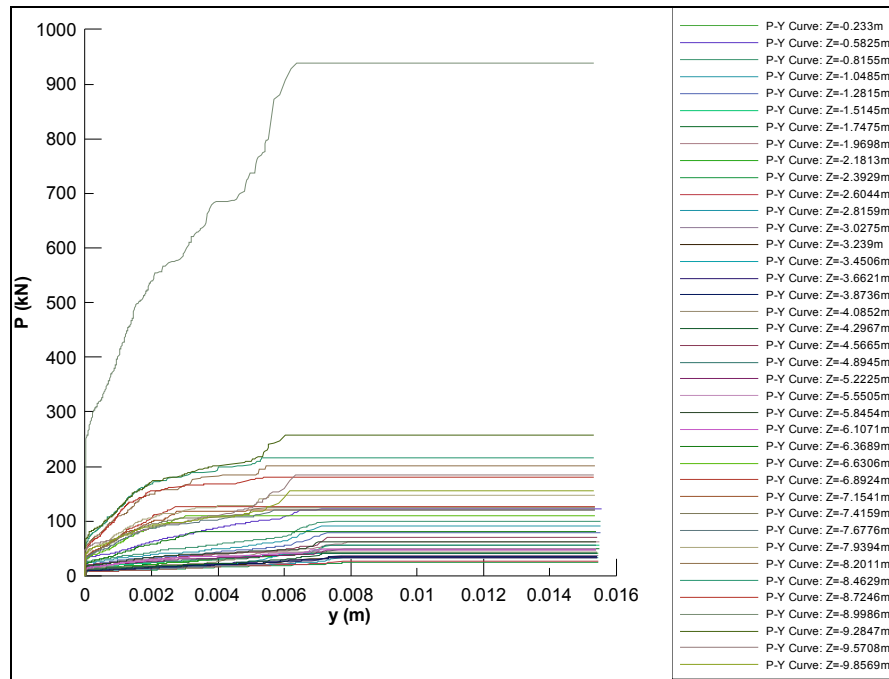


Figure 6.10 Back-calculated p-y curves for QCR1M3

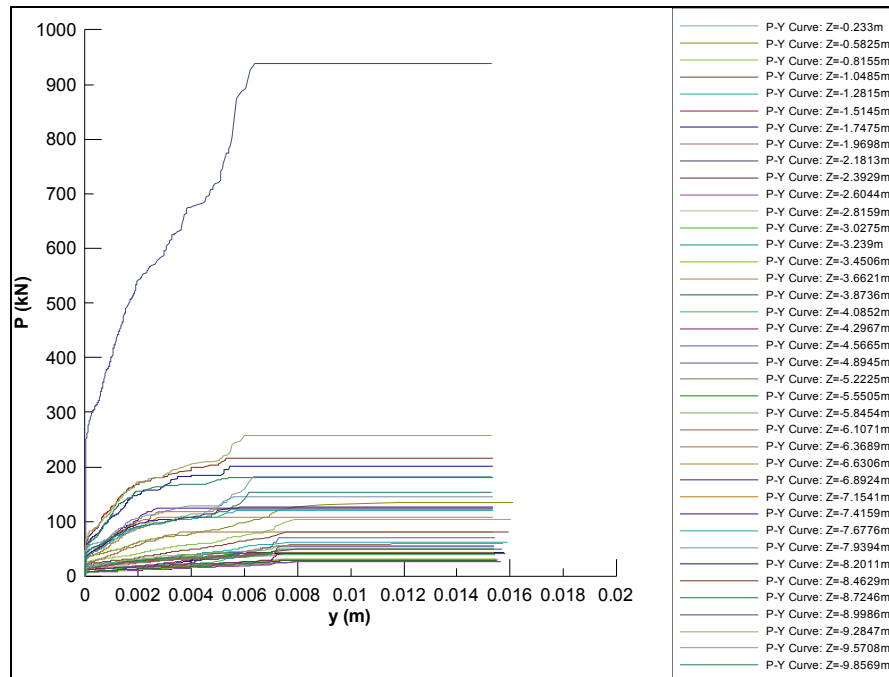


Figure 6.11 Back-calculated p-y curves for QCR1M4

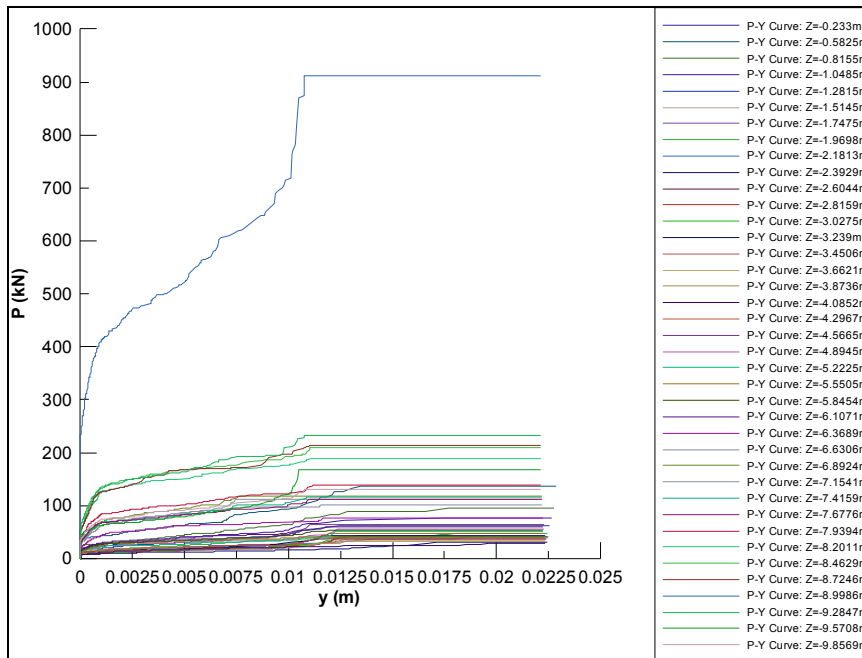


Figure 6.12 Back-calculated p-y curves for QCR2M2

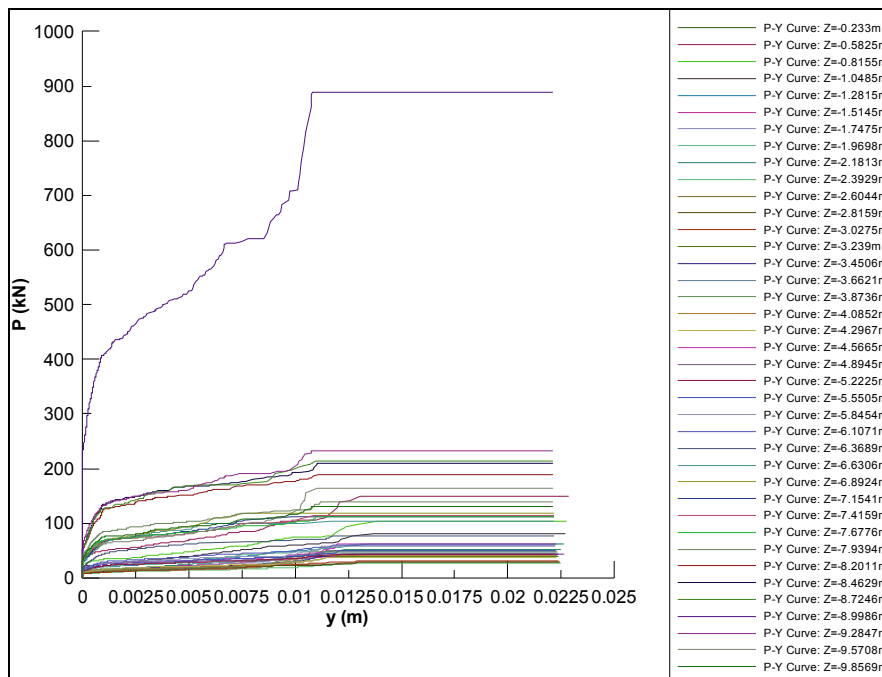


Figure 6.13 Back-calculated p-y curves for QCR2M3

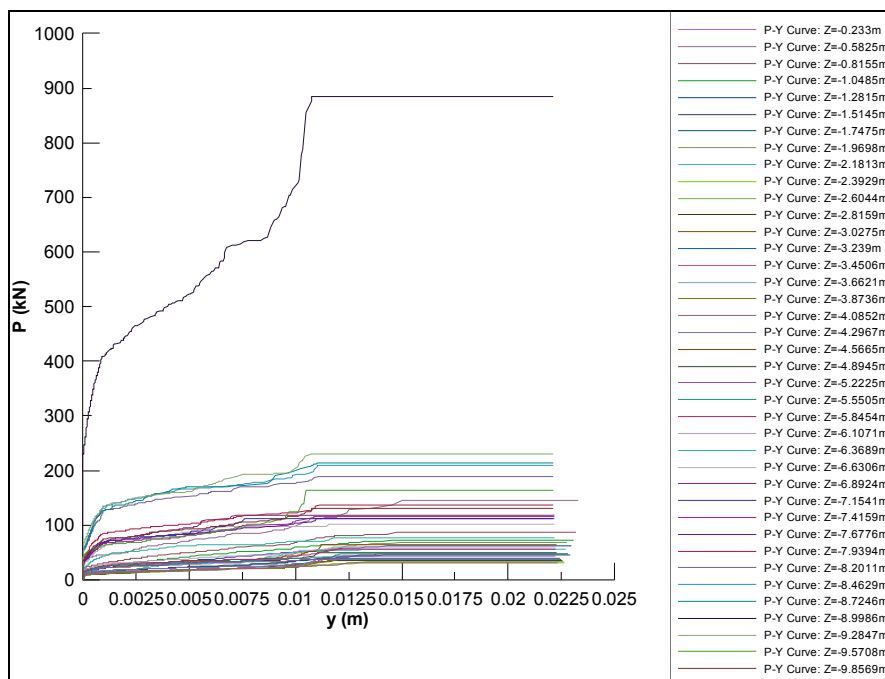


Figure 6.14 Back-calculated p-y curves for QCR2M4

Step 2- Calculating flexure capacity of the pile

The maximum flexure capacity of the pile section was first calculated using Lpile P-M interaction analysis. This was achieved by varying successively the axial thrust P and calculating the corresponding moment capacity M . The analysis was repeated using another software SP-Col for validation. The flexure capacity of the pile section was found to be around 2.5 MN.m. The P-M interaction diagram of the pile and the nonlinear EI-Moment curves are depicted in Figure 6.15 to Figure 6.17.

The purpose of this analysis is to limit the maximum moment along the pile to its flexural capacity, i.e., to exclude mass cases which results in demand to capacity ratio greater than 1.

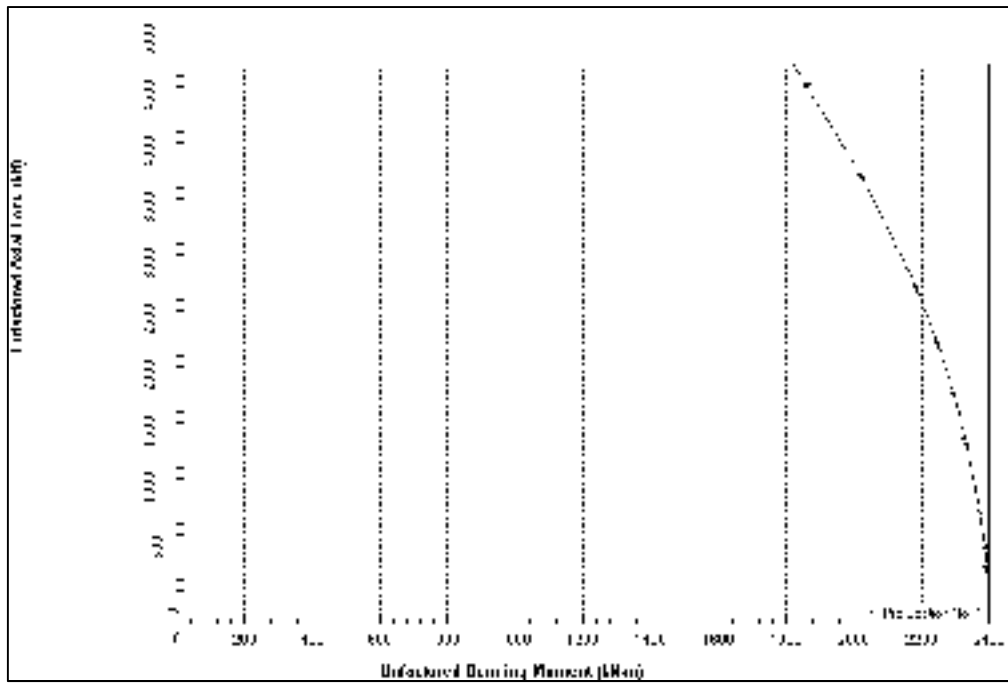


Figure 6.15 P-M interaction curve for the pile section for applied axial loads

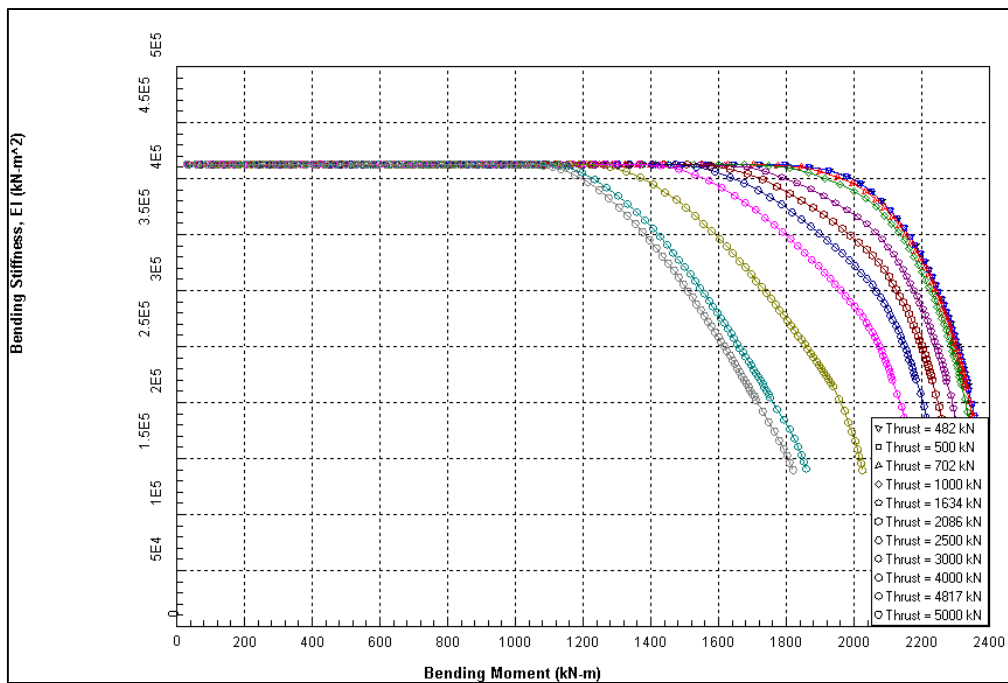


Figure 6.16 Nonlinear EI vs bending moment for the pile section

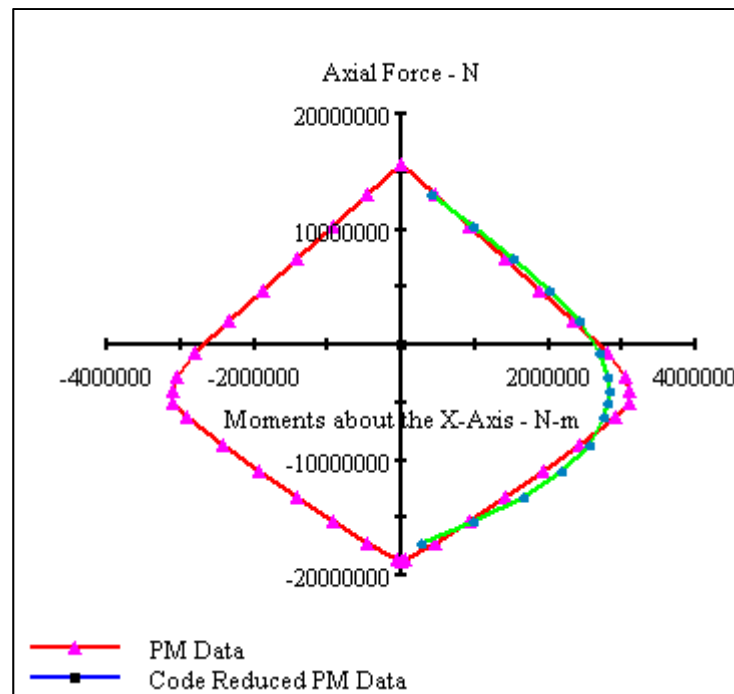


Figure 6.17 P-M interaction envelope

Step 3- Extracting the Maximum Moment at certain depth

Zsoil data are stored in special format files that include the results of all elements in the models including the beam and continuum elements. A VBA code was developed to export the beam results from Zsoil format to matrix format in order to be processed later in Matlab. A Matlab code was written to process the imported data. The Matlab procedure, called `ExtractPsFromSTR`, reads the text files which represent the results from each mass case. The text files contain recorded moments, shear and deformations along the pile for each time instance during the earthquake. `ExtractPsFromSTR` filters each of these files to obtain the maximum moment and to capture its occurrence time and store them in a separate matrix; this matrix is expanded to include the results from the next mass case. The final matrix contains the maximum moments along the pile for each mass case. This matrix is filtered once again to obtain the maximum of maximum moments among all mass cases for each depth along the pile.

This filtering process, explained in the previous paragraph, tests the obtained moment for each mass case by comparing it to the maximum flexural capacity of the pile section. Thus, mass cases resulting in demand to capacity ratio greater than one are excluded from the matrix.

The final obtained bending moments are compared to the bending moments along the pile from the pseudo static analysis. A dynamic to static ratio is then calculated to scale the static p-y curves.

Step 4- Calculating the dynamic/static p-y ratio (DS) for large cyclic stresses

Soil layers during a severe earthquake are exposed to large shear strains within very short time, typically within parts of 10^{th} of seconds. This rapid application to shear strain, with the presence of the water, leads to an increase in the soil pore pressure and makes the soil deposit weaker to resist lateral loads. Pore pressure reduces the friction between soil particles and lubricates the surfaces between these particles which makes it easier for them to move relative to each other. In some cases, this might trigger liquefaction in the soil which is outside the scope of this study. On the soil-pile interface, failure modes have different aspect. When a surrounding soil layer becomes weak and has less lateral resistance, the pile at the failed soil region has no lateral support. A redistribution of the forces in the soil-pile system must take place to accommodate this change and maintain equilibrium. In Winkler model, this means that the spring representing the failed soil layer has lost some or all of its stiffness; therefore the reduction in the spring reaction shall be carried by the neighboring springs until the equilibrium is satisfied. This means that the shear in the neighboring springs is increased and consequently the bending moment is increased as well. The displacements will increased dramatically in the failed layer and less increase will be seen in the stronger layers. The point where the maximum demands, shear and moment, occurs along the pile will shift as well, typically downward. This shift is controlled by several parameters including the stratigraphy of the site, the soil properties and the magnitude and nature of the earthquake signal.

This mechanism of consequential failure is modeled in this study by scaling up the lateral seismic demands. The seismic demands applied to the system were gradually increased by applying a scale factor to the mass at the piles head. That is to say, the mass was kept increasing to insure a failure in the soil layer is formed. Apparently, the stronger soil layers require higher mass values to achieve the failure point.

The maximum moment along the pile from all mass cases at a specific depth represents the maximum moment that can be achieved in the pile considering partial or complete failure of the surrounding soil and neighboring layers. With this in mind, the case which results in maximum possible moment in the pile at certain depth is also the case at which the soil at that depth is deemed to be failed under the applied seismic load. In other words, this soil reached its ultimate seismic capacity P_{u_seism} . Sensibly P_{u_seism} is expected to be smaller than P_{u_static} . The ratio P_{u_seism}/P_{u_static} can be used to scale the original p-y curves of the soil to capture the seismic performance of the soil-pile system during an earthquake. In the following section a proposed method to calculate this ratio is presented.

This concept is employed here to scale the static p-y curves to achieve the dynamic p-y. A new dynamic/static ratio is introduced here. The DS ratio of the pile at depth Z is defined as the ratio of maximum dynamic effect of the pile at Z from seismic load to the static effect at Z from an equivalent static load. The DS ratio is depth dependent. The seismic p-y curves can be obtained from scaling the static p-y curves by DS to obtain lower bounds. The DS factor and seismic p-y curves can be calculated by the following equations:

$$DS = \frac{\text{Dynamic effect}}{\text{static effect}} \quad (6.5)$$

For instance the DS factor of the bending moment can be calculated from the following equation:

$$DS_M = \frac{M_{Dyn-max}^{zi}}{M_{Stat-max}^{zi}} > 1 \quad (6.6)$$

Similarly the DS factor with respect to soil displacement can be calculated from the following equation:

$$DS_y = \frac{y_{Dyn-max}^{zi}}{y_{Stat-max}^{zi}} > 1 \quad (6.7)$$

In order to scale the static p-y curves to obtain equivalent seismic p-y curves, the two components of the curves needs to be scaled independently as follows:

$$p_{Dyn} = \frac{p_{Stat}}{DS_M} \quad (6.8)$$

$$y_{Dyn} = y_{Stat} \times DS_y \quad (6.9)$$

The reason for these separate scaling operations is to satisfy the following two conditions:

$$p_{u_seismic}/p_{u_static} \leq 1 \quad (6.10)$$

$$y_{pu_seismic}/y_{pu_static} \geq 1 \quad (6.11)$$

These two statements represent the typical state of cohesion or cohesionless soils under seismic load.

The equivalent static load case can be obtained by measuring the maximum displacement of the pile head corresponding to $M_{Dyn-max}^{zi}$ which is obtained from the dynamic analysis. The lateral pile head displacement is then applied to the static analysis model such as Lpile.

Comparing the results from both models can then be used to calculate the DS factor as preceded.

6.2.7 Presentation and discussion of results

Results from seismic analyses are presented in Figures AI.1 to AI.55 of appendix AI. The results from the processed data are presented in Figures 6.19 to 6.40 in terms of normalized moment and lateral displacements vs depth for both sites.

The following observations can be made based on the deformed shape and bending moment plots for the pile of both static and dynamic analysis (Figure 6.19 to Figure 6.40):

- The soil in the dynamic analysis has smaller lateral resistance: although the pile head has the same lateral displacement from both cases, it can be observed that lateral deformations along the pile depth from the equivalent static load case are smaller than those from the dynamic analysis. The soil deformations in the static analysis decreased rapidly under the ground surface compared with the seismic load case. Therefore, it can be said that the soil restrains the pile against lateral deformation at shallower depths in the static case— see Figures 6.21, 6.22, 6.27, and 6.28. The lateral deformations converged to zero much quicker than in the dynamic load case. This indicates a deeper point of fixity for the dynamic load case. Yet this finding can be determined from comparing the bending moment diagrams.
- The imbedded length of the pile has significant effect on its performance: It can be noticed from comparing the lateral displacements from static and seismic load cases for Bécancour and Quebec sites, that for long piles the dynamic effect is much apparent. By comparing the depths of point of fixity between the two sites from seismic and static, it can be observed that the longer the pile, the higher is the dynamic effect. – see Figures 6.32, 6.33, 6.38, and 6.39.

- Mass inertial effects on the bending moment diagram are more noticeable in the dynamic analysis: the bending moment of the pile part above the ground is linear in the static load case represented by continuous line connecting the zero moment at the pile head to the maximum moment under the ground surface. In the dynamic load case the line is not continuous – see Figures 6.19 and 6.25. The moment line above the ground surface is steeper than in the line below the ground. This indicates a sudden change in the shear effect just below the ground surface. This effect is not observed in the static analysis. This is due to the fact that currently used p-y curves were driven from the results of full scale tests on piles performed with steady slow cyclic load that produce small shear strains rate in the soil. However, in the dynamic load case the application of the lateral load is much rapid, abrupt and varies with time. The free pile portion responds to the seismic load faster than the embedded part. Therefore, the moment along the pile will suddenly change below the ground surface due to this fact. This change depends on the mass magnitude, the intensity of the seismic load, and the ratio of free to embedded pile.
- The depth of the point of fixity for the static load case is shallower than the dynamic load case: this conclusion is obtained from comparing the bending moment diagrams from the dynamic load case and its equivalent static load case. It can be noticed from all cases that maximum moment from the dynamic load cases occurs at deeper Z than those of equivalent static load cases. This indicates that the soil above the point of fixity from the dynamic load case has failed and do not provide much lateral resistance to the pile as in the case of the equivalent static load.
- The shift in the point of fixity to deeper elevations has several effects on the design of long bridges. In the case of long bridges with deep foundation, the first mode occurs generally in the longitudinal direction of the bridge. The more slender the shafts supporting the piers and superstructure the more flexible the bridge and the higher the fundamental period –see Equations (6.12) and (6.13).

$$T = 2\pi \sqrt{\frac{W}{gK}} \quad (6.12)$$

$$K = c \times \frac{EI_p}{PL_p^3} \quad (6.13)$$

Where

T = fundamental period of the bridge;

W = the weight of the superstructure;

c = constant depends on the I_b/I_c see Figure 6.18;

EI_p = flexure rigidity of pile section; and

L = the distance between the superstructure and the point of fixity of the pile.

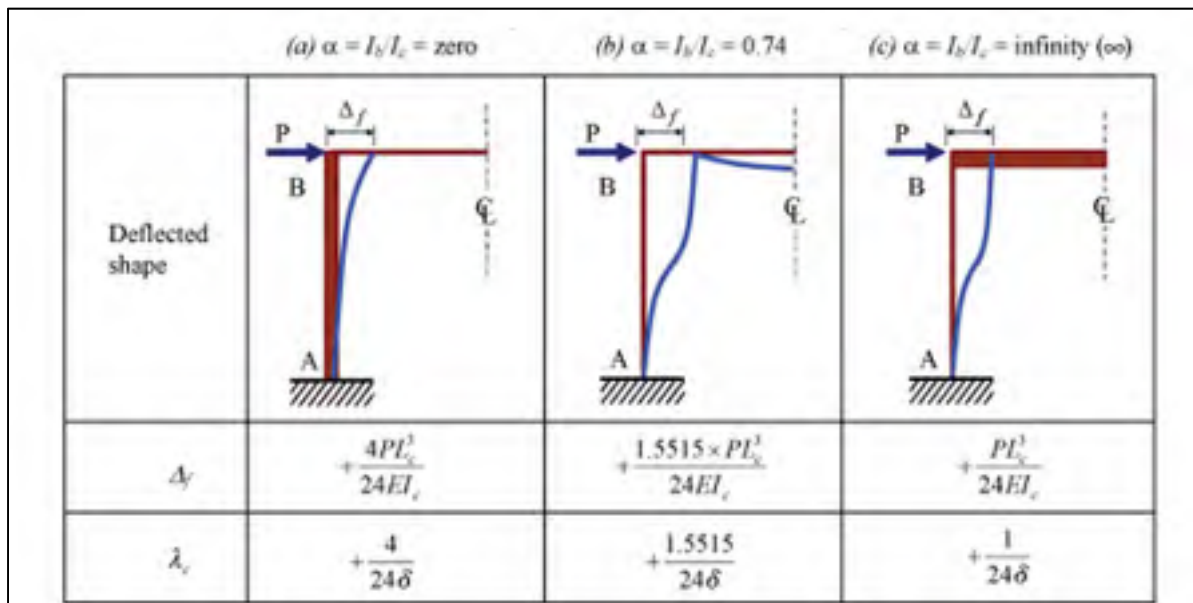


Figure 6.18 Pile head deformation for varying values of I_b/I_c
(Silva, 2008)

- In practice, the designer may choose to integrate the piles model in the global bridge model to accurately estimate the fundamental period of the entire structure. The surrounding soil can also be modeled with one node springs attached to the pile interface and have the p-y curve properties. Limited with time and computation capacity, the

designer might model the pile down to the level of point of fixity which is obtained from a separate calculation. Another option is to include the entire length of the pile in the model and obtain the point of fixity elevation from the global model – normally is the point at which maximum moment occur in the pile. In both cases the shift of point of fixity to deep elevation results in more flexible system, more slender piles and relatively longer fundamental vibration period and significant mass participation. This leads to three direct effects on the design of the bridge:

- (1) Decrease in the seismic demands on the piles.
 - (2) Increase in displacement demands of the superstructure and hence increase in the ductility demand of the bridge.
 - (3) Increase in the seismic demands at the rock-socket part of the pile.
- Reduction in seismic demand on the foundation may results in smaller sections and lowers the cost. However, the increase in the ductility demands increase the design cost significantly. In general, the seismic design philosophy for pile foundation is based on the concept of protected piles approach. This means no failure is allowed to occur in the pile beneath the ground during the earthquake. This is simply because, in most cases, it is not possible to reach the pile at the damaged location to repair after the shake. Instead, the designer allows the failure to occur at selected locations in the pier column, typically at the column base, at which a plastic hinge will form under lateral seismic load. The design of the plastic hinge is controlled by the ductility demands and ductile capacity required by the code and the designer. Design of ductile structures beside its complexity is not a cost effective choice. The special detailing requirement of the plastic hinge zones increases the overall cost of the design, however this cost remains relatively low when compared to the cost of conventional elastic design especially. In addition to the cost factor, the ductile design approach leads to safer structures due to the non-brittle type of failure during earthquake. This behavior is mainly desired because it allows for evacuation of civilians and maintenance of the bridge.

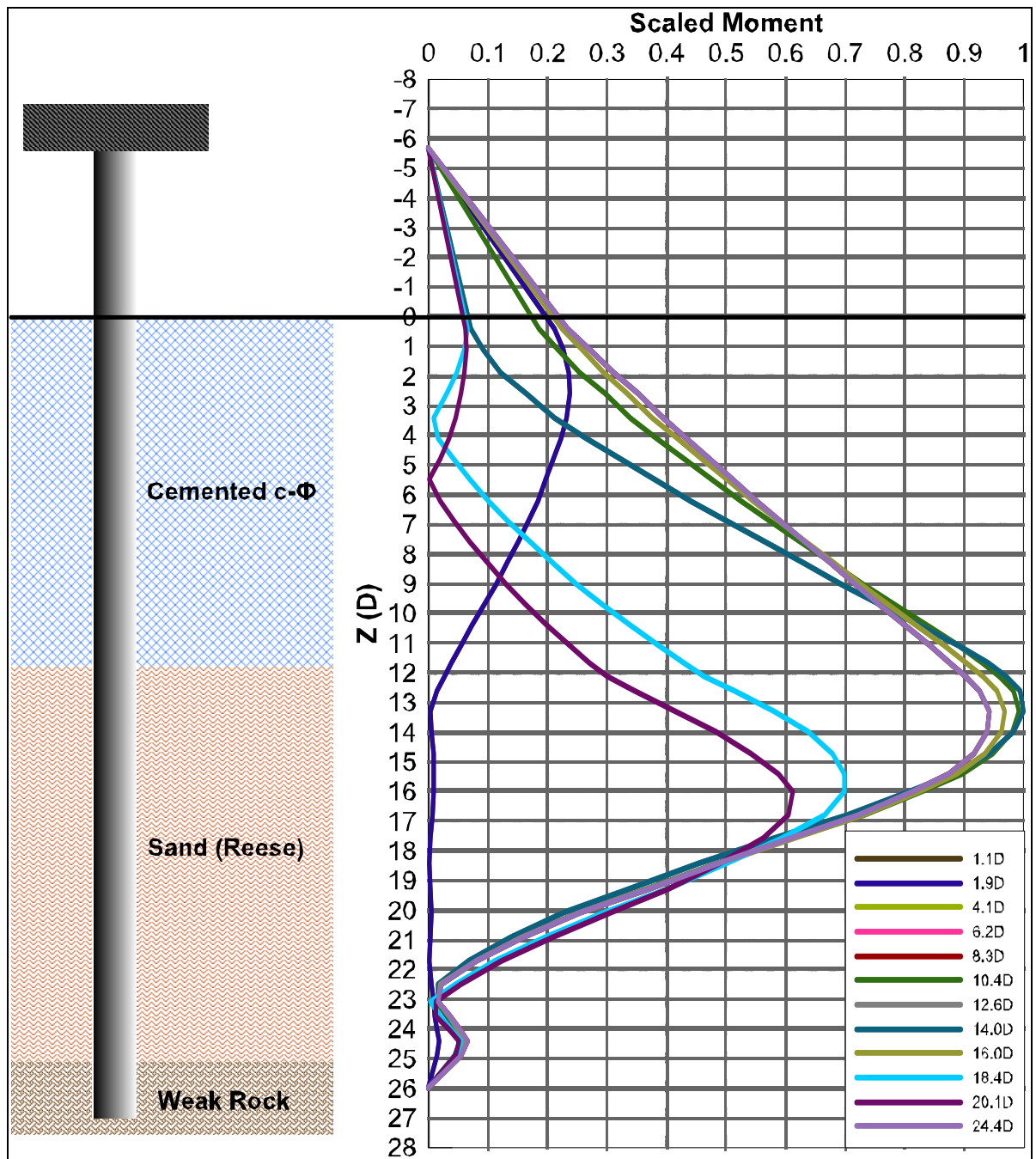


Figure 6.19 BECR1 seismic scaled bending moment

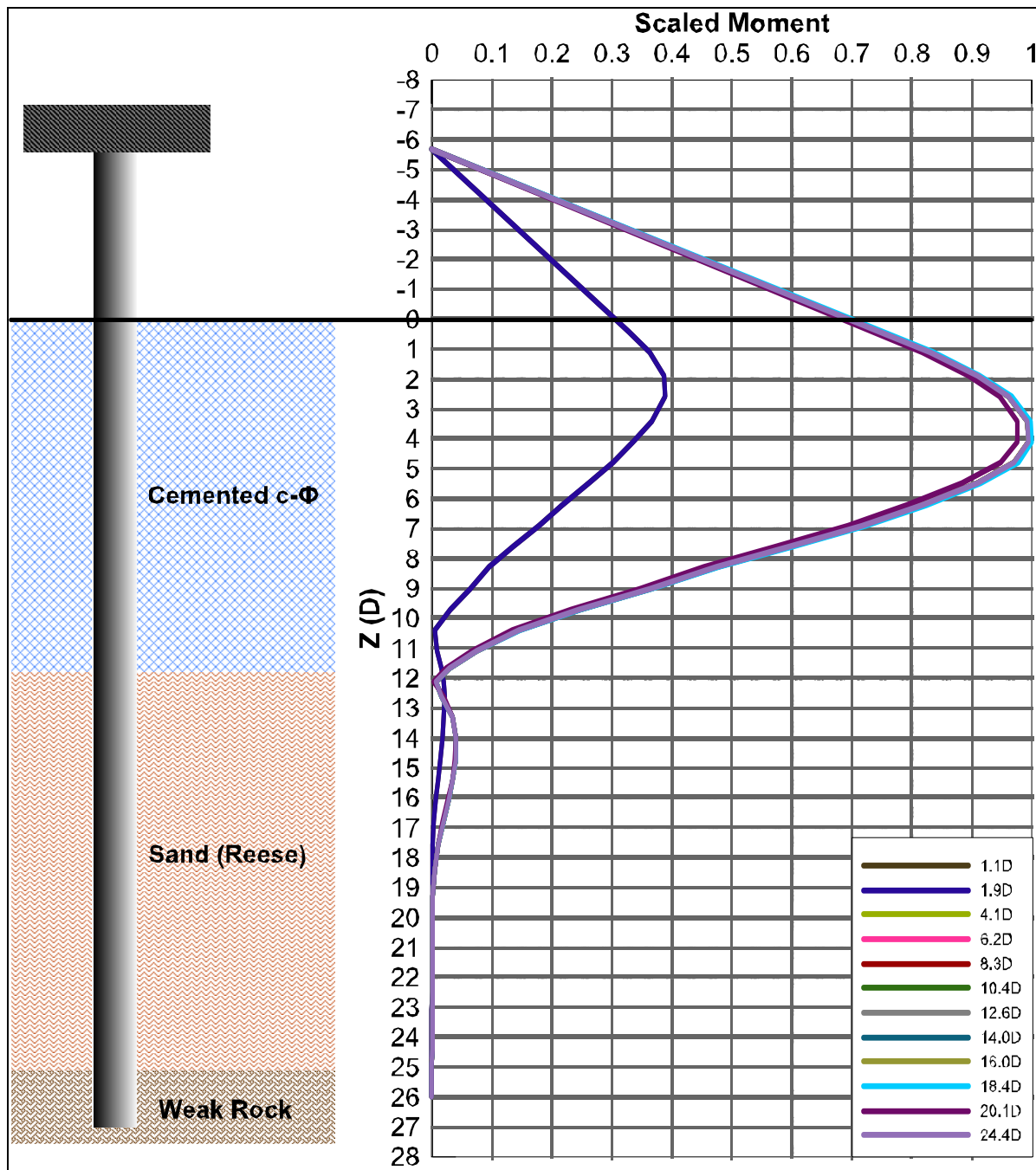


Figure 6.20 BECR1 static scaled bending moment

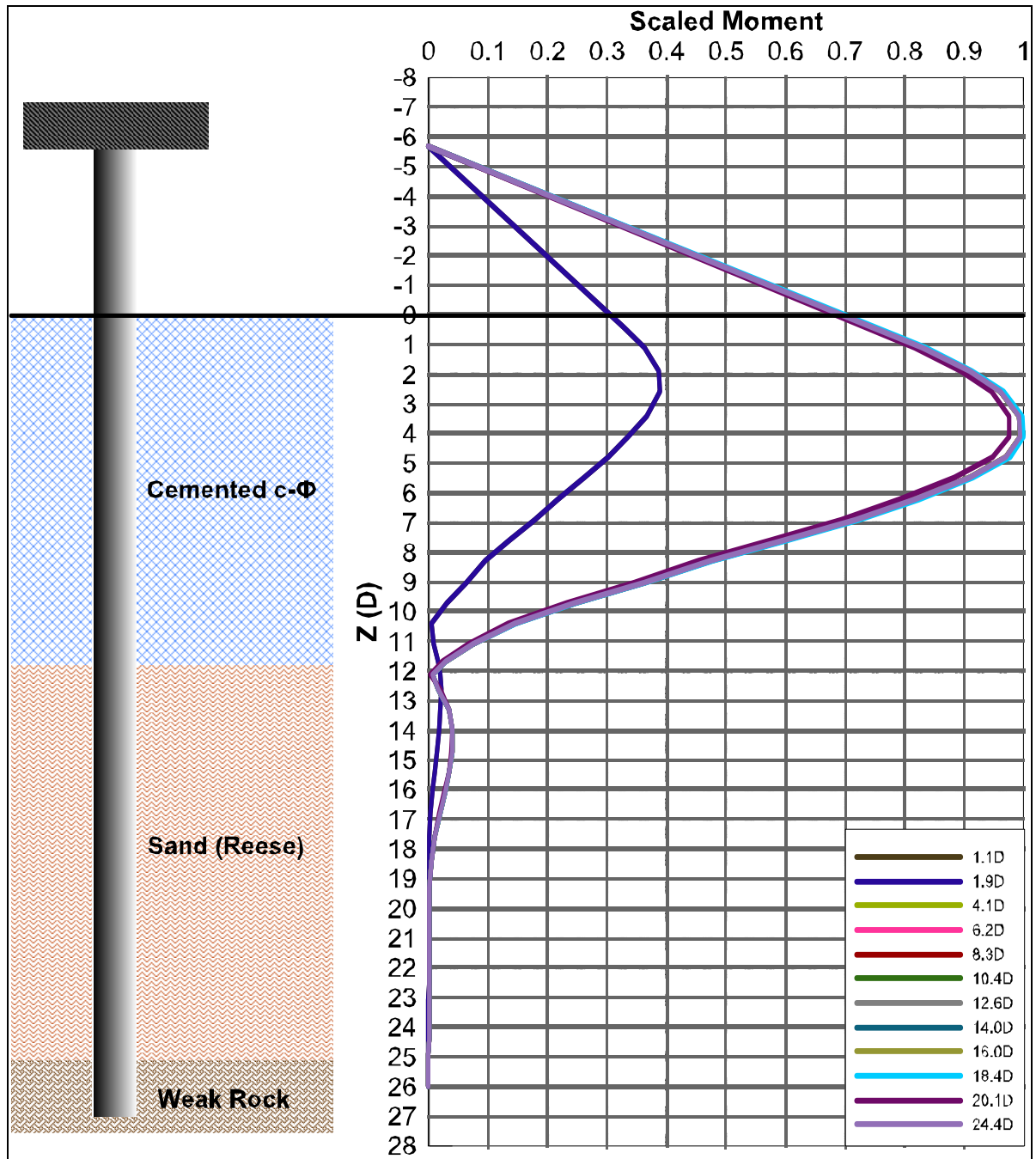


Figure 6.21 BECR1 seismic scaled displacements

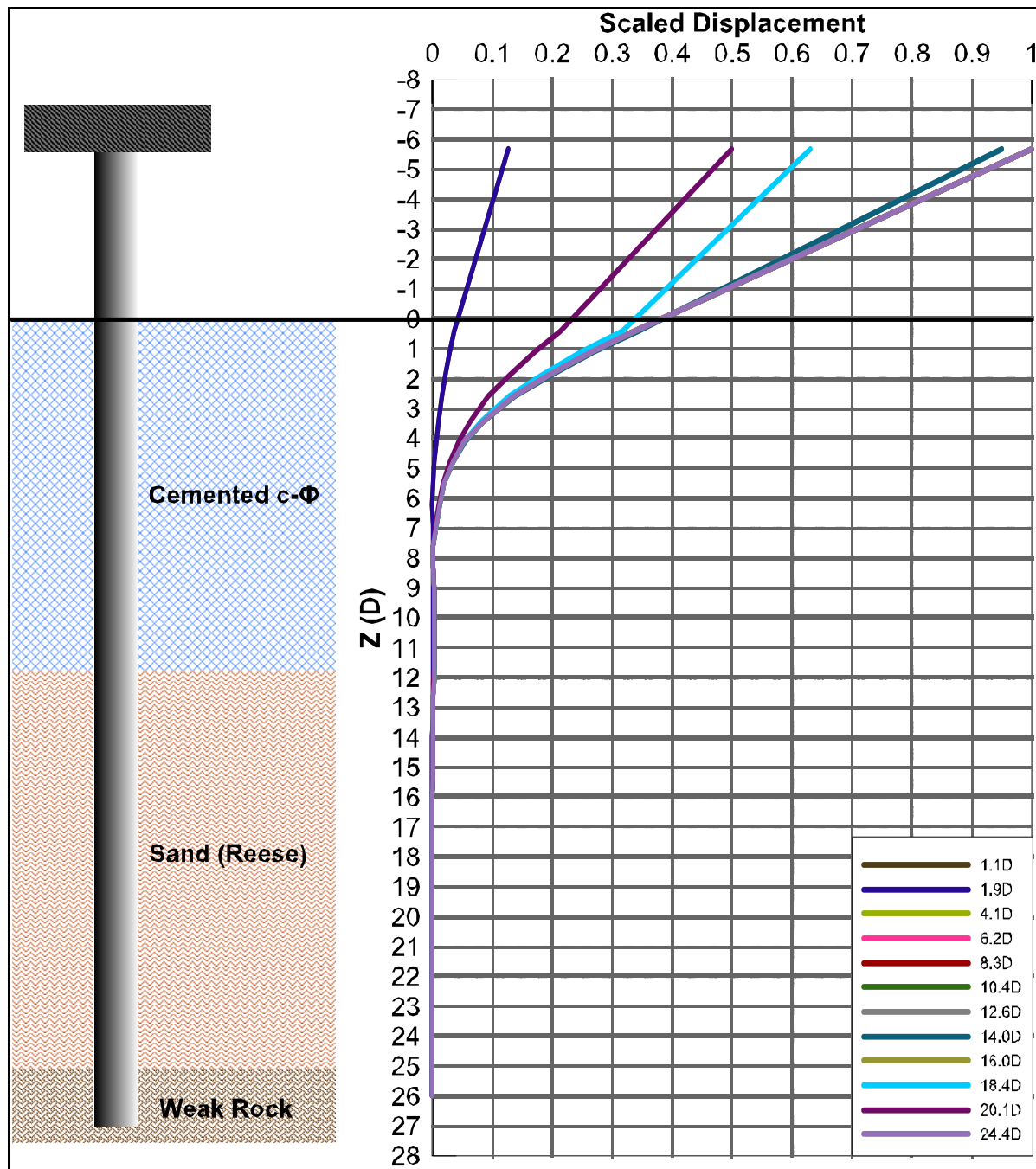


Figure 6.22 BECR1 static scaled displacements

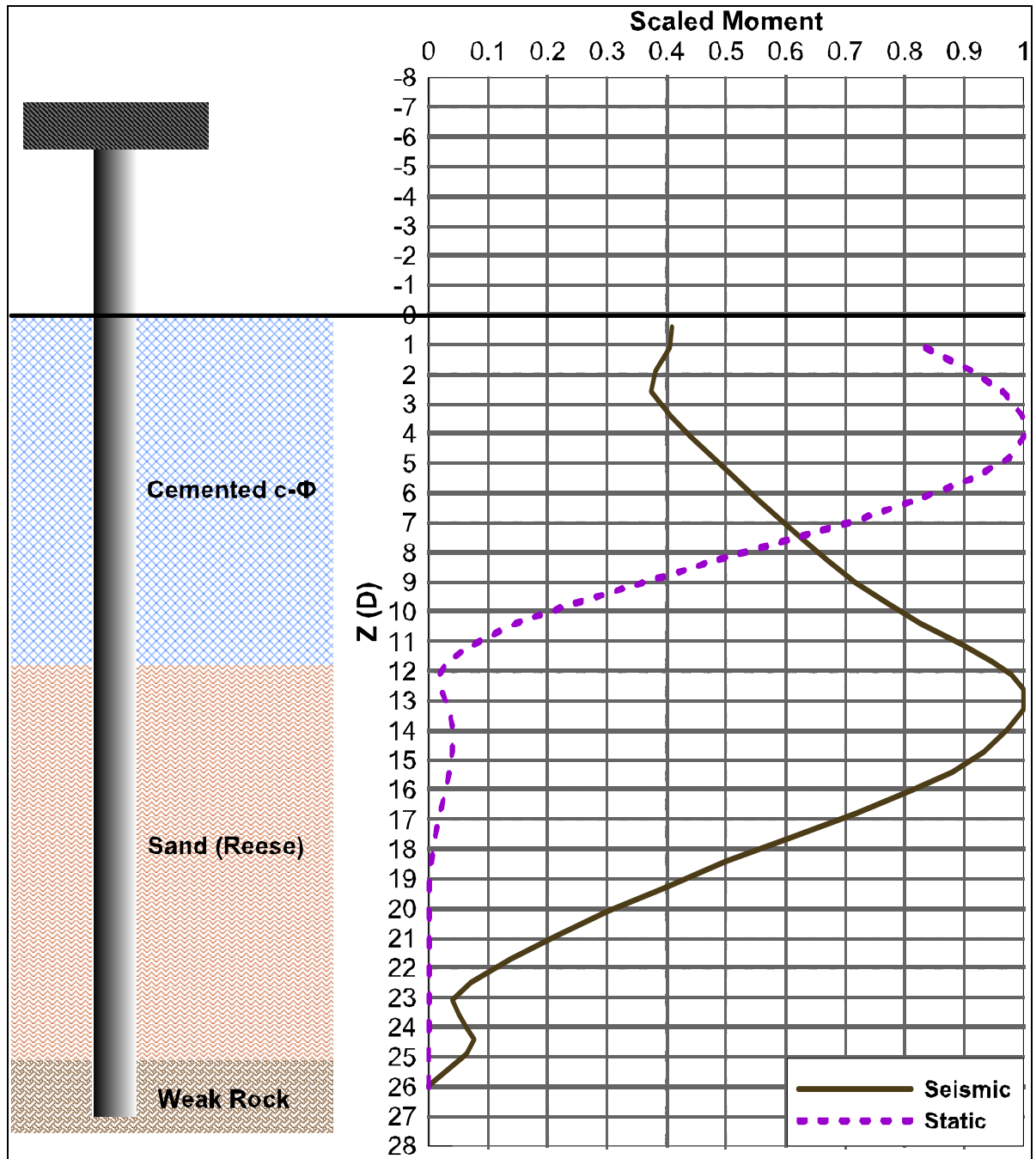


Figure 6.23 BECR1 seismic and static scaled bending moment envelopes

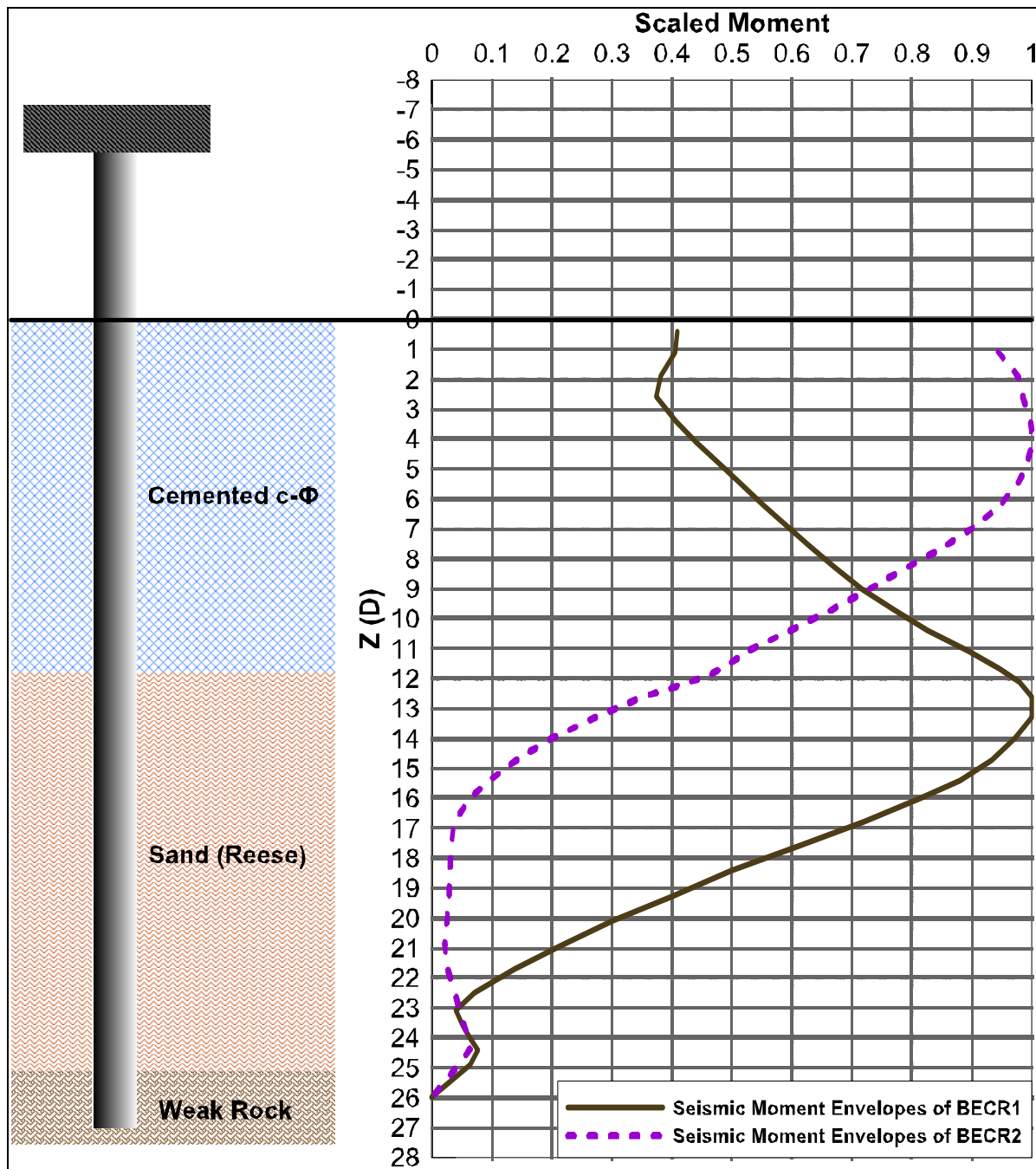


Figure 6.24 Seismic scaled bending moment envelopes of BECR1 and BECR2

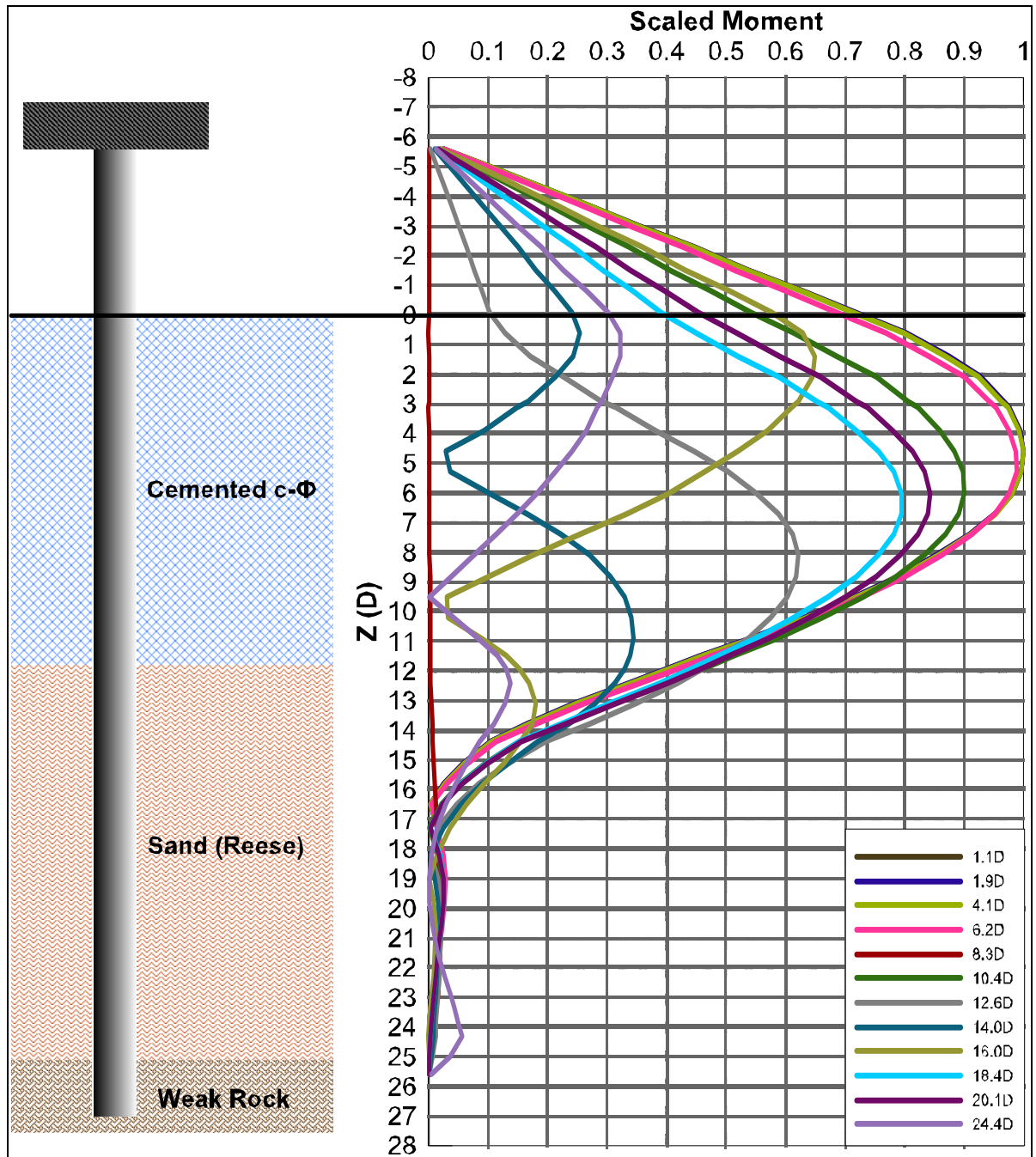


Figure 6.25 BECR2 seismic scaled bending moment

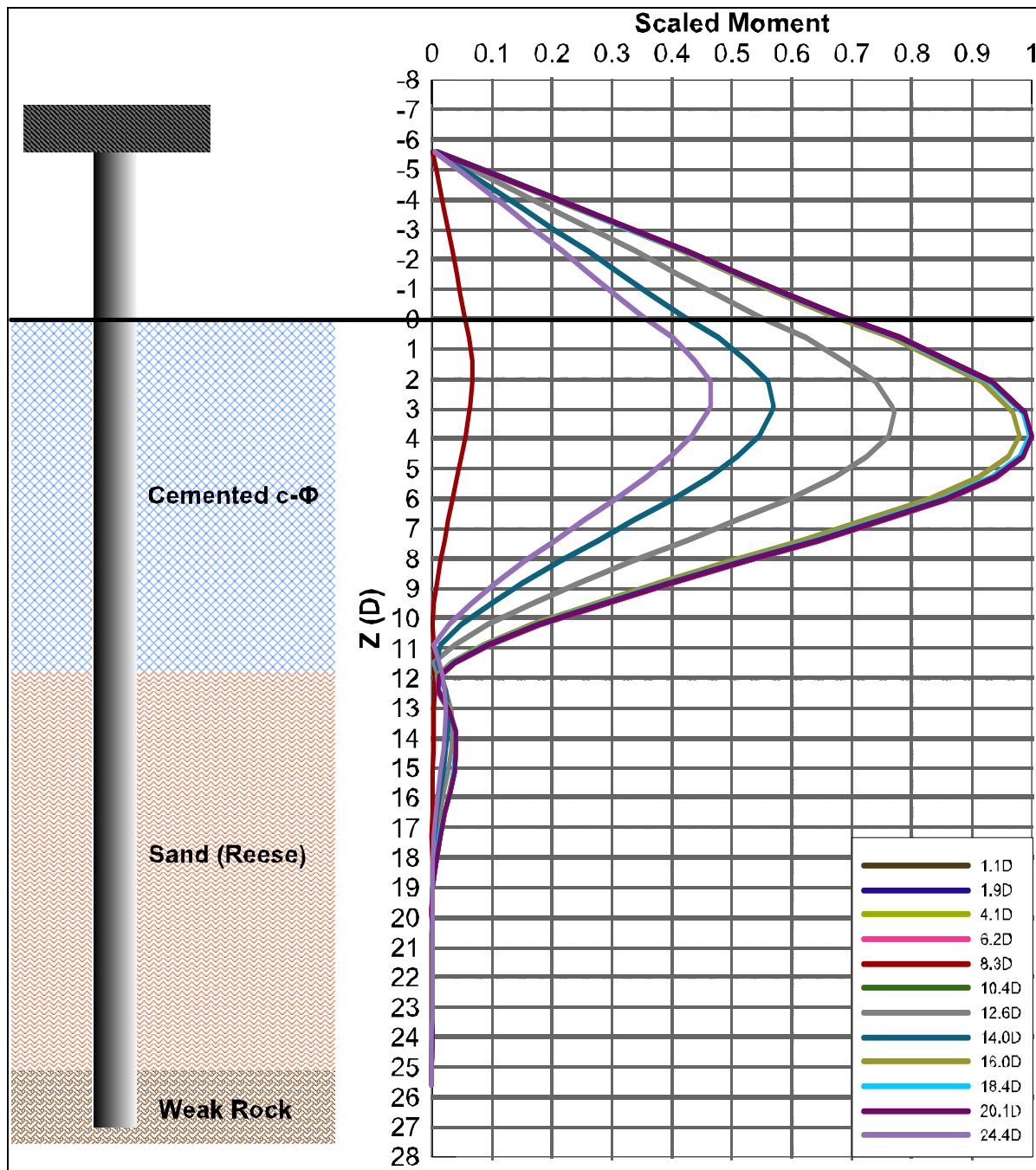


Figure 6.26 BECR2 static scaled bending moment

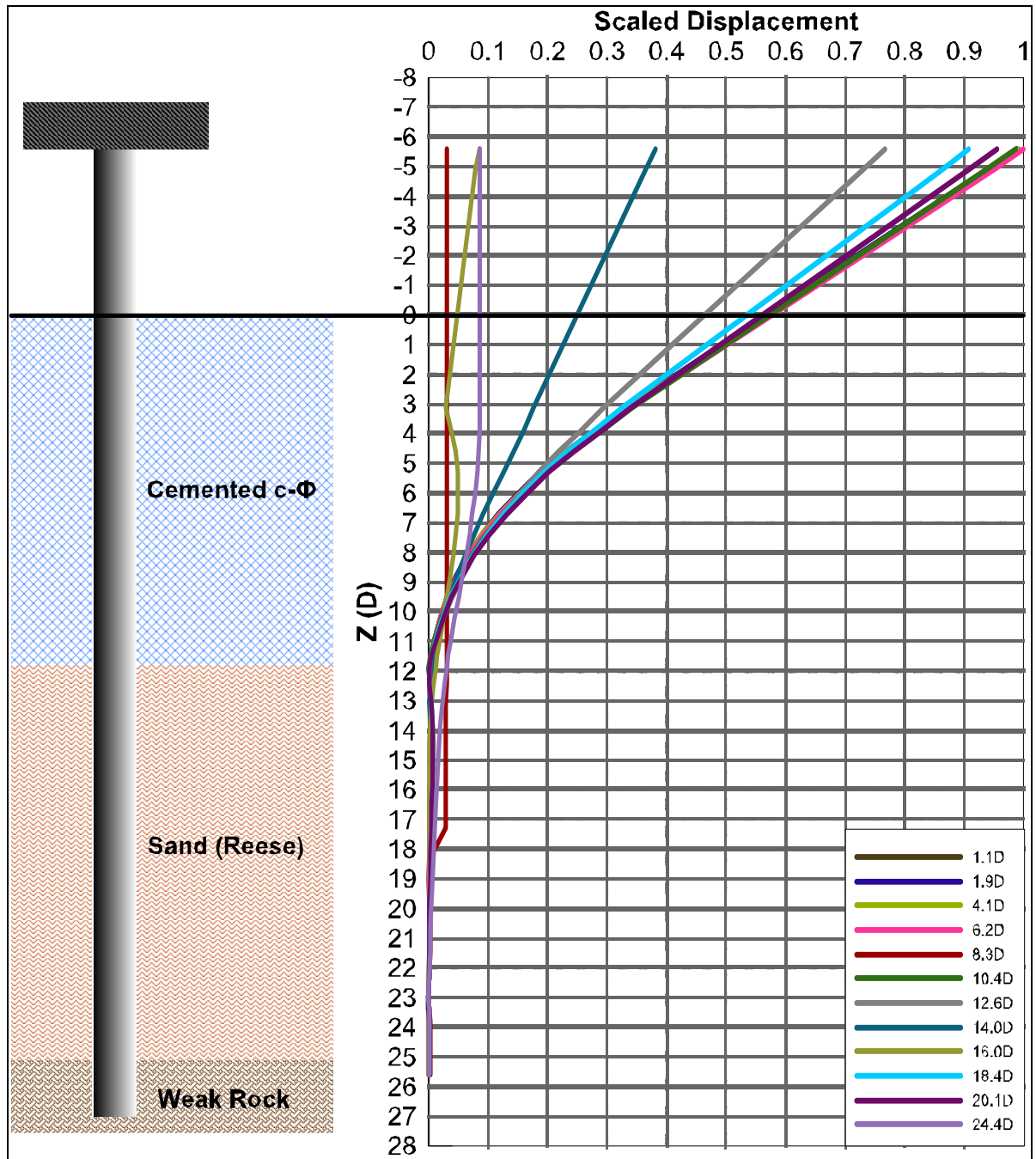


Figure 6.27 BECR2 seismic displacements

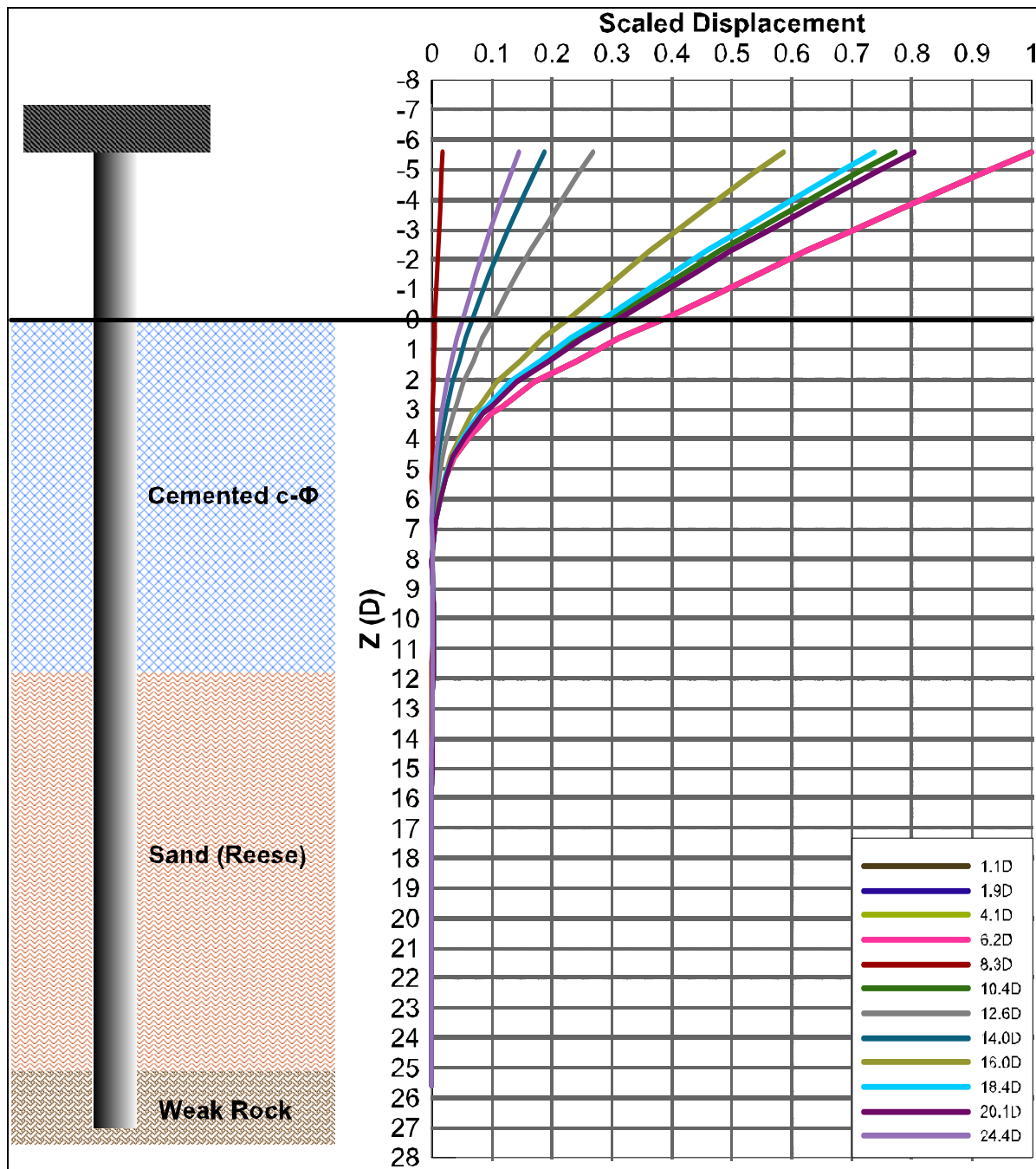


Figure 6.28 BECR2 static displacements

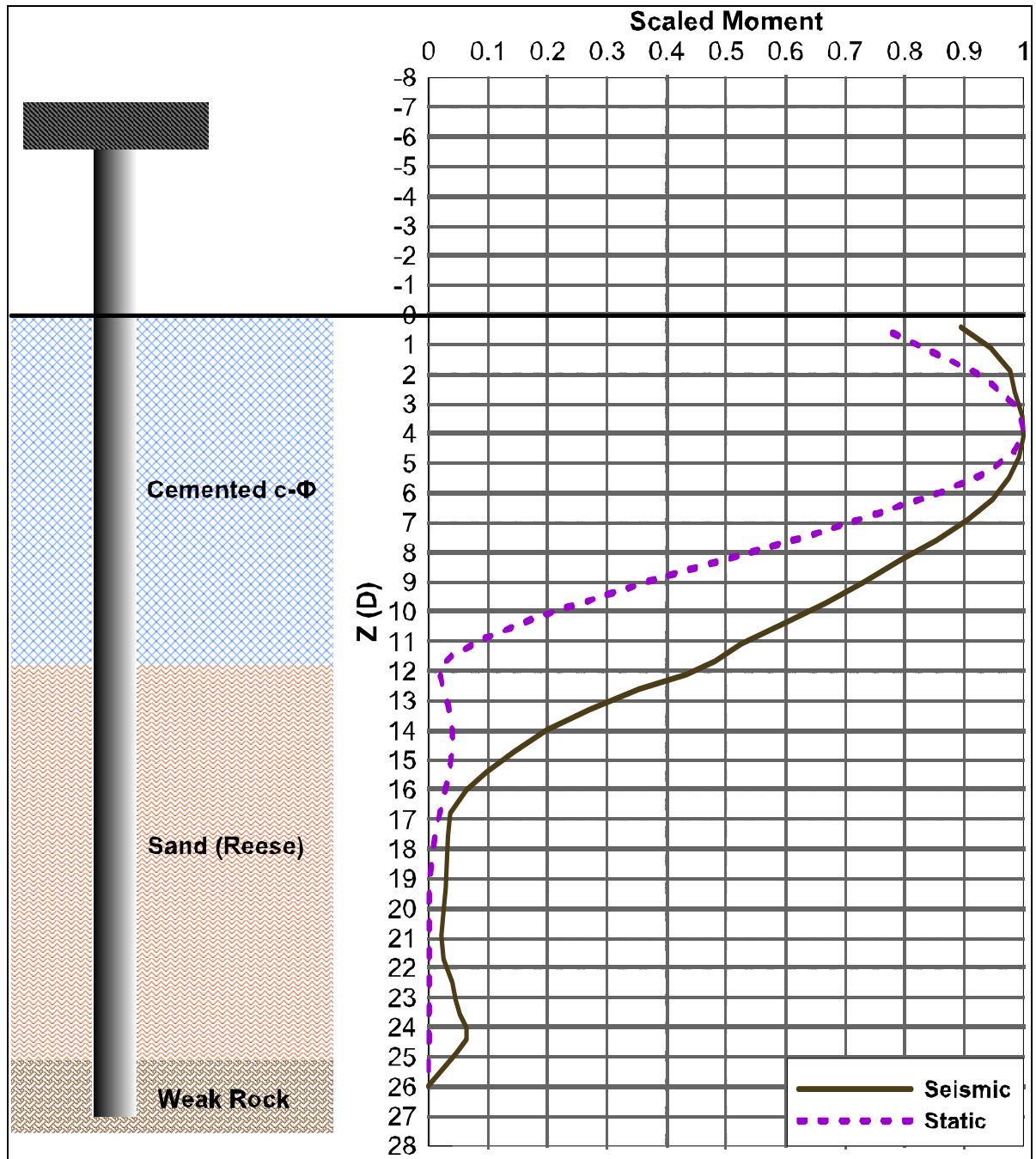


Figure 6.29 BECR2 seismic and static scaled bending moment envelopes

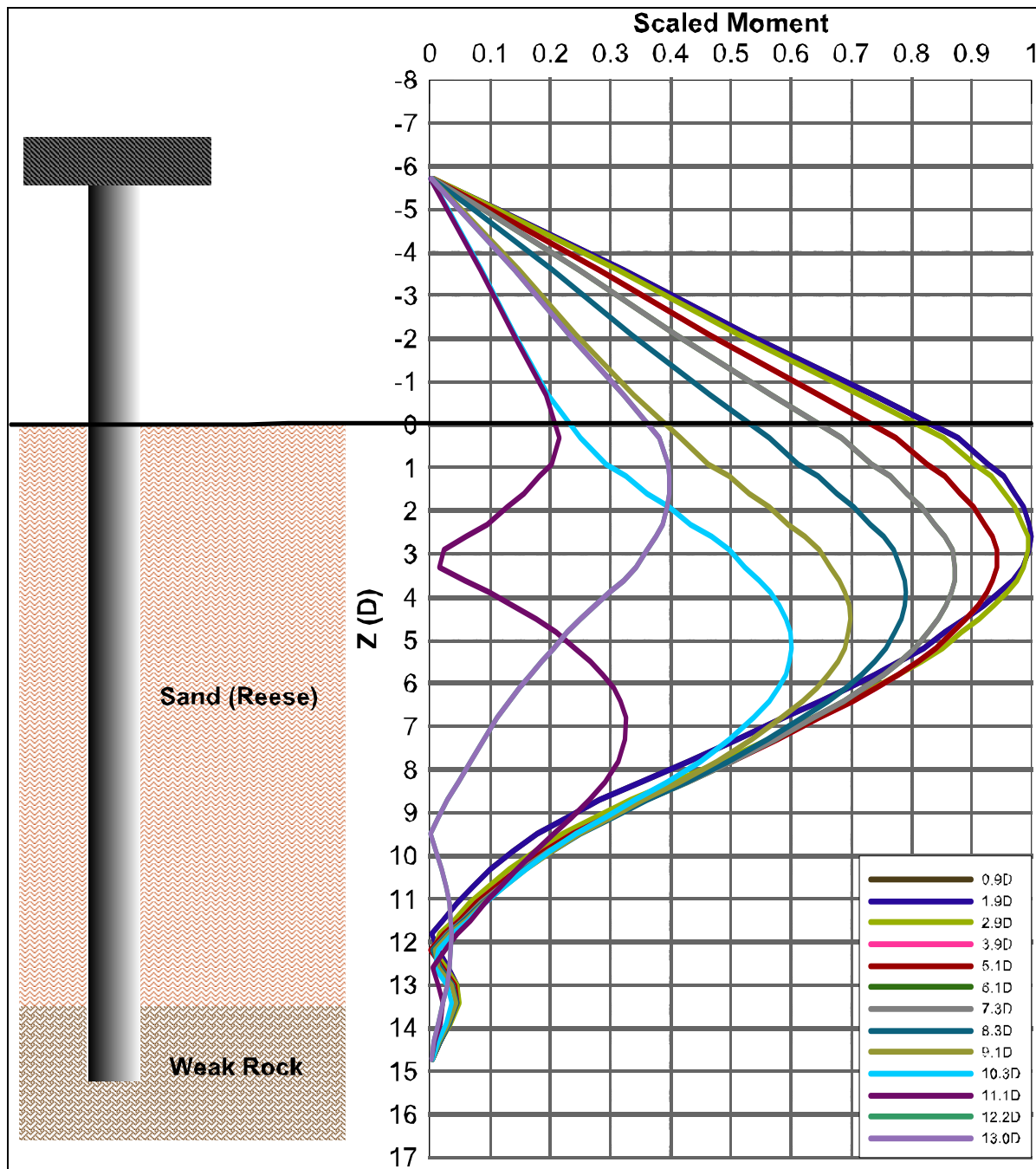


Figure 6.30 QCR1 seismic scaled bending moment

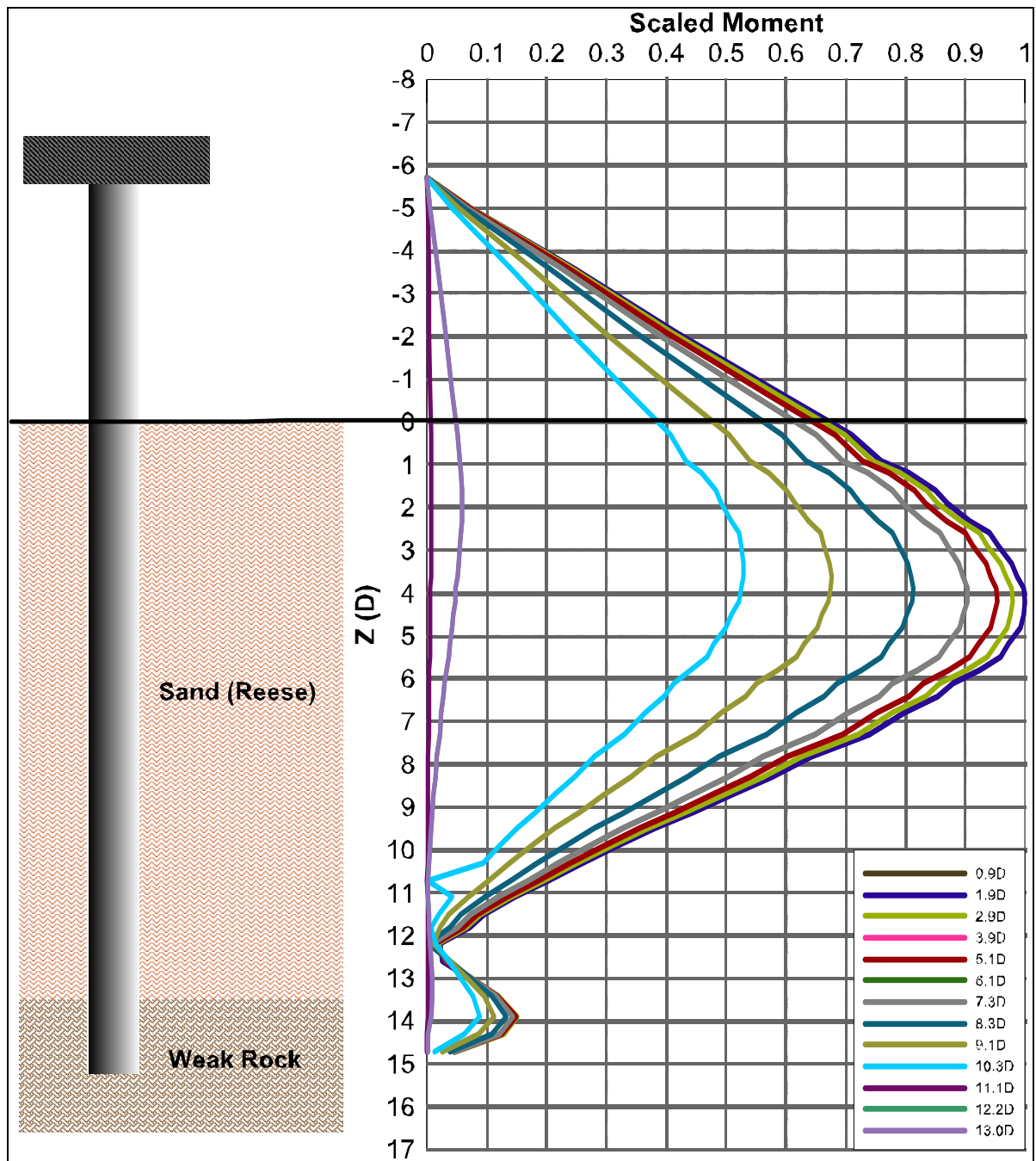


Figure 6.31 QCR1 static scaled bending moment

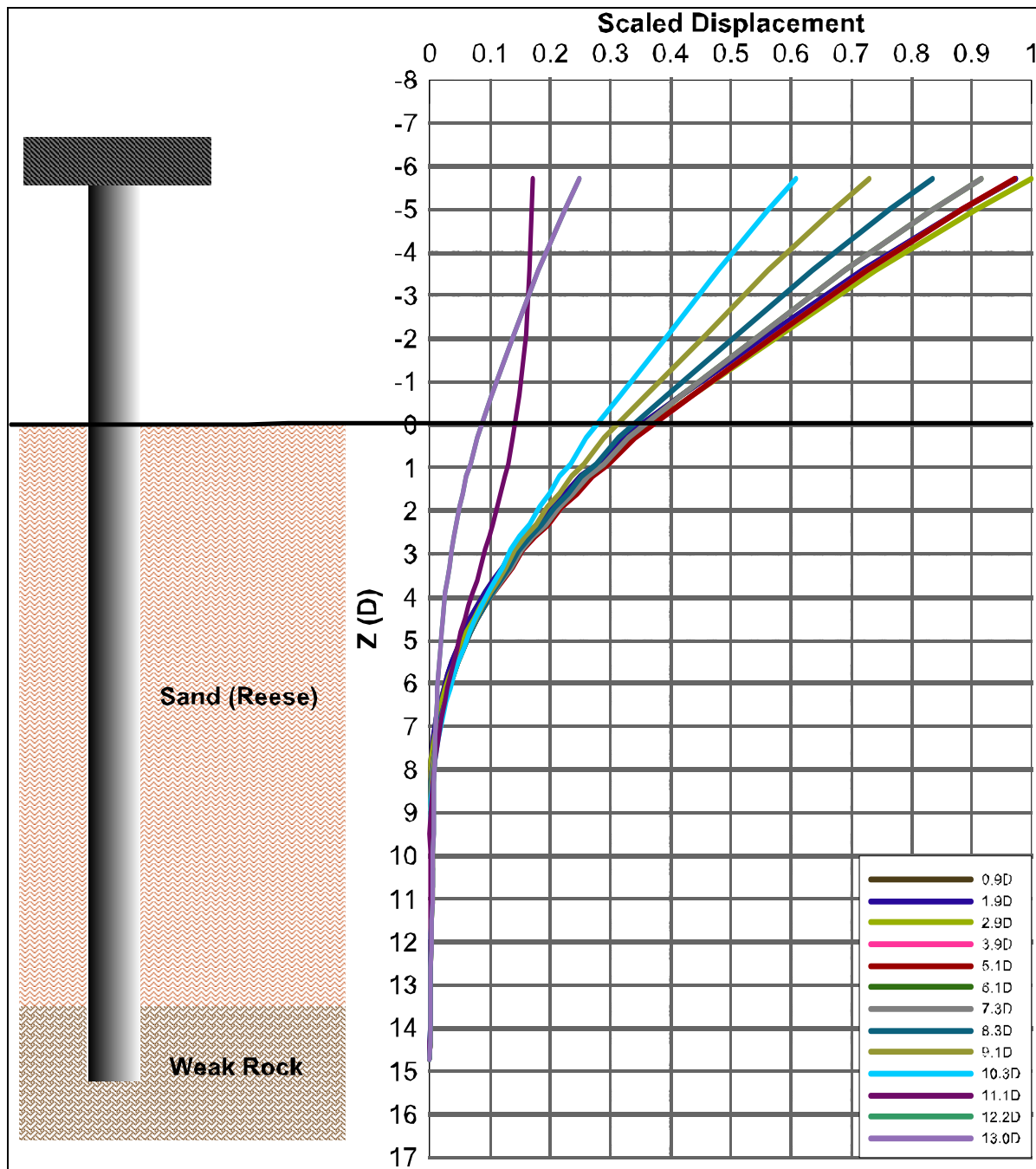


Figure 6.32 QCR1 seismic scaled displacements

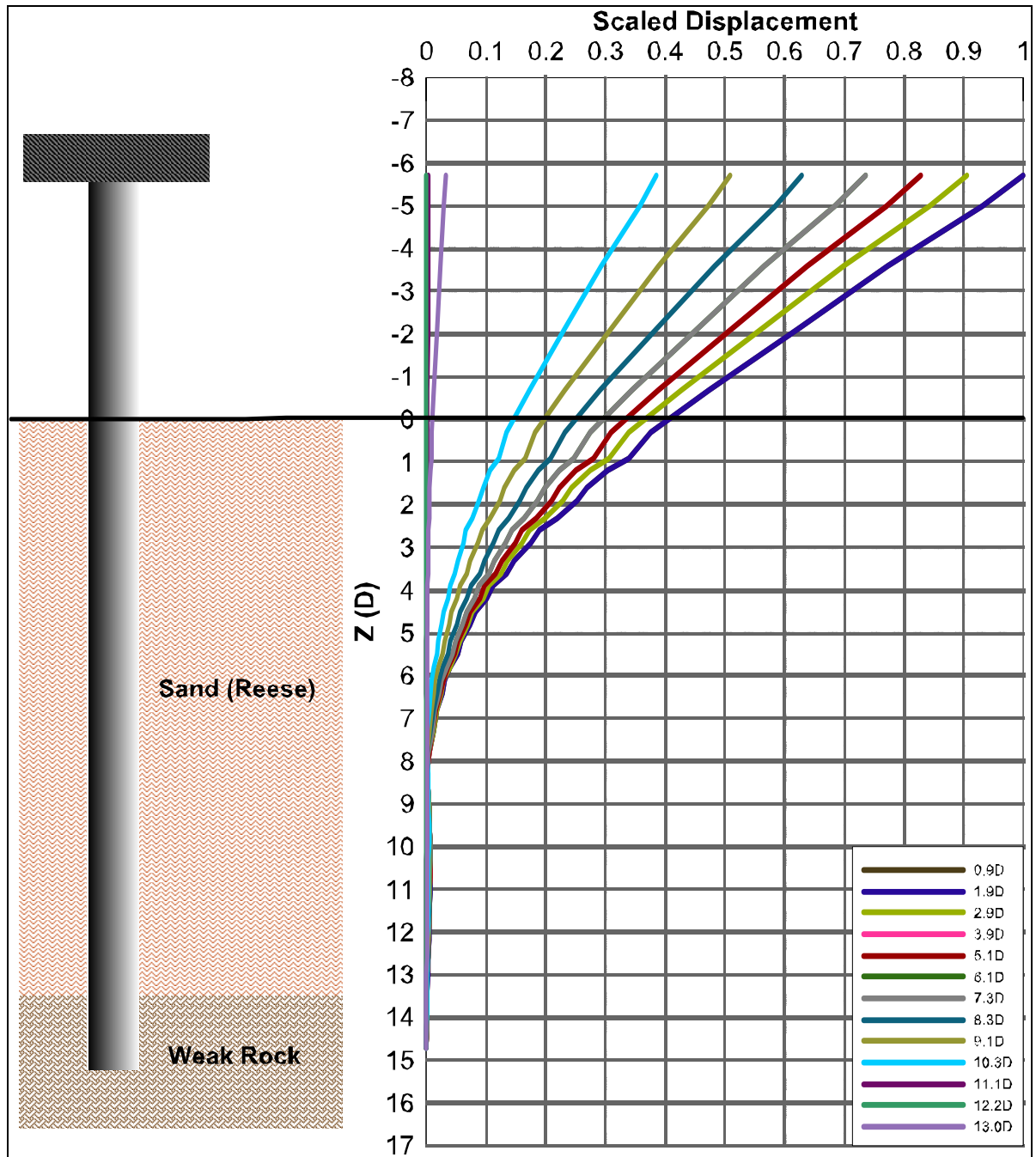


Figure 6.33 QCR1 static scaled displacements

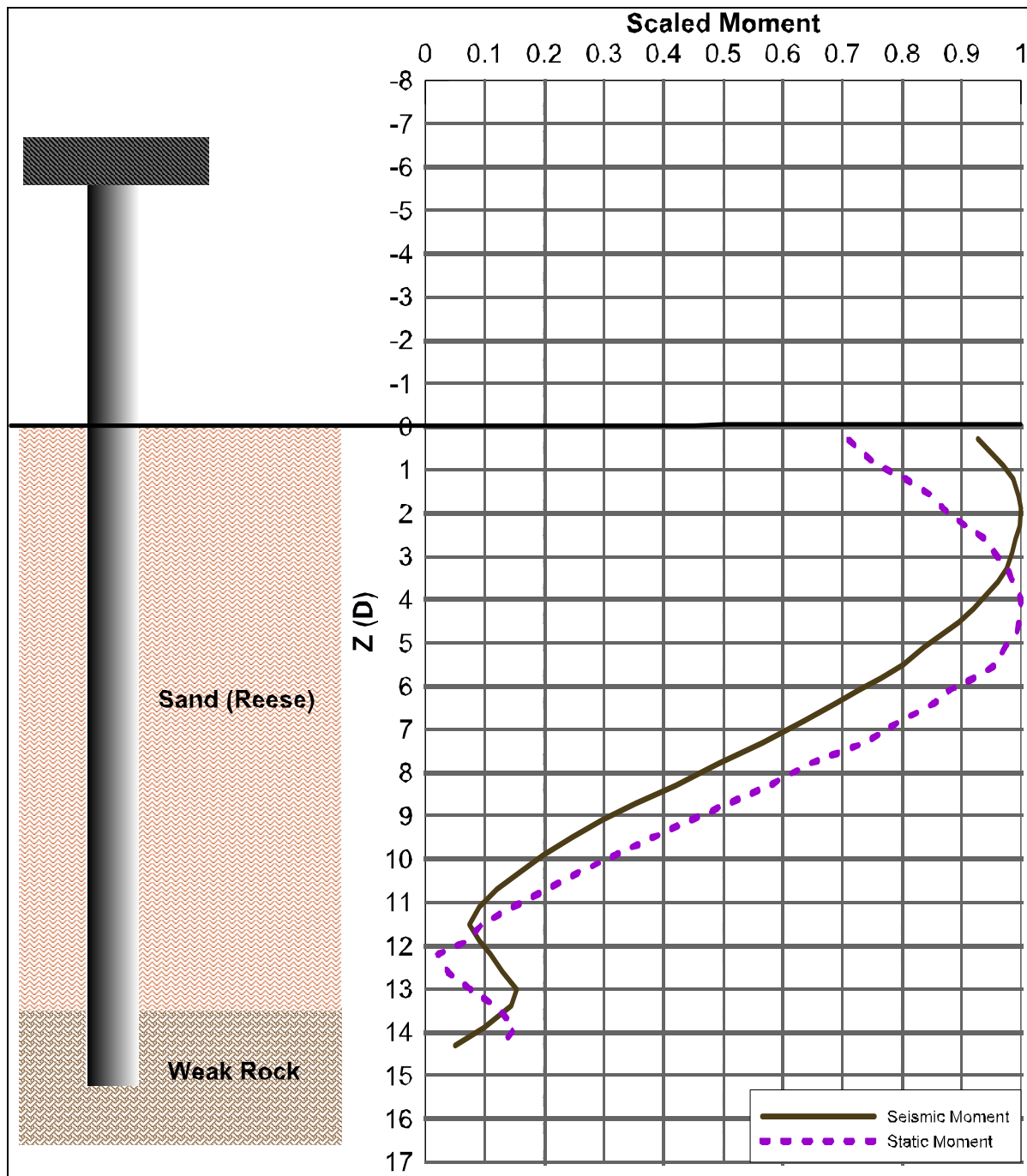


Figure 6.34 QCR1 seismic and static scaled bending moment envelopes

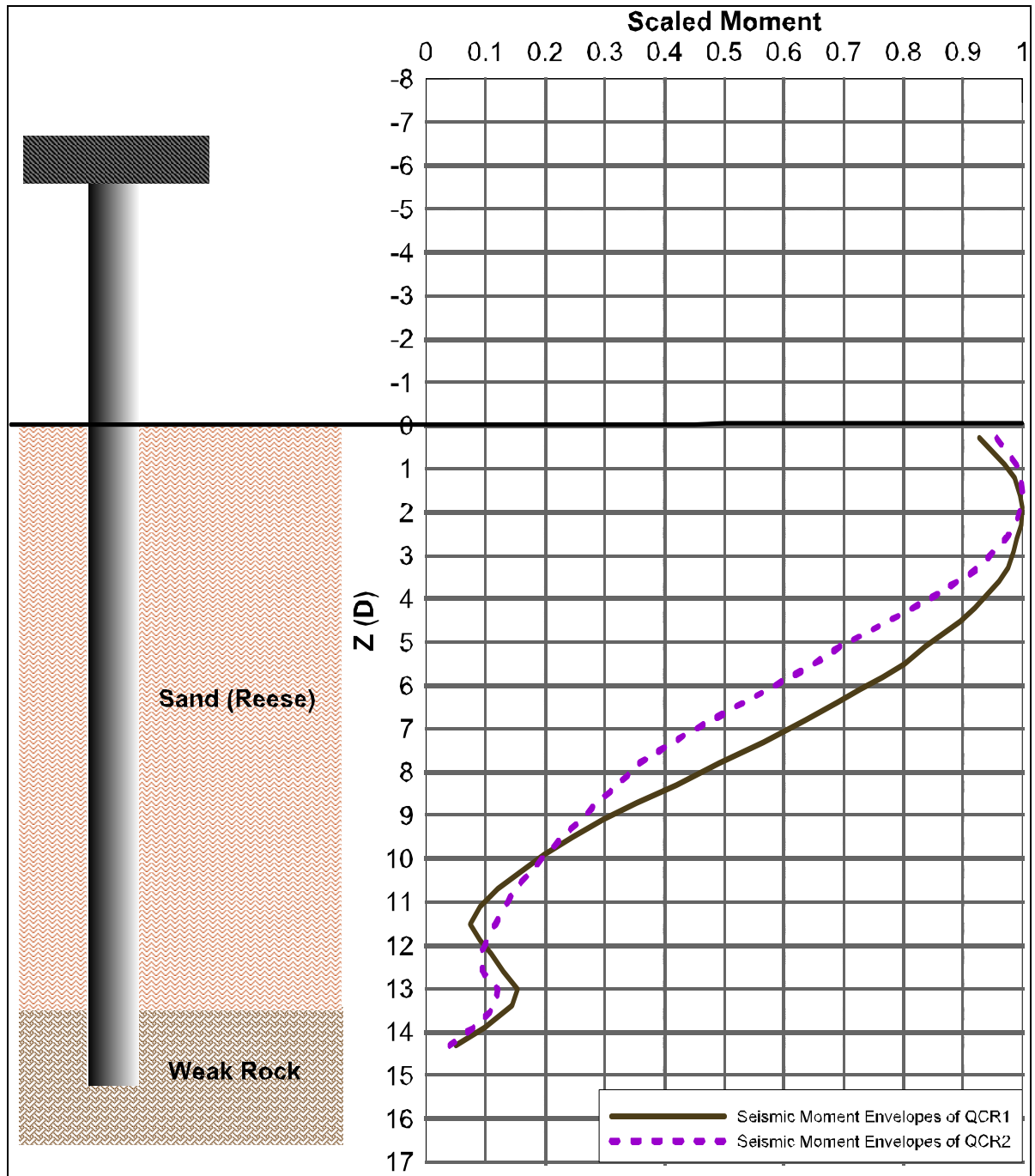


Figure 6.35 Seismic scaled bending moment envelopes of QCR1 and QCR2

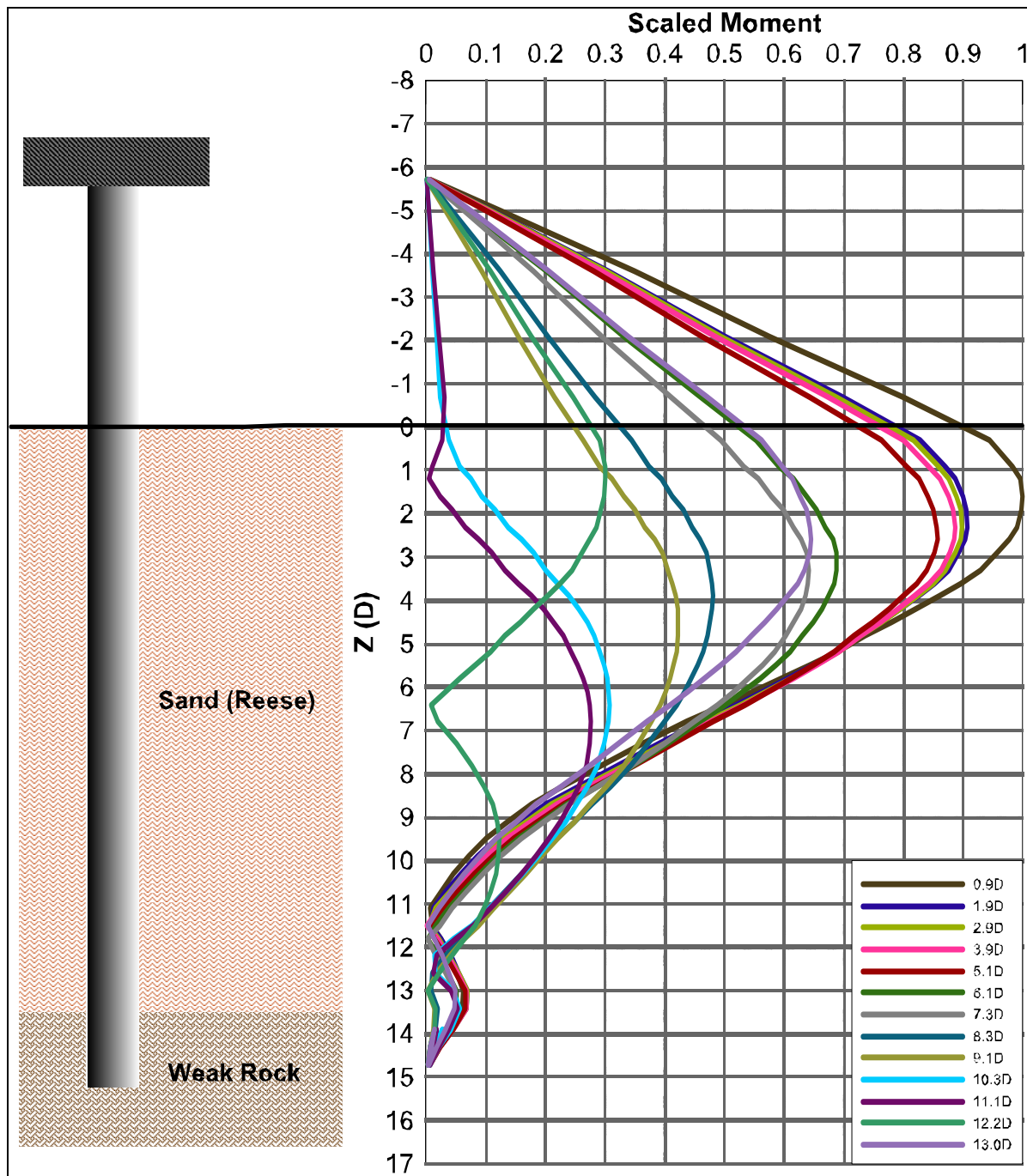


Figure 6.36 QCR2 seismic scaled bending moment

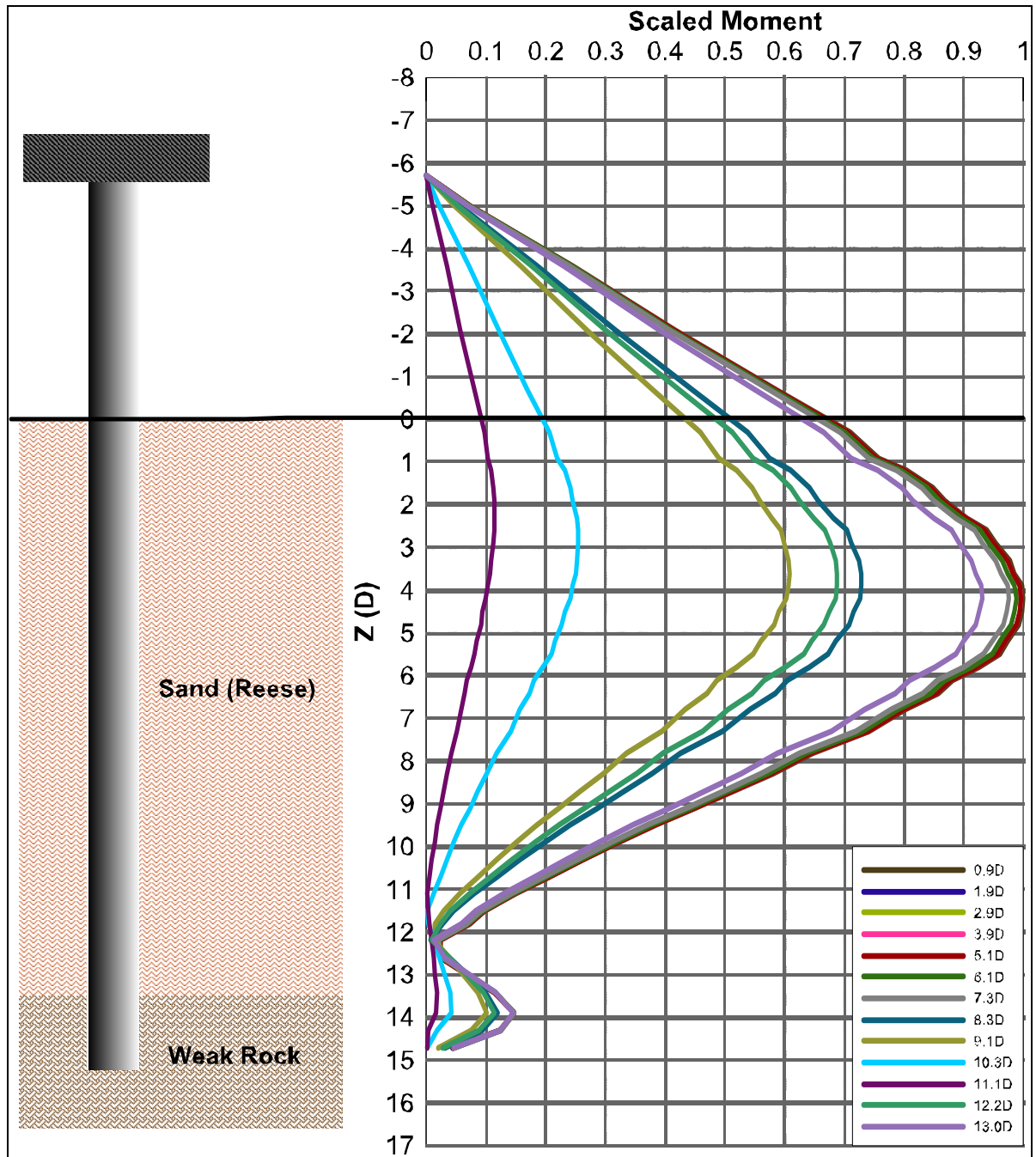


Figure 6.37 QCR2 static scaled bending moment

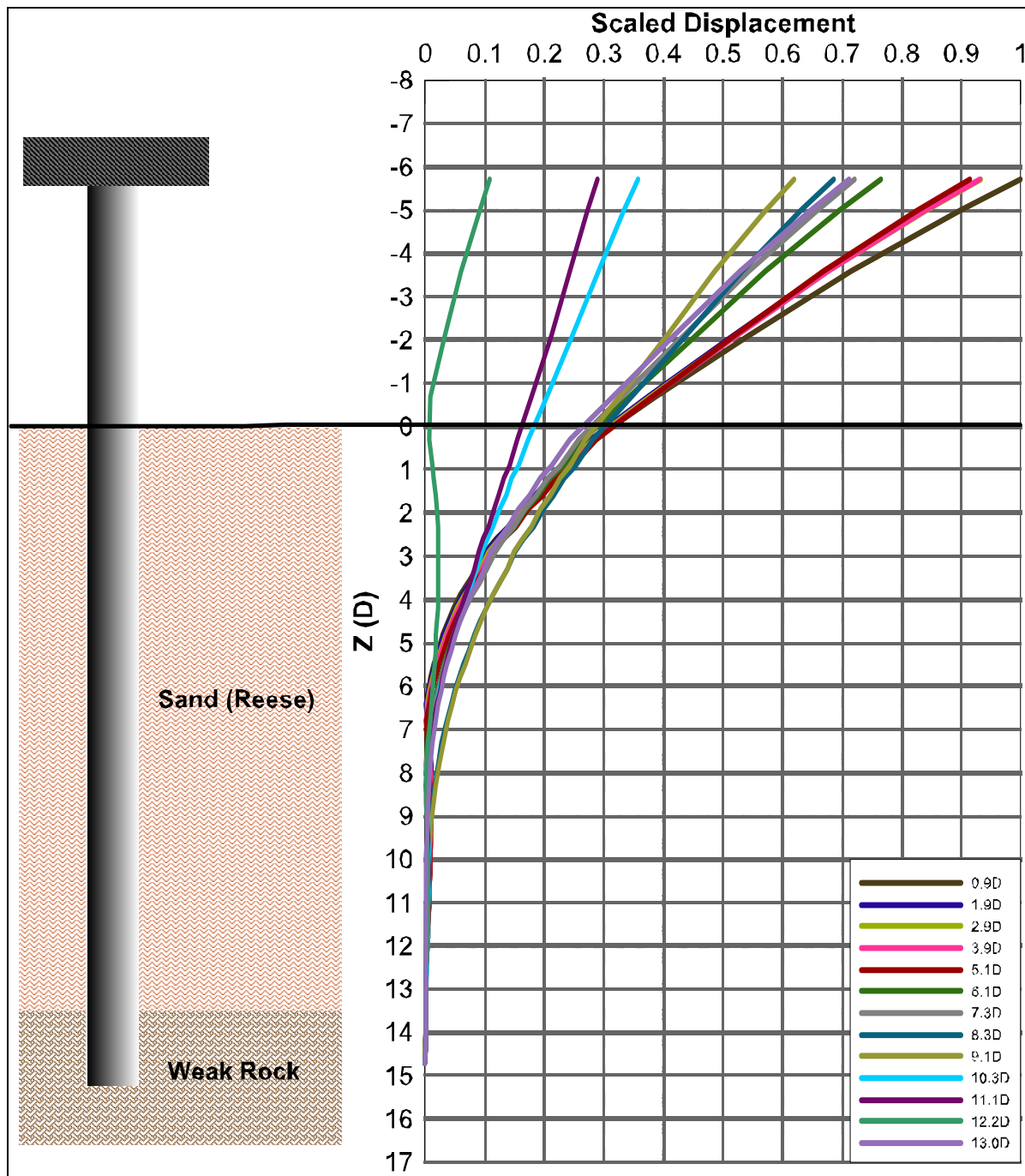


Figure 6.38 QCR2 seismic scaled displacements

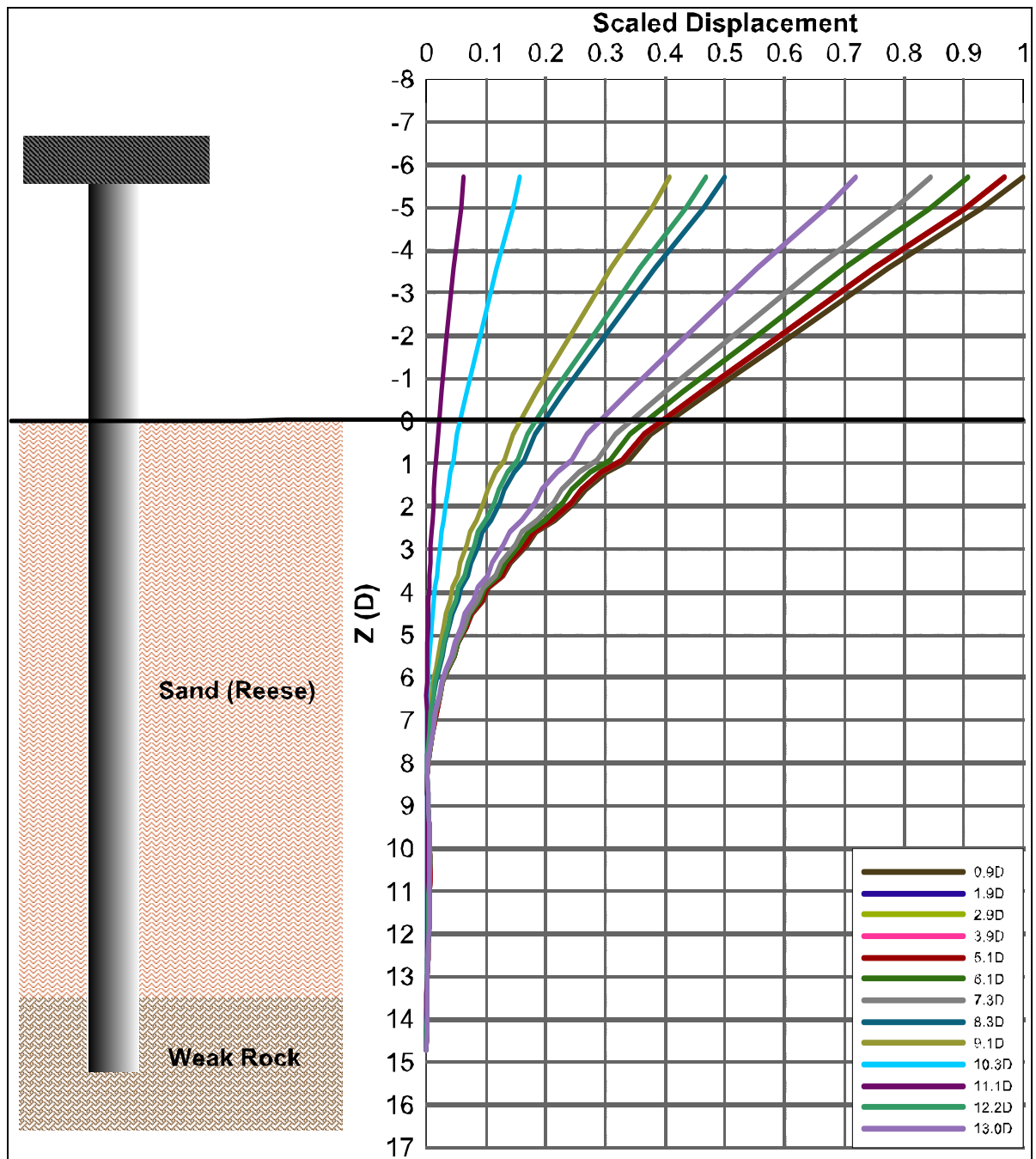


Figure 6.39 QCR2 static scaled displacements

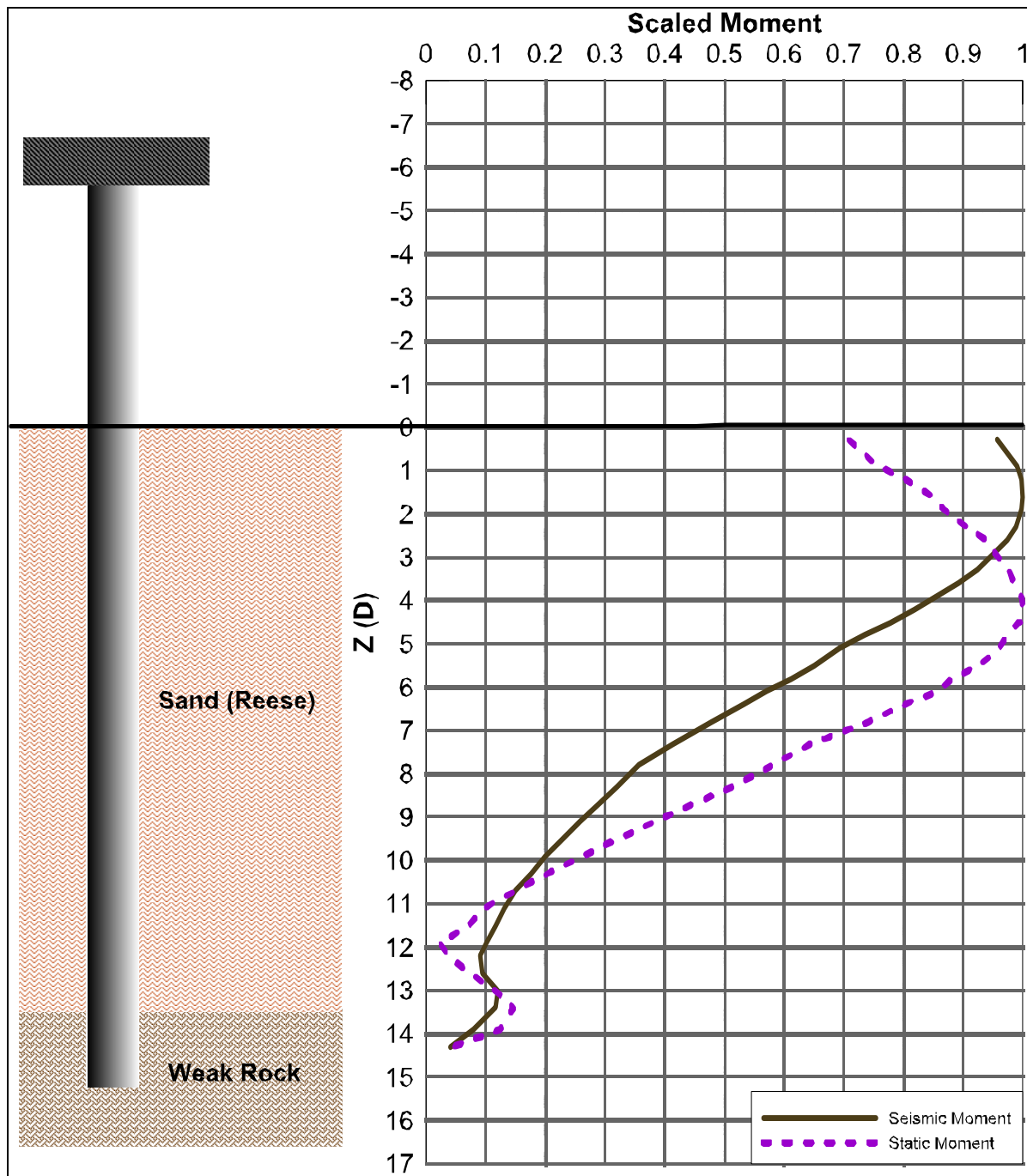


Figure 6.40 QCR2 seismic and static scaled bending moment envelopes

6.2.8 Application of DS ratio in L-Pile and comparison of results

The proposed DS scale which was calculated in the previous step is implemented in Lpile. The results of this implementation are presented and discussed in this section. The DS factor is applied to both components of p-y curves. The p component DS term is less than one and it reduces the ultimate shear capacity of the soil p_u to simulate a weaker soil condition under seismic load. In contrast, the y component DS term is superior to one and it increases the corresponding soil displacement at p_u . Then a static analysis is performed on the pile for the equivalent static load cases. Equivalent static load cases are obtained by matching the pile head displacement from the dynamic analysis as explained in the previous section. Results from Lpile are then compared to results from dynamic analysis in Zsoil.

Lpile has the ability to scale p-y curves by assigning a factor for p or y or both at specific depth. This feature is introduced in Lpile initially to account for the group effect on single pile analysis. Though, it can be used here for the purpose of this study. DS factors were input in Lpile at the depths consistent with beam joints in Zsoil. A comparison between the results from both analyses is presented throughout the plots of Figures 6.41 to 6.48.

The plots indicate that the deformed shape of the pile with scaled p-y curves and static load case match perfectly the deformed shape from seismic load case. The seismic bending moment diagrams match the static results perfectly in terms of the location and value of maximum bending moment and disagree elsewhere along the pile. This variation is visible in the case of BECR1 and is very minimal in the other cases. This indicates that the proposed methodology is satisfactory and yields a good approximation for the seismic behavior of the soil. The proposed approach is capable of predicting the seismic performance of the pile with very simple static analysis.

Several factors affect the determination of the DS ratio such as the rigidity of the pile, the slenderness of the pile and the type of the surrounding soil. The rigidity of the pile as well as its slenderness ratio, i.e. the diameter to length ratio, play significant role in determining the overall flexural behaviors of the pile. For flexible and slender pile, the dominant behavior is flexural bending –see cases A, C, and F, Figure 1.2. However, for rigid or stubby piles the dominant behavior is either complete tilting or shifting of the pile or a combination of both – see cases B, D, and E, Figure 1.2.

Therefore, for the flexible or slender pile case the DS ratio can be determined by Equation 6.6. However, for the rigid pile case, Equation 6.7 can be used considering the pile displacement or rotation at the ground level.

The type of the surrounding soil determines the shape of the p-y curve and therefore the overall performance of the pile under lateral load. However, for the studied sites the soil type varies between sand and silty clay. Therefore, the soil was deemed as c-phi material for the purpose of defining the static p-y. The actual effect of different soil types on the result was therefore not accurately measured in the analysis. However, the proposed procedure can be adapted for a variety of soils as long the static p-y criteria is well defined. The reduction in soil strength is affected by several factors as stated in Chapter 2 including the pore pressure which accumulates rapidly during the earthquake and might lead to liquefaction of the soil. This effect was not considered in this study due to the large number of models and mass levels considered. Further research is recommended to simulate this situation.

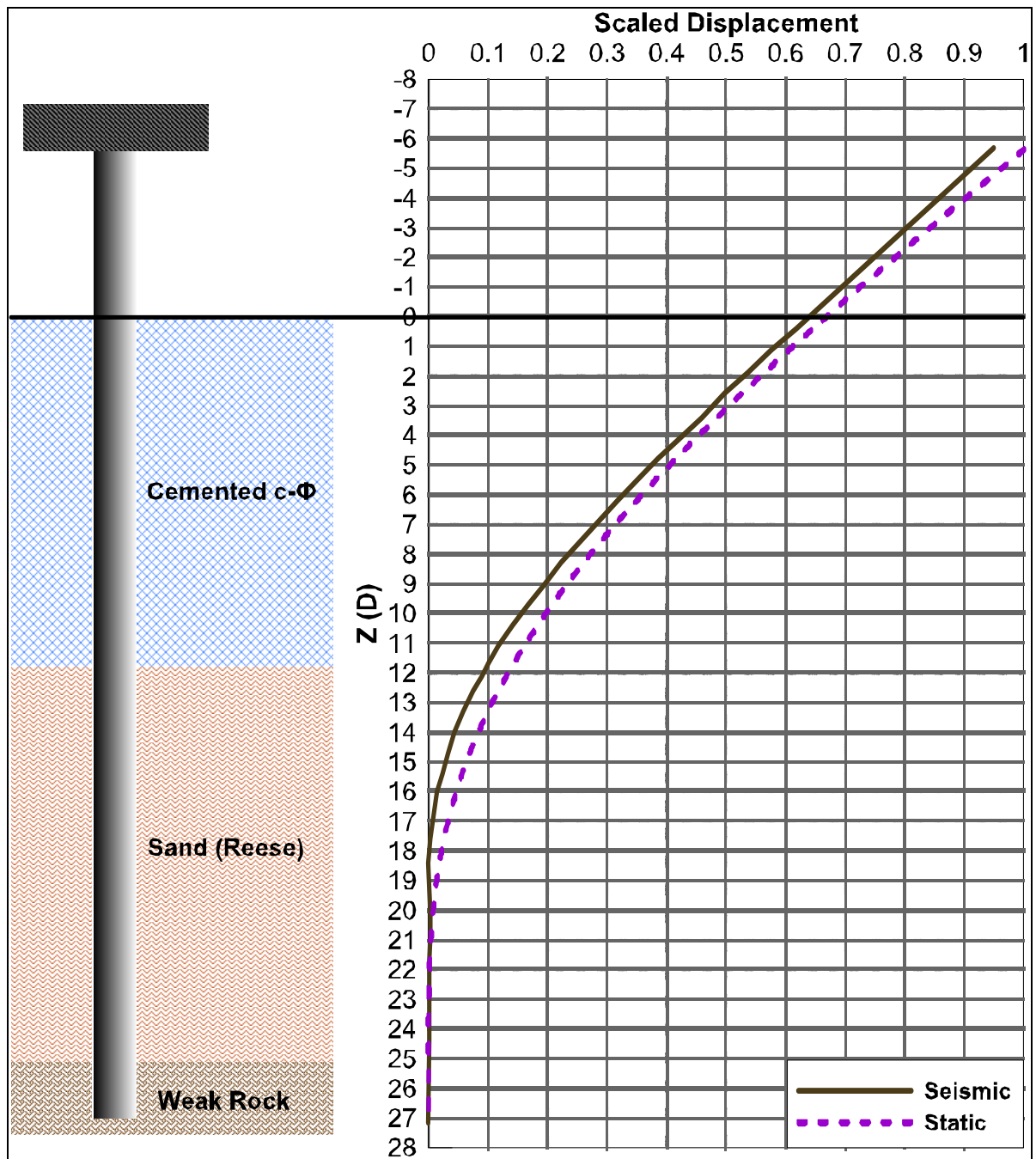


Figure 6.41 Seismic vs static scaled displacements from the modified soil model of BECR1

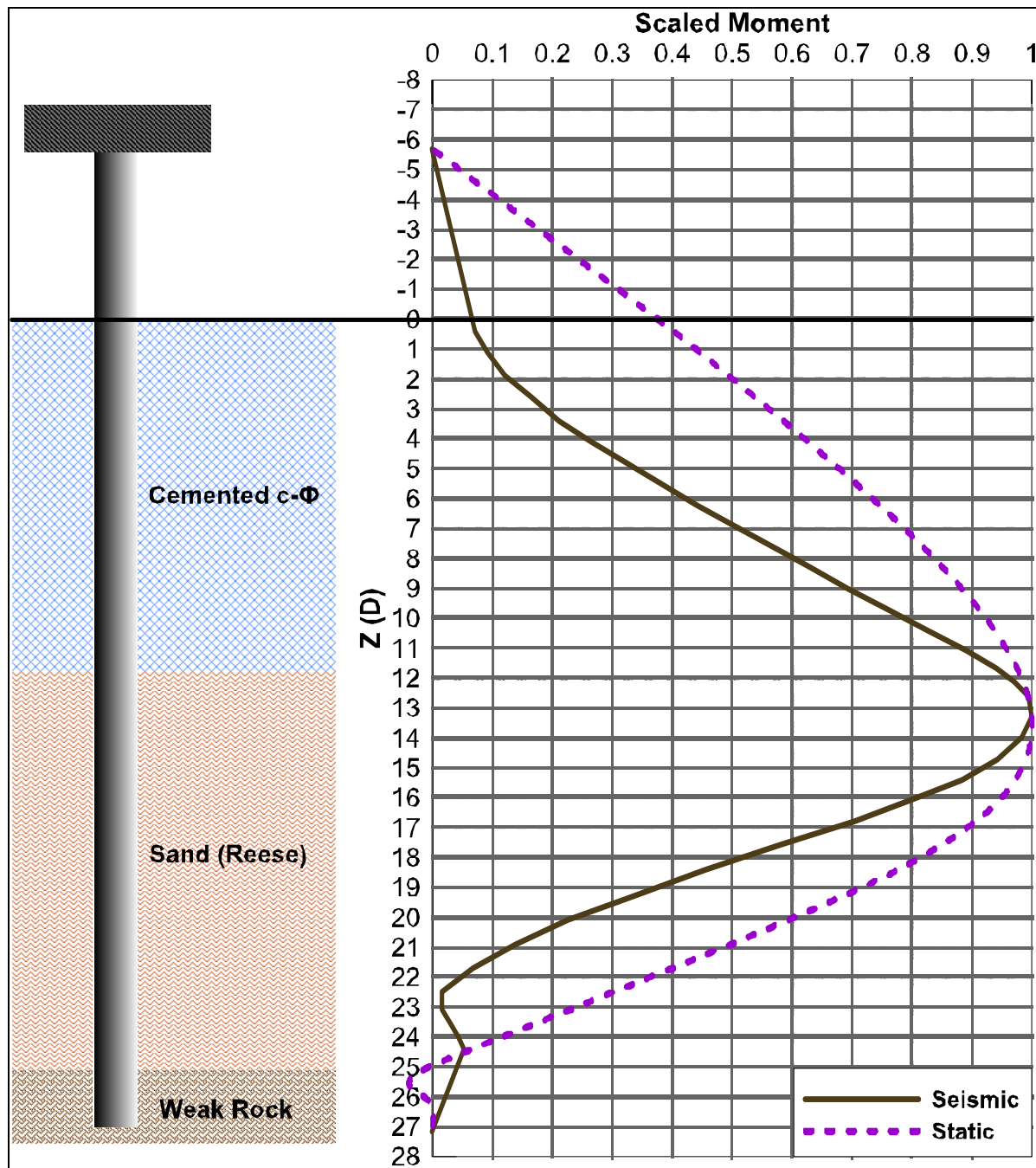


Figure 6.42 Seismic vs static scaled bending moment from the modified soil model of BECR1

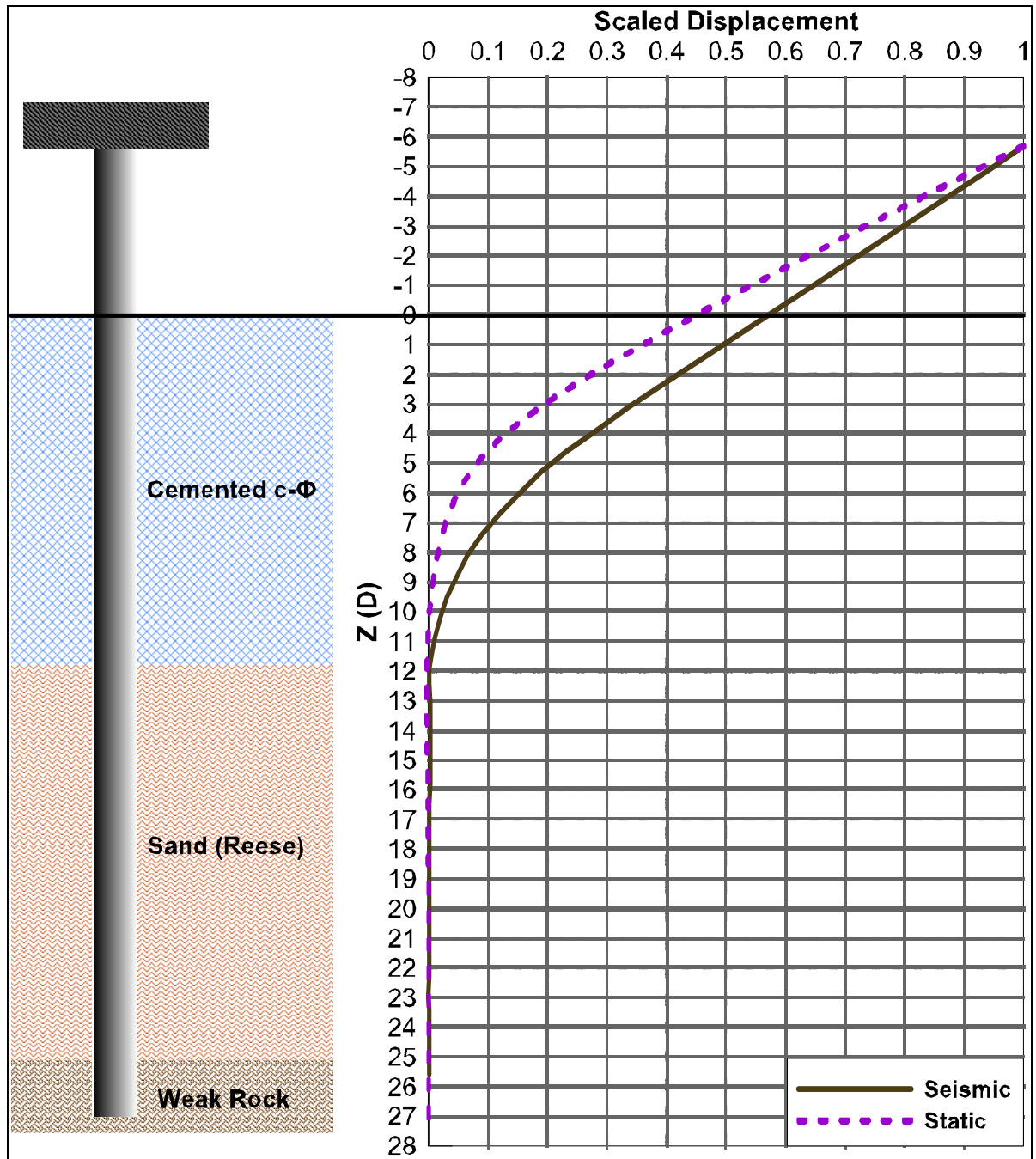


Figure 6.43 Seismic vs static scaled displacements from the modified soil model of BECR1

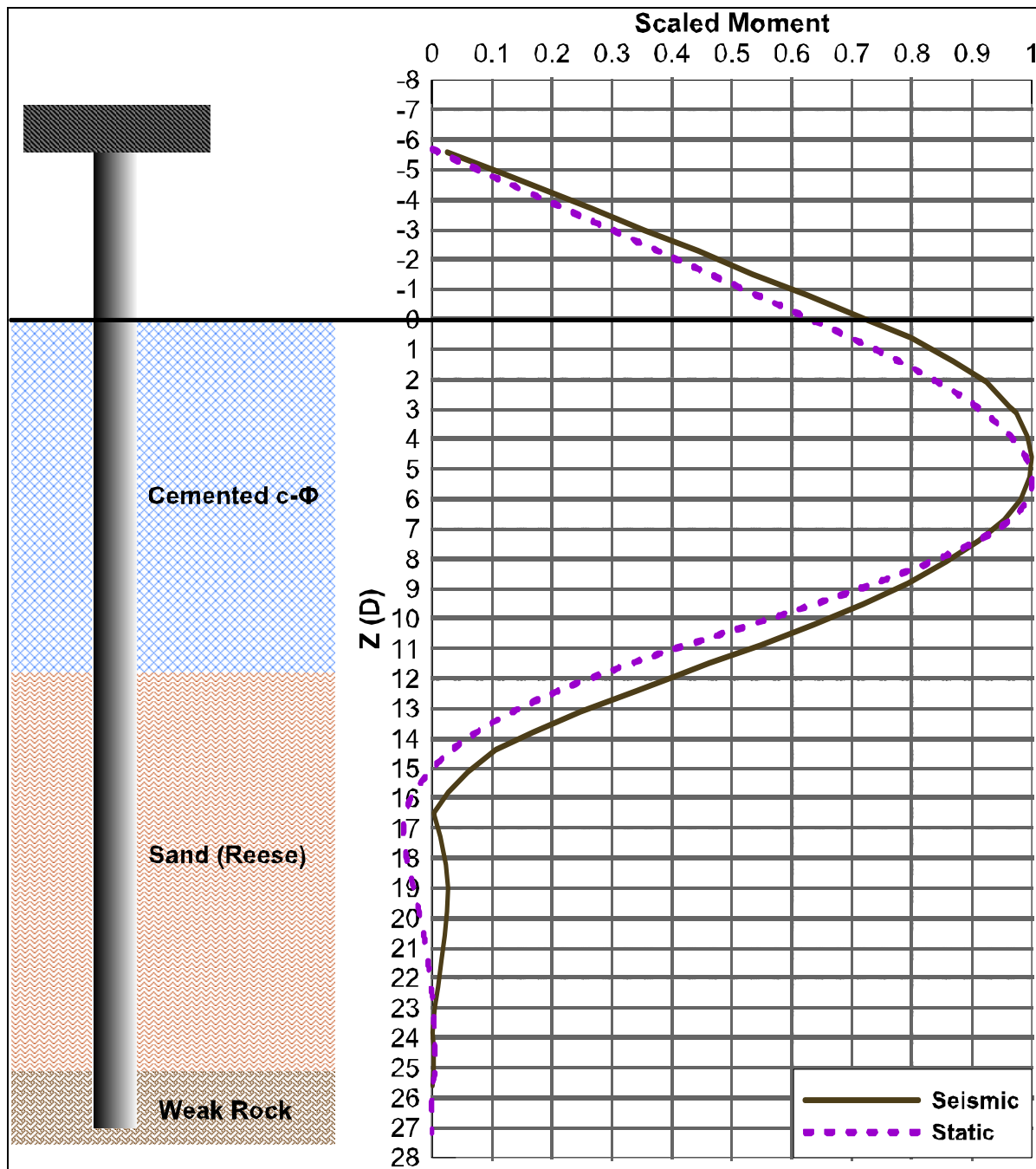


Figure 6.44 Seismic vs static scaled bending moment from the modified soil model of BECR2

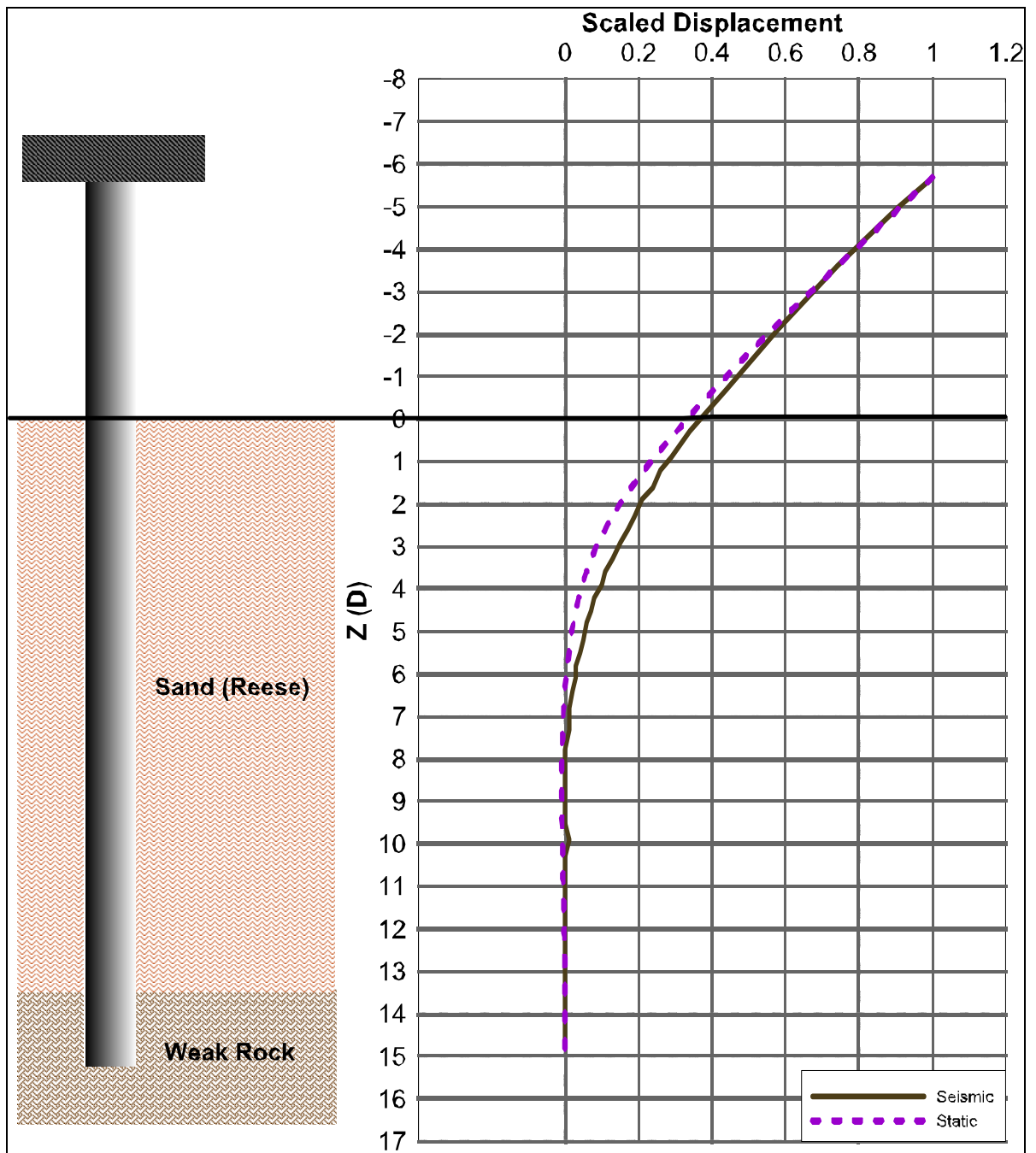


Figure 6.45 Seismic vs static scaled displacements from the modified soil model of QCR1

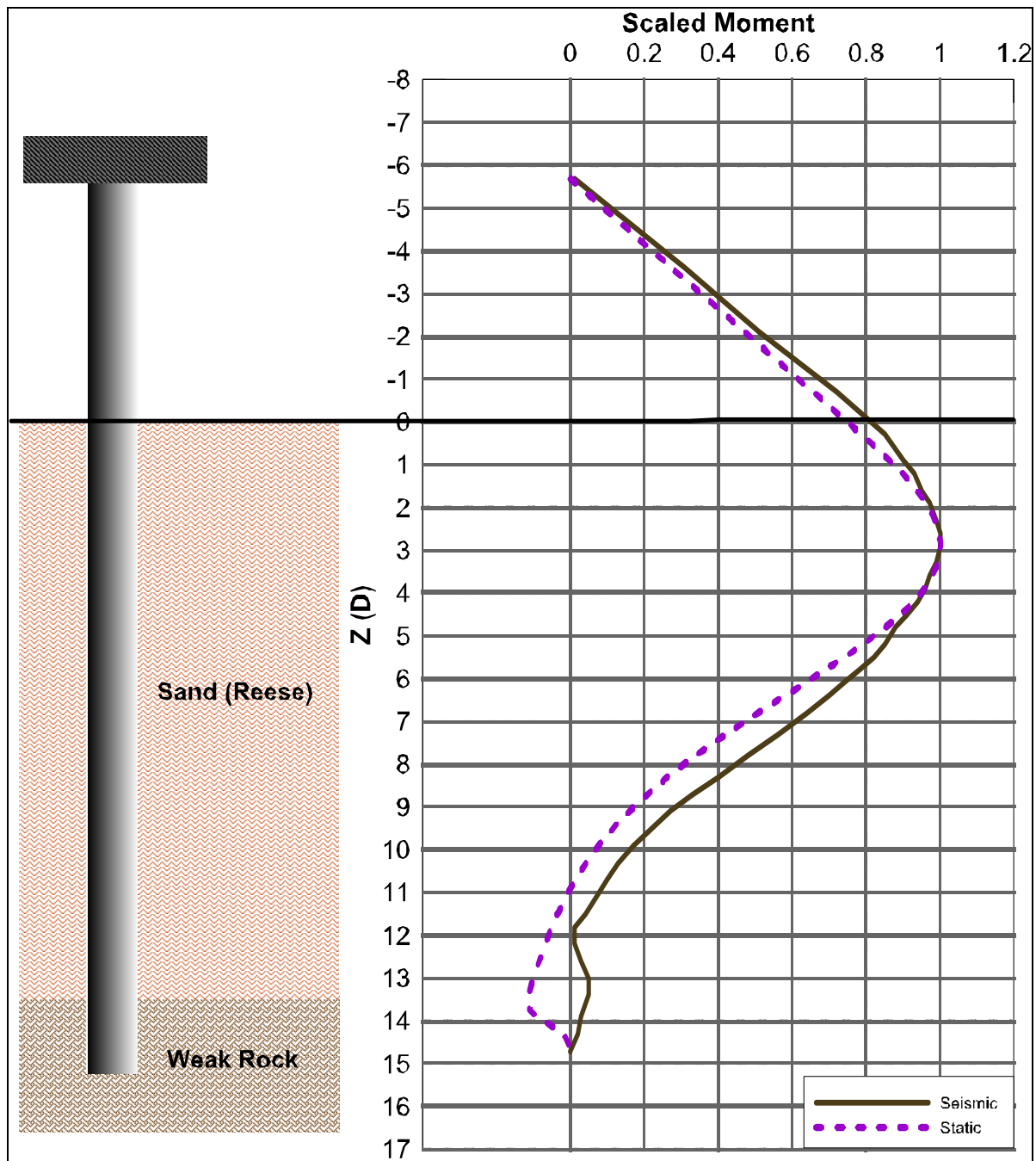


Figure 6.46 Seismic vs static scaled bending moment from the modified soil model of QCR1

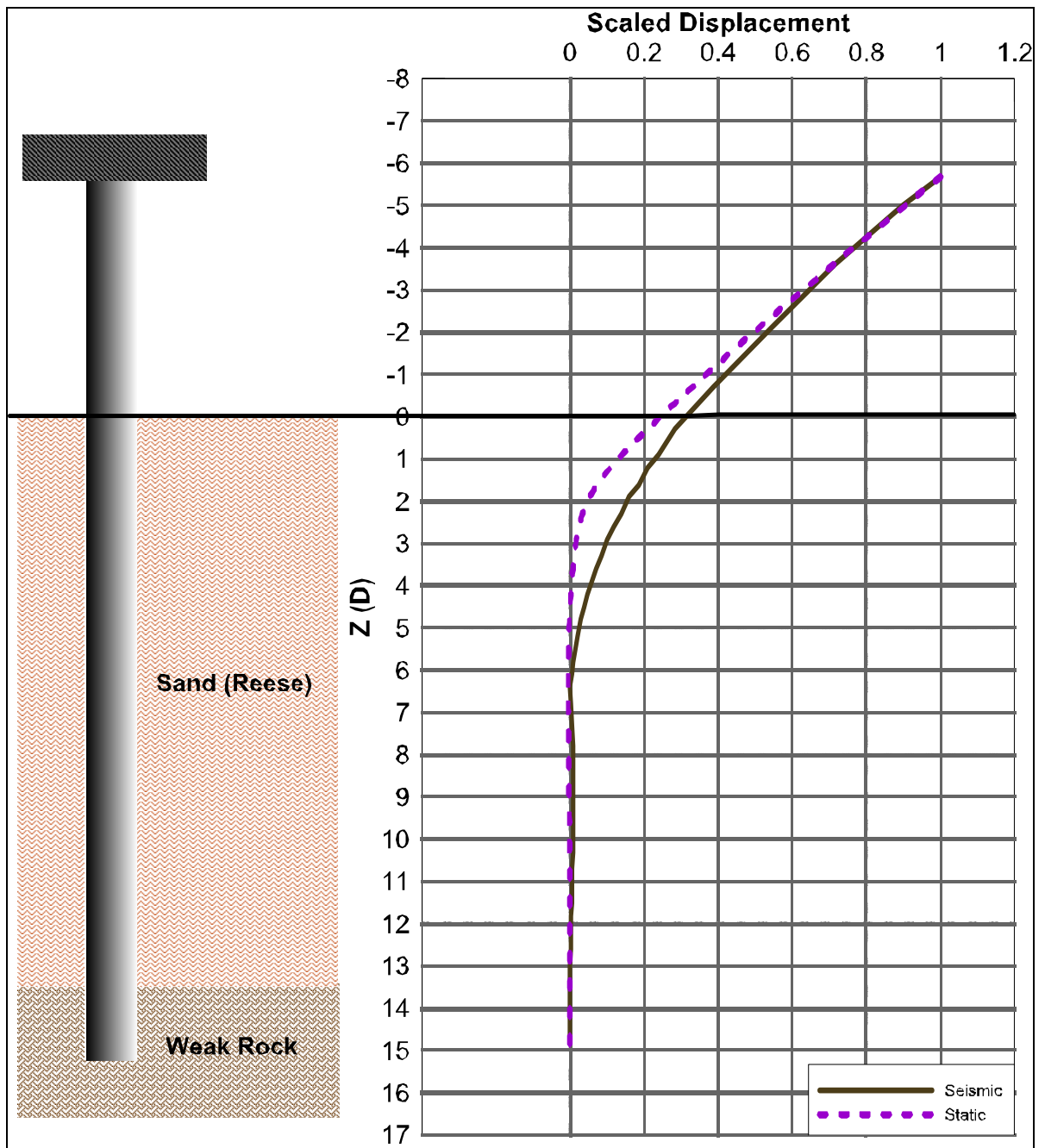


Figure 6.47 Seismic vs static scaled displacements from the modified soil model of QCR2

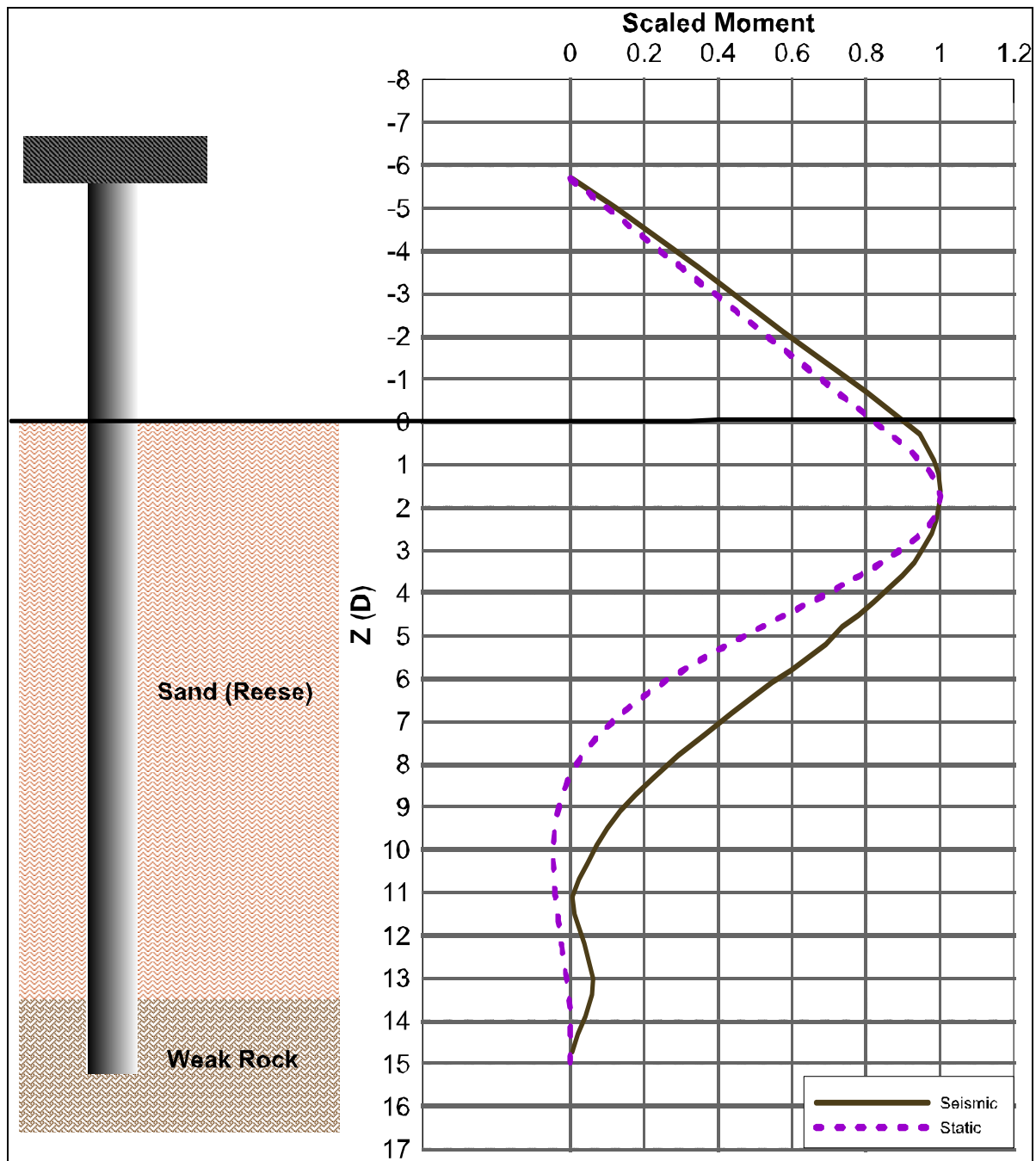


Figure 6.48 Seismic vs static scaled bending moment from the modified soil model of QCR2

CONCLUSIONS AND RECOMMENDATIONS

The research work focused in the nonlinear behavior of seismic soil-structure interaction of deep foundations with particular emphasis on Quebec soils.

Summary:

In summary the following aspects were carried out in this study:

- The study carried out comprehensive nonlinear seismic analyses on soil-pile interaction for Quebec soils.
- It defined the effects of the seismic load on current models of p-y curves by defining a Dynamic to Static ratio DS for P and Y components.
- The study proposed a simplified methodology to evaluate the effect of earthquake load on the commonly used static p-y curves in order to accurately account for the strength loss in soil from earthquake in the design of deep foundation for bridge structures. The proposed method resulted in good results for the selected study cases and it can be potentially applied to other cases.

Conclusions:

The following conclusions can be drawn from this study:

- Generally, the soil in the dynamic analysis has smaller lateral resistance: The soil deformations in the static analysis decreased rapidly under the ground surface compared with the seismic load case. The lateral deformations converged to zero much quicker than in the dynamic load case. Generally, The fixity level for effect of dynamic load is deeper than the one from the static load. Nevertheless, this significance of this shift decreases as the pile length becomes shorter. When the pile length L is less than $15D$, the dynamic effect becomes smaller for piles founded in sand. On the other, when pile is deep the dynamic effect on its PSSI is more apparent.

- The bridge superstructure mass has direct effect on the PSSI. The increase in the deck mass leads to higher inertial effects. For deep piles in good soil during earthquake, this factor might results in pile failure above the ground or at shallow depths which is desirable from the design point of view. The failure of the pile under the ground level is not repairable and therefore is normally forbidden in the design codes. Nevertheless, this can be achieved in the design by varying the section between the pile and the substructure column which extend above the ground and easy to repair in case of failure
- The fixity level from static load case is shallower than the one from dynamic load case: in general the soil above the fixity sees much later disturbance than the soil below. This also reflects the fact that soil modulus of elasticity tends to increase with depth. This fact makes soil laterally stronger below the fixity. The shift in the point of fixity to a deeper elevation means basically that soil above has undergone a big lateral displacement to the point at which it becomes much weaker to resist lateral force. This also means that the pile has less soil to support its lateral movement. In p-y curve language the springs above the fixity have much less stiffness than the ones below. This affects directly the seismic global response of the bridge as well as the pile design.
- The effect of considering seismic PSSI in the design of bridge deep foundation might be significant. In the case of long bridges with deep foundation, the first mode of the bridge occurs typically in the longitudinal direction of the bridge. The more slender the shafts supporting the piers and superstructure the more flexible the bridge and the higher the fundamental period. The shift of point of fixity to deeper elevation results in more flexible system, more slender piles and relatively longer fundamental vibration period. This leads to three direct effects on the design of the bridge:
 - a) Decrease in the seismic demands on the piles,
 - b) Increase in displacement demands of the superstructure and hence increase in the ductility demand of the bridge,
 - c) Increase in the seismic demands at the rock-socket part of the pile.
- The decrease in the demands on the pile is a direct result from the increase in the bridge fundamental period. Nevertheless, the shift in the fixity to lower level, results in

redistribution of forces along the pile and to an increase in the demands on the pile portion underneath the fixity including the socketed part. If the remaining soil depth below fixity is not enough to support the pile laterally or if the socketed part is not deep enough, the bridge might be unstable during an earthquake.

- Therefore, it is recommended to increase the socketed portion of the pile for seismic design of bridges. This increase can be evaluated based on several factors including the pile length and soil type. If increasing the socket portion is not possible or not desired, an increase in the pile diameter, regardless to the decrease in the seismic demands, is recommended in order to increase the rigidity of the structure and obtain lower fundamental period.
- One of the objectives of this study was to assess the effect of seismic loads on current p-y curves for Quebec soils. Results have shown that the proposed reduction factors for Quebec soils can be ranged between 40% and 90% based on the mass of the super structure i.e. the magnitude of the seismic load, the slenderness of the pile. The soil type effect was not accurately measured in this study for the following reasons (i) although the effective soil properties were assumed in the analysis, the pore pressure increase was not simulated, (ii) the type of the soil for the studied sites varied between sand and silty clay and therefore the p-y criteria was defined for c-phi soil, and (iii) initiation of soil liquefaction was not assumed in any of the analysis stages and is considered outside the scope of this study.
- The other objective was to develop a simplified method to be used for SSPSI problem instead of the time history analysis. Results of this study show that it is possible to calculate reduction factors following the same procedure as proposed in this study. The procedure is accurate

Recommendations for the design:

The recommendations drawn from this study to be considered in modeling bridge structures with deep foundation for seismic analysis are as follows:

- The modeling of the soil under seismic conditions with the current p-y curves is not an accurate procedure.
- Considering SPSSI in the analysis impacts the performance of the bridge during earthquakes.
- The direct effect of considering the SPSSI in the analysis is apparent through the relocation of the fixity point and the change of the soil lateral resistance.
- The change in the fixity elevation affects the flexibility of the bridge and increases the demands on the socketed shaft.
- The SPSSI effect is more pronounced in slender shafts ($L/D > 15$).
- The superstructure mass has direct impact on the SPSSI. However, this effect is limited to the shaft capacity.
- Failure of stubby piles is governed by rocking or shifting or a combination of both.
- Failure of slender piles is governed by the formation of plastic hinge.
- For slender piles founded in Quebec soil the reduction in the soil strength is as follows:
 - DS-P is < 1 [0.1-0.6]
 - DS-Y is > 1 [1.1-10]

Future work:

For future work, it is recommended to conduct further analyses considering the following effects:

- Variation of unsupported pile length above the ground,
- Variation of supported pile length below the ground,
- The effect of other types of soil,
- The effect of pile diameter,
- Variation of seismic records.

It is also recommended to conduct a full scale tests on piles under rapid cyclic load.

APPENDIX I

NON-LINEAR TIME HISTORY ANALYSIS RESULTS

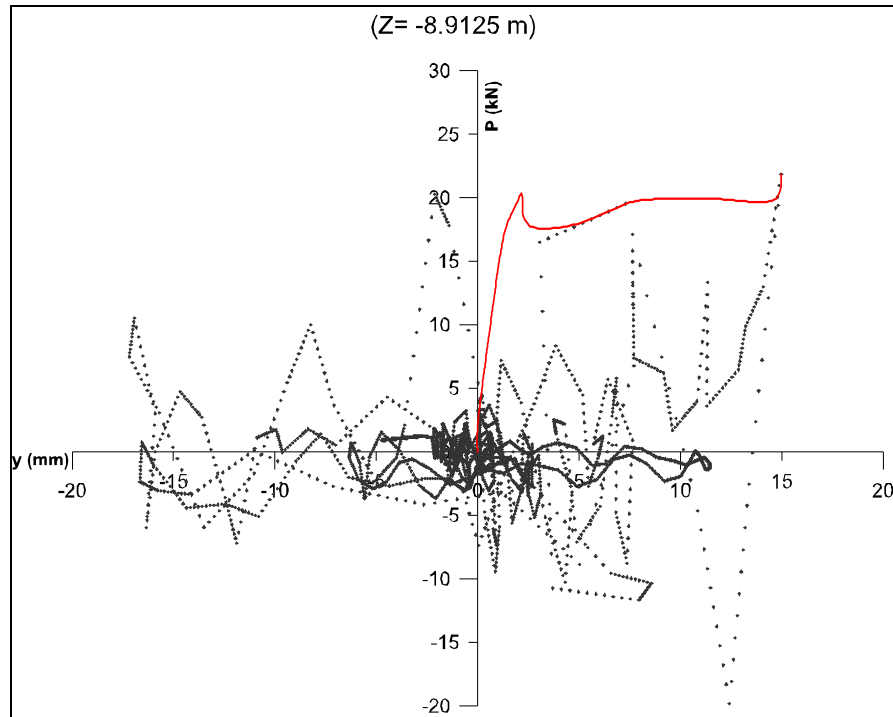


Figure-A I-1 p - y loop of BECR1M2 at $Z=-8.9125$ m and extracted p - y curve (in red)

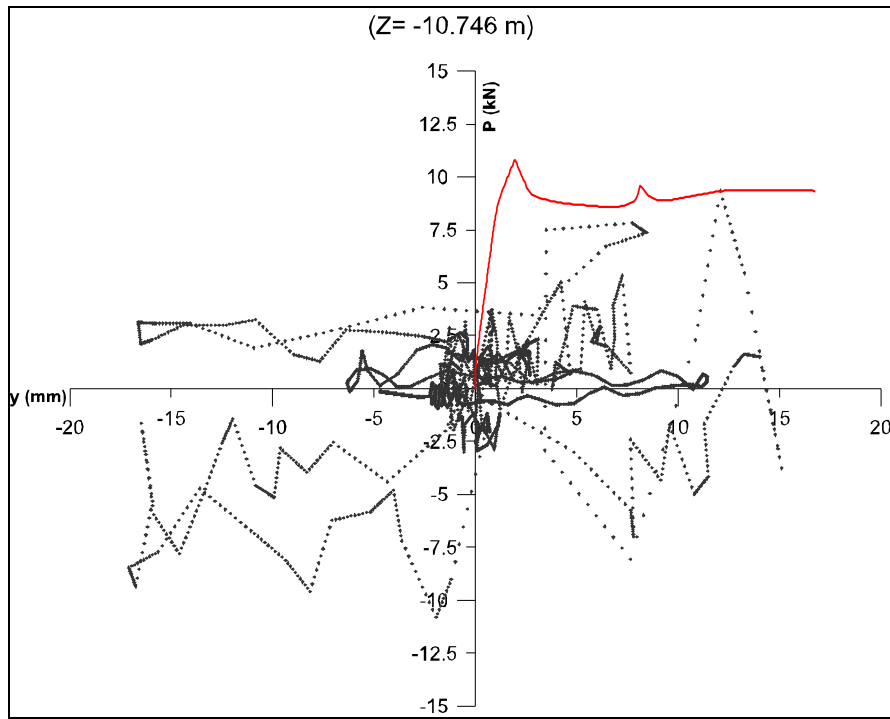


Figure-A I-2 p - y loop of BECR1M2 at $Z=-10.746$ m and extracted p - y curve (in red)

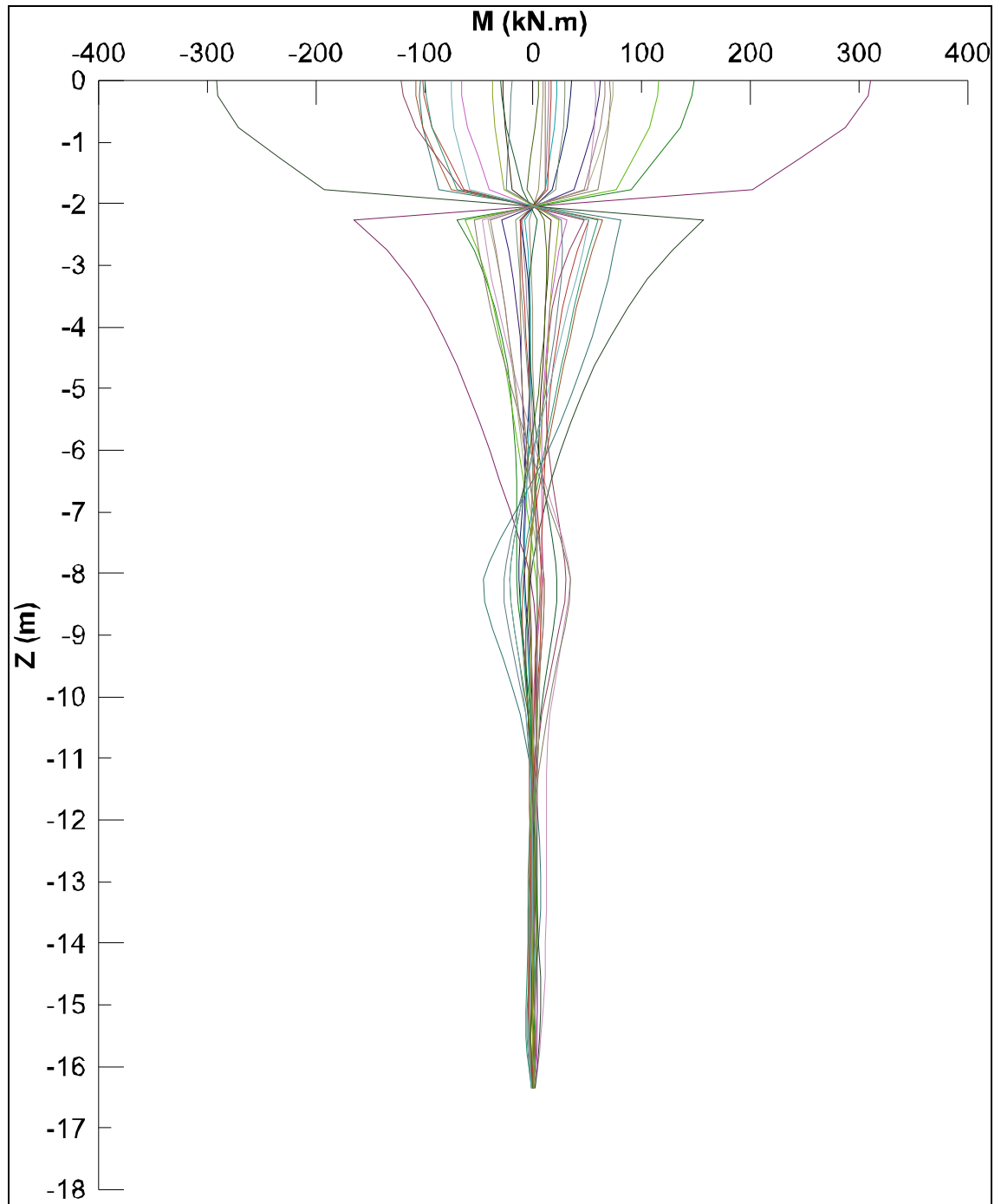


Figure-A I-3 Envelope bending moment with depth of BECR1M2 at pile head

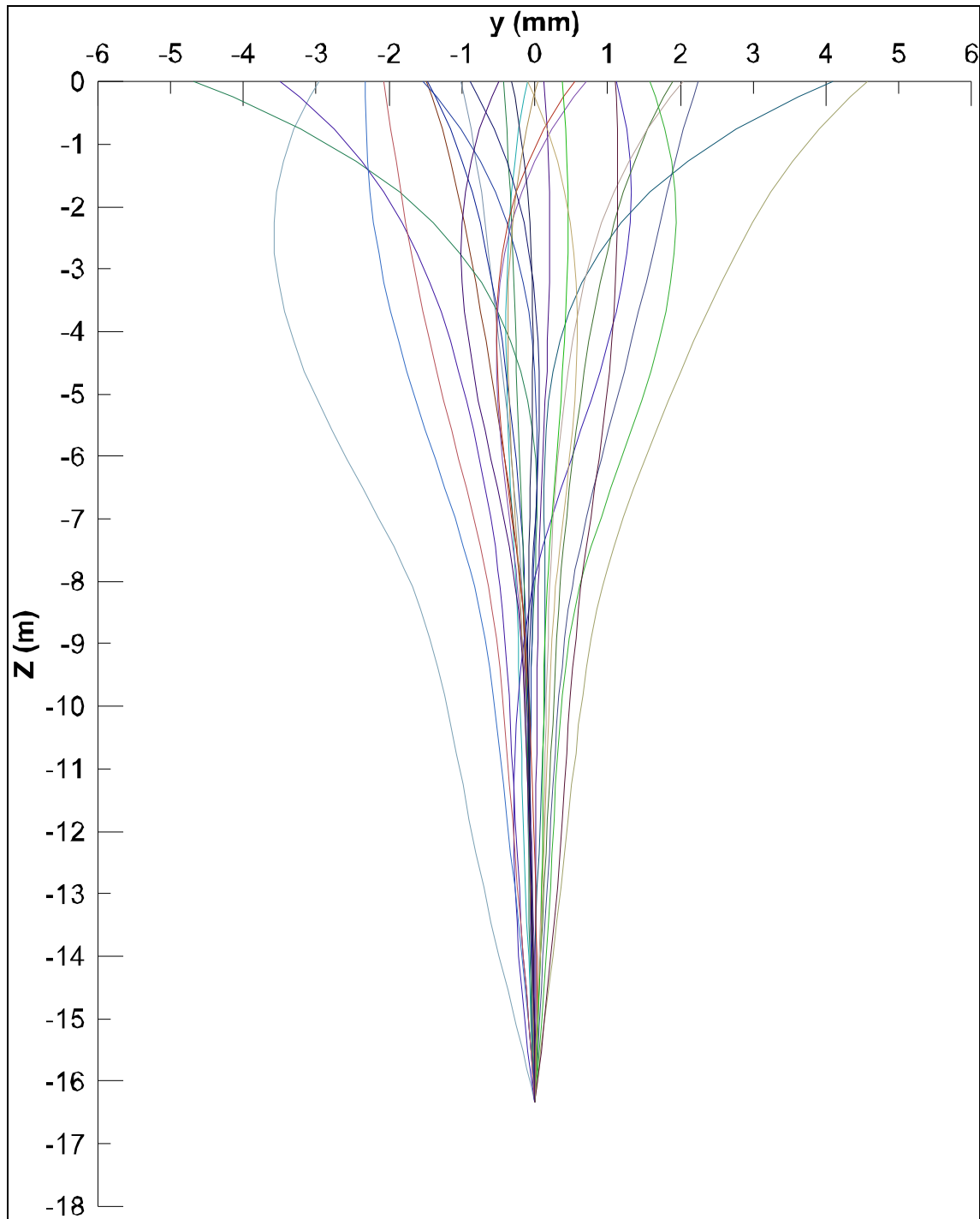


Figure-A I-4 Envelope of displacements with depth of BECR1M2 at pile head

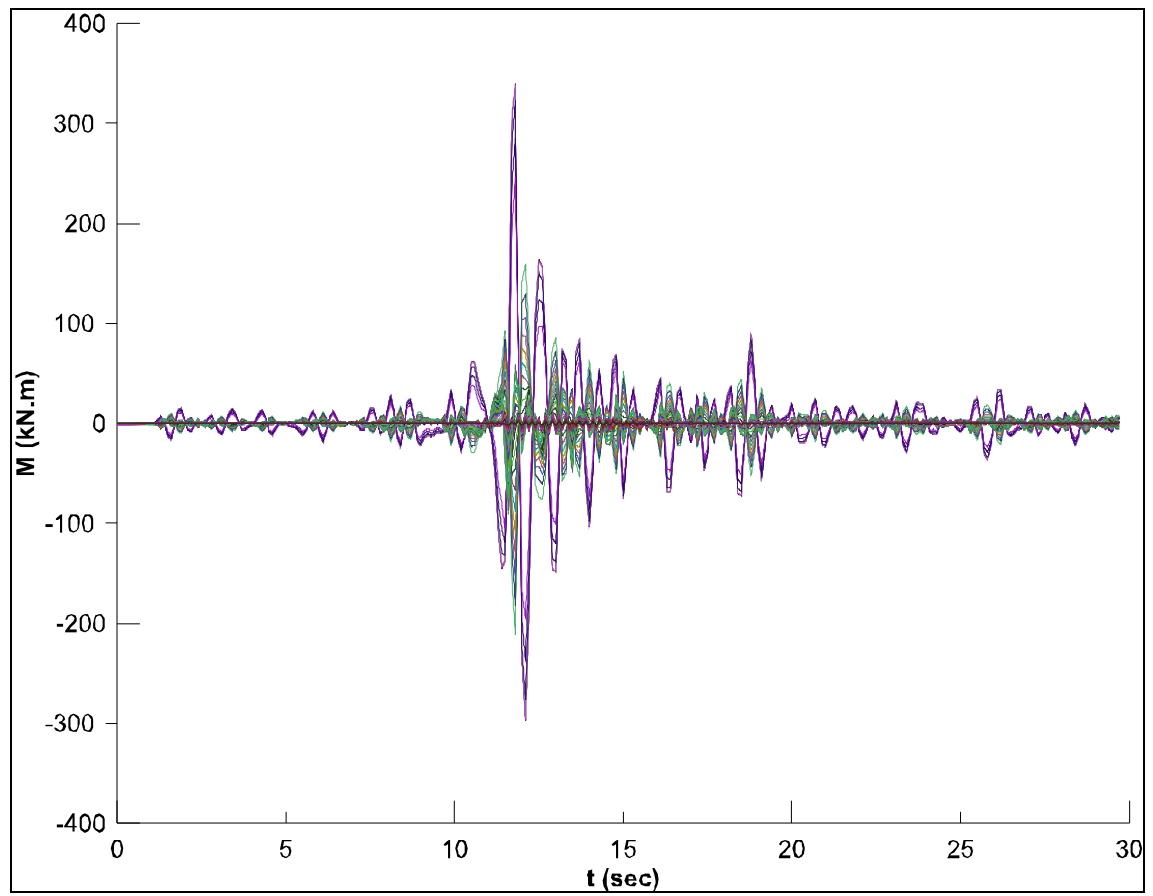


Figure-A I-5 Envelope bending moment with time of BECR1M2 at pile head

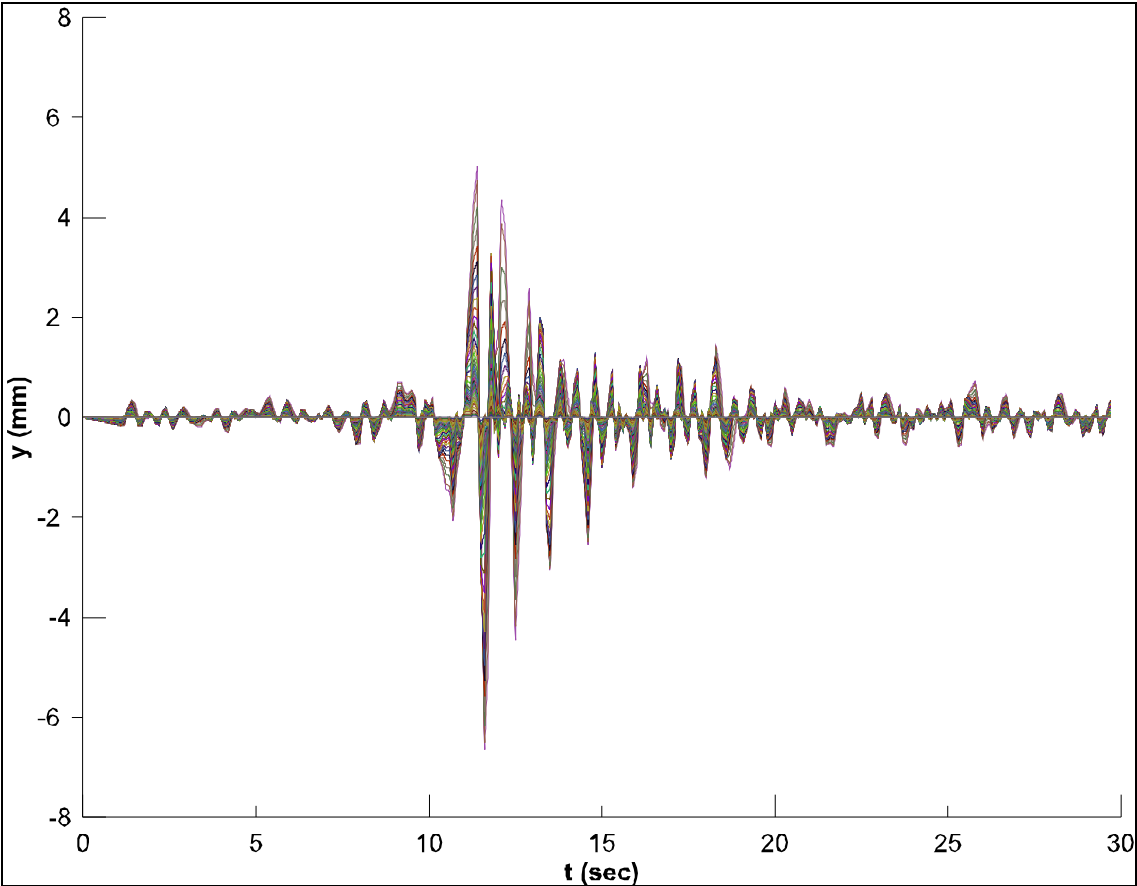


Figure-A I-6 Envelope of displacements with time of BECR1M2 at pile head

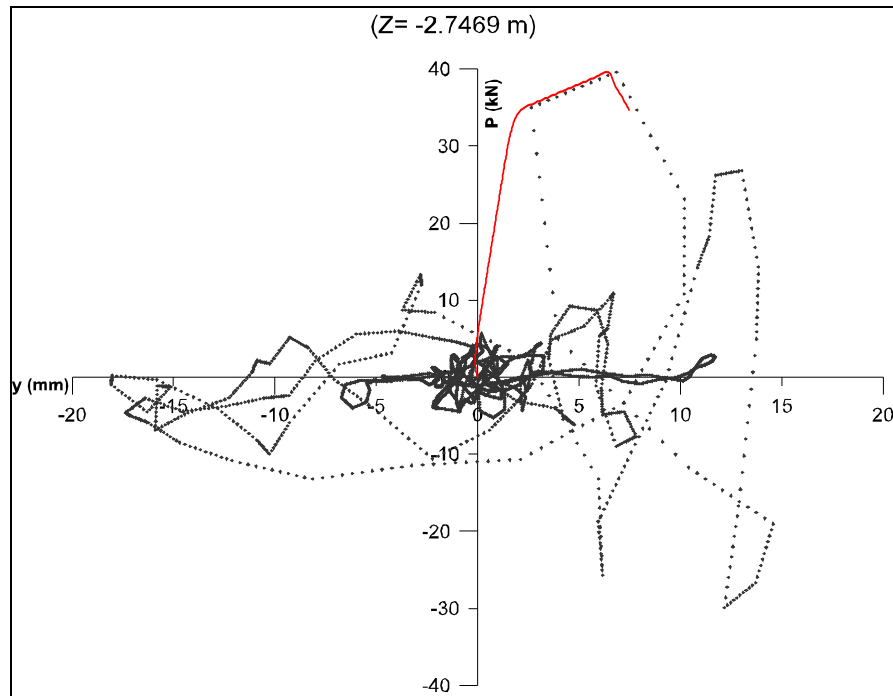


Figure-A I-7 p - y loop of BECR1M3 at $Z=-2.7469$ m and extracted p - y curve (in red)

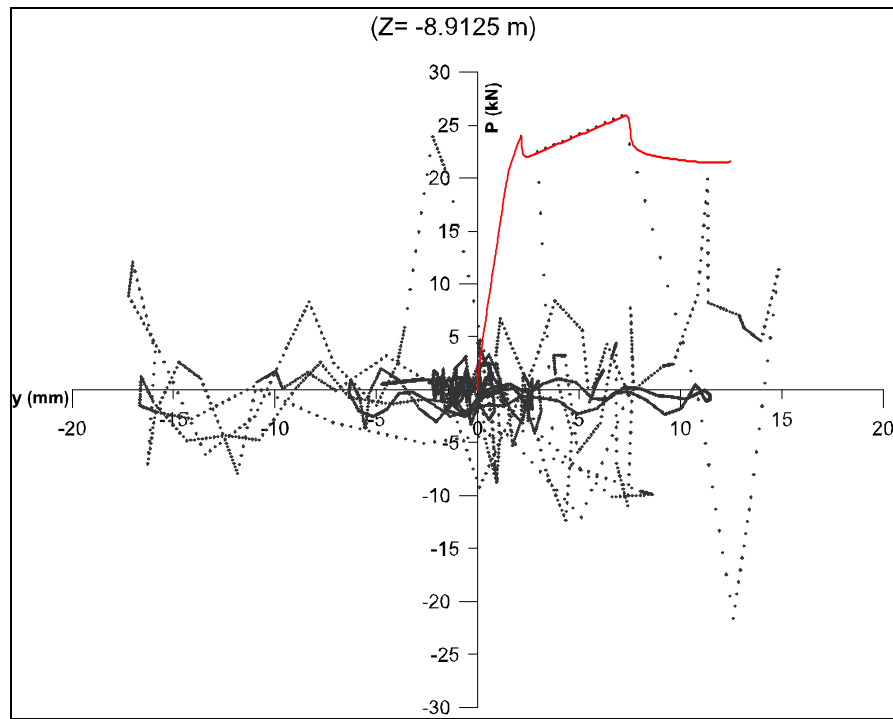


Figure-A I-8 p - y loop of BECR1M3 at $Z=-8.9125$ m and extracted p - y curve (in red)

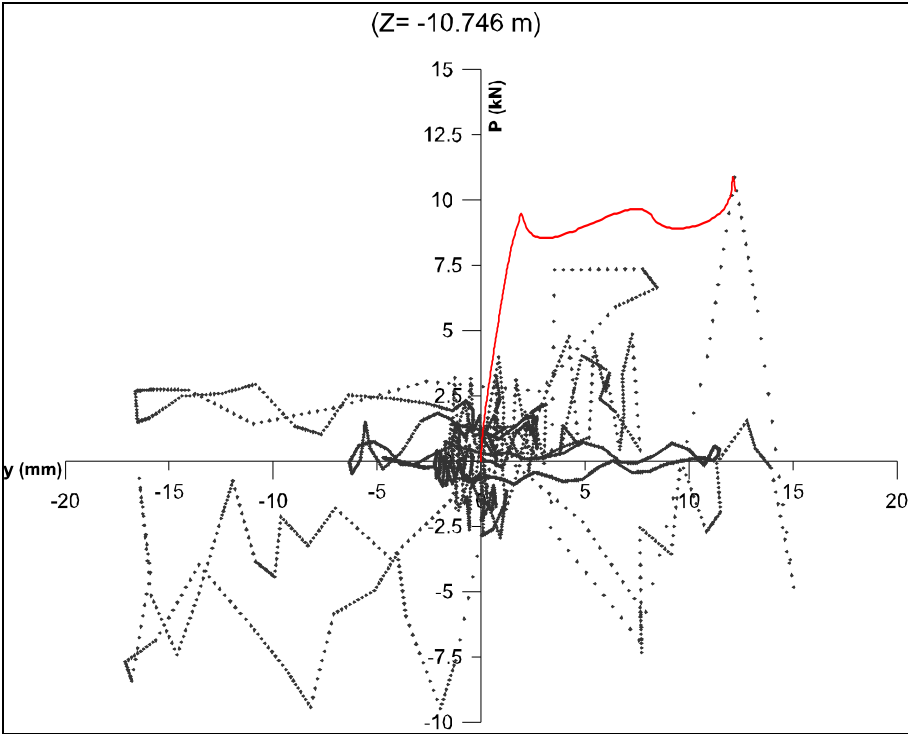


Figure-A I-9 *p-y* loop of BECR1M3 at Z=-10.746 m and extracted *p-y* curve (in red)

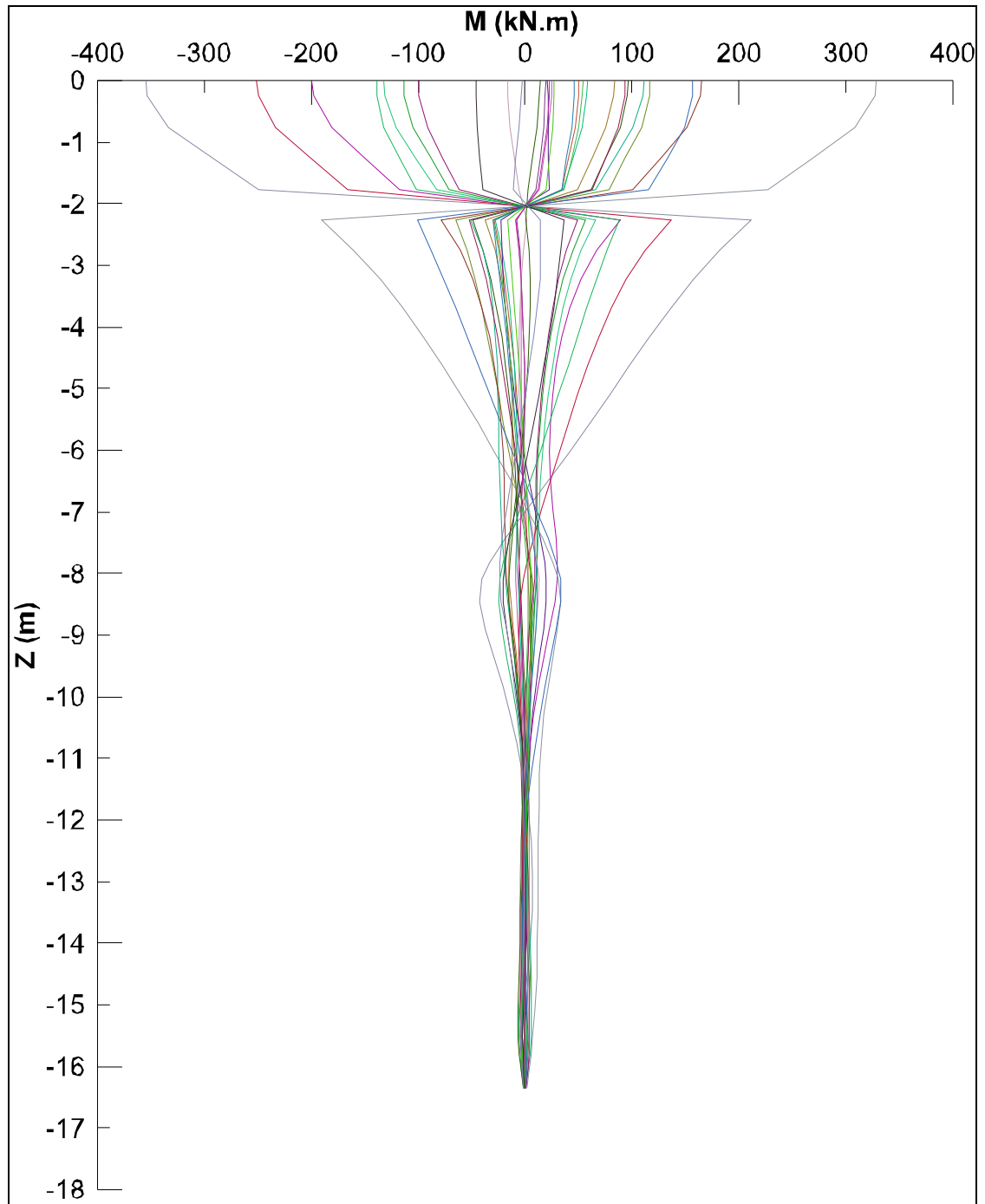


Figure-A I-10 Envelope bending moment with depth of BECR1M3 at pile head

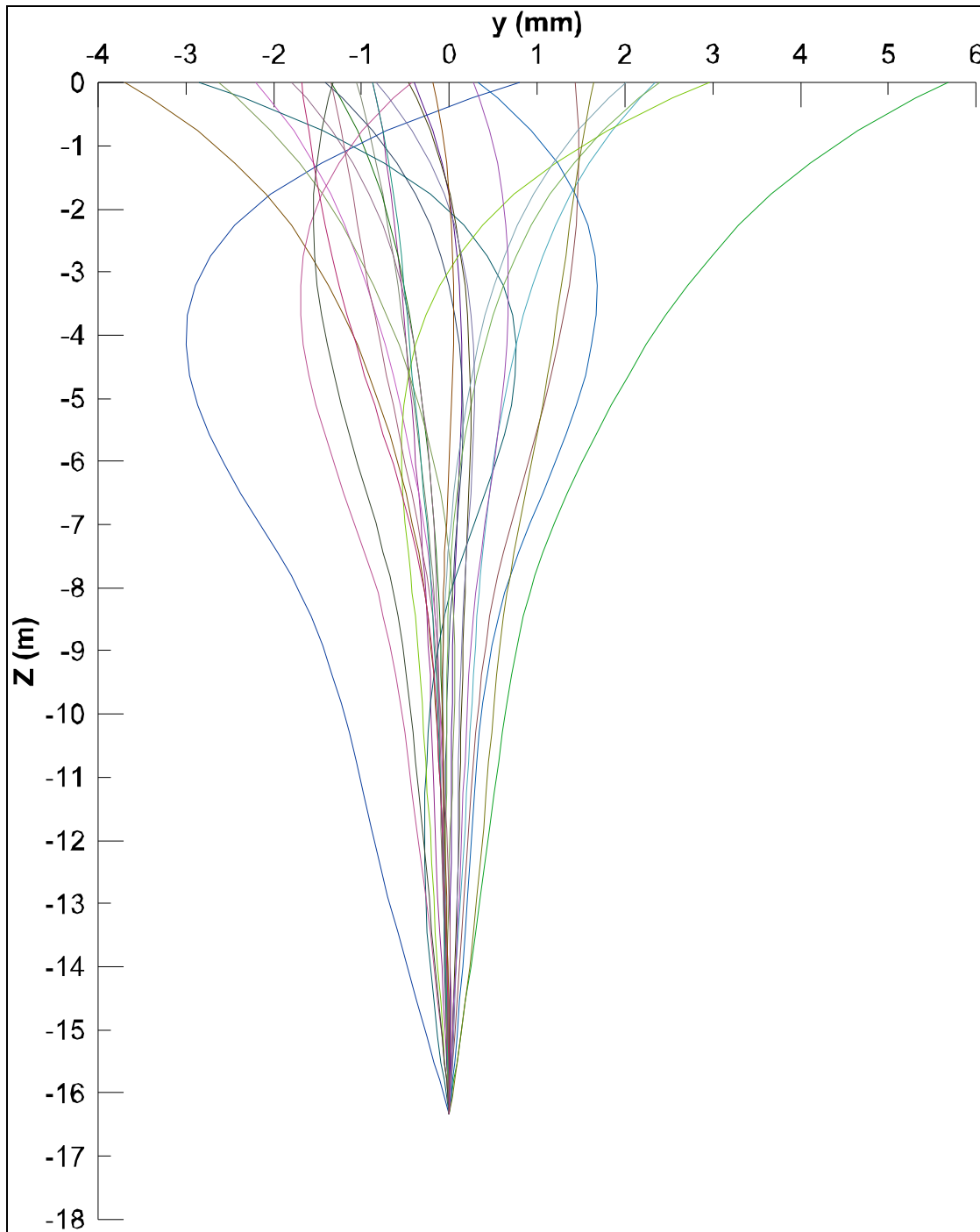


Figure-A I-11 Envelope of displacements with depth of BECR1M3 at pile head

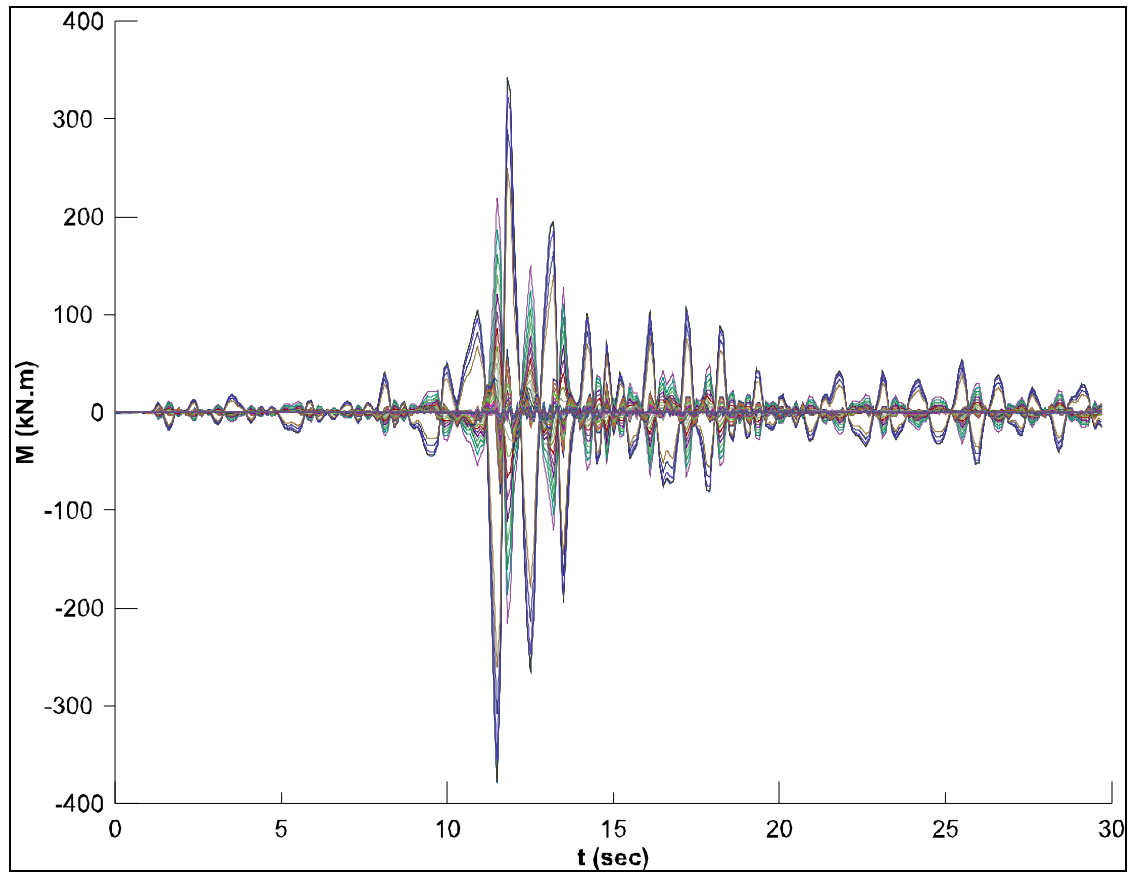


Figure-A I-12 Envelope bending moment with time of BECR1M3 at pile head

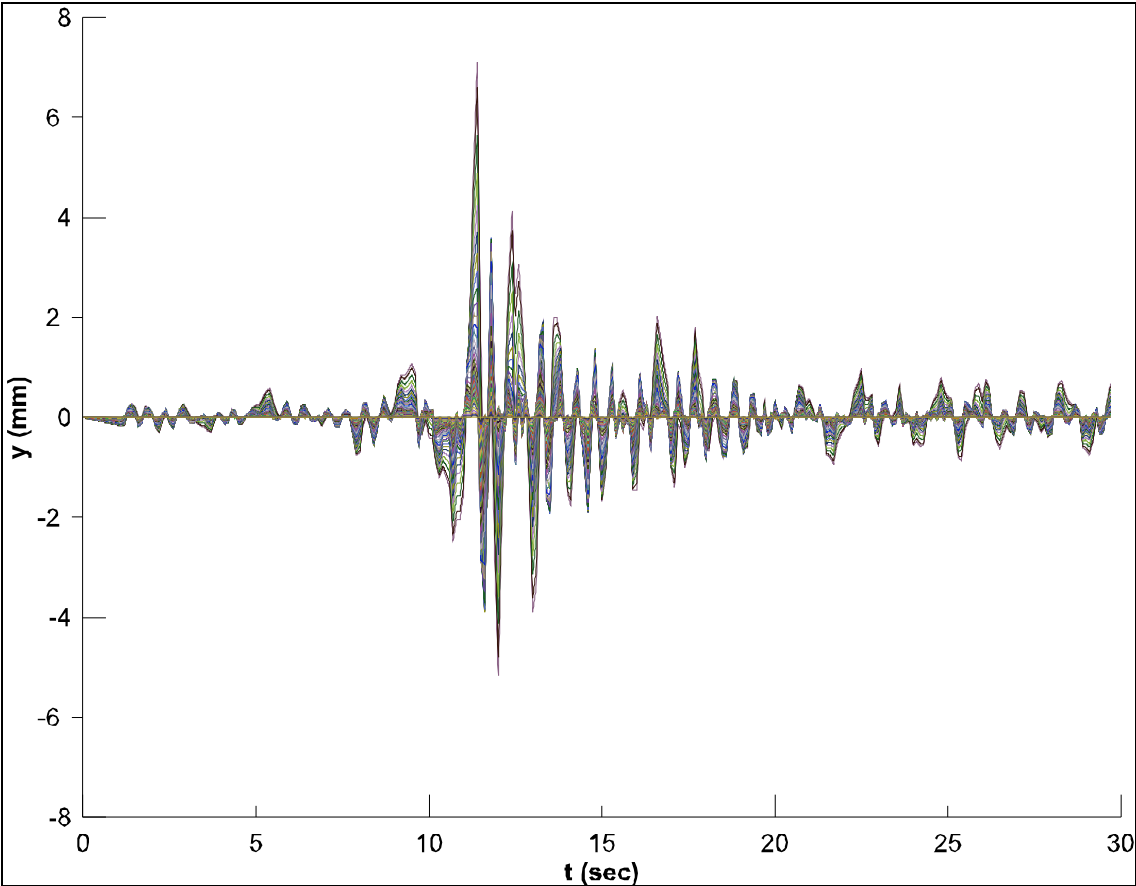


Figure-A I-13 Envelope of displacements with time of BECR1M3 at pile head

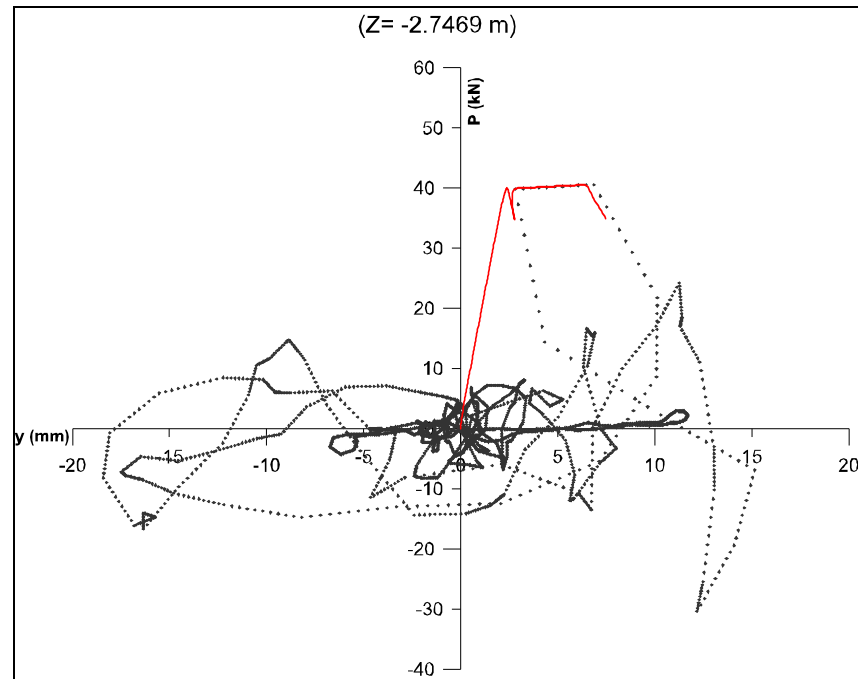


Figure-A I-14 p - y loop of BECR1M4 at $Z=-2.7469$ m and extracted p - y curve (in red)

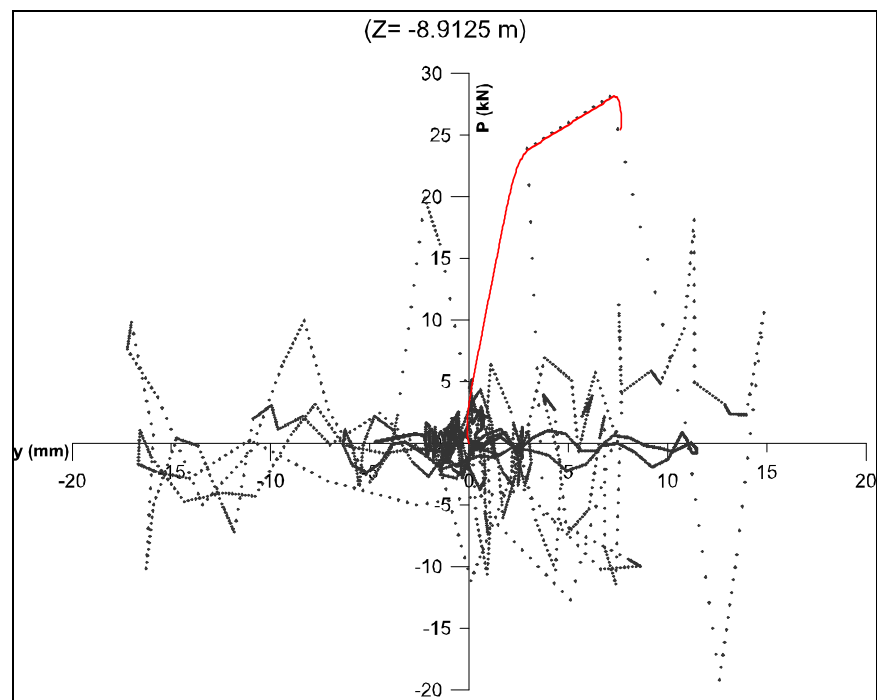


Figure-A I-15 p - y loop of BECR1M4 at $Z=-8.9125$ m and extracted p - y curve (in red)

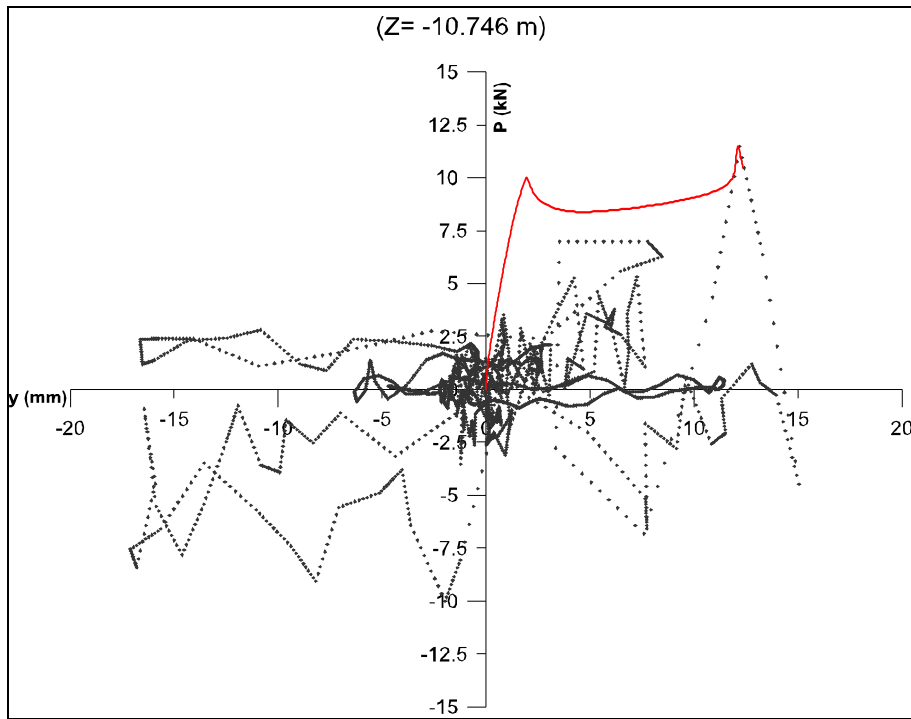


Figure-A I-16 p - y loop of BECR1M4 at $Z=-10.746$ m and extracted p - y curve (in red)

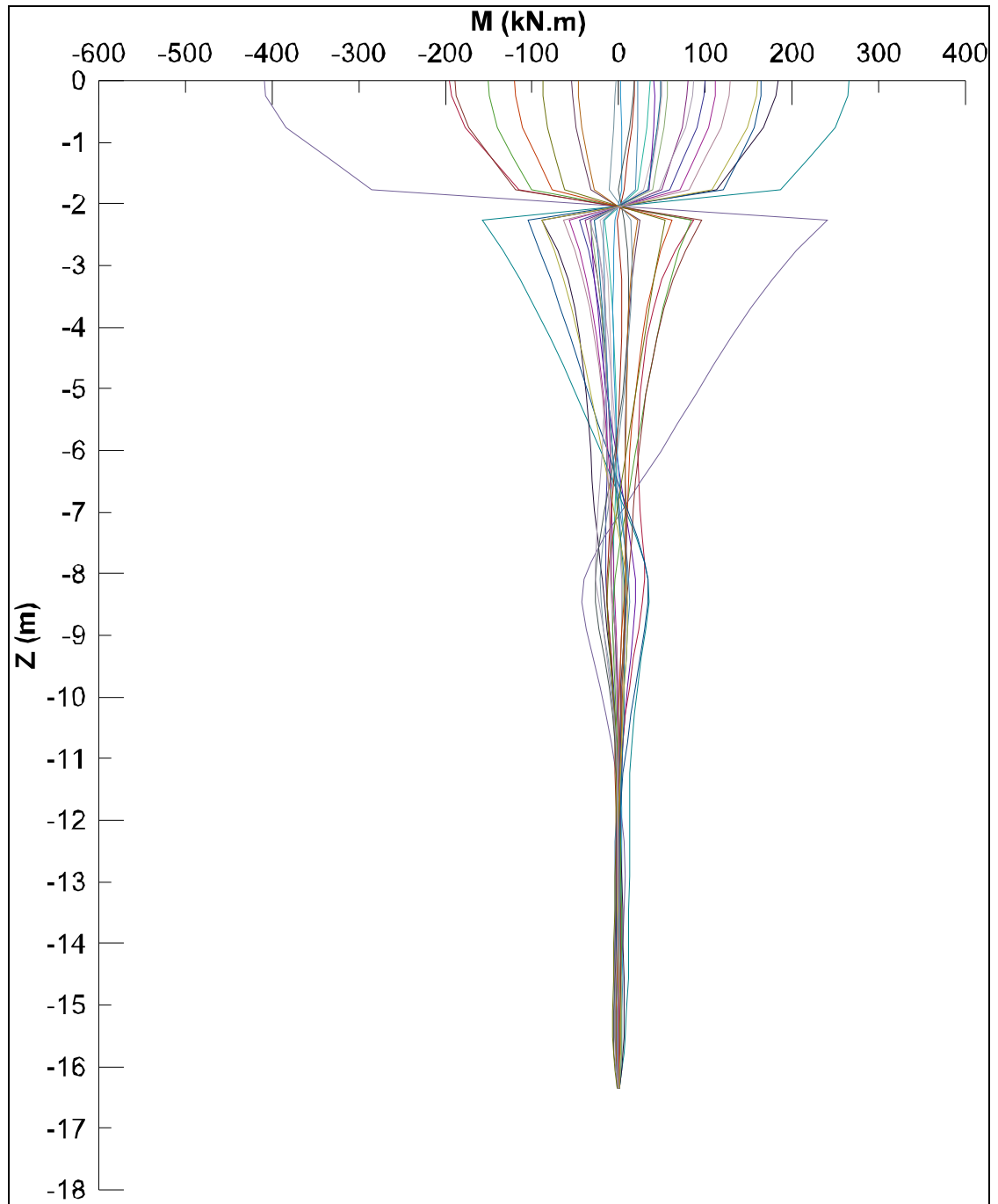


Figure-A I-17 Envelope bending moment with depth for BECR1M4 at pile head

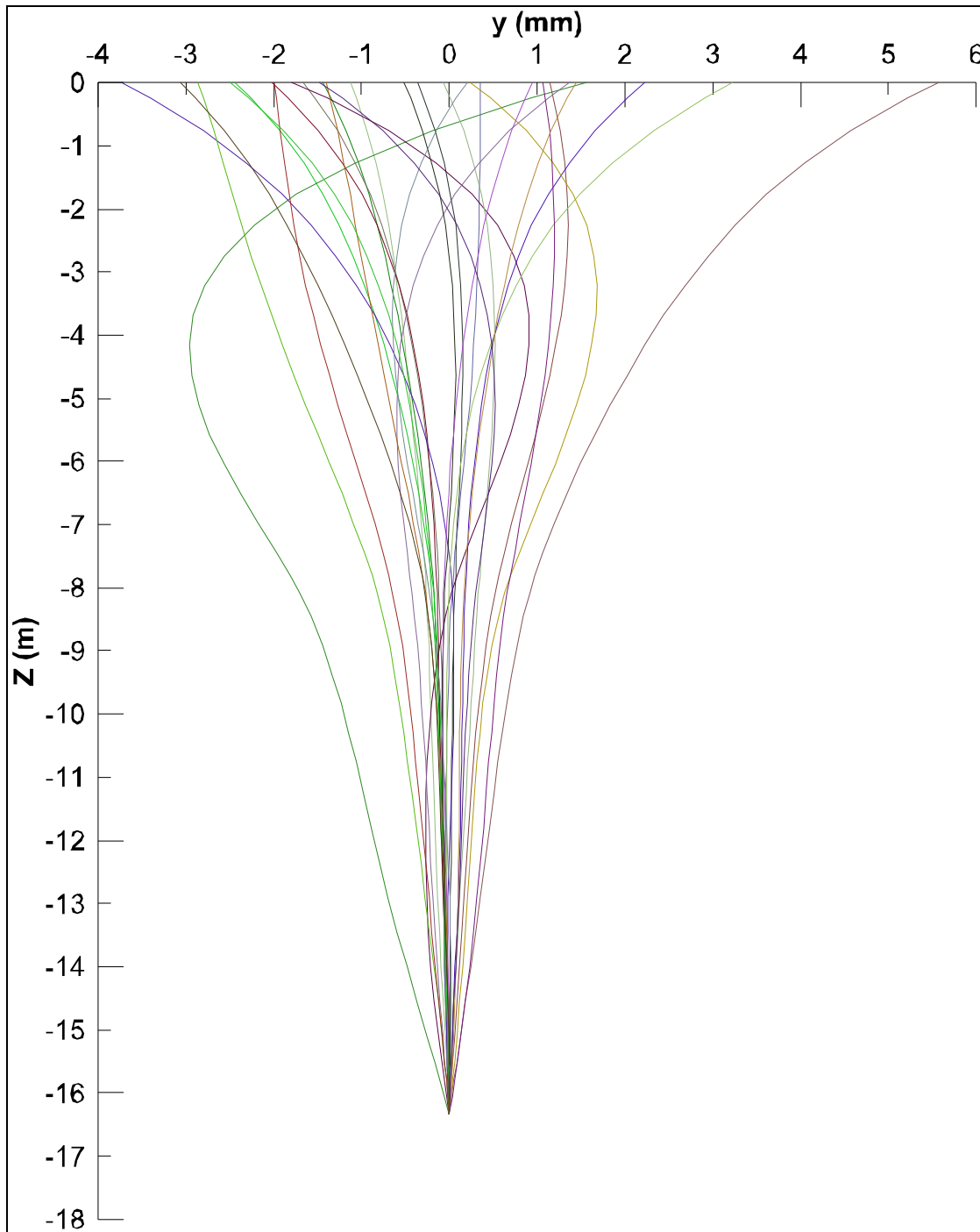


Figure-A I-18 Envelope of displacements with depth of BECR1M4 at pile head

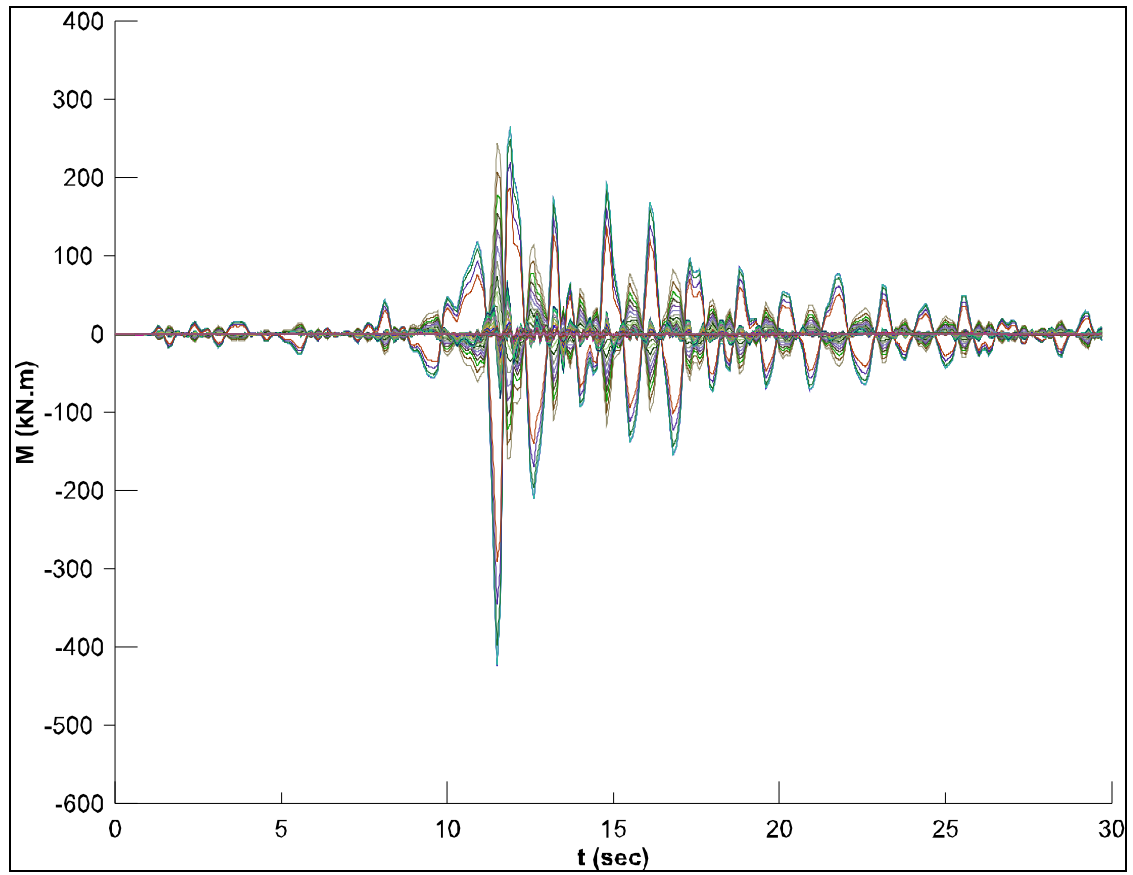


Figure-A I-19 Envelope bending moment with time of BECR1M4 at pile head

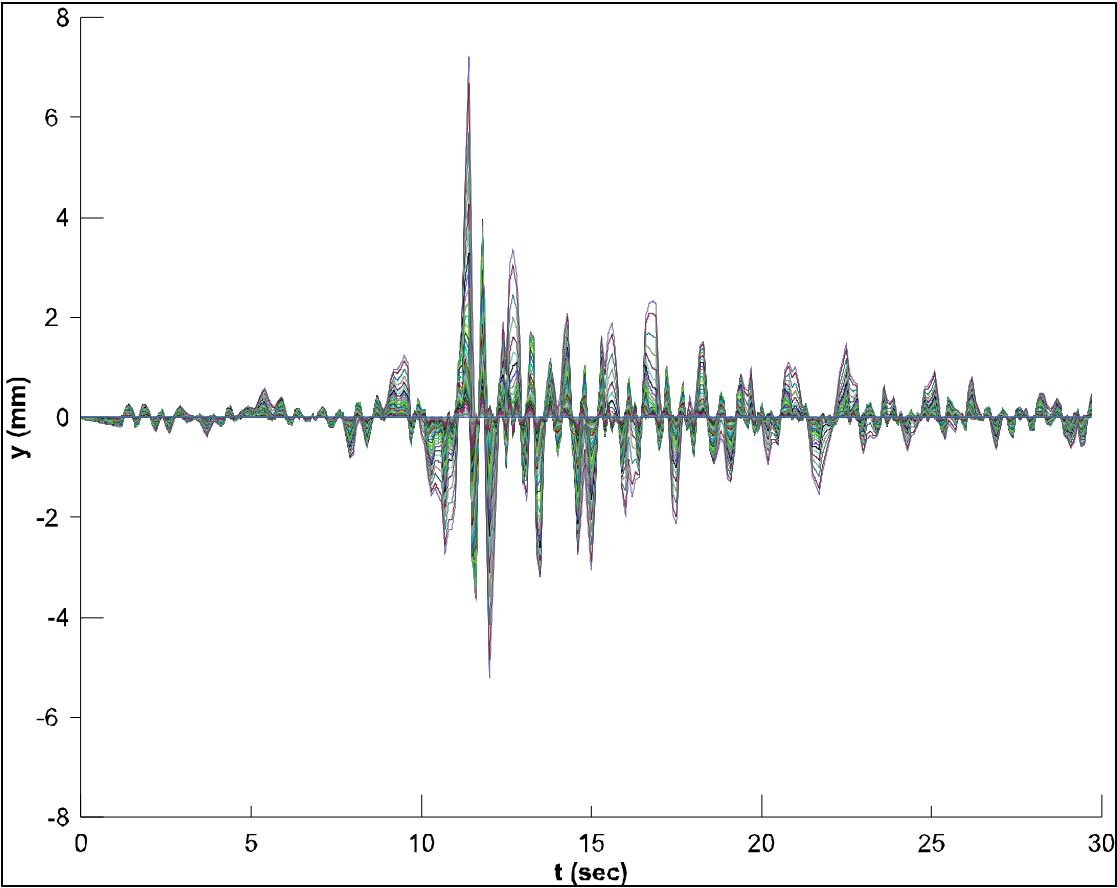


Figure-A I-20 Envelope of displacements with time of BECR1M4 at pile head

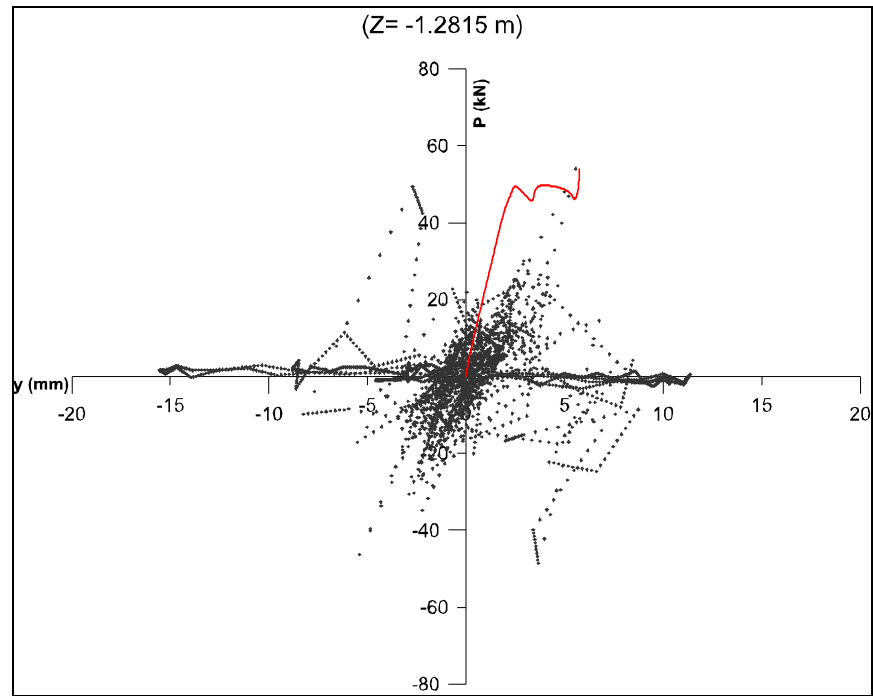


Figure-A I-21 p - y loop of QCR1M2 at $Z=-1.2815$ m and extracted p - y curve (in red)

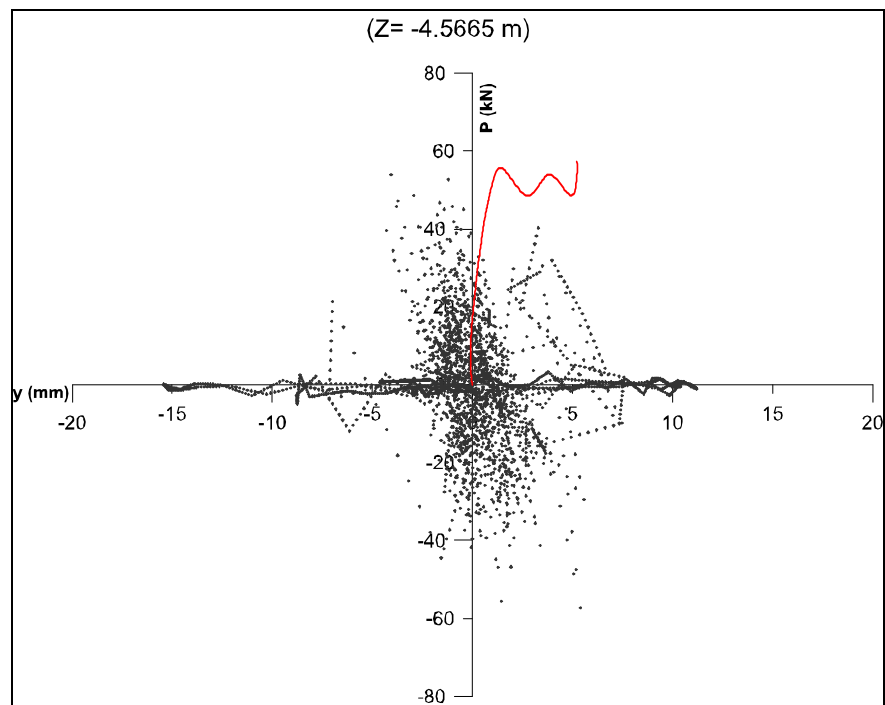


Figure-A I-22 p - y loop of QCR1M2 at $Z=-4.5665$ m and extracted p - y curve (in red)

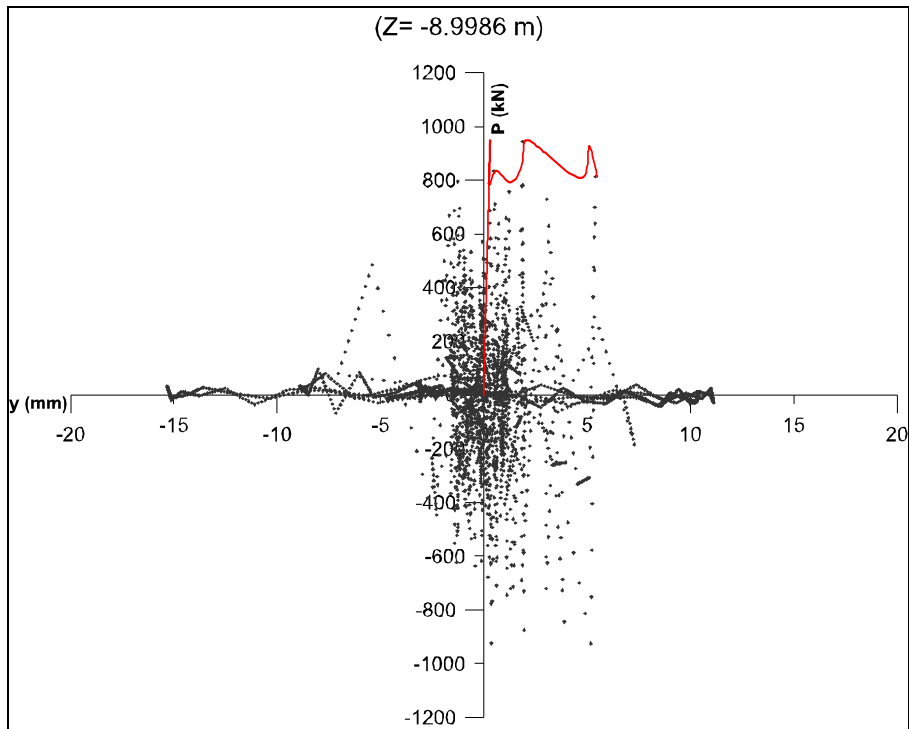


Figure-A I-23 p - y loop of QCR1M2 at $Z=-8.9986$ m and extracted p - y curve (in red)

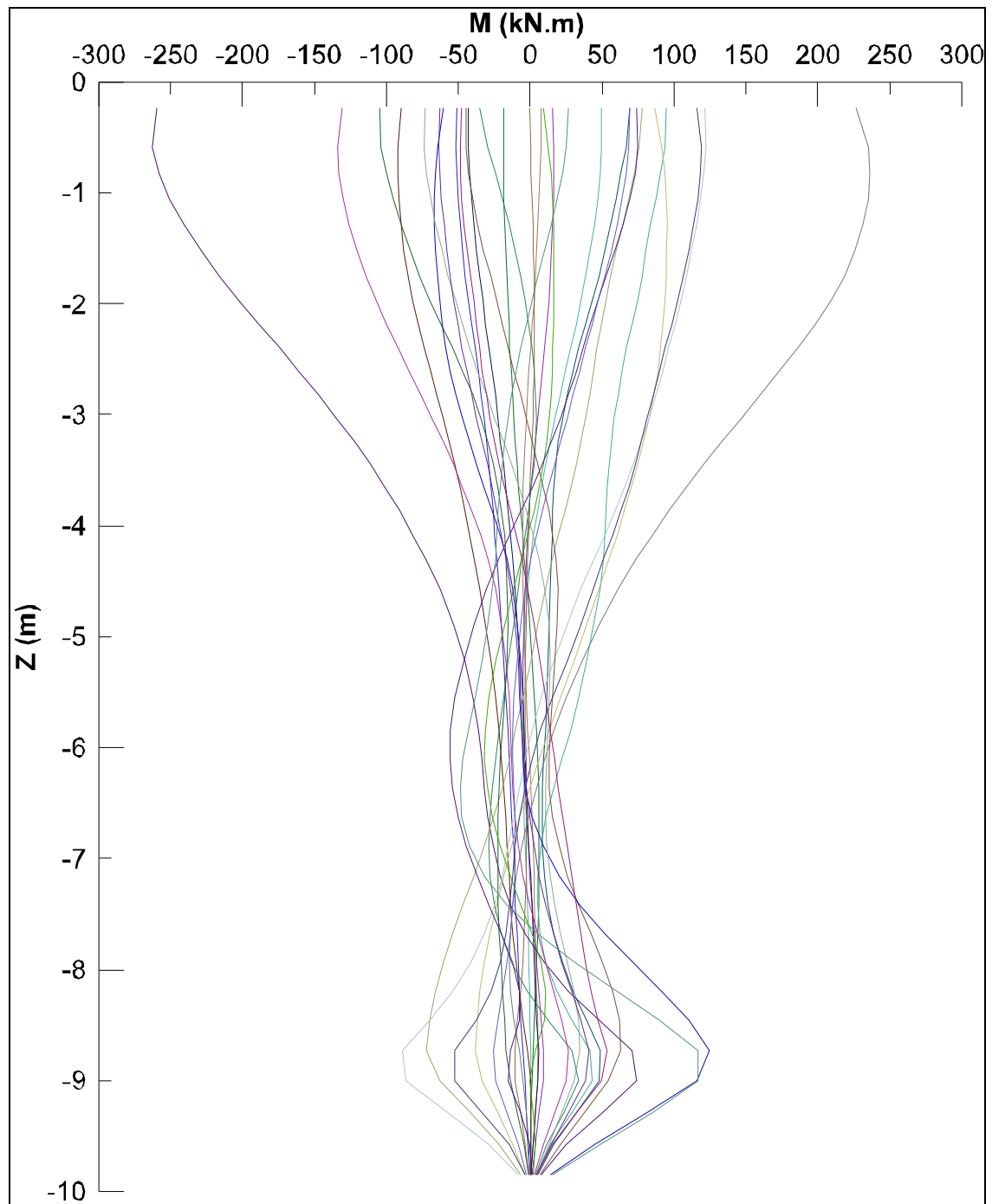


Figure-A I-24 Envelope bending moment with depth of QCR1M2 at pile head

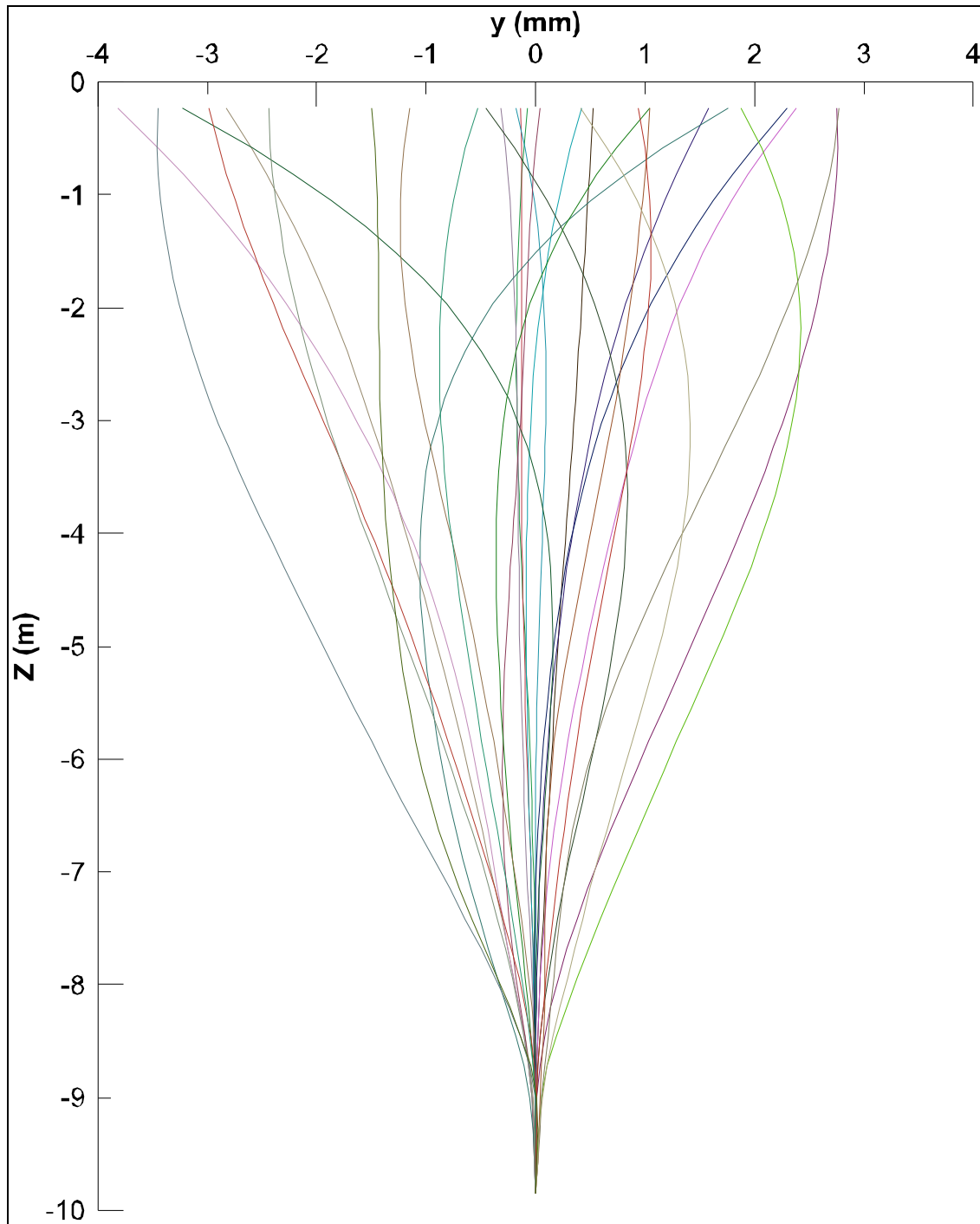


Figure-A I-25 Envelope of displacements with depth of QCR1M3 at pile head

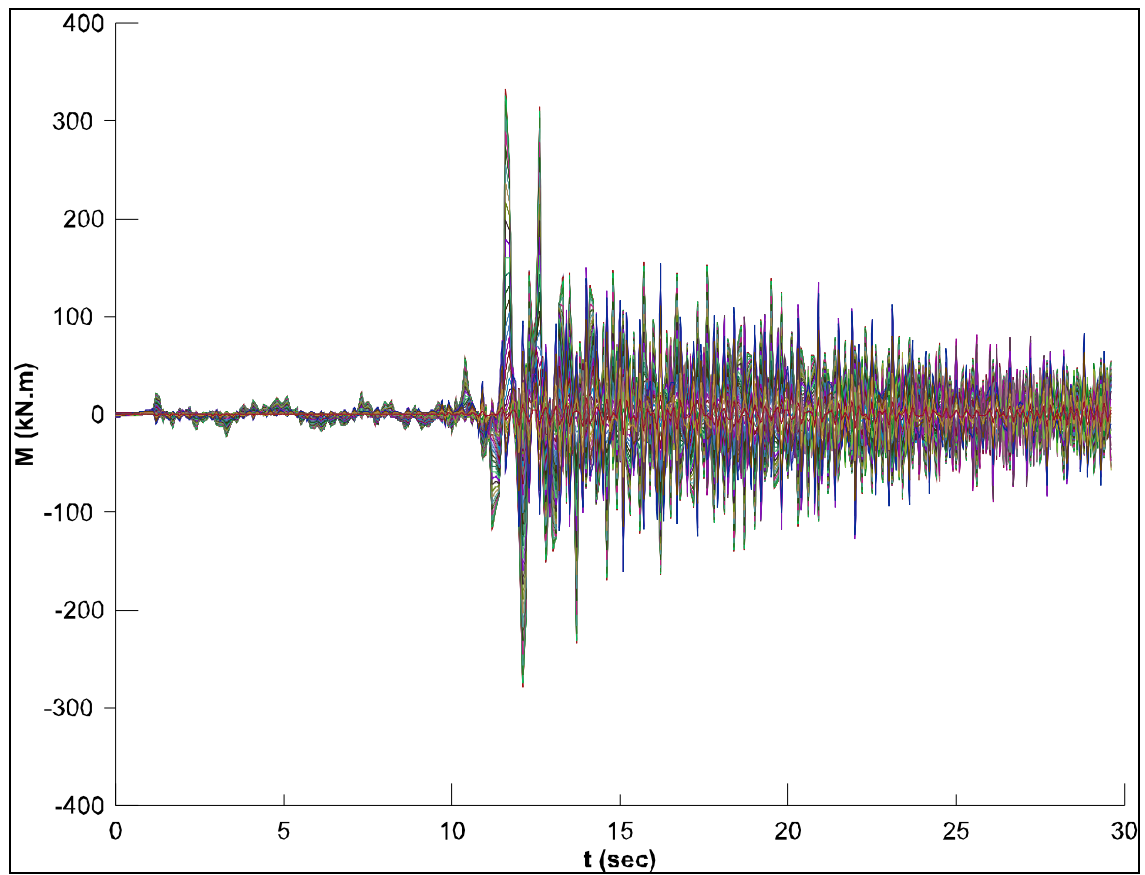


Figure-A I-26 Envelope bending moment with time of QCR1M2 at pile head

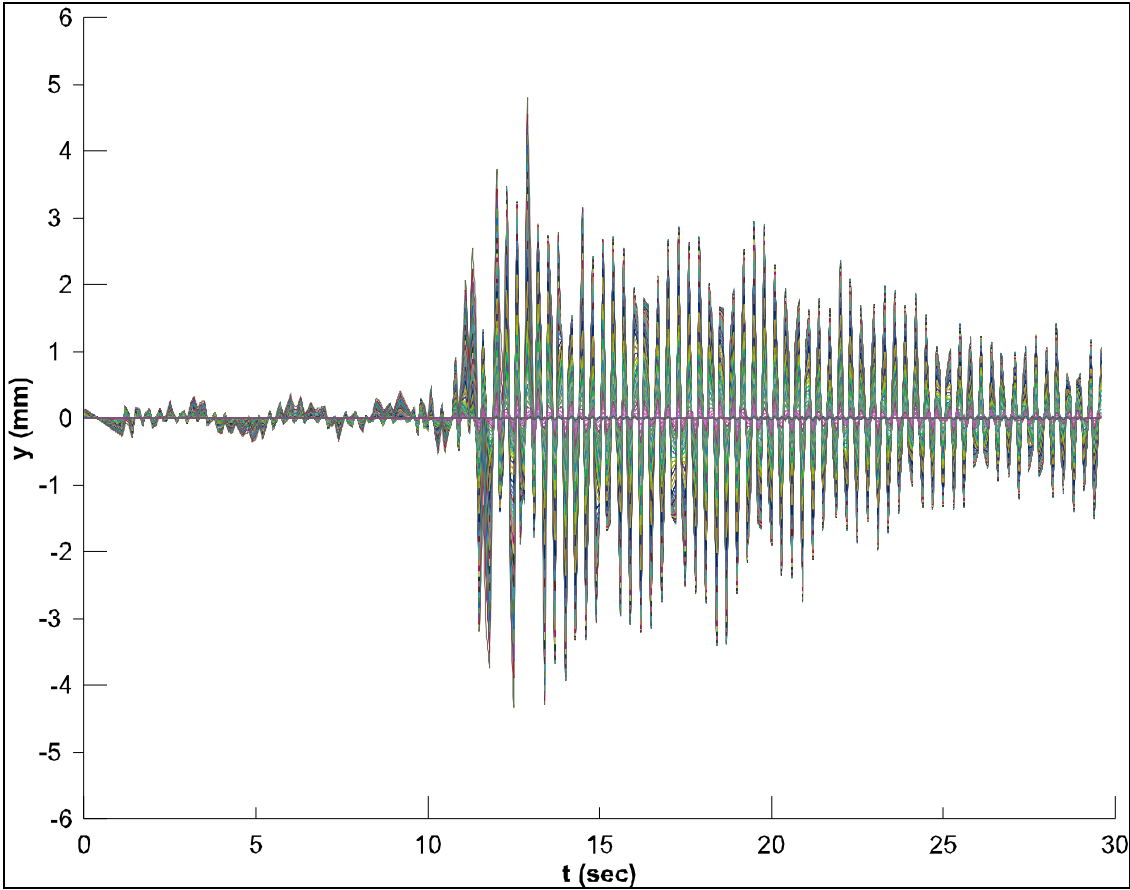


Figure-A I-27 Envelope of displacements with time of QCR1M2 at pile head

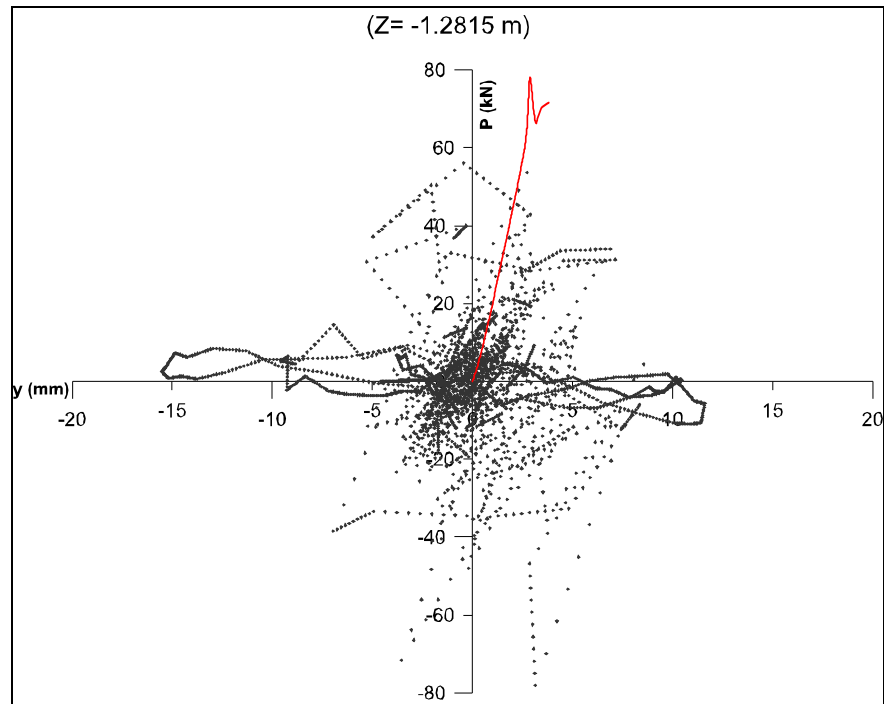


Figure-A I-28 $p-y$ loop of QCR1M3 at $Z=-1.2815$ m and extracted $p-y$ curve (in red)

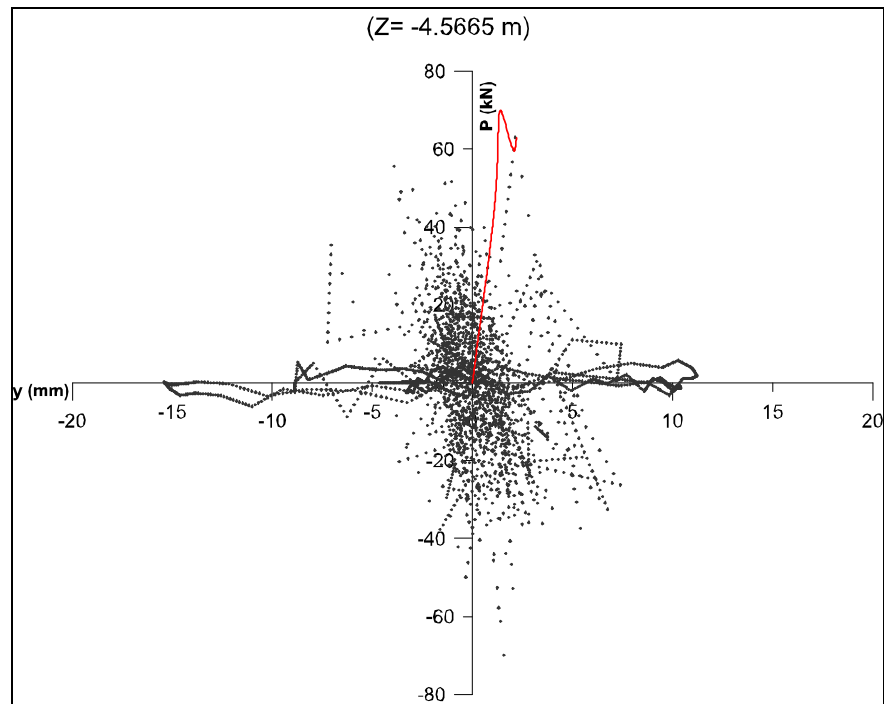


Figure-A I-29 p - y loop of QCR1M3 at $Z=-4.5665$ m and extracted p - y curve (in red)

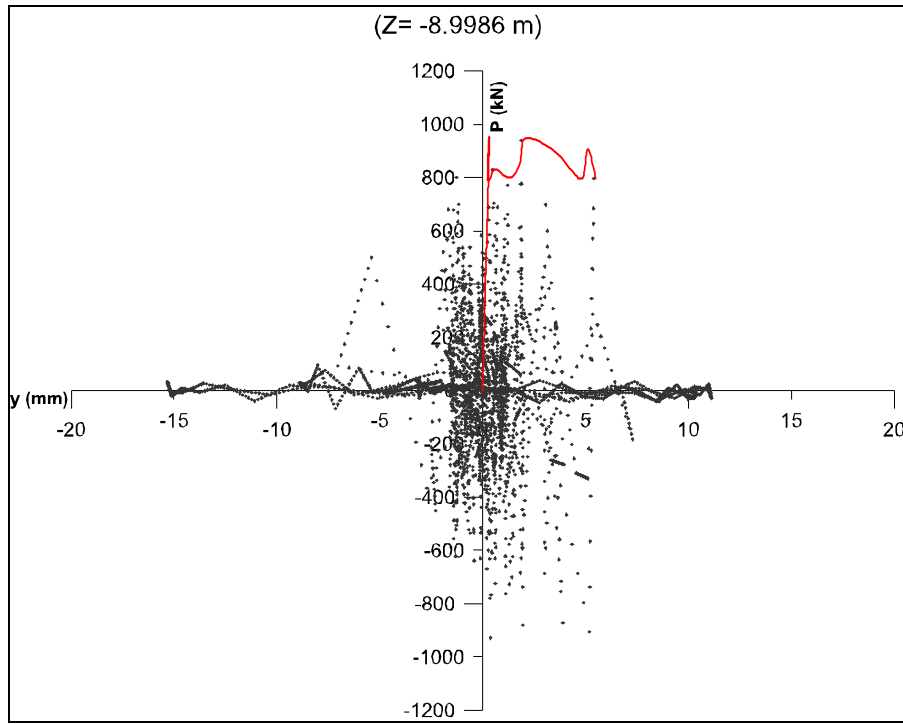


Figure-A I-30 p - y loop of QCR1M3 at $Z=-8.9986$ m and extracted p - y curve (in red)

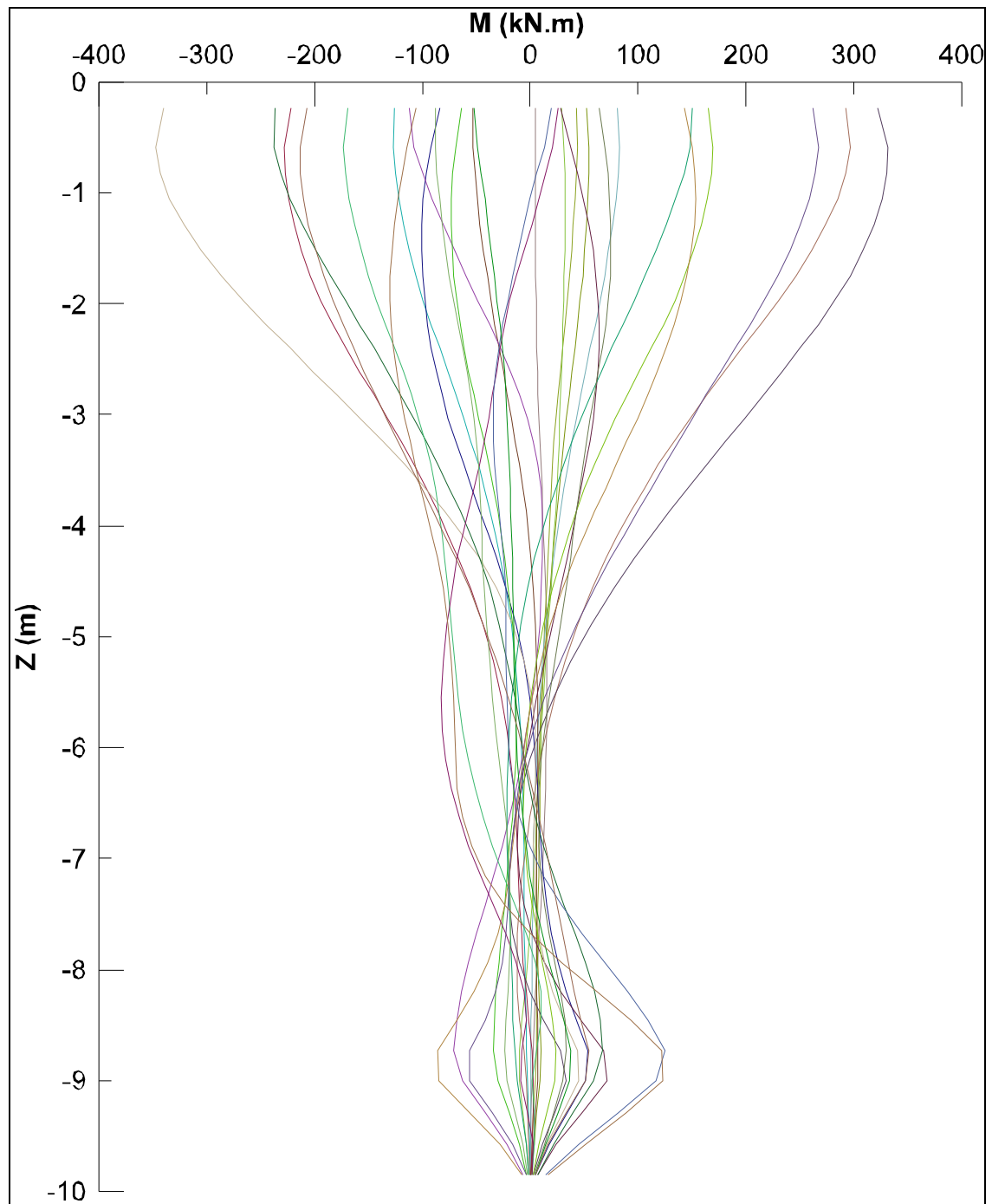


Figure-A I-31 Envelope bending moment with depth of QCR1M3 at pile head

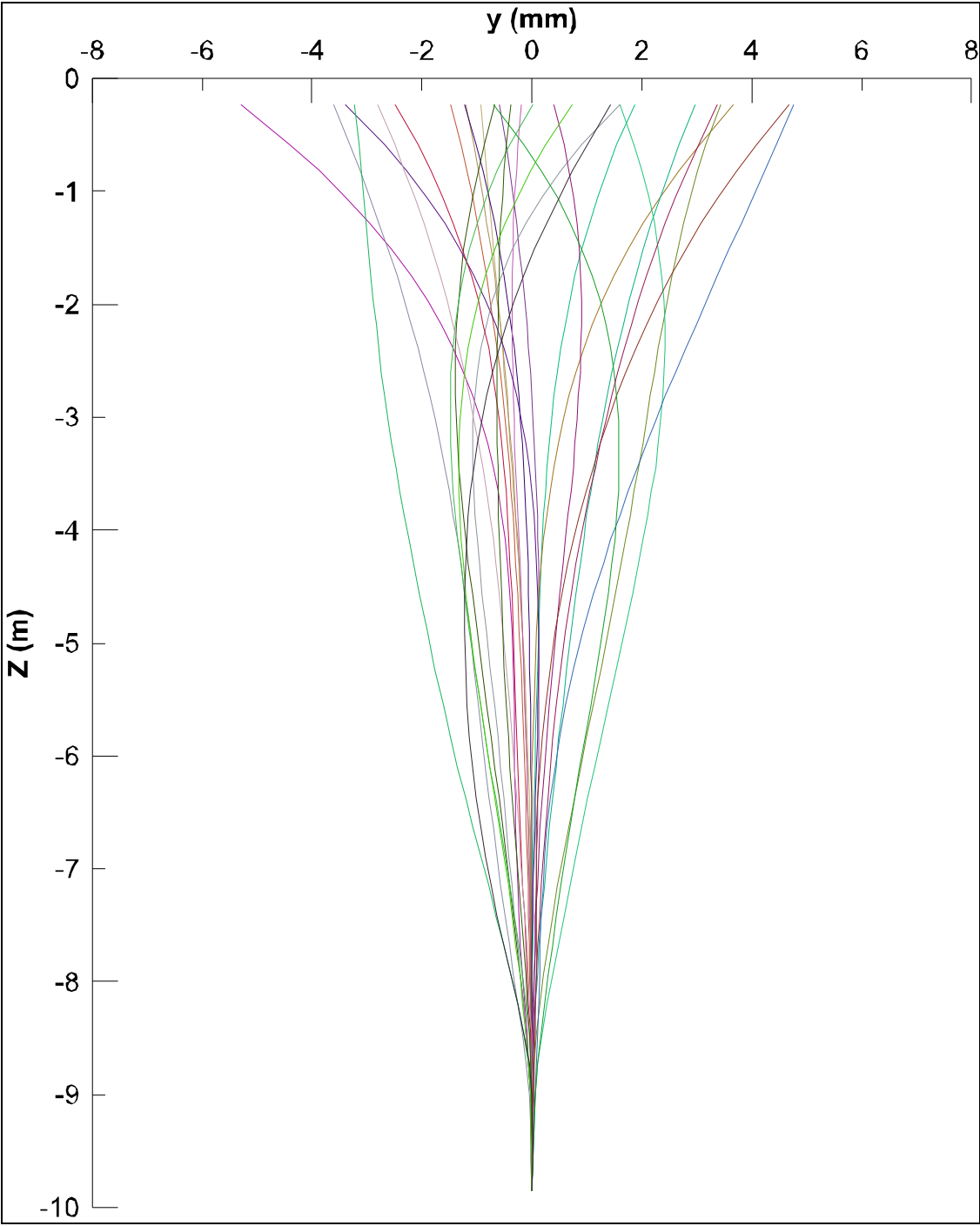


Figure-A I-32 Envelope of displacements with depth of QCR1M3 at pile head

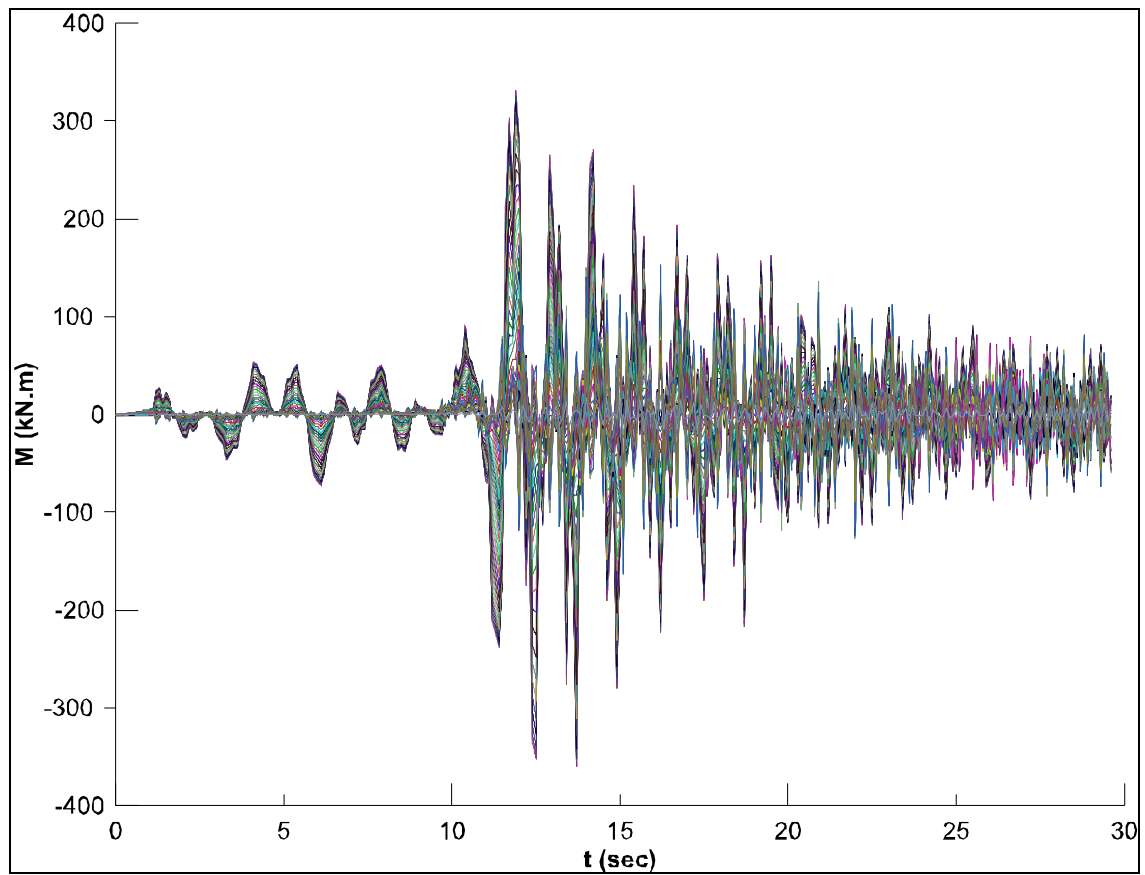


Figure-A I-33 Envelope bending moment with time of QCR1M3 at pile head

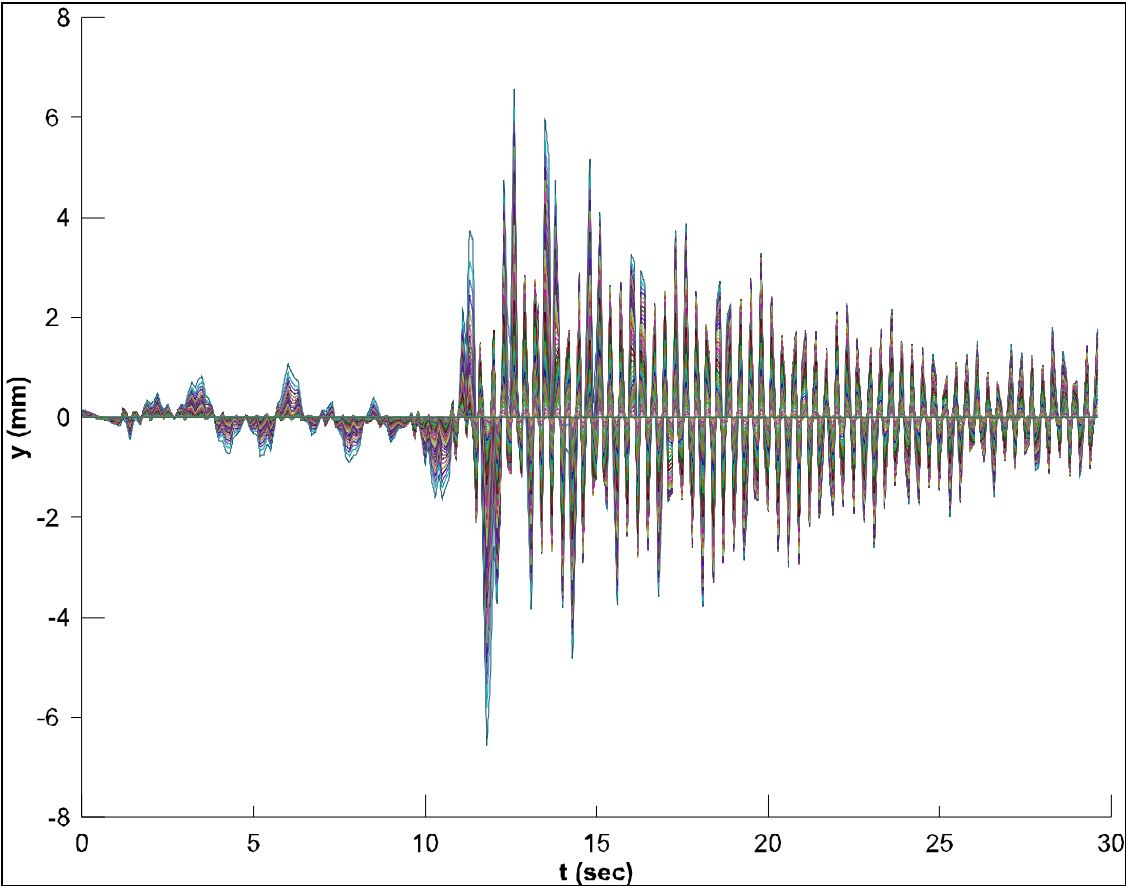


Figure-A I-34 Envelope of displacements with time of QCR1M3 at pile head

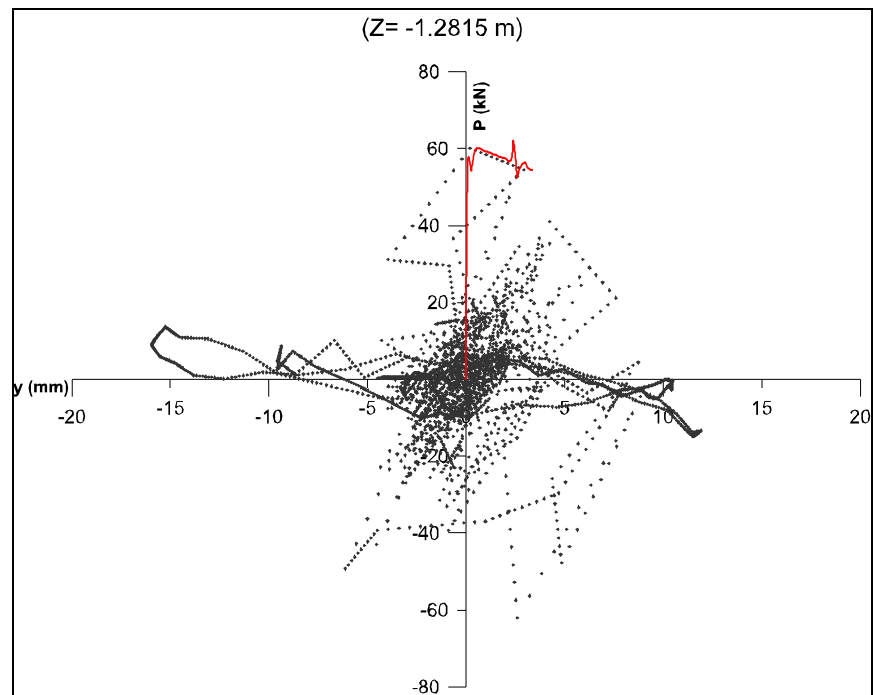


Figure-A I-35 p - y loop of QCR1M4 at $Z = -1.2815$ m and extracted p - y curve (in red)

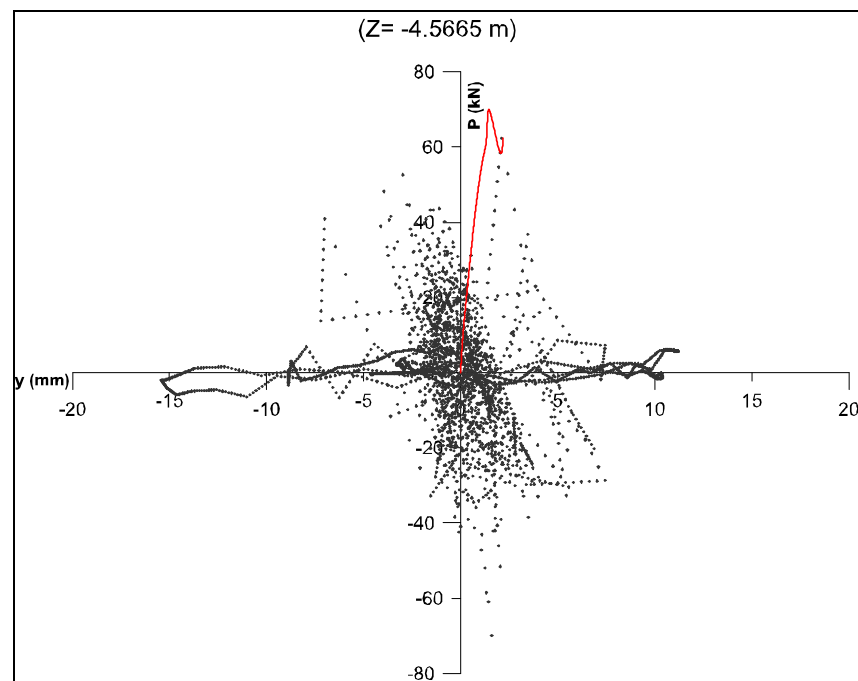


Figure-A I-36 p - y loop of QCR1M4 at $Z=-4.5665$ m and extracted p - y curve (in red)

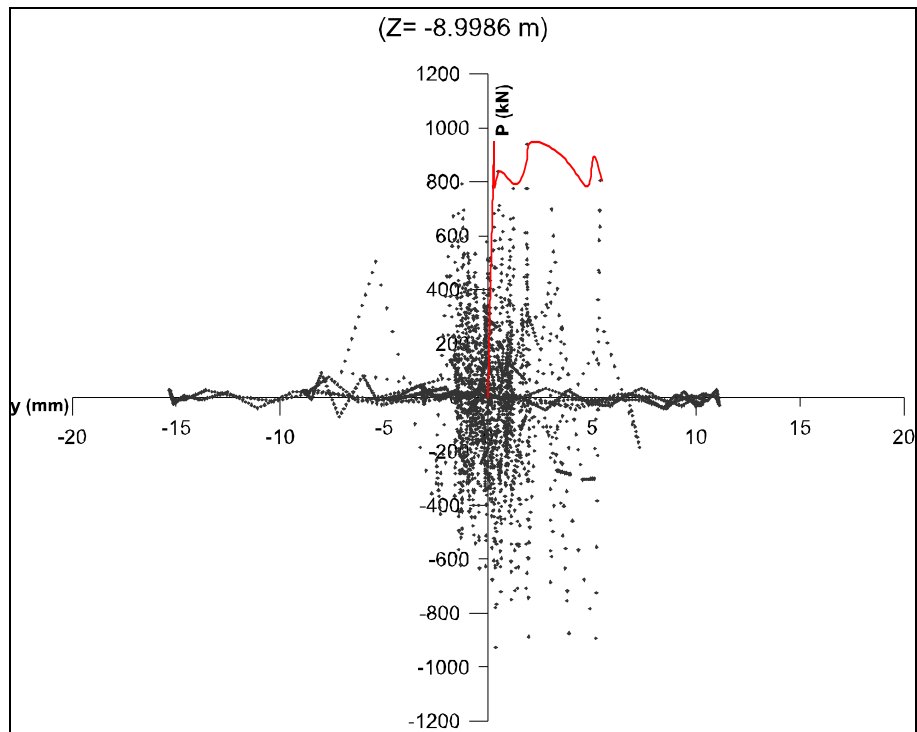


Figure-A I-37 p - y loop of QCR1M4 at $Z=-8.9986$ m and extracted p - y curve (in red)

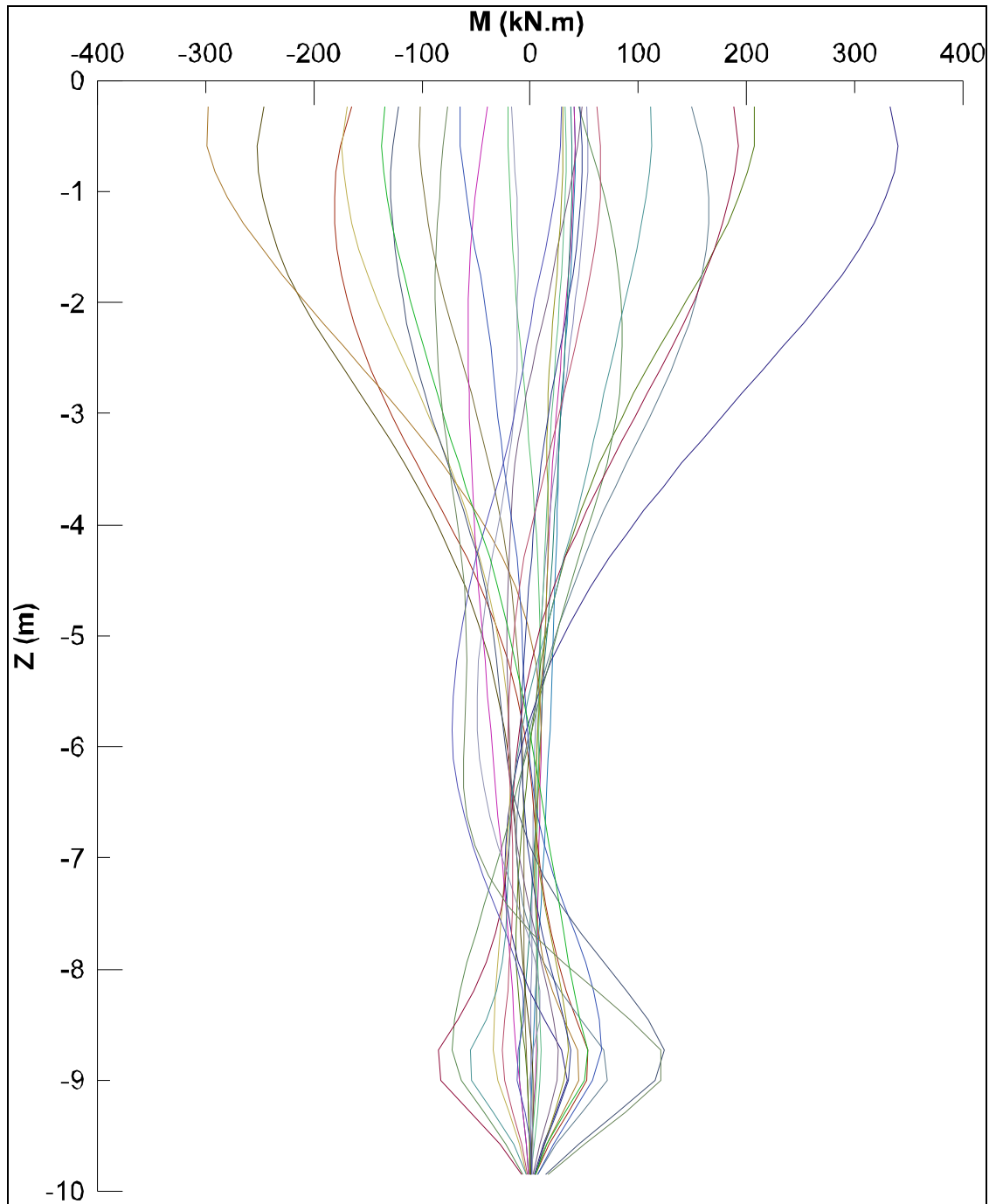


Figure-A I-38 Envelope bending moment with depth of QCR1M4 at pile head

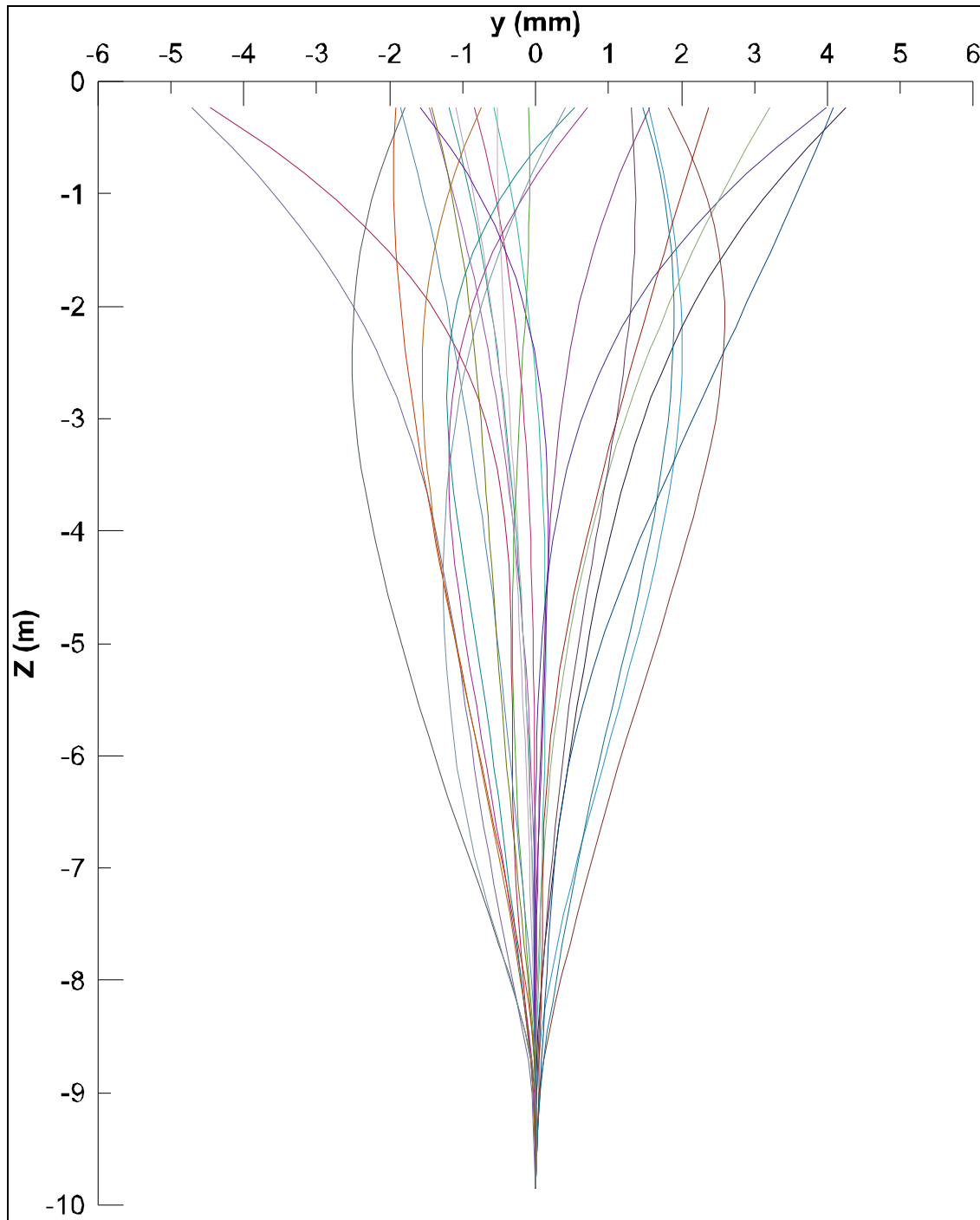


Figure-A I-39 Envelope of displacements with depth of QCR1M4 at pile head

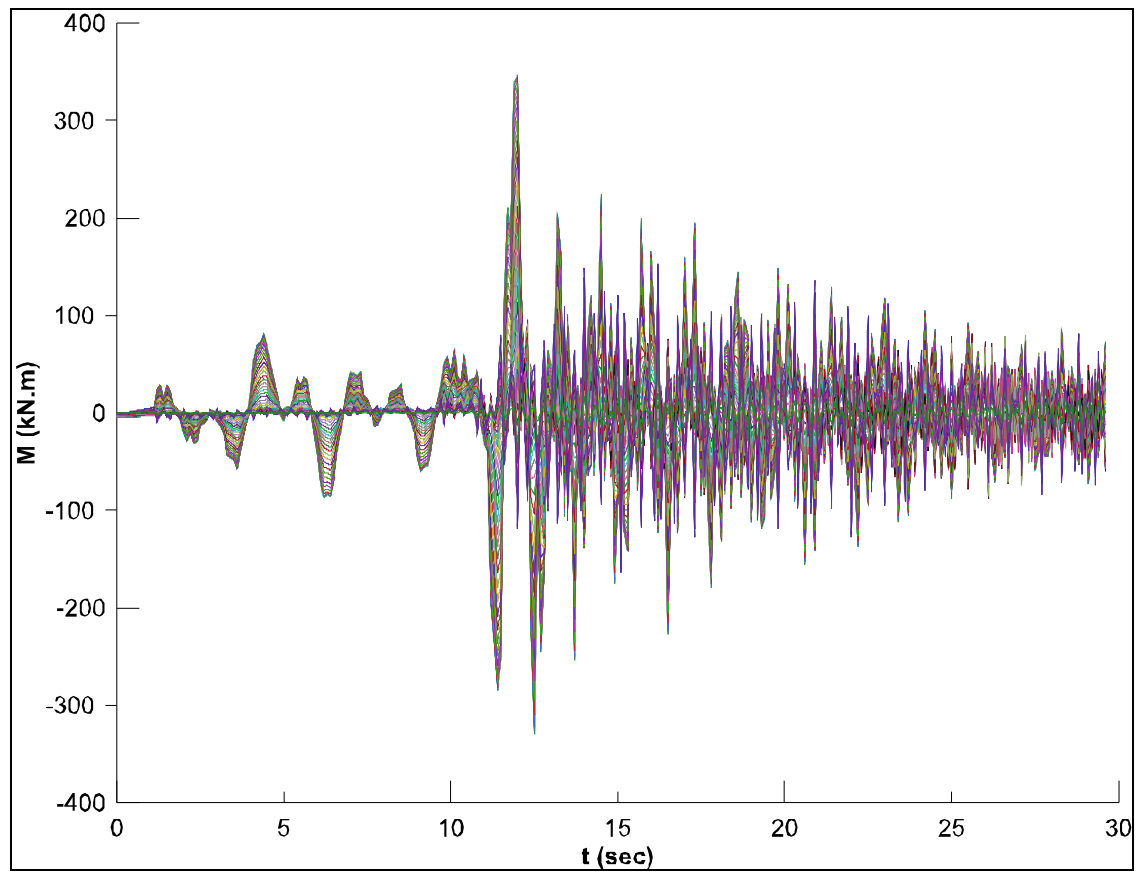


Figure-A I-40 Envelope bending moment with time of QCR1M4 at pile head

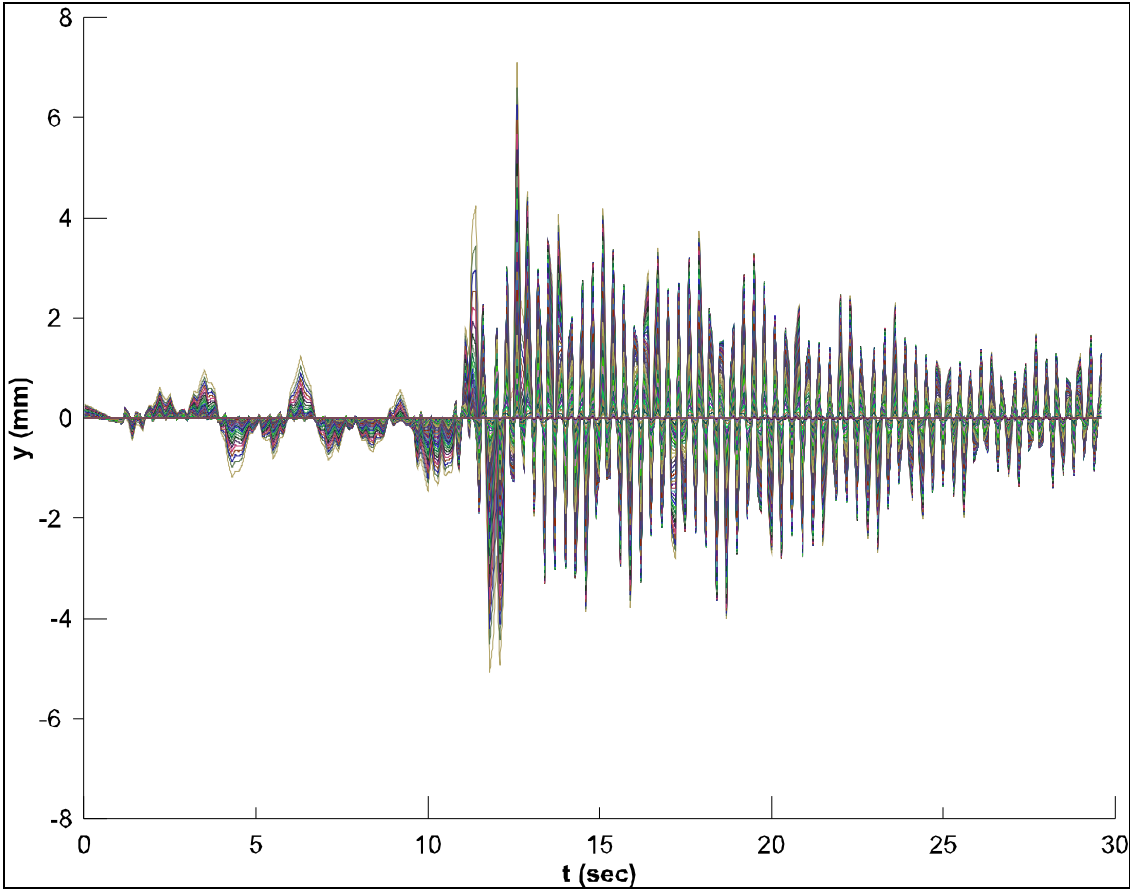


Figure-A I-41 Envelope of displacements with time of QCR1M4 at pile head

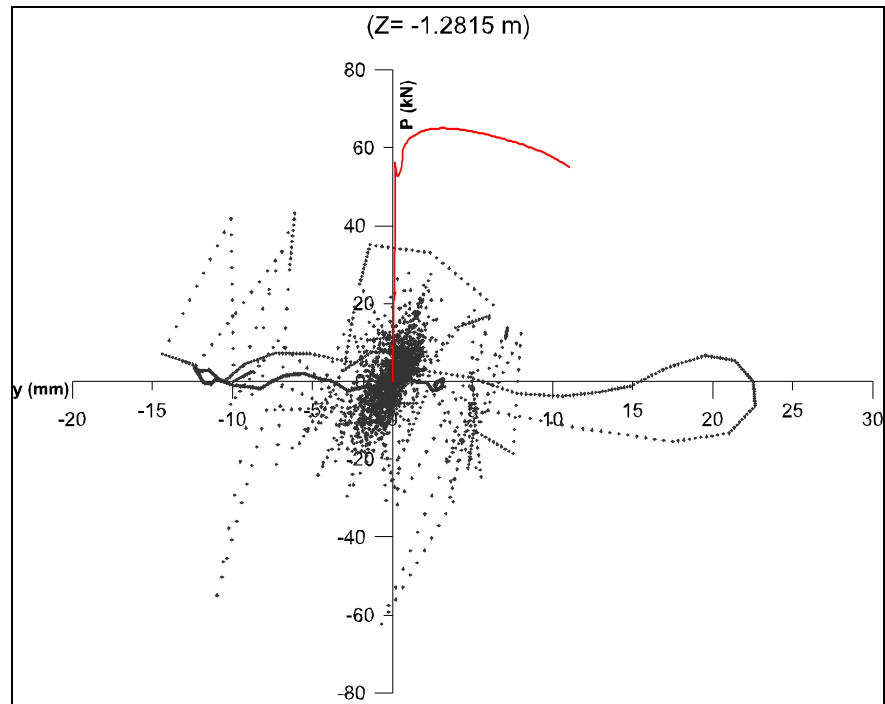


Figure-A I-42 p - y loop of QCR2M2 at $Z=-1.2815$ m and extracted p - y curve (in red)

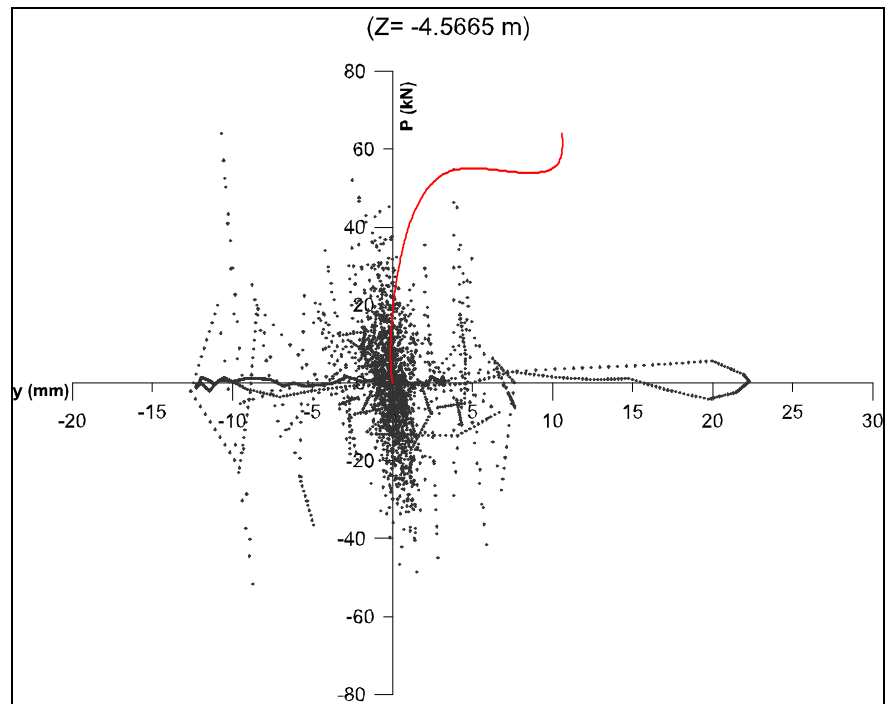


Figure-A I-43 p - y loop of QCR2M2 at $Z=-4.5665$ m and extracted p - y curve (in red)

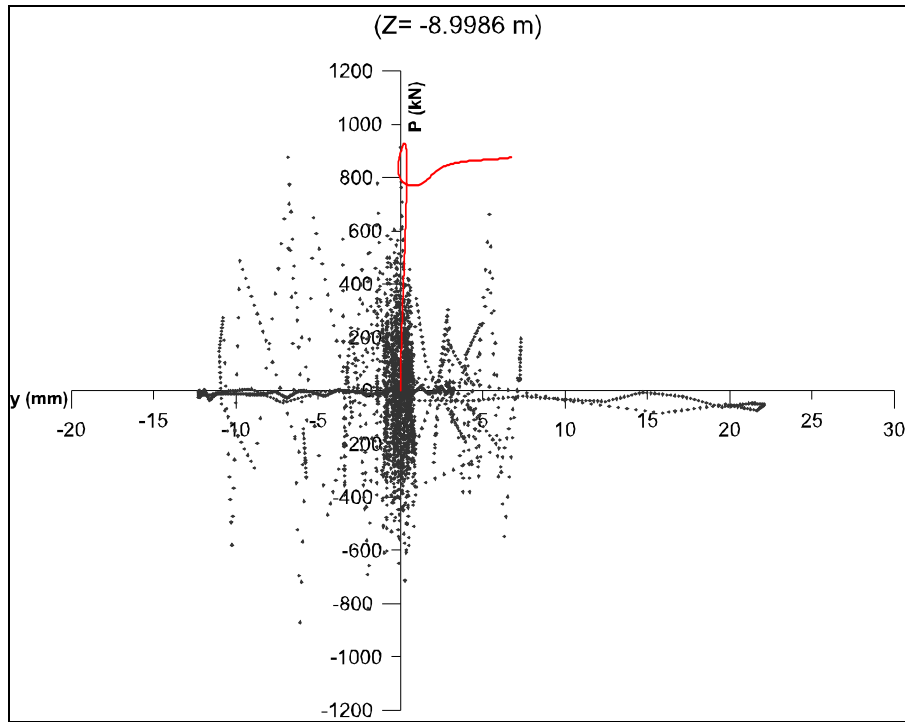


Figure-A I-44 p - y loop of QCR2M2 at $Z=-8.9986$ m and extracted p - y curve (in red)

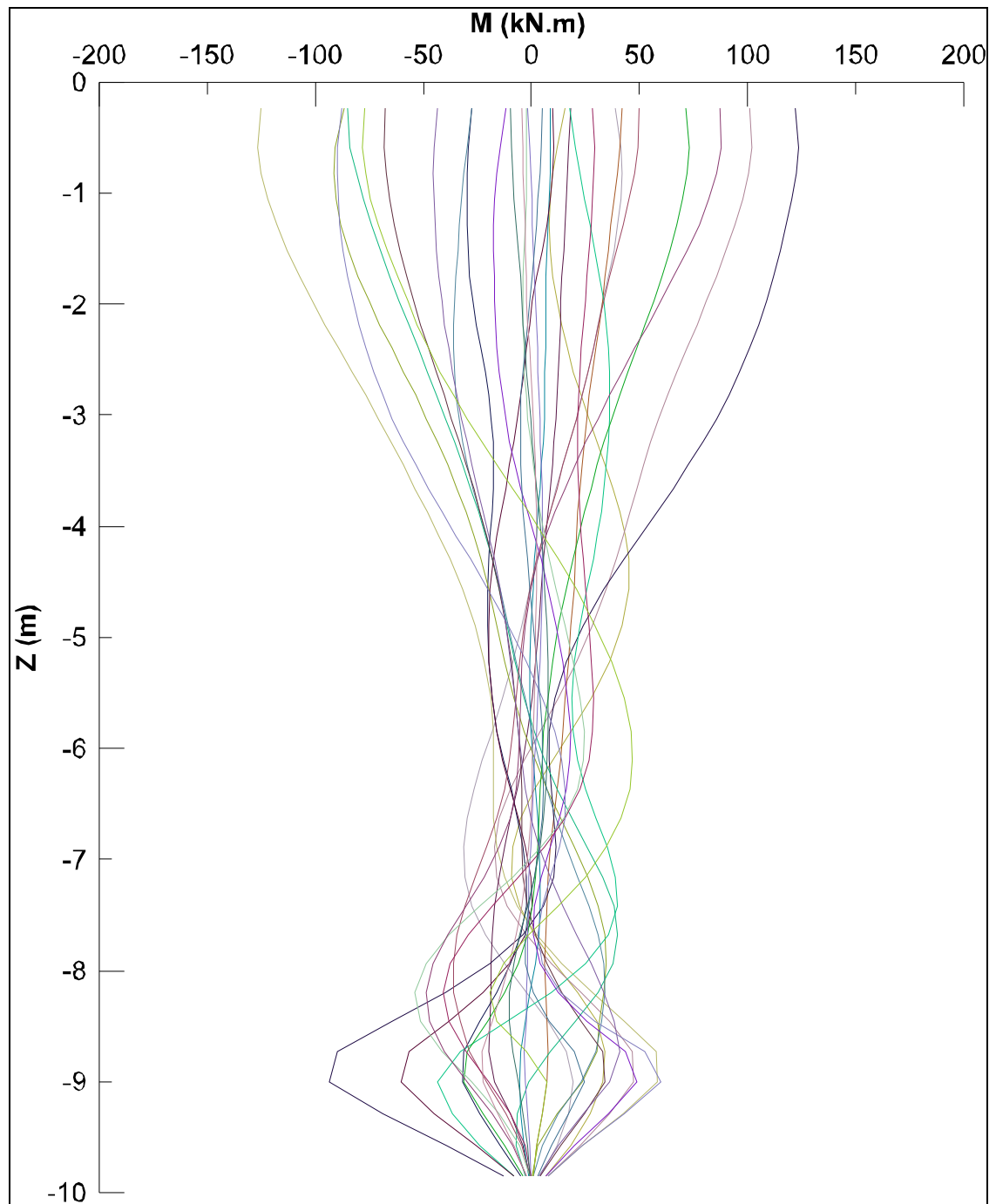


Figure-A I-45 Envelope bending moment with depth of QCR2M2 at pile head

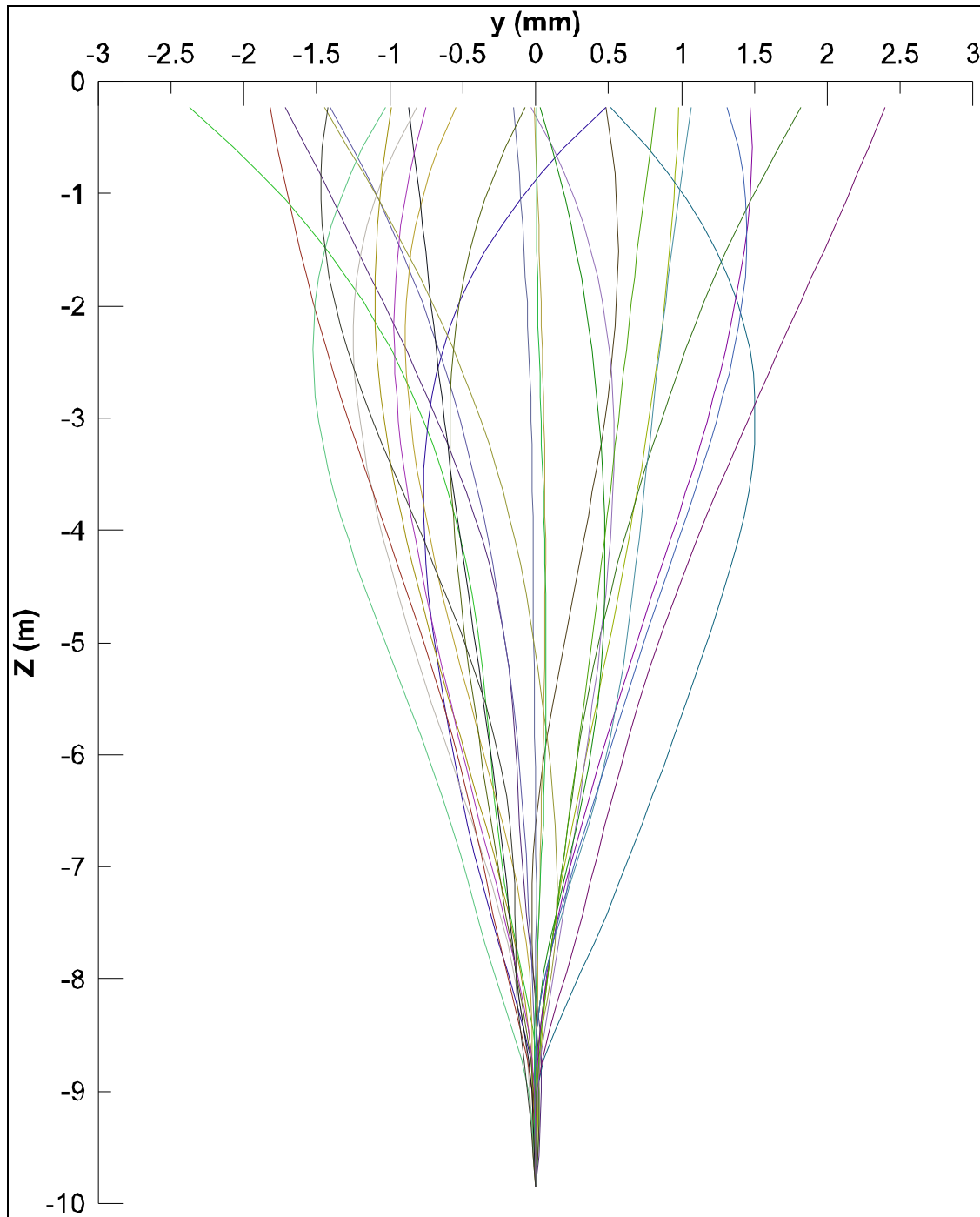


Figure-A I-46 Envelope of displacements with depth of QCR2M2 at pile head

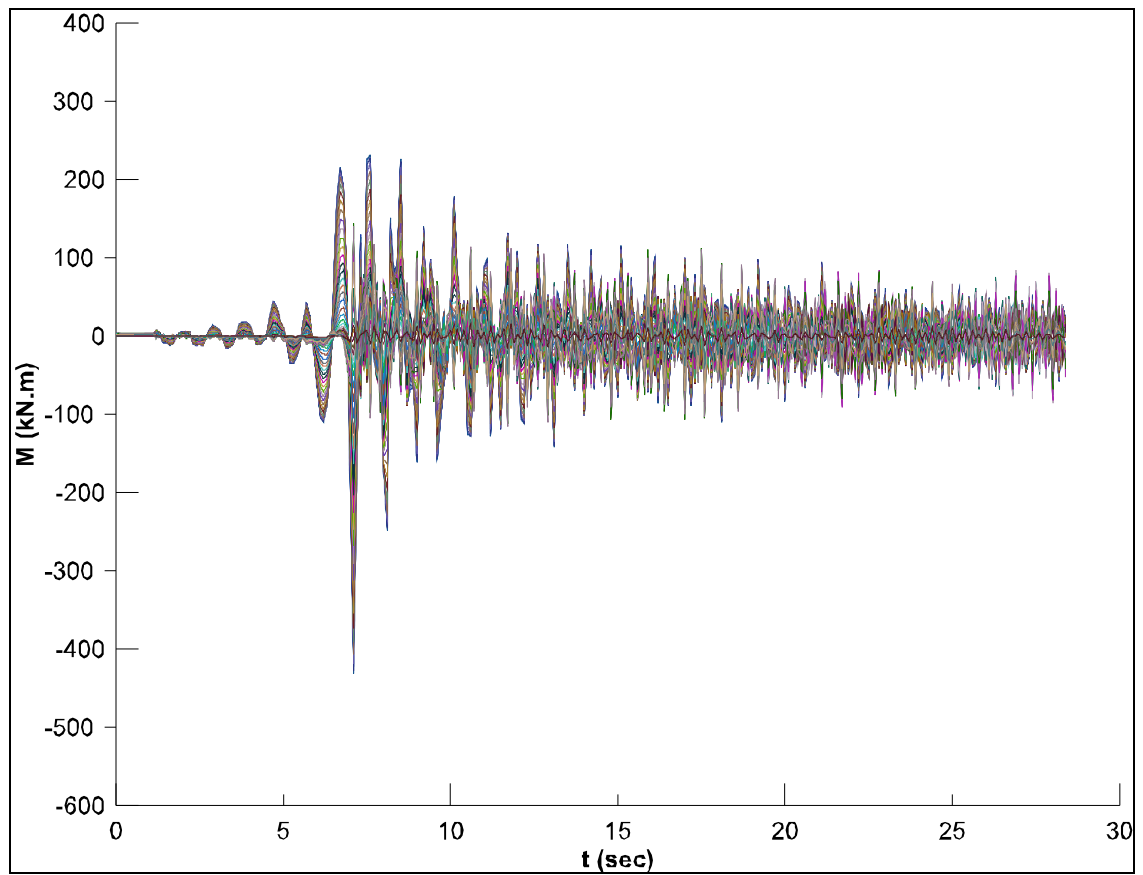


Figure-A I-47 Envelope bending moment with time of QCR2M2 at pile head

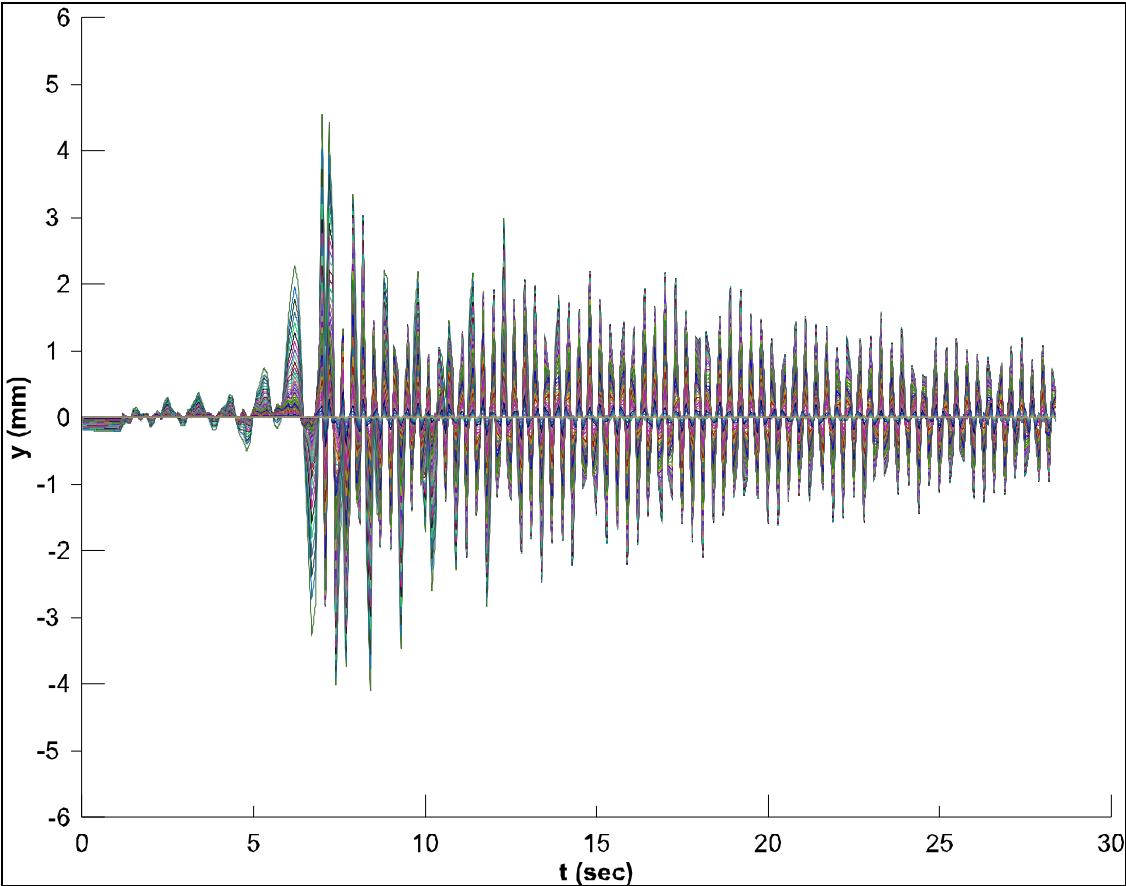


Figure-A I-48 Envelope of displacements with time of QCR2M2 at pile head

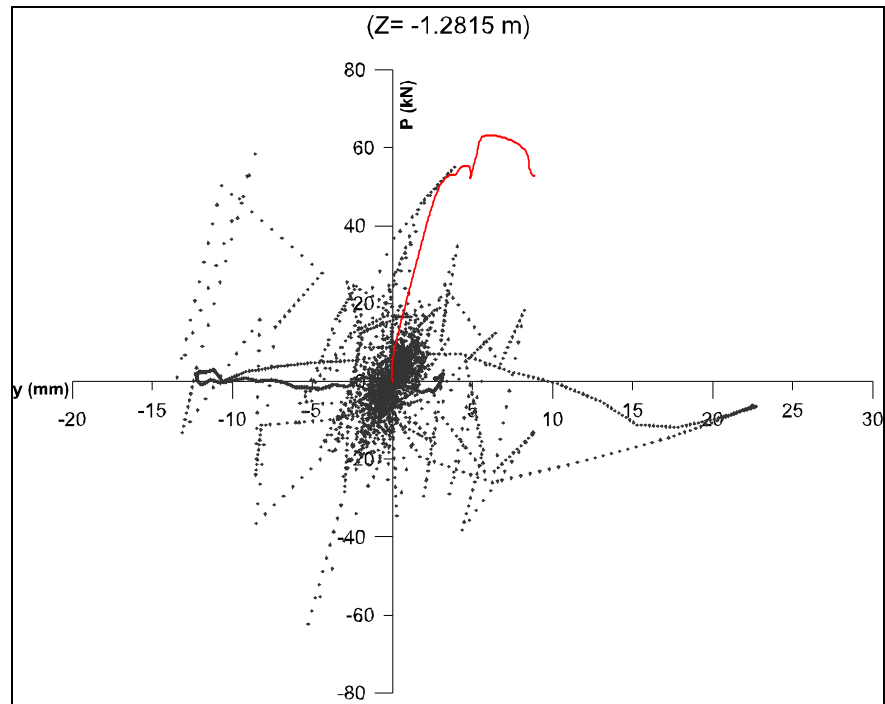


Figure-A I-49 p - y loop of QCR2M3 at $Z=-1.2815$ m and extracted p - y curve (in red)

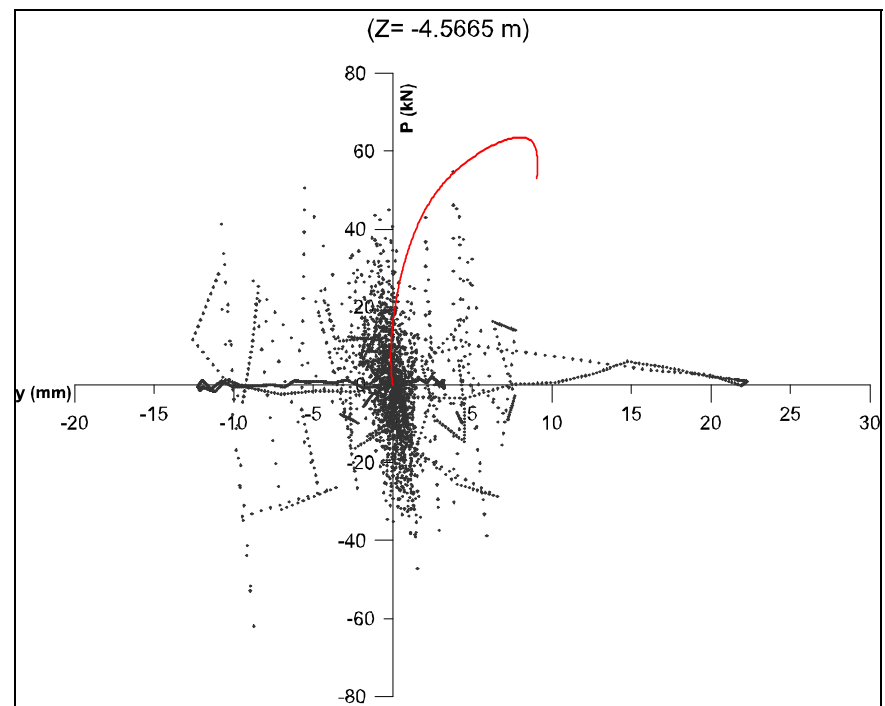


Figure-A I-50 p - y loop of QCR2M3 at $Z=-4.5665$ m and extracted p - y curve (in red)

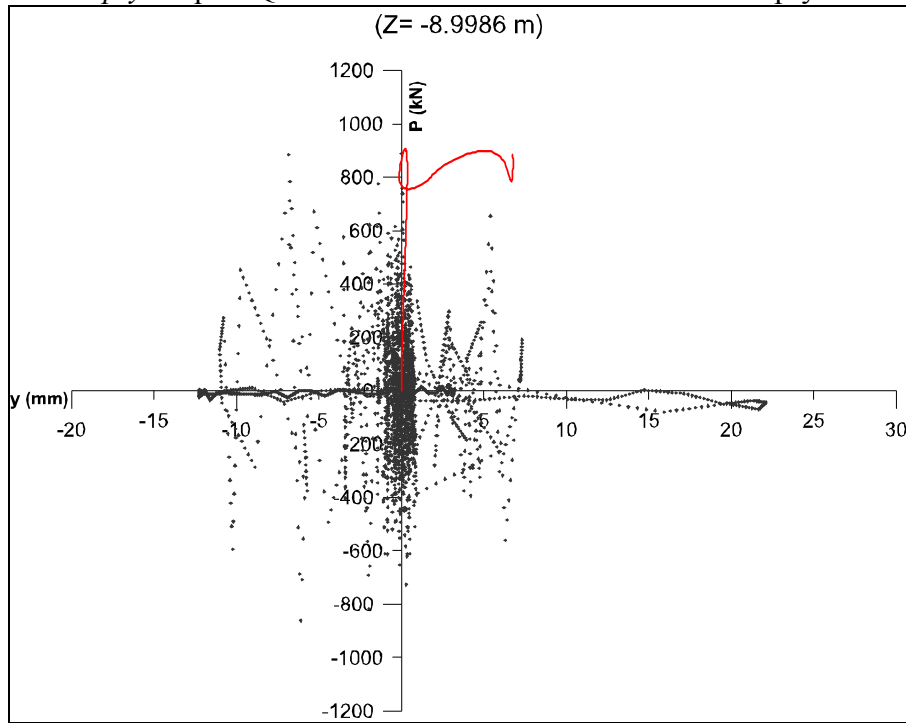


Figure-A I-51 p - y loop of QCR2M3 at $Z=-8.9986$ m and extracted p - y curve (in red)

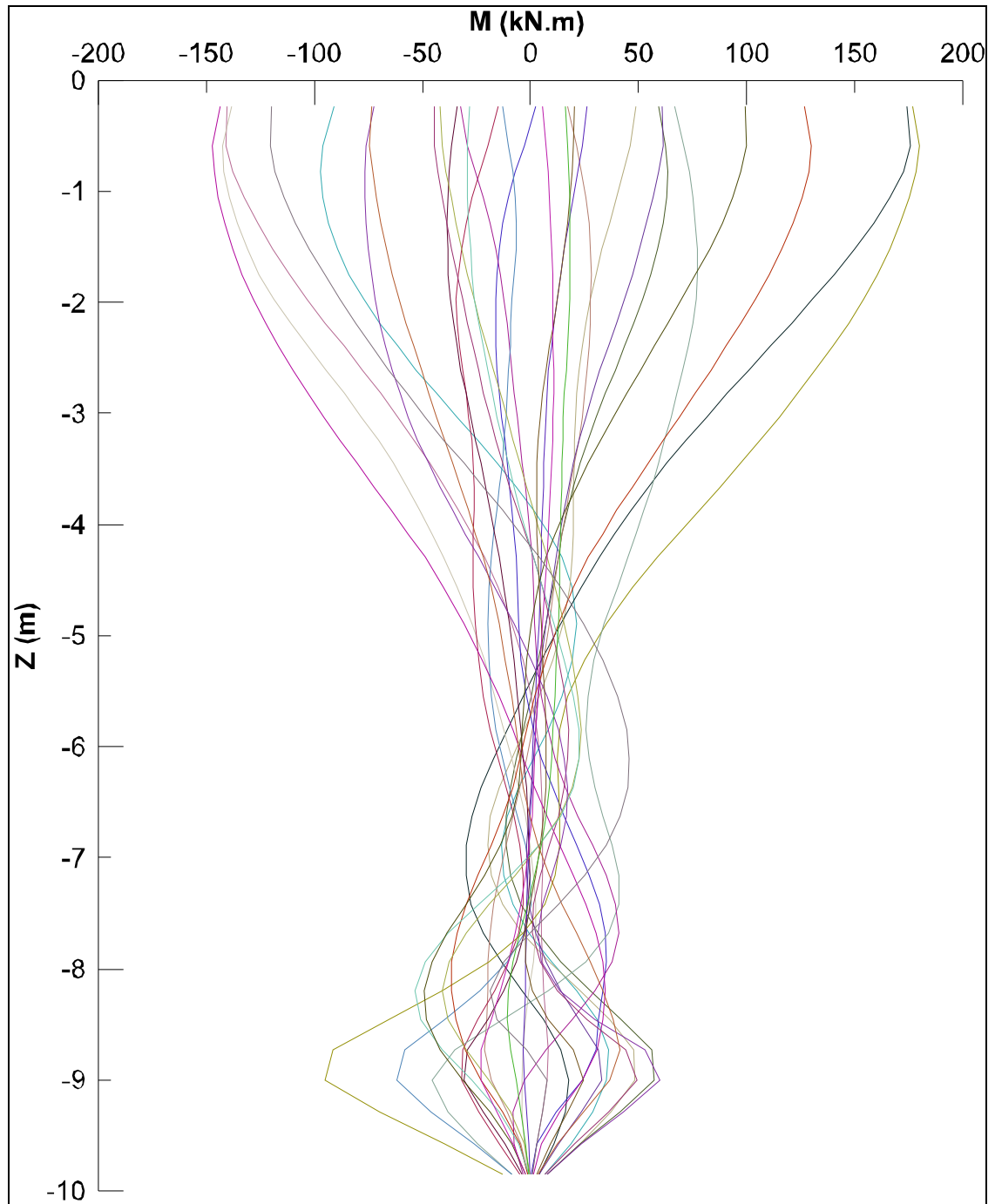


Figure-A I-52 Envelope bending moment with depth of QCR2M3 at pile head

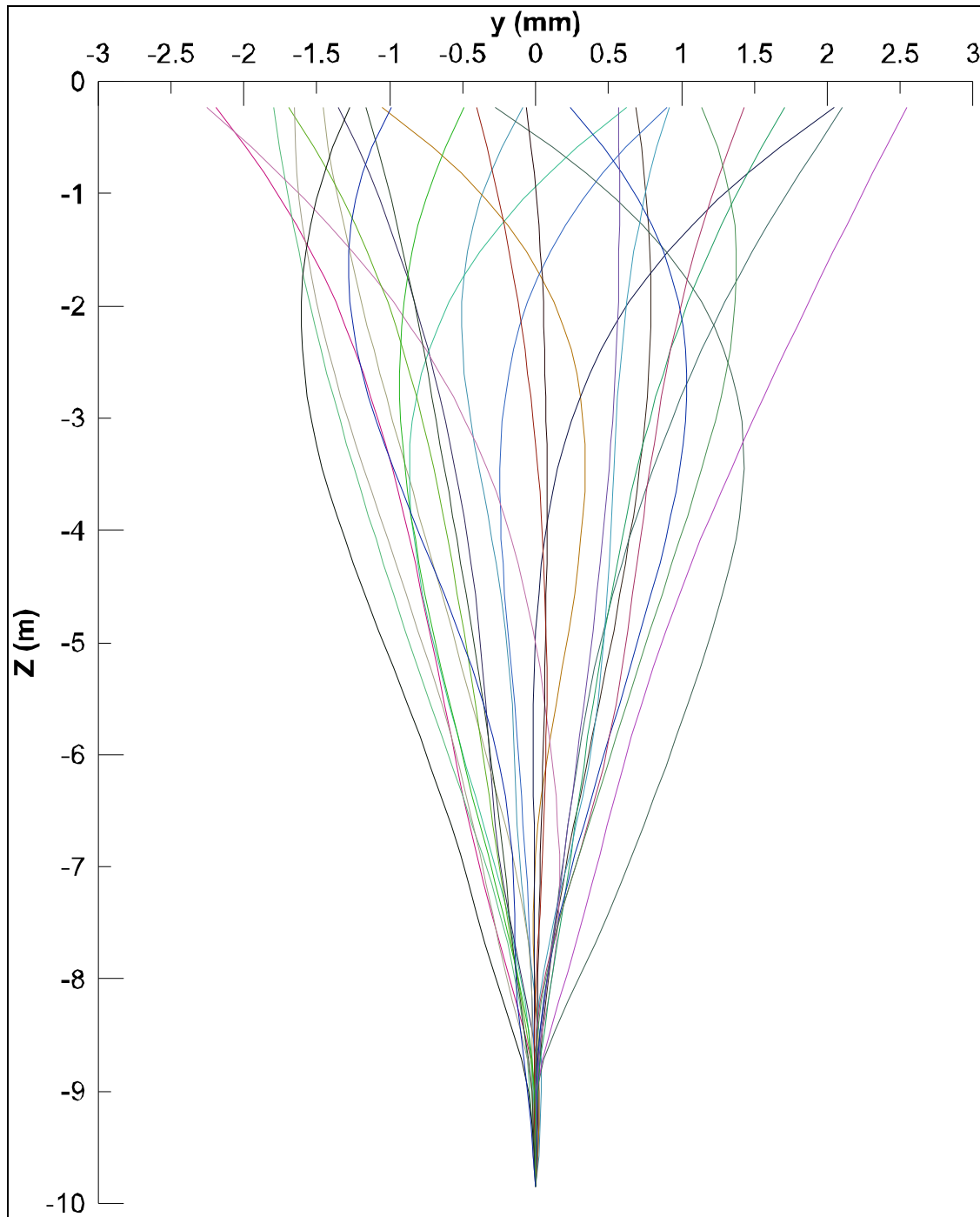


Figure-A I-53 Envelope of displacements with depth of QCR2M3 at pile head

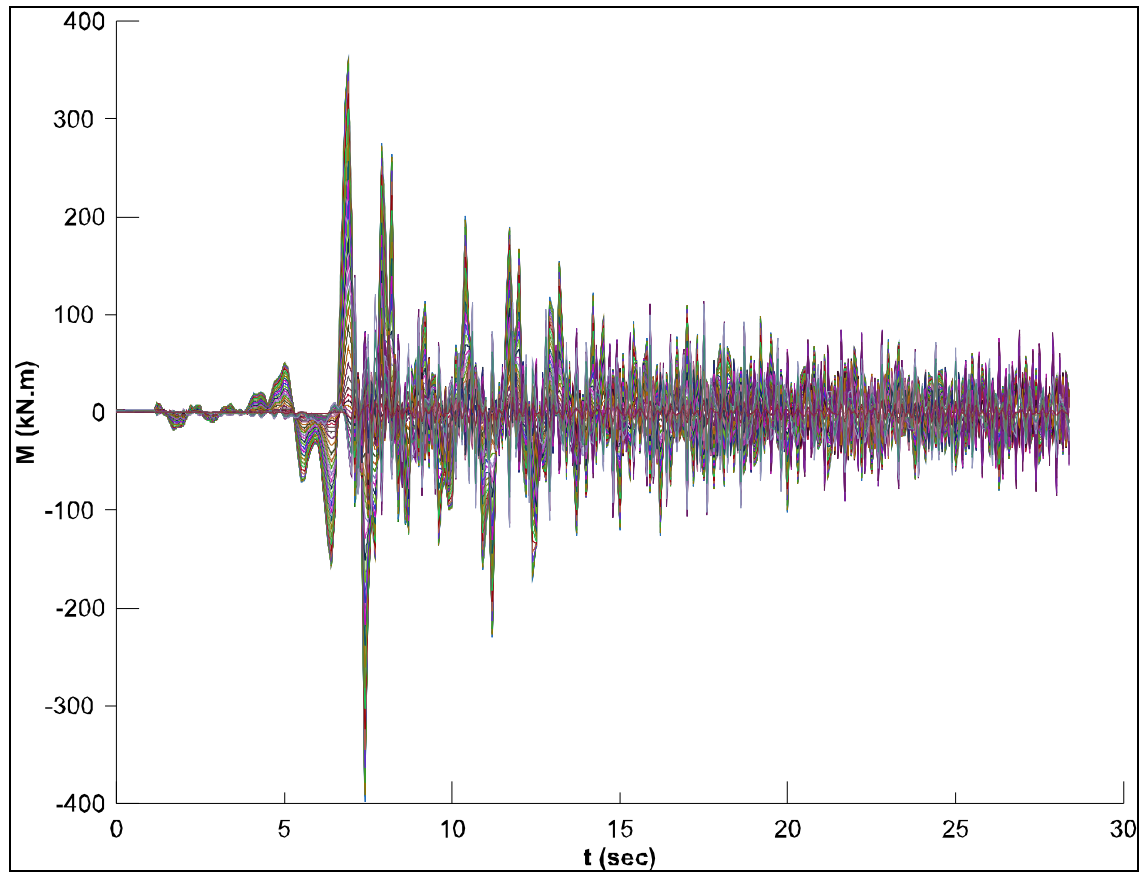


Figure-A I-54 Envelope bending moment with time of QCR2M3 at pile head

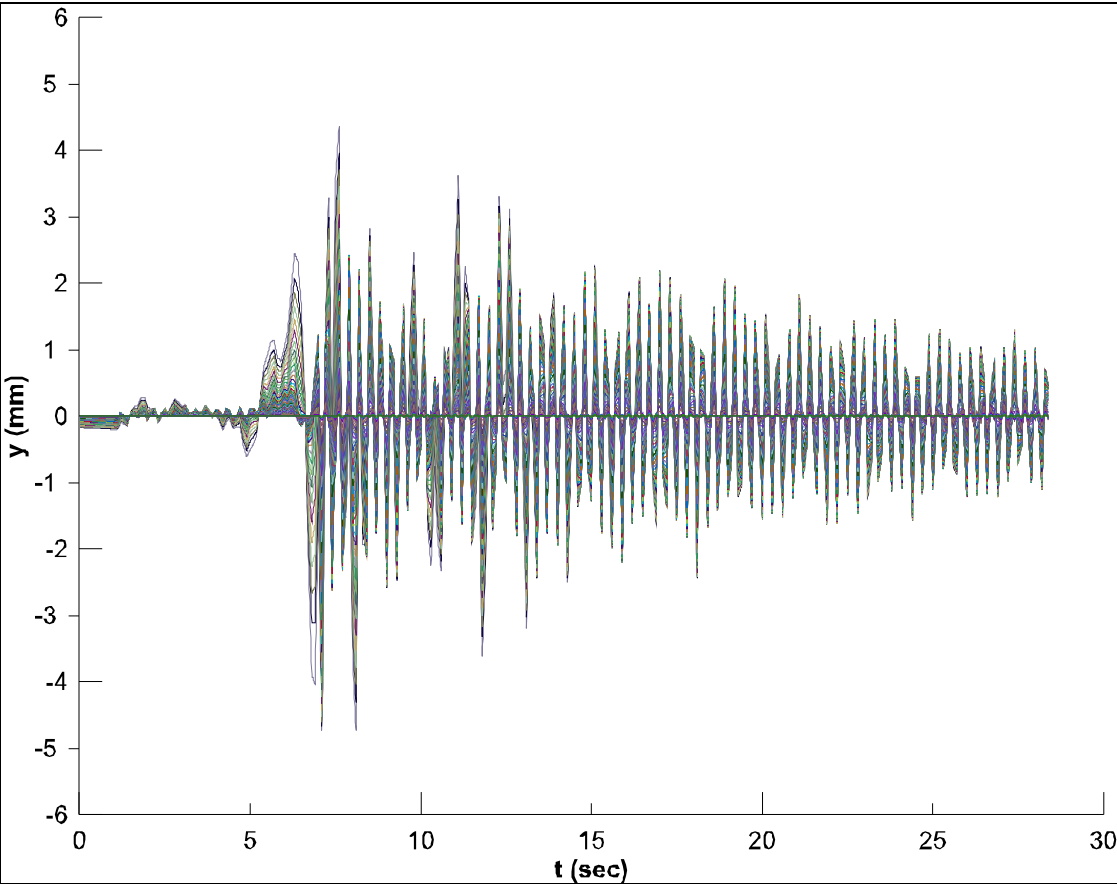


Figure-A I-55 Envelope of displacements with time of QCR2M3 at pile head

BIBLIOGRAPHY

- Adams, J. ; , et S. Halchuk. 2003. *Fourth generation seismic hazard maps of Canada: Values for over 650 Canadian localities intended for the 2005 Building Code of Canada*. Coll. « Geol. Surv. Can. », Open File, 4459, 155 pp p.
- Adams, J.; , P.; Basham et S. Halchuk. 1995. *Northeastern North America earthquake potential—New challenges for seismic hazard mapping*. Coll. « Geol. Surv. Canada ».
- Anderson, J. B.; Townsend, F. C.; Grajales, B. 2003. « Case history evaluation of laterally loaded piles ». *Journal of Geotechnical and Geoenvironmental Engineering*, vol. 129, n° 3, p. 187-196.
- Angelides, D. C.; Roesset, J. M. 1981. « NONLINEAR LATERAL DYNAMIC STIFFNESS OF PILES ». *Journal of Geotechnical and Geoenvironmental Engineering*, vol. 107, n° GT11, p. p. 1443-60.
- Ashford, S.; Juirnarongrit, T. 2003. « Evaluation of Pile Diameter Effect on Initial Modulus of Subgrade Reaction ». *Journal of Geotechnical and Geoenvironmental Engineering*, vol. 129, n° 3, p. 234-242.
- Ashour, M.; Ardalan, H. 2012. « Analysis of pile stabilized slopes based on soil-pile interaction ». *Computers and Geotechnics*, vol. 39, p. 85-97.
- Barton, Y. 1982. « Laterally loaded model piles in sand: Centrifuge tests and finite element analyses ». Ph.D. Dissertation. Cambridge Univ.
- Bea, R. 1988. *PAR User Guidelines: Loadings, Soils, and Pile Characteristics*. Coll. « Rpt. To Joint Industry Project ». Berkeley: Dept. of Civil Eng. And Dept. of Naval Architecture and Offshore Eng., Univ. of California,.
- Bea, R.; Audibert, J. 1979. « Performance of Dynamically Loaded Pile Foundations ». In *Proc. 2nd Intl. Conf. on Behaviour of Offshore Structures*. (London) Vol. 3, p. 728-745.
- Bhomik, S.; Long, J. 1991. « An Analytical Investigation of the Behavior of Laterally Loaded Piles ». In *Proc. Geotech. Eng. Congress*. Vol. 2, p. 1307-1318. ASCE Spec. Pub. 27.
- Bielak, J.; Loukakis, K.; Hisada, Y.; Youshimura, C. 2003. « Domain reduction method for threedimensional earthquake modeling in localized regions. part i: Theory. ». *Bulletin of the seismological Society of America*, n° 93, p. 817–824.

- Blaney, G. W.; Kausel, E.; Roesset, J. M. 1976. « DYNAMIC STIFFNESS OF PILES ». vol. 2, p. 1001-1012.
- Bogard, D.; Matlock, H. 1980. *Simplified Calculation of P-Y Curves for Laterally Loaded Piles in Sands*. Earth Technology Corp.
- Boulanger, Ross W.; Wilson, Dan W.; Kutter, Bruce L.; Brandenburg, Scott J.; Chang, Dongdong. 2004. « Nonlinear FE analyses of soil-pile interaction in liquefying sand ». In *Geotechnical Engineering for Transportation Projects: Proceedings of Geo-Trans 2004, July 27, 2004 - July 31, 2004*. (Los Angeles, CA, United states), 126 I, p. 403-410. Coll. « Geotechnical Special Publication »: American Society of Civil Engineers.
- Brandenburg, Scott J.; Boulanger, Ross W.; Kutter, Bruce L.; Chang, Dongdong. 2005. « Behavior of pile foundations in laterally spreading ground during centrifuge tests ». *Journal of Geotechnical and Geoenvironmental Engineering*, vol. 131, n° 11, p. 1378-1391.
- Briaud, Jean-Louis; Smith, Trevor; Meyer, Barry. 1984. « LATERALLY LOADED PILES AND THE PRESSUREMETER: COMPARISON OF EXISTING METHODS ». In *Laterally Loaded Deep Foundations: Analysis and Performance*. (Kansas City, MO, USA), p. 97-111. Coll. « ASTM Special Technical Publication »: ASTM.
- Broms, B. B. 1964a. « Lateral resistance of piles in cohesionless soils ». *ASCE -- Proceedings -- Journal of the Soil Mechanics and Foundations Division*, vol. 90, n° SM3, Part 1, p. 123-156.
- Broms, B. B. 1964b. « Lateral resistance of piles in cohesive soils ». *ASCE -- Proceedings -- Journal of the Soil Mechanics and Foundations Division*, vol. 90, n° SM2, Part 1, p. 27-63.
- Brown, D. A.; Chine-Feng, Shie; Kumar, M. 1989. « P-Y curves for laterally loaded piles derived from three-dimensional finite element model ». *Numerical models in geomechanics. NUMOG III*, p. 683-690.
- Brown, Dan A.; Shie, Chine-Feng. 1991. « Some numerical experiments with a three dimensional finite element model of a laterally loaded pile ». *Computers and Geotechnics*, vol. 12, n° 2, p. 149-162.
- Budhu, M.; Davies, T. G. 1987. « Nonlinear analysis of laterally loaded piles in cohesionless soils ». *Canadian Geotechnical Journal*, vol. 24, n° 2, p. 289-296.
- Budhu, Muniram; Davies, Trevor G. 1988. « ANALYSIS OF LATERALLY LOADED PILES IN SOFT CLAYS ». *Journal of geotechnical engineering*, vol. 114, n° 1, p. 21-39.

- Cai, Y.; Gould, P.; Desai, C. 1995. « Numerical Implementation of a 3-D Nonlinear Seismic S-P-S-I Methodology ». In *Seismic Analysis and Design for Soil-Pile-Structure Interactions*. p. 96-110. Geotech. Spec. Pub. 70, ASCE.
- Carter, D. 1984. *A Nonlinear Soil Model for Predicting Lateral Pile Response*. Dept. of Civil Eng., Univ. of Auckland.
- David, M. Potts; Potts, David M. 2001. *Finite element analysis in geotechnical engineering : application*. London, Angleterre: London, Angleterre : T. Telford.
- Davies, T. G.; Budhu, M. 1986. « NON-LINEAR ANALYSIS OF LATERALLY LOADED PILES IN HEAVILY OVERCONSOLIDATED CLAYS ». *Geotechnique*, vol. 36, n° 4, p. 527-538.
- Davisson, M.; Gill, H. 1963. « Laterally Loaded Piles in a Layered System ». *J. Soil Mechanics and Foundation Div.*, vol. 89, n° 3, p. 63-64.
- Desai, C. S.; Appel Jr, G. C. 1976. « 3-D ANALYSIS OF LATERALLY LOADED STRUCTURES ». vol. 1, p. 405-418.
- Dobry, R.; Liu, Li. 1999. *Effect of Liquefaction on Lateral Response of Piles by Centrifuge Model Tests*. FHWA-RD-99-165. Washington, D.C.: Workshop on New Approaches to Liquefaction Analysis.
- Dobry, Ricardo; O'Rourke, Michael J.; Roesset, Jose M.; Vicente, Ernesto. 1982. « HORIZONTAL STIFFNESS AND DAMPING OF SINGLE PILES ». *Journal of the Geotechnical Engineering Division*, vol. 108, n° GT3, p. 439-459.
- Dodds, A. M.; Martin, G. R. . 2007a. *Modeling Pile Behavior in Large Pile Groups Under Lateral Loading*. MCEER-07-0004: MCEER, 292 p.
- Dodds, Andrew Mason; Martin, Geoffrey R. 2007b. *Modeling pile behavior in large pile groups under lateral loading*. Coll. « Technical report ». Buffalo, NY: Multidisciplinary Center for Earthquake Engineering Research, University of Southern California., Earth Mechanics Inc., 274 p. p. < <http://worldcat.org/oclc/216723292/viewonline> >.
- Dyson, G. J.; Randolph, M. F. 2001. « Monotonic lateral loading of piles in calcareous sand ». *Journal of Geotechnical and Geoenvironmental Engineering*, vol. 127, n° 4, p. 346-352.
- Emery, J.; Nair, G. 1977. « Dynamic Response of a Single Pile ». In *Proc. 10th Specialty Session, 9th Intl. Conf. Soil Mechanics Fdn. Eng.* (Tokyo), p. 151-158.

- Engineers, McClelland. 1983. *NONSPS: Nonlinear Response Analysis of Soil-Pile-Structure Systems*. Engineering Dept., Computer Programs,, User's Guide 2-26 p.
- Fan, Ke; Gazetas, George; Kaynia, Amir; Kausel, Eduardo; , et Shahid Ahmad. 1991. « Kinematic Seismic Response of Single Piles and Pile Groups ». *Journal of Geotechnical Engineering*, vol. 117, n° 12, p. 1860-1879.
- Finn, Liam. 2010. *Overview of Soil-Structure interaction*. Seminar. Vancouver, British colombia: University of British Colombia.
- FLAC3D-Manual. 2012. *Itasca Consulting Group* (Version 7.0). Minneapolis
- Föppl, A. 1922. *Vorlesungen über Technische Mechanik*, 9th Ed. Leipzig, 258 p.
- Fujii, Shunji; Cubrinovski, Misko; Tokimatsu, Kohji; Hayashi, Tadashi. 1998. « Analyses of damaged and undamaged pile foundations in liquefied soils during the 1995 Kobe Earthquake ». In *Proceedings of the 1998 Conference on Geotechnical Earthquake Engineering and Soil Dynamics III. Part 2 (of 2), August 3, 1998 - August 6, 1998*. (Seattle, WA, USA) Vol. 2, p. 1187-1198. Coll. « Geotechnical Special Publication »: ASCE.
- Gabr, M. A.; Lunne, T.; Powell, J. J. 1994. « P-y analysis of laterally loaded piles in clay using DMT ». *Journal of geotechnical engineering*, vol. 120, n° 5, p. 816-837.
- Gazetas, G. 1991. « Foundation Vibrations ». In *Foundation Engineering Handbook*, 2nd Edition. p. 553-593.
- Gazetas, George; Dobry, Ricardo. 1984. « Horizontal response of piles in layered soils ». *Journal of Geotechnical Engineering*, vol. 110, n° 1, p. 20-40.
- Guoxi, Wu; Finn, W. D. L. 1997a. « Dynamic elastic analysis of pile foundations using finite element method in the frequency domain ». *Canadian geotechnical journal*, vol. 34, n° 1, p. 34-43.
- Guoxi, Wu; Finn, W. D. L. 1997b. « Dynamic nonlinear analysis of pile foundations using finite element method in the time domain ». *Canadian geotechnical journal*, vol. 34, n° 1, p. 44-52.
- Hansbro, S. 1995. « Ultimate Resistance of Laterally Loaded Piles ». In *Proc. Bengt Broms Symposium in Geotech. Eng.* (Singapore), p. 165-170.
- Hetényi, M. 1946. *Beams on elastic foundation; theory with applications in the fields of civil and mechanical engineering*. Ann Arbor: The University of Michigan Press.

- Incorporated, Ensoft. 2007. *LPILE Plus: A Program for the Analysis & Design of Piles and Drilled Shafts Under Lateral Loads*. (Version 5.0.39).
- Jamilokowski, M.; Garassino, A. 1977. « Soil Modulus for Laterally Loaded Piles ». In *Proc. 10th Specialty Session, 9th Intl. Conf. Soil Mechanics Fdn. Eng.* (Tokyo), p. 43-58.
- Juirnarongrit, Teerawut; Ashford, Scott A. 2001. *Effect of pile diameter on p-y curves*. Radisson Hotel, Sacramento, California: California Dept. of Transportation.
- Kagawa, Takaaki; Kraft Jr, Leland M. 1980. « Seismic responses of flexible piles ». *Journal of the Geotechnical Engineering Division*, vol. 106, n° 8, p. 899-918.
- Kagawa, Takaaki; Kraft Jr, Leland M. 1981. « Lateral pile response during earthquakes ». *Journal of the Geotechnical Engineering Division*, vol. 107, n° 12, p. 1713-1731.
- Kausel, Eduardo; Roesset, Jose M.; Waas, Guenter. 1975. « DYNAMIC ANALYSIS OF FOOTINGS ON LAYERED MEDIA ». vol. 101, n° 5, p. 679-693.
- Kay, S.; Kolk, H. J.; van Hooydonk, W. R. 1983. « SITE SPECIFIC DESIGN OF LATERALLY LOADED PILES ». In *Proceedings of the Conference on Geotechnical Practice in Offshore Engineering*. (Austin, Tex, USA), p. 557-580. ASCE.
- Kooijman, A. P. 1989. « Comparison of an elastoplastic quasi three-dimensional model for laterally loaded piles with field tests ». *Numerical models in geomechanics. NUMOG III*, p. 675-682.
- Kuhlemeyer, Roger L. 1979a. « Static and dynamic laterally loaded floating piles ». *American Society of Civil Engineers, Journal of the Geotechnical Engineering Division*, vol. 105, n° 2, p. 289-304.
- Kuhlemeyer, Roger L. 1979b. « Vertical vibration of piles ». *American Society of Civil Engineers, Journal of the Geotechnical Engineering Division*, vol. 105, n° 2, p. 273-287.
- Kulhawy, F.; Chen, Y. 1995. « A Thirty Year Perspective of Broms' Lateral Loading Models, as Applied to Drilled Shafts ». In *Proc. Bengt Broms Symposium in Geotech. Eng.* (Singapore), p. 225-240.
- Lee, M.; Finn, W. 1978. *DESRA-2: Dynamic Effective Stress Response Analysis of Soil Deposits with Energy Transmitting Boundary Including Assessment of Liquefaction Potential*. Coll. « Soil Mechanics »: Dept. of Civil Eng. Univ. of Vancouver, B.C.

- Lewis, K.; Gonzalez, L. 1985. « Finite Element Analysis of Laterally Loaded Drilled Piers in Clay ». In *Proc. 12th Intl. Conf. Soil Mechanics Fdn. Eng.* (Rio de Janiero) Vol. 2, p. 1201-1204.
- Liu, L.; Dobry, R. 1995. *Effect of Liquefaction on Lateral Response of Piles by Centrifuge Model Tests*. SUNY-Buffalo, 7-11 p.
- Lok, M. 1999. « Numerical Modeling of Seismic Soil-Pile-Structure Interaction in Soft Clay ». Berkeley, Univ. of California.
- Makris, N.; Badoni, D. 1995. « Nonlinear seismic response of single piles ». In *Proceedings of the 7th International Conference on Soil Dynamics and Earthquake Engineering, May 1995*. (Crete, Greece), p. 475-475. Computational Mechanics Publ.
- Makris, Nicos. 1994. « Soil-pile interaction during the passage of Rayleigh waves: an analytical solution ». *Earthquake Engineering and Structural Dynamics*, vol. 23, n° 2, p. 153-167.
- Matlock, H. 1962. *Correlations for Design of Laterally Loaded Piles in Soft Clay*. Engineering Science Consultants.
- Matlock, H. 1970. « CORRELATIONS FOR DESIGN OF LATERALLY LOADED PILES IN SOFT CLAY ». vol. 1, p. 577-594.
- Matlock, H.; Bogard, D.; Lam, I. 1981. *BMCOL 76: A Computer Program for the Analysis of Beam-Columns Under Static Axial and Lateral Loading*. Earth Technology Corp.
- Matlock, H.; Foo, S. H. C. 1980. « AXIAL ANALYSIS OF PILES USING A HYSTERETIC AND DEGRADING SOIL MODEL ». *Electronique Industrielle (Paris)*, p. 127-133.
- Matlock, H.; Reese, L. C. 1960. « Generalized solutions for laterally loaded piles ». *ASCE -- Proceedings -- Journal of the Soil Mechanics and Foundations Division*, vol. 86, n° SM5, Part 1, p. 63-91.
- Matlock, Hudson; Foo, Stephen Hoo-Chuen. 1978. *Simulation of lateral pile behavior under earthquake motion*. Austin: Dept. of Civil Engineering, University of Texas.
- McCarthy, David F. (438). 1998. *Essentials of soil mechanics and foundations : basic geotechnics*, 5th. Upper Saddle River, N.J.: Prentice Hall, xiv, 730 p. p.
- McClelland, B.; Focht, J. A., Jr. 1958. « Soil modulus for laterally loaded piles. ». *Trans. A.S.C.E.*, vol. 123, p. 1049-1063.
- Menard, L. 1962. « Comportement d'une Foundation Profonde Soumise a des Efforts de Renversement ». *Sols Soils*, vol. 3, n° 4, p. 9-23.

- Meymand, Philip James. 1998. « Shaking table scale model tests of nonlinear soil-pile-superstructure interaction in soft clay ». 9922971. United States -- California, University of California, Berkeley, 462 p. p. In ProQuest Dissertations & Theses (PQDT). < <http://search.proquest.com/docview/304426318?accountid=10246> >.
- Mindlin, R. D. 1936. « Force at a point in the interior of a semi-infinite solid ». *Physics*, vol. 7, p. 195-202.
- Mylonakis, G.; Syngros, C.; Gazetas, G.; Tazoh, T. 2006. « The role of soil in the collapse of 18 piers of Hanshin Expressway in the Kobe earthquake ». *Earthquake Engineering & Structural Dynamics*, vol. 35, n° 5, p. 547-575.
- NAVFAC. 1982. *Foundations and earth retaining structures design manual DM 7.2*. Alexandria, VA, USA: Dept of Navy.
- Nogami, T.; Konagi, K.; Otani, J. 1988a. « Nonlinear Pile Foundation Model for Time Domain Dynamic Response Analysis ». In *Proc. 9th World Conf. Earthquake Eng.* (Tokyo) Vol. 3, p. 593-598.
- Nogami, T.; Novak, M. 1976. « Soil-pile interaction in vertical vibration ». *Earthquake Engineering and Structural Dynamics*, vol. 4, n° 3, p. 277-293.
- Nogami, T.; Otani, J.; Konagai, K.; Chen, H. 1992. « Nonlinear Soil-Pile Interaction Model for Dynamic Lateral Motion ». *J. Geotech. Eng.*, vol. 118(1), p. 89-106.
- Nogami, T.; Otani, J.; Konagi, K. 1991. « Nonlinear Time Domain Numerical -Model for Pile Group Under Transient Dynamic Forces ». In *Proc. 2nd Intl. Conf. on Recent Advances in Geotech. Eng. and Soil Dyn.* (St. Louis) Vol. 3, p. 881-888.
- Nogami, Toyoaki. 1985. « Nonlinear dynamic winkler model for lateral cyclic response analysis of single piles ». In *Soil Dynamics and Earthquake Engineering, Proceedings of the 2nd International Conference*. (Aboard the Queen Elizabeth 2, New York to Southampton), p. 4. 51-4. 60. Computational Mechanics Ltd.
- Nogami, Toyoaki; Konagai, Kazuo. 1988b. « TIME DOMAIN FLEXURAL RESPONSE OF DYNAMICALLY LOADED SINGLE PILES ». *Journal of Engineering Mechanics*, vol. 114, n° 9, p. 1512-1525.
- Novak, M. 1974. « Dynamic Stiffness and Damping of Piles ». *Can. Geotech. J.*, vol. 11(4), p. 574-598.
- Novak, M. 1977. « Soil-Pile Interaction ». In *Proc. 6th World Conf. Earthquake Eng.* (New Delhi) Vol. 4, p. 97-102.

- Novak, M.; Sheta, M. 1980. « Approximate Approach to Contact Effects of Piles ». *ASCE - Dynamic response of pile foundations, analytical aspects*, p. 53-79.
- Novak, Milos; Aboul-Ella, Fakhry. 1978. « IMPEDANCE FUNCTIONS OF PILES IN LAYERED MEDIA ». vol. 104, n° 3, p. 643-661.
- O'Neill, M.; Gazioglu, S. 1984. *An Evaluation of P-Y Relationships in Clays*. Dept. of Civil Eng., Univ. of Houston.
- O'Neill, M.; Murchison, J. 1983. *An Evaluation of P-Y Relationships in Sands*. Dept. of Civil Eng., Univ. of Houston.
- Parker, F.; Reese, L. 1970. *Experimental and Analytical Study of Behavior of Single Piles in Sands Under Lateral and Axial Loading*. Rpt. 117-2. Austin: Univ. of Texas.
- Pender, M. J. 2004. « Discussion: Evaluation of Pile Diameter Effect on Initial Modulus of Subgrade Reaction ». *J. Geotech. Geoenviron. Eng., ASCE*, , vol. 9, n° 130, p. 981-982.
- Pender, M.; Pranjoto, S. 1996. « Gapping Effects During Cyclic Lateral Loading of Piles in Clay ». In *Proc. 11th World Conf. Earthquake Eng. (Acapulco)*.
- Penzien, J.; Scheffey, C. F.; Parmelee, R. A. 1964. « Seismic analysis of bridges on long piles ». *ASCE -- Proceedings, Journal of the Engineering Mechanics Division*, vol. 90, n° EM3, Part 1, p. 223-254.
- Poulos, H. 1971a. « Behaviour of Laterally Loaded Piles: Part 1 - Single Piles ». *J. Soil Mechanics and Foundation Div., ASCE*, vol. 97(5), p. 711-731.
- Poulos, H. 1971b. « Behaviour of Laterally Loaded Piles: Part 2 - Group Piles ». *J. Soil Mechanics and Foundation Div., ASCE*, vol. 97(5), p. 733-751.
- Poulos, H. G. 1989. « Pile behaviour - theory and application ». *Geotechnique*, vol. 39, n° 3, p. 365-415.
- Poulos, H.; Davis, E. 1980. *Pile Foundation Analysis and Design*. John Wiley and Sons.
- Poulos, Harry G. 1982. « Single pile response to cyclic lateral load ». *Journal of the Geotechnical Engineering Division*, vol. 108, n° GT3, p. 355-375.
- Randolph, M. F. 1981. « RESPONSE OF FLEXIBLE PILES TO LATERAL LOADING ». *Geotechnique*, vol. 31, n° 2, p. 247-259.
- Randolph, M. F.; Houlsby, G. T. 1984. « Limiting pressure on a circular pile loaded laterally in cohesive soil ». *Geotechnique*, vol. 34, n° 4, p. 613-623.

- Randolph, Mark F.; Wroth, C. Peter. 1978. « ANALYSIS OF DEFORMATION OF VERTICALLY LOADED PILES ». vol. 104, n° 12, p. 1465-1488.
- Reese, L. C. 1997. « Analysis of laterally loaded piles in weak rock ». *Journal of Geotechnical and Geoenvironmental Engineering*, vol. 123, n° 11, p. 1010-1017.
- Reese, L.; Cox, W.; Koop, F. 1974. « Analysis of Laterally Loaded Piles in Sand ». In *Proc. 6th Offshore Technology Conf. (Houston)* Vol. 2, p. 473-483.
- Reese, L.; Wang, S. 1989. « Documentation of Computer Program SHAFT1 Version 1.1: Drilled Shafts Under Axial Loading ». *Ensoft, Inc.*
- Reese, Lymon. 2006. *Analysis and design of shallow and deep foundations*. Hoboken N.J.: John Wiley.
- Reese, Lymon. 2009. *Single piles and pile groups under lateral loading*. London: Taylor & Francis.
- Reese, Lymon C. 1977. « Laterally loaded piles: Program documentation ». *American Society of Civil Engineers, Journal of the Geotechnical Engineering Division*, vol. 103, n° 4, p. 287-305.
- Reese, Lymon C. 1984. « BEHAVIOR UNDER LATERAL LOADING OF PILES SUPPORTING OFFSHORE STRUCTURES ». In., p. 399-448. New York, NY, USA: John Wiley & Sons.
- Reese, Lymon C.; Cox, William R.; Koop, Francis D. 1975. « Field Testing and Analysis of Laterally Loaded Piles in Stiff Clay ». p. 671-690.
- Reese, Lymon C.; Wang, Shin Tower. 1986. « METHOD OF ANALYSIS OF PILES UNDER LATERAL LOADING ». In *Marine Geotechnology and Nearshore/Offshore Structures*. (Shanghai, China), p. 199-211. Coll. « ASTM Special Technical Publication »: ASTM.
- Robertson, Peter K.; Davies, Michael P.; Campanella, Richard G. 1989. « Design of laterally loaded driven piles using the flat dilatometer ». *Geotechnical Testing Journal*, vol. 12, n° 1, p. 30-38.
- Robertson, Peter K.; Hughes, John M. O.; Campanella, Richard G.; Sy, Alex. 1984. « Design of laterally loaded displacement piles using a driven pressuremeter ». In *Laterally Loaded Deep Foundations: Analysis and Performance*. (Kansas City, MO, USA), p. 229-238. Coll. « ASTM Special Technical Publication »: ASTM.

- Rowe, P. W. 1956. « Single pile subject to horizontal force ». *Geotechnique*, vol. 6, n° 2, p. 70-85.
- Scott, R. F. 1979. « CYCLIC STATIC MODEL PILE TESTS IN CENTRIFUGE ». *Proceedings of the Annual Offshore Technology Conference*, vol. v, n° 2, p. 1159-1168.
- Silva, Pedro; Badie, Sameh S. . 2008. « Optimum Beam-to-Column Stiffness Ratio of Portal Frames under Lateral Loads ». *Structural Design - Discussions on design issues for structural engineers*.
- Society, Canadian Geotechnical. 2006. *Canadian Foundation Engineering Manual*, 4th. Vancouver, B.C.: Canadian Geotechnical Society, xvi, 488 p. p.
- Stevens, J. B.; Audibert, J. M. E. 1979. « RE-EXAMINATION OF P-Y CURVE FORMULATIONS ». *Proceedings of the Annual Offshore Technology Conference*, vol. v, n° 1, p. 397-403.
- Swane, I. C.; Poulos, H. G. 1984. « SHAKEDOWN ANALYSIS OF A LATERALLY LOADED PILE TESTED IN STIFF CLAY ». In *Fourth Australia-New Zealand Conference on Geomechanics: Geomechanics - Interaction, Preprints of Papers*. (Perth, Aust), 84 /2, p. 165-169. Coll. « National Conference Publication - Institution of Engineers, Australia »: Inst of Engineers.
- Terzaghi, K. 1955. « Evaluation of coefficients of subgrade reaction ». *Geotechnique*, vol. 5, n° 4, p. 297-326.
- Trochianis, A.; Bielak, J.; Christiano, P. 1988. *A Three-Dimensional Nonlinear Study of Piles Leading to the Development of a Simplified Model*. Coll. « Rpt. R-88-176 »: Dept. of Civil Eng., Carnegie Inst. of Technology.
- Truty, A; Zimmermann, Th. . 2010. *Dynamic Soil-Structure Interaction Using Domain Reduction Method (DRM) Zsoil Tutorial Manual*. Coll. « Dynamics in ZSoil ».
- Urao, K.; Masuda, K.; Kitamura, E.; Miyamoto, Y.; Fukuoka, A. 1992. « Dynamic behaviors of a composite foundation ». In *Proceedings of the Tenth World Conference on Earthquake Engineering. 10 vols, Jul 19 - 24 1992*. (Madrid, Spain), p. 1801-1801. Coll. « Proceedings of the World Conference on Earthquake Engineering »: Publ by A.A. Balkema.
- Vasquez, Lymon C. Rees; Shin Tower Wang; Luis. 2006. *Analysis of a group of piles subjected to axial and lateral loading* (February 2006). Technical Manual. Austin, Texas: ENSOFT, INC.

- Ventura, Carlos. 2010. *Visualization of Soil-Structure Interaction Effects*. Seminar. Vancouver, British Colombia: University of British Colombia.
- Wang, Lymon C. Rees; Shin-Tower. 2006. *Verification of computer program LPILE as a valid tool for design of a single pile under lateral loading*. Coll. « LPILE verification notes ».
- Winkler, E. (182). 1876. *Die Lehre von der Elastizitat und Festigkeit*, . Verlag.
- Wolf, John P.; Song, Chongmin. 2002. « Some cornerstones of dynamic soil-structure interaction ». *Engineering Structures*, vol. 24, n° 1, p. 13-28.
- Wong, Patrick C. W.; Kulhawy, Fred H.; Ingraffea, Anthony R. 1989. « Numerical modeling of interface behavior for drilled shaft foundations under generalized loading ». In *Foundation Engineering: Current Principles and Practices, June 25, 1989 - June 29, 1989*. (Evanston, IL, USA), p. 565-579. Publ by ASCE.
- Yegian, M.; Wright, S. 1973. « Lateral Soil resistance - Displacement Relationships for Pile Foundations in Soft Clays ». In *Proc. 5th Offshore Technology Conf.* (Houston) Vol. 2, p. 663-676.
- Youshimura, C.; Bielak, J.; Hisada, Y.; Fernandez, A. . 2003. « Domain reduction method for threed-imensional earthquake modeling in localized regions. part ii: Verification and applications ». *Bulletin of the seismological Society of America*, n° 93, p. 825–840.